COKE DEACTIVATION DURING CATALYTIC COAL OILS HYDROTREATMENT

By

HONG-JU CHANG

Bachelor of Science
Tunghai University
Taichung, Taiwan
1973

Master of Science
Oklahoma State University
Stillwater, Oklahoma
1977

Submitted to the Faculty of the Graduate College
of the Oklahoma State University
in partial fulfillment of the requirements
for the Degree of
DOCTOR OF PHILOSOPHY
December, 1982

COKE DEACTIVATION DURING CATALYTIC

COAL OILS HYDROTREATMENT

Thesis Approved:

Billy L Cypres
Thesis Adviser

Mayis Seapan

Archibald G. Hill

R. N. Maddox

Zuhair al-Shaieb

Norman N Durham
Dean of the Graduate College

PREFACE

The objective of this study was to investigate catalyst deactivation due to coke deposition during hydrotreatment of coal derived liquids. In order to observe this coke deactivation in a reasonable period of time, a suitable combination of a catalyst (Shell 324 NiMo/Al_2O_3) and a feedstock (SRC mixture) was chosen. Severe reactor plugging was encountered during the initial phase of this study. Much effort has been given to solve this problem. Elemental analyses showed that silica in the catalyst was not a major factor causing the plugging. However, experience and literature search revealed that hydrotreatment of SRC oils could result in heavy residue accumulating in the reactor and causing plugging. By recognizing these facts, the hydrotreating system was modified to tolerate heavy residue precipitation, and thus, to eliminate the plugging problem.

After the reactor plugging was solved, the subsequent experimental runs with various catalyst-oil contact times were rather smooth. These experiments have generated useful data for the investigation of catalyst deactivation mechanisms and kintics. A reaction-deactivation model was developed to consistently interpret these experimental results, and more importantly, to predict better catalysts for SRC oils hydrotreatment.

I am deeply indebted to my thesis adviser, Professor Billy L. Crynes, for his intelligent guidance and invaluable suggestions during various

phases of my graduate study and thesis work. I am very thankful to Dr. M. Seapan for his cooperation in this study, and to Dr. Z. Al-Shaieb for his great help in catalyst analyses during the initial phase of this study. I would like to express my sincere appreciation to Dr. R. N. Maddox, Dr. A. L. Hill and other faculty in the School of Chemical Engineering.

I would like to thank Mr. E. E. McCroskey and Mr. C. Baker, the storeroom managers, for their cooperation in equipment setup, and Steve Smith and Steve Parker for their help in equipment operations and sample analyses. I am grateful to Ms. Teresa Tackett for her patience in typing and editing this thesis.

Financial support from the School of Chemical Engineering and the Department of Energy is sincerely appreciated.

Finally, I would like to express my deepest sincerity to my parents, my wife, little daughter, all other family members and friends for their understanding and support.

TABLE OF CONTENTS

LIST OF TABLES

LIST OF FIGURES

CHAPTER I

INTRODUCTION

Since the Mideast oil embargo of 1973, worldwide oil prices have soared up more than ten times to $40 a barrel in 1981. Although the current oil price has been edging down because of decreasing demand due to conservation and economic recession and because of increasing worldwide oil exploration, this declining price is only a temproary relief to a depressed world economy. The conservation and exploration have started leveling off and the economy will soon recover. This may set the conditions for another oil price shock. In order to be free from uncertain oil imports, the United States has launched intense research and development efforts to utilize alternative energy resources.

Among many alternatives, coal seems to provide the most immediate solution due to its large reserve and being readily accessible. Liquefaction is one of the most promising ways to utilize coal because of limited supply of crude oils and the glaring fact that the U.S. is overwhelmingly dependent on gasoline and diesel powered vehicles; this means coal liquefaction products could help as transportation fuels.

Since coal liquids could potentially replace conventional petroleum fuels, and are the main concern in this study, a brief

description of the currently active coal liquefaction processes will be given below:

Indirect Liquefaction: Coal is first gasified by reacting with oxygen and steam to produce CO and H_2. The gaseous products are purified to remove heteroatom containing compounds and then treated in the presence of an iron or a cobalt catalyst to produce liquid hydrocarbons. The commercial process SASOL operated in South Africa belongs to this category.

Solvent Refining: Almost all processes that operate on the principle of hydrogen addition use a liquid solvent of some type. In the solvent refining processes, coal is dissolved in a donor solvent which is derived from coal itself. Solvent Refined Coal (SRC) and Exxon Donor Solvent (EDS) processes are the typical processes in this category. The latter one extracts coal with a catalytically hydrogenated recycle solvent to produce synthetic crudes (Epperly, 1980). Whereas the former process extracts coal with a recycle solvent saturated with hydrogen to produce low sulfur fuels (Lewis, 1981).

Catalytic Liquefaction: In these processes a coal slurry is treated with hydrogen in the presence of a catalyst at pressures and temperatures in the range of 14-30 MPa and 350-460 C respectively. Typical process under this category is the H-Coal process which uses an ebullated bed reactor (Johnson et al., 1974).

Except from indirect liquefaction process, the coal liquids as produced require further upgrading before they can be used as boiler, home heating and transportation fuels, and feedstocks for various chemicals production. This is necessary because:

1. Coal liquids contain large amounts of polynuclear aromatic compounds, and are low in hydrogen.

2. Coal liquids contain high percentages of heteroatoms such as nitrogen, sulfur, oxygen and inorganics. These will cause environmental and equipment problems upon combustion, stability difficulties upon storage, and result in catalyst poisoning upon catalytic cracking or reforming.

While coal liquids can be upgraded to chemical feedstocks and clean fuels, many problems still need to be resolved. Rapid catalyst activity decay is among the toughest problems during hydrotreating. This decreased catalyst life is an important factor in determining the commercial feasibility of the process. Coking is largely responsible for this rapid catalyst activity decay.

This study is a part of a program carried out in the School of Chemical Engineering at Oklahoma State University aimed at finding better catalysts for upgrading liquids derived from coal-to-oil processes. A combination of a catalyst and a coal oil feedstock has been chosen so that only coke deposition is the primary deactivation mechanism, and that the deactivation can be studied in a reasonable period of time. A number of analytical instruments has been used in this study to fulfill the following objectives:

1. To simulate industrial hydrotreatment operation and to support the study on the feasibility of coal liquefaction.

2. To determine changes in catalyst properties including pore size, pore volume, surface area and coke content as functions of catalyst-oil contact time and position within the reactor bed.

3. To study the catalyst decaying mechanisms and catalyst life.

4. To study the effects of catalyst support properties on the catalyst performance including activity and its maintenance.

CHAPTER II

LITERATURE REVIEW

The main objective of this study is to understand the catalyst deactivation due to coke formation during coal liquids hydrotreatment. Available information in the literature on the nature of coke, mechanism of coke formation and coke deactivation kinetics will be discussed in detail. Since this deactivation study concerns coal liquid hydrotreatment, knowledge of the properties of coal liquids, the chemistry and kinetics of hydrotreatment, and hydrotreating catalysts are also essential. Therefore, a general overview of coal liquids and their hydrotreatment will be given to enhance the understanding of the main subject, coke deactivation mechanism and kinetics.

Properties of Coal Derived Liquids

Processing of coal derived liquids require detail understanding on their properties. These properties are influenced by widely varied ranks, types and fields of the parent coals. In general, coal structure consists of stacked lamellae derived by two dimensional interconnection of aromatic and hydroaromatic clusters. The interlamellar distances are less than 1 nm apart. Ether, ester and amide groups as well as short aliphatic chains constitute some of the numerous types

of possible connecting links between polycyclic clusters. Elements such as nitrogen, oxygen and sulfur are present in the heterocyclic structure as well as in the form of different functional groups. Hypothetical coal models have been presented (Huntington, 1966; Given, 1960; Davidson, 1980).

In addition to the coal origin the type of liquefaction process and its operating conditions also play a major role in determining the properties of coal liquids. The catalytically produced coal liquids have better properties than thermally produced in terms of lower heteroatoms and higher hydrogen contents, preferred boiling range, reduced asphaltenes and increased stability. The results of gas and liquid chromatographic (GLC) and field ionization mass spectrometric (FIMS) analyses have shown that thermally produced liquids contain large amounts of a few individual compounds, whereas catalytically produced liquids contain a more even distribution of components (Whitehurst et al., 1979a). This is further revealed in Table I which presents the mass spectroscopic data of Synthoil (from a fixed bed process), SRC-I and its recycle solvent (Schiller, 1977). Table I indicates that the SRC recycle solvent has high concentrations of naphthalene and phenol; SRC-I concentrates in naphthalene, biphenyl and anthracene; while catalytically produced Synthoil liquid has a more even distribution of components.

Kershaw et al. (1980a, 1980b) studied the effects of temperature and catalysts on the chemical nature of coal hydrogenation oils using C^{13} - and C^{14} - n.m.r., infrared, ultraviolet, fluorescence and phosphorescence spectroscopic methods. The results showed an increase

TABLE I

COMPOSITION OF COAL DERIVED LIQUIDS
(Schiller 1977)

	SRC-I Recycle Solvent		Synthoil[a] W. Virginia Bituminous Coal	SRC-I W. Kentucky 9-14 Coal
	Pittsburg #8 Coal	Illinois #6 Coal		
Benzenes	1.05	1.60	-	-
Tetralin	8.12	5.75	1.70	-
Tetrahydroacenaphthene/ Dihydronaphthalene	-	-	1.64	- 0.22
Naphthalene	27.70	21.80	3.74	14.27
Acenaphthene/Biphenyl	6.31	9.75	9.01	12.57
Fluorene/Acenaphthylene	3.25	4.67	3.71	7.60
Phenanthrene/Anthracene	4.77	5.92	1.58	16.55
Dihydropyrene	-	1.59	6.85	7.00
Pyrene/Fluoranthene	1.13	1.87	1.82	4.49
Chrysene/Triphenylene	-	-	1.26	0.42
Binaphthyl	-	-	0.95	-
Benzopyrene	-	-	1.36	-
Dibenzoanthracene	-	-	0.40	-
Tetrahydroquinoline	0.23	0.26	0.67	-
Indole	0.38	0.13	0.41	-
Quinoline	9.89	8.43	1.07	1.36
Phenylpyridine/Tetrahydroacridine	1.39	2.74	1.77	3.00
Carbazole	0.18	0.59	0.68	2.56
Acridine	0.89	1.38	0.52	4.17
Naphthenobenzoquinoline	-	-	0.15	0.09
Azapyrene/Benzocarbazole	-	-	0.42	0.69
Benzacridine	-	-	0.10	-

TABLE I (Continued)

	SRC-I Recycle Solvent		Synthoil[a] W. Virginia Bituminous Coal	SRC-I W. Kentucky 9-14 Coal
	Pittsburg #8 Coal	Illinois #6 Coal		
Phenol	27.80	21.50	9.03	0.13
Indanol	-	-	2.30	0.88
Dibenzofuran	9.23	8.53	4.50	9.78
Hydroxyanthracene	0.20	0.59	0.29	-
Benzonaphthofuran	-	0.64	2.85	1.74
Benzo(def)phenanthrene	-	-	-	-
Benz(ghi)perylene	-	-	0.71	-
Coronene	-	-	0.11	-

a. 55-65% of product to distillate.

in operating temperature in the range of 400-700°C during coal liquefaction resulted decreases of molecular weight and viscosity of the product oils as well as a decrease in the percentage of polar compounds in the oils. Increasing the amount of liquefaction catalyst also gave the same positive results.

Coal liquids may contain up to 1 wt% of sulfur, 2 wt% of nitrogen and up to 5 wt% of oxygen. Sulfur compounds which are not present in Table I but are common to coal liquids are thiophenes, benzothiophenes, dibenzothiophenes and benzonaphthothiophenes. Common nitrogen compounds in coal liquids are quinolines, acridines, carbazoles and indoles; and common oxygen compounds are phenols, dibenzofurans, benzonaphthofurans and indanols (Crynes, 1981a; Shultz et al., 1977; Bodzek and Marzec, 1981). Mineral contents in coal liquids are also significantly high, which may appear as organic or inorganic compounds. The major mineral elements in coal liquids are Al, Ca, Fe, Mg, Si and Ti; the minor and trace mineral elements are B, Ba, Co, Cu, Cr, Mn, Mo, Ni, K, Na, Sr, Sn and V (Hauster et al., 1981; McGinnis, 1978).

Coal liquids contain significant quantities of asphaltenes and preasphaltenes, especially SRC-I which may contain up to 80 wt% of these undesirable fractions (Greskovich et al., 1977). The C/H atomic ratio, aromaticity, density and viscosity increase as the concentrations of asphaltenes and preasphaltenes increase. Although no solvents have generally been accepted to define asphaltenes and preasphaltenes, asphaltenes are usually referred to heptane insoluble and benzene soluble material which appears to be monofunctional species with molecular weight range from 300 to 1000; and preasphaltenes are

usually referred to benzene insoluble and pyridine soluble material which appears to be polyfunctional species having molecular weight higher than 400 (Whitehurst et al., 1976; Sternberg et al., 1975). Both asphaltenes and preasphaltenes contain large quantities of heteroatoms and ash which are difficult to be removed.

Dickie and Yen (1967) have postulated that the asphaltene particles consist of planar sheets of condensed aromatic rings and saturated carbon chains, and a loose net of naphthenic rings. Average diameters are in the range of 2-8 nm according to their model.

Coal liquids are not stable when stored in air. Several investigators (Finseth et al., 1979; Karn et al., 1974; Lin et al., 1974; Brinkman et al., 1979; O'Rear et al., 1980; Given et al., 1977) have observed property changes of the coal oils derived from Synthoil, H-Coal, COED and SRC processes. Significant increases in viscosity and high molecular weight components along with the formation of gum and other deposits after the oils have been stored under an oxygen atmosphere for a period of time have been reported. However, only slight change in properties when storing under nitrogen atmosphere has been observed. This instability is apparently caused by the formation and reaction of oxygen containing compounds. The oxygen content in coal oils has been found to associate with high viscosity and large molecular components (Heck, 1978; Stein et al., 1978).

In the study of the H-Coal process oil vacuum bottom with small angle X-ray scattering, Ho and Briggs (1981) observed that the formation of micelles in solution from the oil was as high as 49%. The percentage depends upon the concentrations and molecular sizes of asphaltenes,

preasphaltenes and the solvent. Most micelles were spherical with a diameter of 2.2-3.8 nm. Size in the range of 8-10 nm were also observed. They further noticed the appearance of a low level floc composing of three or more micelles in the solution upon extended sitting.

In summary, properties of coal liquids depend on the parent coals, production methods and process variables. Coal liquids are unstable in air and contain high concentrations of heteroatoms, ash, asphaltenes and preasphaltenes. These undesirable constituents cause processing difficulties in refining and equipment problems upon combustion. Nitrogen and sulfur further cause environmental problems upon combustion. These coal liquids are, therefore, not ready to serve as feed to conventional equipment using conventional petroleum stocks without further treatment.

Reaction Networks

The important global reactions that occur under the hydrotreating conditions are:

Hydrogenation:	Unsaturates $\longrightarrow$ Saturates
Hydrodenitrogenation: (HDN)	N-compounds $\longrightarrow$ Hydrocarbons + NH_3
Hydrodesulfurization: (HDS)	S-compounds $\longrightarrow$ Hydrocarbons + H_2S
Hydrodeoxygenation: (HDO)	O-compounds $\longrightarrow$ Hydrocarbons + H_2O
Demetallization:	Ash and/or metal compounds $\longrightarrow$ Hydrocarbons + metal deposits

The complexity of coal liquids precludes detailed studies on the kinetics and mechanisms of the above reactions as well as the role of catalysts in these reactions. An understanding of hydrotreatment processes can be gained through studies made on individual compounds that occur in coal liquids. Numerous studies have been made on representative heterocyclic compounds. Only hydrogenation and hydrodenitrogenation reactions will be discussed in some detail here since the hydrogen and nitrogen contents in oils are referred to catalyst activity and are the main concern in this study. The other reactions have been described elsewhere (Gates et al., 1979; Daly, 1978; Lee and Butt, 1977; Owens and Amberg, 1962a and 1962b; Krishnamurthy et al., 1981; Badilla-Ohlbaum et al., 1979a and 1979b).

Hydrogenation

The hydrogenation of aromatic hydrocarbons on hydrotreating catalysts has been studied by several investigators. Veluswamy (1977) studied the mechanisms of phenanthrene and pyrene hydrogenation on sulfided $NiMo/Al_2O_3$ and NiW/Al_2O_3 catalysts at temperatures of 200-340°C, a pressure of 3.5 MPa and a reaction time of 2 hours. The results are presented in Figures 1 and 2. The reaction network of phenanthrene shows that the first reaction step involves preferential hydrogenation of one end benzene ring resulting in 1,2,3,4-tetrahydrophenanthrene [3]. Hydrogenation at the 9,10-position of the inner rings occurs to a markedly lower extent. Subsequent hydrogenation of [3] is a fast step leading to [5]. The residual inner aromatic ring in [5] is somewhat sterically hindered, and consequently

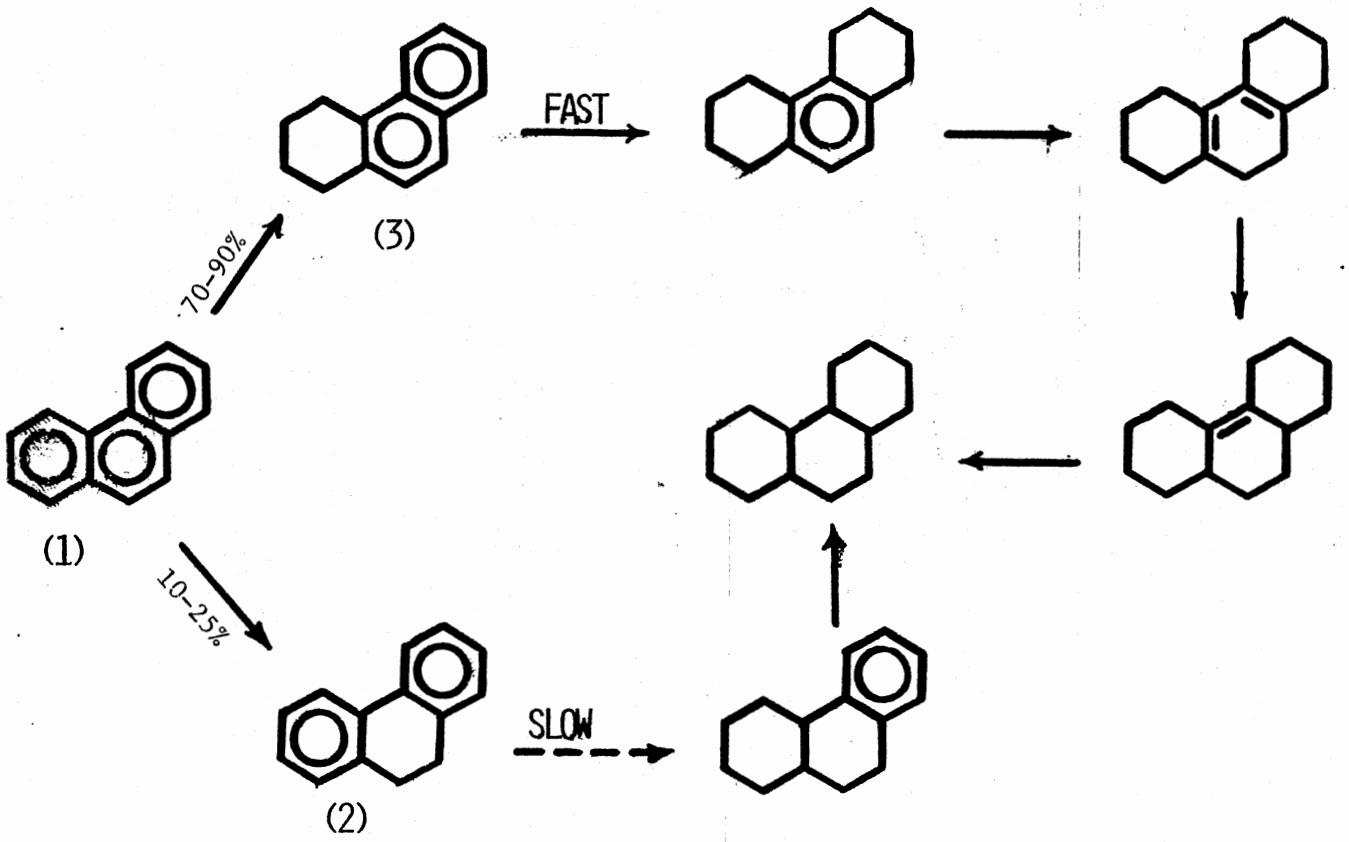

Catalysts: Sulfided $NiMo/Al_2O_3$ or NiW/Al_2O_3

Figure 1. Reaction Network for Hydrogenation of Phenanthrene at 200-340°C (Veluswamy, 1977)

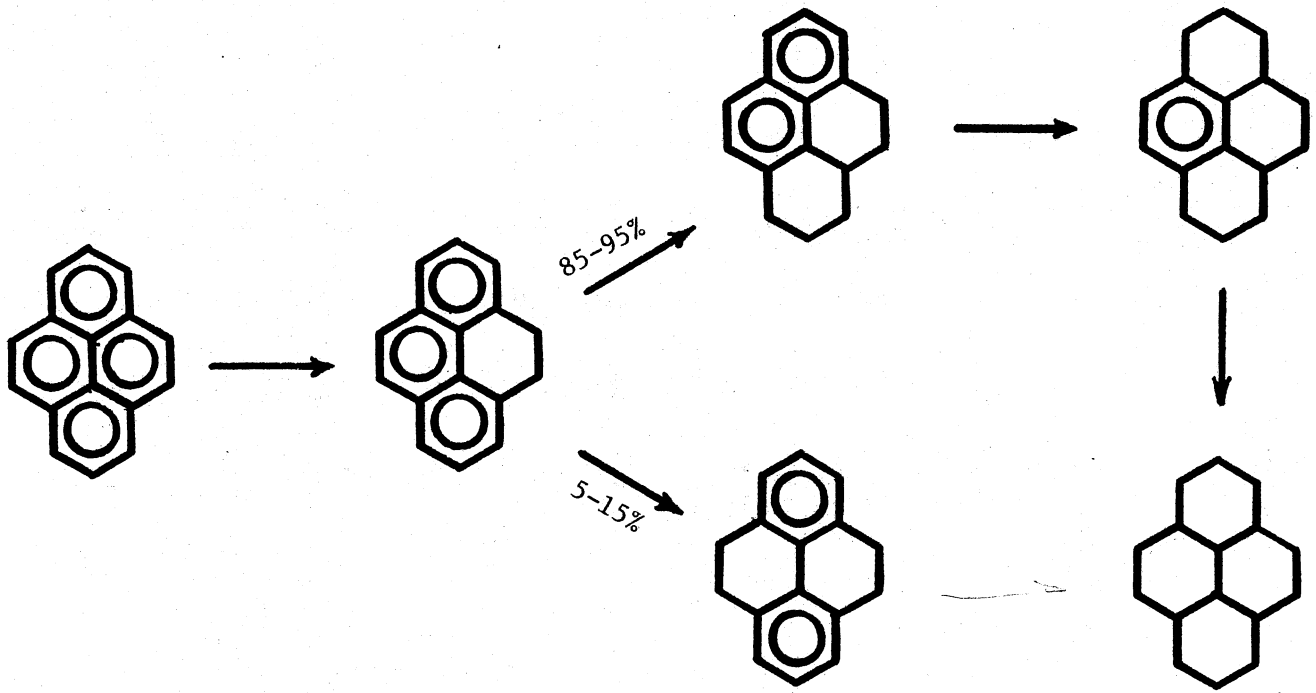

Catalyst: Sulfided NiW/Al_2O_3

Figure 2. Reaction Network for Hydrogenation of Pyrene at 200-340 C (Veluswamy, 1977)

the subsequent steps leading to complete hydrogenation are relatively low. Hydrogenation of pyrene proceeds in a similar stepwise manner: the hydrogenation with preferential formation of intermediates having strainless hydroaromatic rings and characterized by minimal steric interference with subsequent hydrogenation of residual aromatic rings.

The above studies of phenanthrene and pyrene hydrogenation were made at low temperatures of 200-340°C. No cracking was indicated. In contrast, Badilla-Ohlbaum et al. (1979) studied phenanthrene hydrogenation and hydrocracking over a sulfided $NiMo/Al_2O_3$ catalyst at temperatures higher than 500°C. As Figure 3 shows, tetrahydrophenanthrene [3] and 9,10-dihydrophenanthrene undergo hydrocracking to form alkyl- naphthalene and biphenyl as well as further hydrogenation. Figure 3 also shows that at relatively high temperatures, phenanthrene and hydrophenanthrenes undergo hydrogenation-dehydrogenation equilibrium reactions. Sullivan et al. (1964), Huan et al. (1977) and Wu and Haynes (1975) also reported similar observations.

Sapre and Gates (1981) have studied hydrogenation of aromatic compounds in a batch reactor at 7.6 MPa and 325°C in the presence of partciles of sulfided $CoMo/Al_2O_3$ catalyst. The compounds studies were benzene, biphenyl, naphthalene and 2-phenylnaphthalene. The reaction networks are shown in Figure 4 Each reaction network involves reversible hydrogenation of aromatic hydrocarbon (e.g., naphthalene) to give a hydroaromatic hydrocarbon (e.g., tetralin), which experienced further, slow hydrogenation (e.g., to decalin). Slow isomerization reactions of biphenyl to give methylcyclopentyl-

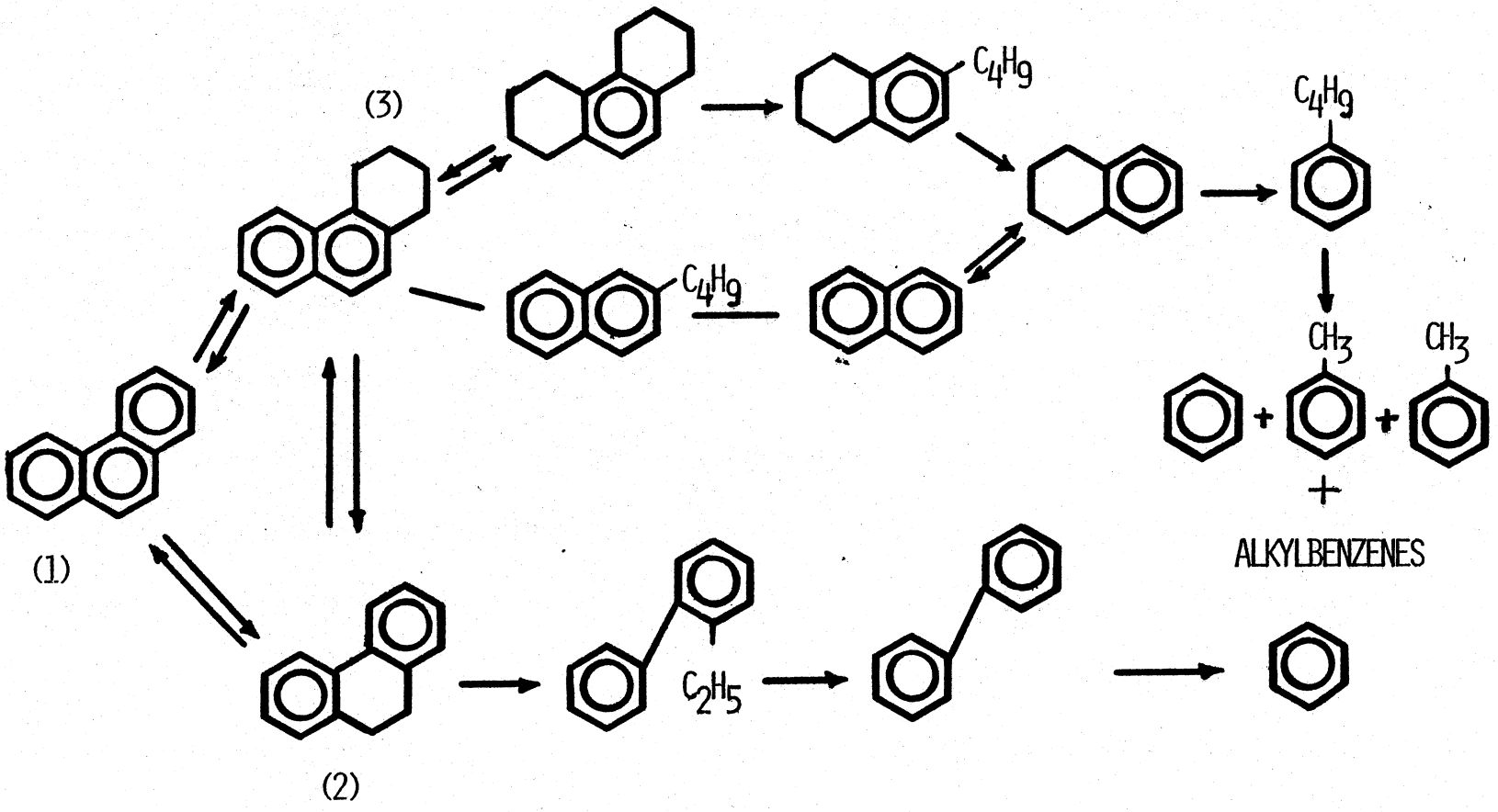

Catalyst: Sulfided $NiMo/Al_2O_3$

Figure 3. Reaction Network for Hydrogenation of Phenanthrene over 500°C (Badilla-Ohlbaum et al., 1979)

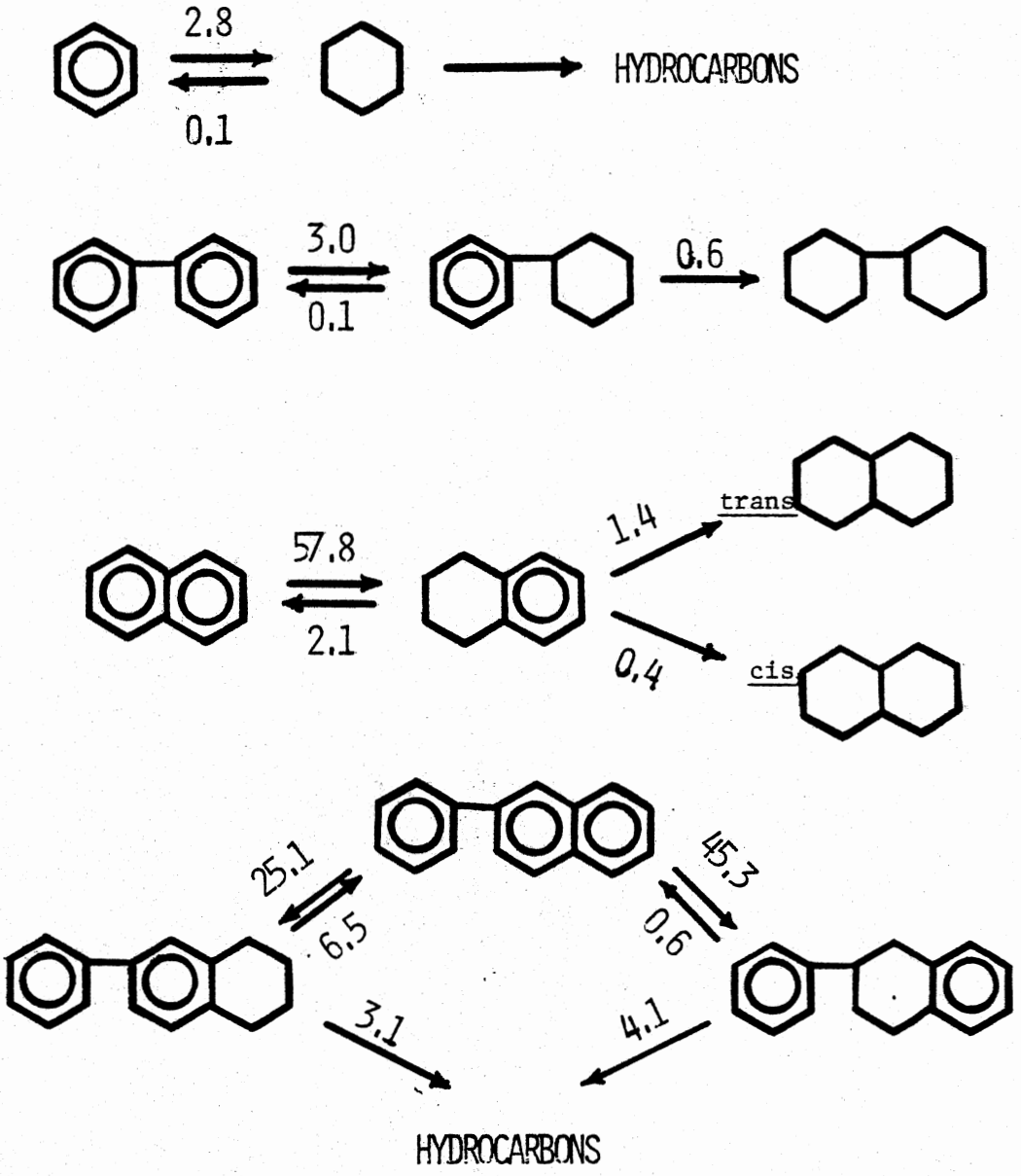

Catalyst: Sulfided $CoMo/Al_2O_3$
Pressure: 7.6 MPa; The numbers are pseudo-first-order rate constants in $m^3/s/kg$-catalyst

Figure 4. Reaction Networks for Hydrogenation of Benzene, Biphenyl, Naphthalene, and 2-phenylnaphthalene at 325 C (Sapre and Gates, 1981)

benzenes were also observed. The kinetic in each step can be approximated as pseudo first order reaction. The pseudo first order rate constants in Figure 4 show that benzene and biphenyl have nearly the same reactivities, and naphthalene and 2-phenylnaphthalene have nearly the same reactivities, but one order of magnitude greater than that of benzene.

From these pure compound studies, one can see that the hydrogenation products of one to four ring aromatics are mainly cyclic compounds, hydro-aromatics and alkyl-aromatics. Since these one to four ring aromatics are the main constituents of coal liquids, naturally the hydrogenated coal liquids contain more saturates and more smaller aromatics than do the raw coal liquid; the viscosity and the boiling point ranges of the hydrogenated oils are also reduced.

Hydrodenitrogenation (HDN)

Most of the nitrogen present in coal liquids are found in heterocyclic compounds which can be classified into basic and non-basic compounds. Examples of non-basic compounds are pyrrole, indole and carbazole; and basic are pyridine, quinoline and acridine. The reaction network of indole hydrodenitrogenation (HDN) over commercial hydrotreating and some novel catalysts at 350°C and 7.0 MPa was studied and proposed by Stern (1979), as shown in Figure 5. The HDN mechanisms of basic compounds have been studied by a number of investigators and reviewed by Katzer and Sivasubramanian (1979). The reaction network for pyridine HDN as demonstrated by McIlvried (1971) on sulfided $CoNiMo/Al_2O_3$ and by Sonnemans et al. (1974) on unsulfided Mo/Al_2O_3

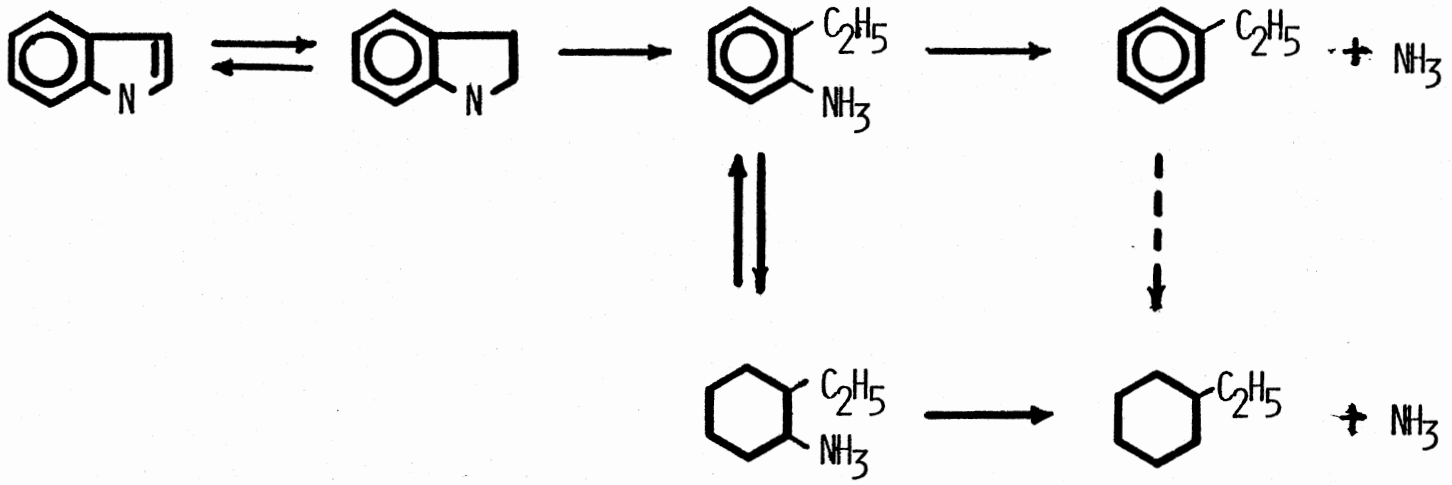

Catalysts: common and novel hydrotreating catalysts
Temperature: 350°C
Pressure: 7.0 MPa

Figure 5. Reaction Network for Hydrodenitrogenation of Indole (Stern, 1979)

catalyst is:

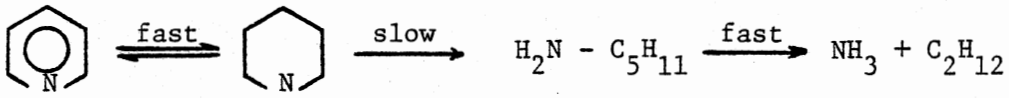

Sonnemans et al. (1974) found that piperidine can undergo disproportionation reactions that can be quite important in the overall reaction scheme. Figures 6 and 7 present the reaction networks and associated reaction kinetics for quinoline and acridine HDN as reported by Gates et al. (1979). The pseudo first order rate constants for each reaction in the networks are given for the reaction conditions indicated. These results show that HDN first involves hydrogenation of the aromatic rings, with hydrogenation of the nitrogen containing ring being favored kinetically, which is followed by carbon-nitrogen bond scission. The carbon-nitrogen bond scission occurs only in saturated rings. The aniline type species are stabilized by resonance with the aromatic ring, and thus the aromatic ring may require hydrogenation prior to carbon-nitrogen bond scission. Because of the bifunctional nature of HDN reactions, catalysts having both hydrogenation and bond breaking activities are required. Under typical commercial reaction conditions, the carbon-nitrogen bond breaking is not characterized as a rate limiting step, as shown in Figures 6 and 7.

The pseudo first order rate constants for HDN of multi-ring, nitrogen containing, aromatic compounds containing up to five rings at 367 C and 14.0 MPa catalyzed by $NiMo/Al_2O_3$ fall in the following decreasing order: Dibenz-[c,h]acridine > Quinoline > Carbazole > Acridine > Benz[c]acridine > Benz[a]acridine (Shih, 1977; Gates, 1979). $NiMo/Al_2O_3$ catalyst is more active than $CoMo/Al_2O_3$ for these

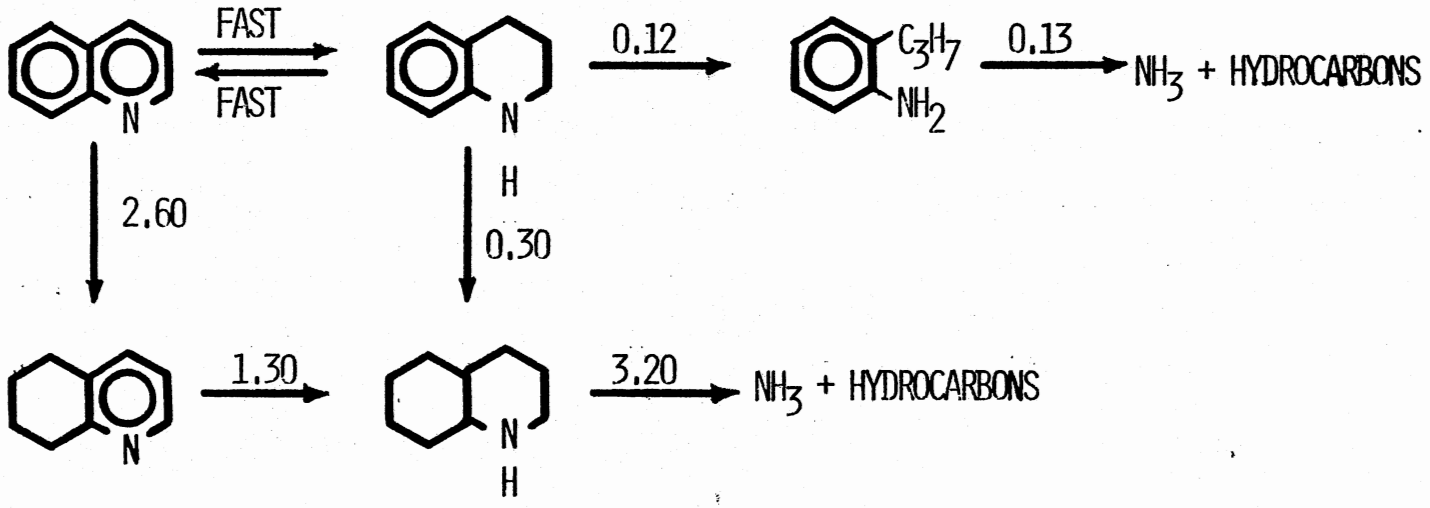

Catalyst: Sulfided $NiMo/Al_2O_3$
Temperature: 342 C
Pressure: 13.9 MPa; The numbers are pseudo-first-order rate constants in kg-oil/min/kg-catalyst

Figure 6. Reaction Network for Hydrodenitrogenation of Quinoline (Gates et al., 1979)

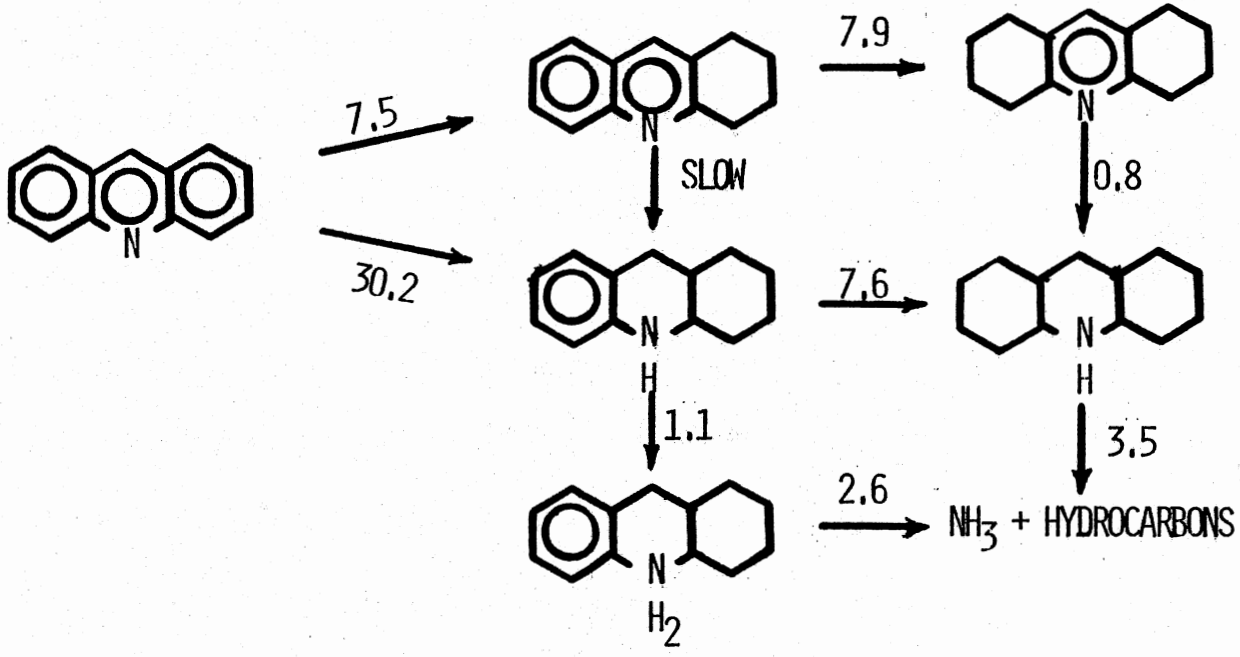

Catalyst: Sulfided $NiMo/Al_2O_3$
Temperature: 342 C
Pressure: 13.9 MPa; The numbers are pseudo-first-order rate constant in kg-oil/min/kg-catalyst

Figure 7. Reaction Network for Hydrodenitrogenation of Acridine (Gates et al., 1979)

hydrodenitrogenation reactions.

Cocchetto and Satterfield (1981) studied quinoline HDN over a presulfided $NiMo/Al_2O_3$ catalyst at 375 C and 7.0 MPa. The equilibrium constants for the reversible steps were theoretically calculated and compared to the experimental data. The results show that the HDN pathways of minimal hydrogen consumption are not thermodynamically favored under representative conditions of industrial interest. So the burden of selectively hydrotreating is placed solely on the catalyst. Satterfield et al. (1975, 1980, 1981) also studied the effects of hydrogen sulfide and thiophene on the HDN of pyridine and quinoline. The presence of thiophene and/or hydrogen sulfide has dual effects on the reaction kinetics. Thiophene and hydrogen sulfide inhibit the hydrogenation reaction of pyridine and quinoline at lower temperatures, and reduce the overall reaction rate. At higher temperatures, the hydrogen sulfide promotes the scissions of C - N bonds and enhances the overall rate of HDN reaction. In the presence of sulfur containing compounds, thermodynamic equilibrium of pyridine and piperidine is not reached, caused by both inhibition of pyridine hydrogenation and enhancement of piperidine hydrogenolysis.

Satterfied et al.(1975) showed that increasing nitrogen concentration severely inhibits hydrodesulfurization of thiophene, whereas the presence of sulfur compounds can promote the hydrodenitrogenation of pyridine and quinoline. Gates et al. (1979) investigated the interactions between quinoline, indole, dibenzothiophene and naphthalene in n-hexadecane over a $NiMo/Al_2O_3$ catalyst. The results showed that increasing concentration of naphthalene or indole (a non-basic nitrogen compound) has no effect on the reactions of quinoline

and dibenzothiophene. However, the presence of quinoline, a basic nitrogen compound, severely reduced hydrogenation and hydrosulfurization reaction rates. When the initial quinoline concentration was increased from 0.0 to 0.5 wt%, the rate of naphthalene hydrogenation was reduced by thirty-fold and hydrodesulfurization was reduced by three-fold.

From these pure compound HDN studies, one can expect that, in order to remove nitrogen from coal liquids, consumption of a large quantity of expensive hydrogen is necessary. In the meanwhile, basic nitrogen compounds in coal liquid reduce the catalyst activity; but presulfiding of the catalyst improves the activity and selectivity of the catalyst for HDN reactions.

Hydrotreatment of Coal Derived Liquids

The type of coal liquid has profound effects on the results of hydrotreatment. Under severe hydrotreating conditions, most coal liquids can be upgraded to refinery feeds and clean fuels. This has been demonstrated by a number of investigators (Caspers et al., 1981: Frumkin et al., 1981; Fant and Barton, 1978; Hildebrand, 1979; O'Rear et al., 1981; Potts et al., 1981; Ryan, 1979; Shih et al., 1980; Sullivan et al., 1979, 1980). However, severe reactor plugging and rapid catalyst deactivation have often been encountered, especially in processing heavy residuum such as SRC-I (Bowman et al., 1980; Sullivan, 1981; Stein et al., 1978; Ahmed, 1979). This catalyst deactivation will be discussed in more details later.

Basic nitrogen containing compounds in coal liquids can have detrimental effects on the hydrotreatment as expected from pure compound

studies discussed earlier. This has been reported by Sivasubramanian and Crynes (1980) and Mitchell (1980). The former authors studied the nitrogen compound effects by doctoring a raw anthracene oil with quinoline to various concentrations. Both undoctored and doctored feedstocks were hydrotreated over presulfided $CoMo/Al_2O_3$ catalysts in a trickle bed reactor at 370 C and 10.4 MPa. Of the three catalysts tested, increasing nitrogen concentrations more severely affected sulfur removal ability of that catalyst with the lowest HDN activity.

Process Variable Effects

Hydrotreatment of coal liquids is typically achieved in the conventional down flow trickle bed reactors in the presence of hydrogen under a wide range of operating conditions. Other reactors such as expanded bed and ebullated bed have also been used (Potts et al., 1978; Johnson et al., 1974). Typically, the operating pressures range from 10 to 20 MPa, temperatures range from 300 to 450 C, with space times from less than 0.5 to 5.0 hours and hydrogen to oil feed ratios from 500 to 4000 std. m^3 H_2/m^3 oil.

The effects of temperature on the reaction rate is apparent. The rate constant can be correlated with Arrhenius plots, from which the pre-exponential factors and the activation energies are calculated. The apparent activation energies for various types of pseudo first order reactions of coal liquids over commercial hydrotreating catalysts are generally reported to fall into the range of 50-200 KJ/mole (Seapan and Crynes, 1981). While the rate of reaction increases with increasing temperature, thermodynamic equilibrium favors the dehydro-

genation and cracking. This results in excess coke formation and thus rapid catalyst deactivation and reactor bed plugging (Ahmed, 1979).

Hydrogen pressure is not included in the rate equation in most cases; except in the work by Qader (1972), Caldwell (1979) and Heck and Stein (1977). The effects of increasing hydrogen pressure is to increase hydrogen solubility in the oil resulting in a higher reaction rate. At temperatures between 100 and 400 C and hydrogen pressures between 3.5 and 20.7 MPa, the solubility of hydrogen in creosote oil was reported to increase linearly with hydrogen pressure (Prather et al., 1977). However, increasing hydrogen pressure beyond 7.0 MPa during hydrotreating raw anthracene oil and Synthiol liquid has been observed to have less significant effects on the heteroatom removal rates over presulfided $CoMo/Al_2O_3$ catalysts (Soni, 1977; Sooter, 1977; Garg et al., 1981). This may be due to the fact that there is a large excess of hydrogen available in the oil during reaction at higher pressure.

Kinetics of Hydrotreatment

The kinetics of coal liquids hydrotreatment has been extensively reviewed by Seapan and Crynes (1981). Global rates of reaction are generally used to represent the results from trickle bed reactor studies, although a few studies have been designed to decouple the physical processes from the intrinsic kinetics (Ahmed, 1979). The majority of investigators have concluded that their data can be adequately represented by a simple first order kinetic model (White et al., 1968; Jacobs et al., 1971; deRosset, 1976; Ahmed, 1979; Wiser, 1977, 1978).

However, the second order rate expression can generally give a better fit to the data over the range of operating conditions, especially for feedstocks with a wide boiling range (Heck and Stein, 1977; Heck, 1977: Stein et al., 1978; Shih et al., 1980; Soni and Crynes, 1981; Mehta, 1978; Angevine et al., 1979). This higher than first order dependence is a necessary result of the lumping of thousands different compounds present in coal liquids (Katzer, 1976). Theoretical discussions of Weekman (1968) also show that a mixture of several parallel first order reactions exhibits an overall kinetic order higher than unity.

In addition to the simple first and second order reactions, modifications of the first order forms also appear in the literature. Dividing the feedstock into reactive and relatively less reactive sub-groups was proposed by Sooter (1974), Garg et al. (1979, 1980) and Struck (1969). Satchell (1974) modeled the hydrodenitrogenation of a coal liquid by dividing it into several boiling ranges and assuming that the HDN reactivity is a linear function of the boiling range.

In the laboratory, the ideal plug flow model is generally used to interpret the hydrotreatment data from trickle bed studies. However, low liquid flow rates in these laboratory trickle bed reactors often make the reactor performance deviate from ideality. Several approaches have been developed to account for this non-ideality (Henry and Gilbert, 1973; Mears, 1974; Shah, 1979; Satterfield, 1975; Doraiswamy, 1975). Among these, the first two approaches have been widely accepted for the design and scaleup of the trickle bed reactor. Henry and Gilbert (1973) incorporated the liquid holdup and obtained the following equation for a first order reaction:

$$\ln \frac{C_i}{C_o} = \frac{k_1(1-\varepsilon_b)\,\eta h_L}{LHSV} \qquad (1)$$

where

C_i, C_o = inlet and outlet concentrations, respectively

k_1 = first order Kinetic constant

ε_b = porosity of the reactor bed

η = effectiveness factor

h_L = total liquid holdup

LHSV = liquid hourly space velocity

When the liquid holdup, h_L is replaced by Satterfield's et al. correlation (1969), the following equation is obtained:

$$\ln \frac{C_i}{C_o} \alpha\ (L)^{1/3}(LHSV)^{-2/3}(d_p)^{-2/3}(\nu_L)^{1/3} \qquad (2)$$

for liquid Reynold numbers between 10 and 600, where

L = total reactor length

d_p = particle diameter

ν_L = kinematic viscosity of the liquid

Mears (1974) attributed the dependency of the effectiveness factor on the liquid flow rate to the incomplete wetting of the catalyst at low liquid flow rates and obtained the following equation for the first order reactions:

$$\ln \frac{C_i}{C_o} = \frac{k_1(1-\varepsilon_b)\eta}{LHSV}\left[1 - \exp(-\gamma\,(L)^{0.4}(LHSV)^{0.4})\right] \qquad (3)$$

where γ is a correction factor accounting for the effect of viscosity, surface tension, density and particle diameter.

Hydrotreating Catalysts

Typical hydrotreating catalysts are a combination of Co, Ni, Mo and W in oxide forms on a alumina or silica-alumina support. Other active metals such as Fe, Cr, and Pt are occasionally used (McKinley, 1975). The concentrations of MoO_3 or WO range from 10 to 20 wt% and the promoters, CoO or NiO, range from 0 to 5 wt%. The Ni-Mo supported catalysts are generally more active in hydrogenation and hydrodenitrogenation than the catalysts of other combinations, whereas the Co-Mo supported catalyst is more preferred for hydrodesulfurization. This is due to the fact that Ni is more active in hydrogenation which is an important step for hydrodenitrogenation but less so in hydrodesulfurization.

The most commonly used supports are gamma type (γ) alumina and silica-alumina which have medium surface areas and micropore diameters in the range of 150×10^3 - 300×10^3 m^2/kg and 5-20 nm, respectively. Increasing pore size can be achieved with the sacrifice of surface area and vice versa. Therefore there must exist an optimal value for hydrotreating a particular oil at a fixed set of operating conditions. Riley (1978) studied hydrotreatment of heavy feeds containing up to 20% asphaltenes over $CoMo/Al_2O_3$ catalysts with various pore sizes. The results showed that the hydrodesulfurization activity increased with pore size, to a maximum and then decreased. The optimal pore diameter was in the range of 10-20 nm. Sooter (1974) in his hydrotreatment study with raw anthracene oil, reported that the reduction of pore diameter from 6.6 to 5.0 nm had a detrimental effect on sulfur removal. Mineav et al. (1975) and Nakamura et al. (1979) in their studies with residual oils over $CoMo/Al_2O_3$ and $NiMo/Al_2O_3$ catalysts observed

that the catalysts with larger pores and pore volumes had higher activity and stability.

Stein et al. (1978) reported that the hydrotreatment of SRC-I/solvent mixture over smaller diameter (5-10 nm) NiMo/Al_2O_3 catalysts resulted in two phase products, i.e., gas and heavy liquid, and reactor plugging. However, these two phase products and plugging did not happen when a larger diameter cataylst (pore diameter in the range of 10-20 nm) was used. Two phase products were apparently caused by selectively hydrotreating the light fraction in the oil. Since the heavy fraction generally contains compounds having molecular sizes between 3 and 10 nm, these large molecules can not diffuse into the pores having the same dimensions as the molecules.

Catalyst Deactivation

Deactivation Mechanisms

Rapid catalyst deactivation during coal liquefaction and coal liquid upgrading has been a major concern and often been reported in the literature (Curtis et al., 1981; Mitchell, 1980; Stanulonis et al., 1976; Sivasubramanian et al., 1980; Ahmed, 1979). Catalyst deactivation could be due to poison adsorption, sintering, and mineral and/or coke depositions.

Basic nitrogen compounds can reduce catalyst activities, as discussed earlier, because they can strongly adsorb on the surface acidic sites which play important roles in hydrogenation and hydrocracking reactions. Hollway and Nelson (1977) reported that in spent catalysts from the Synthoil process, Auger electron data indicated the presence

of nitrogen on the catalyst surface and speculated the presence of ntirogen containing compounds. Berg and McCandless (1980) in their coal liquid hydrogenation study found that nitrogen compounds primarily disappear from the liquid by irreversible adsorption on the catalyst substrate rather than by chemical reaction to ammonia. Poisoning of the hydrotreating catalyst by basic nitrogen compounds should be significant only during the first few hours of the startup period and be reversible after that period.

Sintering results in change in physical and/or chemical properties of the catalyst, such as surface area, pore volume, pore size and states of the active species. Polinski et al. (1981) observed that the surface area decreased and pore size increased during a liquefaction process using a $CoMo/Al_2O_3$ catalyst at 13.9 MPa and 440 C. However, under normal hydrotreating conditions, this sintering effect is not significant. This can be seen from the facts that after regeneration of the spent catalyst from hydrotreating low ash coal liquids, essentially all the surface area and pore size were recovered. Moreover, the activities of these regenerated catalysts were also recovered (Crynes, 1981b; Ahmed, 1979).

Mineral matter from feedstocks can deposit on the catalyst covering the active sites and restricting the pore mouths, resulting in permanent loss of catalyst activity. Some of the deposited metals such as iron, nickle, cobalt and their oxides can even catalyze coking reaction at relatively low temperatures, 350-600 C (Baker, 1972). Weisser and Landa (1973) have reviewed the work of several European and Russian researchers and reported that vanadium at low concentration has little significant deactivating influence on $CoMo/Al_2O_3$ catalysts.

However, they noted that the presence of alkali metals along with vanadium results in even higher deactivation rates. In coal tar hydrogenation, arsenic has been observed to significantly poison the catalyst.

Stanulonis et al. (1976) have observed relatively higher inorganic deposits on the catalysts near the reactor inlet in the Synthoil process for coal liquefaction. On the other hand, Holloway and Nelson (1977) in their studies with the spent catalysts from the Synthoil process observed that most of the inorganic materials are concentrated near the reactor outlet. Holloway and Newson (1977) also observed that Fe and Ti penetrated into the catalyst pellet up to a depth of 200 μm with a relatively high concentration near the outer surface. Sivasubramanian et al. (1980) used X-ray microprobe to study aged hydrotreating catalysts, and reported that silicon, a major constituent of the clay in coal, was found in the exterior 100 μm of the catalysts, while iron mainly existed in the exterior crust and associated with sulfur as FeS_x. The study by Tamm et al. (1981) on residuum hydroprocessing clearly showed that vanadium and nickle can penetrate half way into a catalyst pellet of 1.6 mm diameter extrudate, while iron mainly deposits on the catalyst periphery.

In the hydrotreatment of petroluem feedstocks, catalyst activity decay is rapid initially, followed by a slow decline period. The former is due to coke formation on the catalyst surface which soon reaches an equilibrium level. The metal deposition is responsible for the stage of slow decay (Dautzenberg et al., 1978). However, in heavy coal liquid hydrotreatment, due to high asphaltenes and aromatics contents in the feedstock, coke may continuously build up on the catalyst

without approaching an equilibrium, until the catalyst is completely deactivated (deRosset et al., 1979). In this case, the effect of metal deposition is not significant, and coking becomes the primary deactivation mechanism. Coking deactivation is the main interest in this study and will be discussed in detail.

Mechanisms of Coke Formation

The structure of coke and the mechanisms of coke formation are complex and not fully understood. Most reported work on coking is from studies of catalytic cracking. Haldman and Botty (1959) have studied the coke from the catalytic cracking of gas oils over a silica-alumina catalyst. Their results from X-ray diffraction, nitrogen adsorption, and light and electron microscopies showed that the carbon deposit was a finely divided, highly dispersed phase present within the ultimate pore structure of the catalyst. X-ray diffraction indicated that the coke deposit consisted largely of pseudo graphitic structure together with considerable amount of poorly orgainzed carbonaceous material. The coke was characterized as low density particles consisting of thin, filmy, aggregates of sizes less tha 10 nm. The H/C atomic ratio determined by Haldeman and Botty (1959) was 0.4-0.5. This suggests that a considerable fraction of aliphatic and/or alicyclic fragments (H/C = 2) was present in the deposit, since the H/C atomic ratio of a condensed ring of 1 nm diameter is approximately 0.30, and of 1.4 nm diameter is 0.25.

Baker and Harris (1978) studied the mechanisms of coke formation, and classified coke into three main types: amorphous, filamentous and graphite platelets. These types would not be distinguished during a

routine analysis of the spent catalysts, but merely referred to collectively as "coke". As discussed by Baker and Harris (1978), condensation and polymerization reactions play a major role in amorphous carbon formation. Although some hydrogen is removed during condensation, a significant amount still remains in the deposit. As the temperature is raised, dehydrogenation reactions reduce the hydrogen content. Filamentous carbon is produced by the catalytic decomposition of carbon containing gases on small metal particles such as iron, cobalt and nickel and their oxides. The graphitic deposit is formed indirectly, at the expense of the other two deposit forms and also requires the participation of a catalyst. The graphite carbon can form only at elevated temperatures higher than 1000 C. Therefore, only amorphous and filamentous types of carbon deposits are significant in hydrotreating catalysts.

In the study with acidic silica-alumina and neutral silica gel, Appleby et al. (1962) reported that coke formation proceeds mainly through aromatic molecules serving as coke precursors. The aromatics could be present in the feedstock or may form as intermediates in the process. Definite correlations were found relating strong coking tendencies to large aromatic molecules and acid-base interactions between the catalyst and several aromatics and their alkyl derivatives. As a result of their observations, these investigators postulated a carbonium-ion mechanism involving growth of polynuclear aromatic polymers via dehydrogenation, cracking, and condensation reactions to form coke. This theory was later supported by Eberly et al. (1966), who studied coke formation during catalytic cracking of pure hydrocarbon

and n-hexadecane at 445 and 500 C over a silica-alumina catalyst. The results of infrared analyses indicated that coke mainly contains aromatic rings and some methyl groups, the relative amount depends on the feed. The more aromatic the feed is, the more aromatics in the coke. They concluded that aromatic compounds are generally much more strongly adsorbed than the more saturated hydrocarbons. These strongly adsorbed species are believed to form coke on the surface as the reactions proceed.

The work of Uchida et al. (1975) disclosed that in the dehydrogenation of n-butane over silica-chromia, coke deposits preferentially at Lewis acid sites over the Bronsted acid sites. Although both types are known to be active in dehydrogenation.

Madison and Roberts (1958) in their pyrolysis experiments at temperatures of 450 C and higher observed that nitrogen containing heterocyclic aromatic compounds have a hgher coking tendency than their hdyrocarbon analogs: Quinoline and acridine pyrolyzed to give more coke than naphthalene and anthracene. They also observed that aromatics with one or more methylene groups bridging the aromatic nuclei had a strong tendency towards condensation and hence coking. These observations were later confirmed by Lewis and Edstrom (1963) who studied the thermal reactivity of eighty-four polynuclear aromatic hydrocarbons, and reported that thermal condensation reactivity was dependent on molecular size. Furimsky (1978) has experimentally studied spent hydrotreating catalysts and reported that coke contained higher concentrations of oxygen and nitrogen than the corresponding feedstock.

All the above studies suggest that aromatic compounds, especially polar aromatic compounds having strong adsorption tendency and having high cracking and condensation reactivities, tend to form more coke than do the other compounds.

Temperature and pressure have definite effects on coke formation. As expected, the effect of temperature is strong, although not like the characteristics of chemcial reactions which follow the Arrhenius relationship. Voorhies (1945) has shown coke formation on catalysts from fixed bed cracking of gas oil to be a linear function of temperature. Ternan et al. (1979) showed that the amount of coke on catalysts was strongly dependent on the temperature during hydrodesulfurization of heavy oil. Rudershausen and Watson (1954) observed that the coking rate decreased with an increase in hydrogen partial pressure and suggested Langmuir-Hinshelwood type kinetics for coke formation. The effects of catalyst properties on coke formation are also important. Ahmed (1979) hydrotreated a Synthoil liquid dissolved in raw anthracene oil and determined the coke contents and surface areas of the spent catalysts. He found that there was more accumulation of carbonaceous material on the $CoMo/Al_2O_3$ catalysts relative to $NiMo/Al_2O_3$ catalysts, and that $CoMo/Al_2O_3$ lost more surface area than did $NiMo/Al_2O_3$. This may be due to the higher hydrogenation power of nickel catalyst.

Ternan et al. (1979) have made a detailed study of the coke formation during hydrodesulfurization of heavy residual oils over various promoted MoO_3/Al_2O_3 catalysts. They reported that at a MoO_3 concentration of 2.2 wt% and a promoter/molybdenum atomic ratio of one, the amount of coke on the catalyst was almost unaffected by the type of promoter used: Ti, V, Cr, Mn, Fe, Co, Ni, Cu or Zn. On the other hand,

the molybdenum content on the catalyst had a strong effect on coke formation. Coke on catalyst decreased rapidly with increasing molybdenum content until a MoO_3 concentration of 5 wt% was reached. For a nickel promoted catalyst, the coke formation was maximized at a Ni/Mo atomic ratio of one. However, the sulfur removal was also maximized at this ratio. Presulfiding can help suppress coke formation. This has been investigated by Takatsuka et al. (1979), who reported that the presulfiding of a $NiCoMo/Al_2O_3$ catalyst decreased coke deposits and thus increased catalyst life during residual oil hydrodesulfurization.

Coke on a catalyst surface can be multilayered. By assuming than a coke monolayer has the effective area of an aromatic molecule, less than 8 wt% of coke is enough to occupy a monolayer on a catalyst having a surface area of 200×10^3 m^2/kg. In residual and coal oils hydrotreatment, spent catalysts typically contain 10-30 wt% coke and still possess considerable fractional surface area and activity (Ahmed, 1979). This suggests that coke may preferentially or randomly deposit on certain sites of the catalyst surface and grow three dimensionally as the reactions proceed. This is in contrast to depositing as a monolayer and covering all the active surface.

Coke deposits on porous catalysts can seriously alter the intraparticle transport characteristics of the catalyst by reducing the pore volume, blocking the pore mouth and introducing restrictions in the catalysts. Semiquantitative results from scanning Auger microscopic and electron microprobe analyses have shown that coke primarily deposits on the outer shell of a catalyst pellet and decreases toward the

center of the pellet (Bouwman and Toneman, 1980; Tamm et al.,1981; Berg and McCandless, 1981).

Duraiswamy (1973) studied the effect of coke on the catalytic hydrocracking of a heavy oil and concluded that at higher coke levels (5-6 wt%), pore diffusion was the rate controlling step, but not so at a lower coke level. Prashers et al. (1978) measured the effective diffivities of hydrocarbons in fresh and plant aged cracking catalysts, and reported that the effective diffusivities of the spent catalysts were reduced by more than three-fold by the deposits, while the surface area and pore volume were reduced by three and two-fold, respectively. The higher the deposit, the more the effective diffusivity was reduced.

Kinetics of Catalyst Deactivation

The mechanism of coke formation in coal liquids hydrotreatment is very complex since coal liquids contain thousands of compounds. However, coke formation can be viewed as the result of a sequence of side reactions from feedstock, intermediates, products, or any combination of the three. This scheme can be simplified as follows:

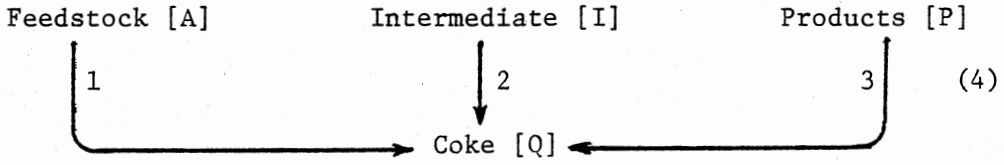

Depending on the relative contribution of the individual routes, the coke deactivation mechanisms can be classified into parallel, series and independent fouling. If coke forms mainly by route 1 only, then this is parallel fouling; if mainly by routes 2 and 3, it is series; and if equally by all three routes, then it is independent fouling.

This scheme can also represent other fouling mechanisms such as poisoning.

Reaction kinetics studies are quite complex for most industrial systems. When catalyst deactivation, especially in the case of diffusional limitation, is occurring, the kinetics become even more complex. The kinetics and mechanistic details of catalyst deactivation were first discussed by Wheeler (1951, 1955). He identified two types of poisoning, homogeneous and pore mouth poisoning aspects depending on the relative rates of poisoning and diffusion. For the uniform poisoning, the fractional activity left, F, relative to the fraction poisoned, α, is:

$$\text{for } \eta = 1, \quad F = 1 - \alpha \tag{5}$$

$$\text{for } \eta << 1, \quad F = (1 - \alpha)^{1/2} \tag{6}$$

where η is the effectiveness factor. Pore mouth poisoning is more of a rate taxation than when uniform poisoning prevails.

Reviews of the work on catalysts deactivation have been given by several authors (Butt, 1972, 1980; Wojciechowski, 1974; Carberry, 1976; Froment, 1980; Levenspiel, 1972). Levenspiel (1972) and his co-worker have fruitfully analyzed the deactivation-reaction problem in simple yet representative terms which encompass a wide diversity of poisoning-fouling precursor networks. Their approach assumes nth order catalytic reaction and activity decay. Following Levenspiel (1972), the main reaction rate is given by

$$R_A = \frac{dA}{dt} = -k_A A^n a \tag{7}$$

and the activity decline rate is given by

$$R_q = \frac{da}{dt} = - k_g (A,I,P)^m a^d \tag{8}$$

where

$$a = \frac{\text{rate at time t}}{\text{rate at time zero}}$$

k_A, k_q = intrinsic rate constants for main and fouling reactions respectively

n,m = order of reactant dependencies

d = order of deactivation

When diffusion of the reactant and/or poison precursor is to be anticipated, the respective Thiele moduli for reactant and poison, h_A and h_q, will determine the distribution of poison within the porous catalyst and thus the activity-selectivity behavior. Khang and Levenspiel (1972) have shown that at low Thiele moduli, the poison deposits uniformly on the pellet for both parallel and series poisoning. At high Thiele moduli, the poison deposit proceeds from the outer core of the catalyst pellet toward the center for parallel poisoning, and from center to outer core for series fouling. Khang and Levenspiel (1972) solved the diffusion-reaction equations for each of the reaction networks to establish the mean activity of the pellet and concluded that the order of deactivation, d, in equation (8) varies with the Thiele modulus and the deactivation mechanisms, i.e., parallel, series, and independent foulings.

Wojciechowski (1974) has used the power law decay of zero, first and higher orders, and competing first and second order decay to summarize the catalyst decay kinetics proposed by earlier researchers. Application of his generalized decay equation to cumene cracking was demonstrated to be satisfactory. John et al. (1974) studied the catalytic cracking of a gas oil in a fixed bed reactor and found that

coke on catalyst could reach an equilibrium level in a relatively short period while the catalyst activity continued to decline. They thus concluded that coke on the catalyst can not be a measure of the catalyst activity, and the catalyst activity is solely a function of time on stream.

These power law reaction-deactivation functions have the merit of adequately describing a number of deactivation-time on stream observations such as exponential, hyperbolic and power law decay, as noted by Levenspiel (1972). Carberry and Gorring (1966) viewed the deactivation process in terms of gas-solid noncatalytic reaction under conditions where the shell progressive model can be invoked. Their application of the shell progressive model and coking, poisoning and deactivation in general is inspired by the fact that observations of catalyst decay in petroleum processing have been correlated in terms of the Voorhies equation (1945), which states that the extent of poisoning, coking, or fouling, α, is relative to time on stream, t, by:

$$\alpha = Kt^n \tag{9}$$

where K is the proportional constant, and n is the order of time dependency which is equal to 1/2 in Voorhies' observation (1945). Carberry and Gorring (1966) have interpreted that a value of n = 1/2 is an indication of a diffusionally affected deactivation event. In practice, plots of α versus t on ln-ln coordinates generally have shown that the order with respect to time on stream have a value of 1/2, though values of n greater or smaller than 1/2 have been observed, as noted by Carberry (1976).

Froment and Bischoff (1961) have studied the catalyst fouling behavior in a fixed bed reactor in the absence of diffusional limitations. Instead of relating to time on stream, they explicitly related the activity decline to coke on catalyst. Two forms of activity decay function, exponential and hyperbolic, were used to investigate the parallel and series mechanisms. This approach of carbon related activity decay requires a rate equation for the coke formation, coupled with that for the main reaction. This approach is able to predict coke profiles in the reactor. For the system investigated by Froment and Bischoff (1961), the carbon profile in the reactor was descending from the entrance in the case of a parallel fouling, and ascending in the case of series fouling. The descending profile in parallel fouling implies that the rate and temperature profiles exhibit peak values whose loci travel down through the reactor as time proceeds.

van Zoonen (1965) employed the ideal by Froment and Bischoff (1961) and assumed that the rates of coke formation and desired reaction are inversely proportional to coke on catalyst. A set of equations were derived describing the fixed bed hydroisomerization of olefins over a silica-alumina supported nickel sulfided catalyst. The relations have been found for coke on catalyst as a function of time and space; conversion as a function of time; useful catalyst life; and average coke on catalyst as a function of time. The last relation shows that for very long process periods, the equation of average coke-time on stream approaches the so called Voorhies equation (equation (9)). From his experimental data, van Zoonen (1965) found

that the hydroisomerization reaction rates decreased with increasing pellet size and increased with increasing catalyst specific pore volume. The specific surface area was of only secondary importance. van Zoonen (1965) noted that the reason why rates are inversely proportional to the coke content of the catalyst may well be that pore entrances are obstructed by growing coke "plugs" through which the reactants must diffuse.

Froment and his co-workers (Dumez and Froment, 1976; De Pauw and Froment, 1975; Froment, 1976) have extended their earlier work (Froment and Bischoff, 1961) to a more general approach based on Langmuir-Hinshelwood catalytic mechanisms. Their later work uses the data of coke and temperature profiles, and conversion from butene deyhdrogenation and n-pentane isomerization in a fixed bed reactor under various temperatures and pressures to demonstrate the validity of their approach.

Masamune and Smith (1966) mathematically evaluated the activity decay of catalyst pellets for first order, isothermal reactions in the cases of parallel, series and independent fouling. The deactivation function of the catalyst was expressed in terms of coke on catalyst. The governing equations for all three cases were solved numerically. The results of activity profiles show that for parallel and independent fouling, the maximum catalyst activity exists at the center of the pellet, whereas it exists at the pellet surface for the series fouling. The catalyst activity was presented as an effectiveness factor which is a function of both Thiele modulus and time on stream. They concluded that for series and independent deactivation, the catalyst pellet of lowest intraphase resistance yields the highest

activity and the longest life, whereas for a simultaneous (parallel) deactivation, a pellet exhibiting an intermediate level of intraphase resistance gives the highest activity, particularly at longer process time.

Murakami et al. (1968) experimentally confirmed the theoretical developments of Masamune and Smith (1966). The former authors used the disproportionation of toluene as a sample parallel reaction scheme, and dehydrogenation of primary alcohols as a sample series reaction scheme. The results show that at lower temperatures the intraparticle diffusion resistance is relatively small: coke deposition occurs from the inner part of the pellet for the series fouling, while it occurs from the outer part for the parallel fouling. However, at higher temperatures where the diffusional effect is relatively large, deposition occurs from the outer part in both fouling schemes.

Ozawa and Bischoff (1968) applied Masamune and Smith's analysis (1966) to explain the experimental data from catalytic cracking of n-hexadecane over a silica-alumina catalyst. The parallel fouling mechanism was found to be in reasonable agreement with the experimental observations at various temperatures except for the initial period of very rapid activity decline.

Lee and Butt (1973) have expanded Masamune and Smith's work (1966) to analyze more complicated systems. From the analyses which assumed coke deposition as the deactivation parameter, one, and perhaps the most important conclusion is that some degree of diffusional limitation benefits catalyst efficiency and life (Masamune and Smith, 1966; Murakami et al., 1968; Lee and Butt, 1973). Polinski et al. (1981) treated catalyst aging as a modified shrinking core model, which is

able to account for diffusional resistance due to pore clogging. The results indicate that larger diameter catalysts with a greater diffusional resistance tend to reduce the rate of poisoning and thus increase the catalyst life. They also presented experimental data for reactions involving a synthesized coal gasification product with different diameter catalyst pellets to illustrate the validity of their conclusion. Polinski et al. (1981) further used preliminary aging data from a continuous coal liquefaction unit (H-Coal) to test the theory in catalytic coal liquefaction over commercial $CoMo/Al_2O_3$ catalyst extrudates of 0.8 mm and 1.6 mm diameters. The data indicated that although the initial activity of the smaller diameter catalyst was higher, it deactivated much more rapidly than did the larger catalyst. After approximately 50 hours on stream, the activity of the larger diameter catalyst became higher and remained that way throughout the remainder of the test, which lasted approximately 100 hours. The ratio of the activities of the larger to smaller diameter catalyst actually increased continuously with time on stream.

Froment (1980) and Beeckman and Froment (1979, 1980) have developed a statistical method to analyze catalyst deactivation in terms of active site coverage and pore blockage by coke deposition. Their model assumes that there is no diffusional limitation effect on the rate of the main reaction, and that the concentrations of the reactants are uniform inside the pores of the catalyst particle. The active sites inside the catalyst are assumed to have deterministic or stochastic distribution. The relationship between the deactivation function and the coke content was derived for single ended pores. Froment (1980) further noted that the corresponding deactivation functions

are not necessarily identical and they have to be specifically related to the composition of the reacting mixture and the operating conditions. The knowledge of the coke content on the catalyst is an essential piece of information.

Pore Mouth Plugging

The models presented thus far were mainly developed for gas phase reaction-deactivations in which pore mouth reduction caused by coke or metal was not a main consideration. However, in coal liquids and residual oils hydrotreatment, pore mouth reduction along with reactant exclusion could play an important role in catalyst deactivation since heavy oils contain a large quantity of large size, highly condensed compounds which are coke precursors and have difficulty diffusing into pores of the same order of sizes.

Ahmed (1979) has studied the hydrotreatment of a coal derived liquid over commercial $NiMo/Al_2O_3$ and $CoMo/Al_2O_3$ catalysts in a trickle bed reactor. He observed that the most frequent pore sizes of the spent catalysts remained essentially unchanged, whereas the pore volumes and surface areas were severely reduced. He thus proposed an independent pore mouth plugging model based on Wheeler's pore mouth poisoning, and assumed that the rate of poisoned fraction of the pore is linearly proportional to the unpoisoned fraction. This model has successfully explained the experimental results.

Chiou and Olson (1978) have modified the model by Masamune and Smith (1966) to account for pore plugging and geometrical exclusion due to high coke content in aged H-Coal catalyst. The correlation of effective diffusivity made by Satterfield et al. (1973) was incorporated.

The results demonstrate that physical properties of both catalyst and reacting molecules have a decisive effect on the loss of the catalyst life and the nature of coke formation.

Newson (1975) proposed a pore plugging model to describe catalyst deactivation in axial flow trickle bed reactors. Wheeler's pore model, which assumes a Maxwellian or log normal distribution was used in describing catalyst pore size distribution. In hydrotreatment of residual oils, Newson (1975) assumed that the desulfurization reaction takes place in parallel with the demetallization and coking reactions, and that the catalyst pore plugging is due to deposition of reaction products, i.e., mineral and coke. The model has been used to semi-quantitatively describe catalyst deactivation data, in terms of catalyst life, available in the literature. Here the catalyst life was defined as the catalyst-oil contact time at which the catalyst can never give a desirable activity under the most severe allowable operational conditions. With all other conditions kept essentially the same, the following results have been obtained:

1. Decreasing liquid hourly space velocity (LHSV) from 1.0 to 0.5 at 75% sulfur conversion level increases catalyst life from 600 to 3500 hours.

2. Decreasing sulfur conversion level from 75 to 63% at a LHSV of 1.0 increases the catalyst life from 600 to 1500 hours.

3. Increasing total reactor pressure from 5.6 to 10.4 MPa at a LHSV of 0.7 and a sulfur removal level of 75% increases catalyst life from 800 to 1400 hours.

4. With a normal pore size distribution, increasing average catalyst pore diameter from 4.0 to 6.5 nm increases catalyst life

from 700 to 1400 hours.

5. Decreasing catalyst pellet diameter from 0.4 to 0.2 mm increases catalyst life from 500 to 1100 hours.

Note that the last two observations are a contradiction to the prediction that diffusional resistance can increase the catalyst life: Masamune and Smith (1966), Murakami et al. (1968), Lee and Butt (1973), and Polinski et al. (1981).

Hughes and Mann (1978) have proposed a theory of fouling to predict catalyst activity loss while accounting for changes in catalyst porous structure. They assumed the catalyst porous structure to consist of a set of idealized, parallel, non-intersecting pores of variable radius but each of a certain length. The foulant has been speculated to accumulate within the pores by simultaneous penetration and thickening. The volume of foulant is expressed in terms of pore volume, specific surface area and pore size distribution. In the case of pore mouth plugging, the rate of catalyst activity loss is predicted to be rapid during the initial period, but approach an asymptotic value with increased foulant content. Hughes and Mann (1978) studied the hydrodesulfurization of thiophene using $CoMo/Al_2O_3$ catalysts which were aged to various coke levels. Analyses of the resulting hydrodesulfurization data revealed that the pore diffusional effect is negligible and the catalyst activity loss is mainly due to pore mouth plugging. The decrease in catalyst activity was observed to be related to the amount of coke deposited, as predicted by their model (Hughes and Mann, 1978).

Dautzenberg et al. (1978) proposed a model to interpret the activity loss during hydrodesulfurization of residual oils having a

high metal content. They analyzed the hydrodesulfurization data to predict the effect of inorganic deposits on the activity of an equilibrium-coked catalyst. They reported heavy coke deposition on the catalyst surface during the initial periods. With increased oil-catalyst contact time, the coke content approached a more or less constant level. They hydrodesulfurization as well as demetallization reactions were observed to be pore diffusion limited. In the activity decay model, the pore radius is related to the vanadium content on the catalyst surface. The fractional activity remaining was observed to be independent of pressure, temperature and space time but does depend on the relative catalyst age. Note that in their modeling, Dautzenberg et al. (1978) assumed pore plugging to be due to inorganic depositions only. This assumption can be valid only for equilibrium-coked catalysts in which the inorganic deposit is the dominant decay mechanism. Alternately, their model may be applied to the initial period where coking is the dominant decaying mechanism.

Literature Summary

This literature review above can be summarized as follows:

1. The properties of coal derived liquids depend on the parent coal, production method and process variables. In general, coal liquids are hydrogen deficient, high molecular weight hydrocarbons containing significant concentrations of highly condensed aromatic and heterocyclic compounds. The heteroatoms exist in the high boiling fraction and are associated with condensed aromatic rings. This makes the heteroatoms removal difficult. Molecular sizes of coal liquid

are large (1-5 nm) and are difficult to diffuse into small catalyst pores (5-20 nm) for reactions. The coal liquids are also unstable during storage under an oxygen atmosphere.

2. Hydrogenation of condensed aromatic compounds proceeds preferentially with saturation of end benzene rings. Hydrocracking of the benzene does not occur until the ring is saturated at typical hydrotreating conditions. The kinetics of both overall hydrogenation and individual steps can be represented by first order reactions.

3. Hydrodenitrogenation proceeds via saturation of the heterocyclic ring, followed by ring fracture and subsequent removal of the nitrogen as ammonia. The more condensed the heterocyclic aromatics are, the more hydrogen is required to remove a nitrogen atom. Most of the studies indicate that hydrodenitrogenation is first order with respect to the concentration of the nitrogen species.

4. Basic nitrogen compounds can adsorb on the acidic active sites and greatly reduce the catalyst hydrotreating activity. Hydrogen sulfide can promote the hydrotreating activity. Hydrogen sulfide can promote the hydrodenitrogenation activity and selectivity, it can also help prevent coke formation on the catalyst and maintain activity.

5. Increasing hydrogen pressure can significantly increase hydrogenation and heteroatom removal rates. High hydrogen pressure can also help by suppressing coke formation. These effects become less significant at higher pressure.

6. Although second order power law can represent hydrotreating kinetics better than the first order, the latter one has been reported to be satisfactory and have been frequently used.

7. Although other reactor configurations are common, hydrotreatment studies are generally conducted in trickle bed reactors. The hydrodynamics of the reactor can play an important role in affecting data. Low liquid flow rate in laboratory trickle bed reactors may cause incomplete wetting, low liquid holdup and thus non-ideality. Several models have been proposed to interpret the deviation from ideal plug flow reactor.

8. Presulfided $CoMo/Al_2O_3$ and $NiMo/Al_2O_3$ are the most commonly used and the most effective catalysts in coal liquid upgrading. The latter catalyst is more effective for nitrogen removal. The support properties appear to have more of an effect on hydrotreating than does the amount and type of active metal on the catalyst. Pore size is an especially important characteristic in determining catalyst activity and life in heavy coal liquids hydrotreatment.

9. Deactivation of hydrotreating catalysts can be due to poison adsorption, sintering, and metal and coke deposits. Among these, coke deposition is the primary deactivation mechanism and is a major concern since it can cover active sites and plug pore mouths rapidly during coal oils hydrotreatment.

10. Coke on hydrotreating catalysts is mainly amorphous, highly condensed and hydrogen deficient carbonaceous material which does not dissolve in oil at hydrotreating conditions. Coke forms via adsorption, condensation and polymerization of feedstock, intermediates and products.

11. Aromatic compounds, especially polar aromatics and the aromatic rings bridged by one or more methylene groups have stronger adsorption tendency, higher cracking and condensation reactivities,

and thus tend to form more coke than do the other compounds.

12. The rate and amount of coke formation depend on the catalyst properties and operating conditions as well as the liquid properties. Initial rate of coke formation can often be described by half order power law relationships. Coke depositions quickly level off after the initial period of rapid formation. Both increasing hydrogen pressure and presulfiding the catalyst can help suppress coke formation.

13. Coke deposits can deactivate the catalyst in two ways: by covering the active sites and blocking the pore mouths.

14. Coke on catalyst can be multilayered and deposits mainly on the outer shell of the catalyst pellet, thus severely restricting pore diffusion.

15. Depending on the relative contribution of the feedstock, intermediates and products, the coke deactivation mechanisms in coal liquids hydrotreatment can be described by parallel, series and independent fouling.

16. The power law reaction-deactivation function can generally adequately describe a number of deactivation-time on stream observations such as exponential, hyperbolic and power law decay. In the presence of diffusional restrictions, the observed order of deactivation varies with the decay mechanism and the Thiele modulus.

17. When coke is used as the deactivation parameter, coke profiles versus time and space can also be predicted. These coke profiles are important information in understanding coke deactivation mechanisms.

18. The incorporation of pore mouth plugging in modeling coking deactivation during coal liquids hydrotreatment is necessary, since coke mainly deposits at the outer shell of the catalyst pellet and

the sizes of coal liquid molecules are significant to catalyst pore sizes.

19. Both experimental data and theoretical predictions show that pore diffusional resistance could have beneficial or have detrimental effect on the catalyst life. Whether the diffusional resistance is beneficial or detrimental to the catalyst life under coking deactivation environment solely depends on the system studied, i.e., oil, catalyst and process conditions, and can only be determined experimentally.

CHAPTER III

EXPERIMENTAL EQUIPMENT

The objectives of this study are to assess the activity and activity decay of a $NiMo/Al_2O_3$ catalyst for hydrotreating coal-derived liquids in a trickle bed reactor. In order to accomplish this, an experimental system has been designed to meet the following requirements:

1. The system should be able to hydrotreat coal liquids having different physical and chemical properties. These liquids may be very viscous at room temperature, and contain ash.

2. The reactor heating system should be able to provide flat axial temperature profiles of up to 482 C (900 F) along the catalyst bed.

3. The system should be capable of operating at constant pressures up to 25 MPa (3500 psig).

4. Sampling should be possible without disturbing normal operation.

5. The reactor and other parts in the system should be easily replaceable.

6. The system should be capable of operating on a 24-hour continuous basis. Pressure, temperature and flow controls should be automatic during normal operations. The experimental system should

also include data logging instruments for continuous recording of the process variables.

7. An automatic safety system consisting of detectors for combustible gases, fire and smoke, sudden pressure losses and over pressurization with rupture release lines and provision for safe shut down should be incorporated in the overall experimental set up.

In order to achieve these requirements, and hence the objectives, an experimental system, henceforth referred to as Catalyst Life Test Unit (CLTU), consisting of three trickle bed reactors in parallel has been designed and constructed by Ahmed (1979). Considering the hazards involved in handling hydrogen and coal-derived liquids under severe hydrotreating conditions of high temperatures and pressures, the CLTU is housed in a high pressure cell in the Oklahoma State University Hazardous Reaction Laboratory. In this laboratory all the recording instruments and controllers are located in a control room inside the main building. The reactors with associated heating (temperature control) and pressure control accessories, oil feed pump, high pressure fluid flow lines, scrubber for vent gases, and etc. are located in a high pressure test cell outside the building. Three sides of this cell have common walls made up of stainless steel with the main building. The fourth side of the cell (west wall) is a blow out wall containing only an exhaust fan and opens toward a hillock.

Several modifications have been made to meet the specific requirements in this study. These modifications include pressurized feed and separation systems. An overall flow scheme of the CLTU used is shown in Figure 8. The feed oil is transferred to the feed tanks by gravity

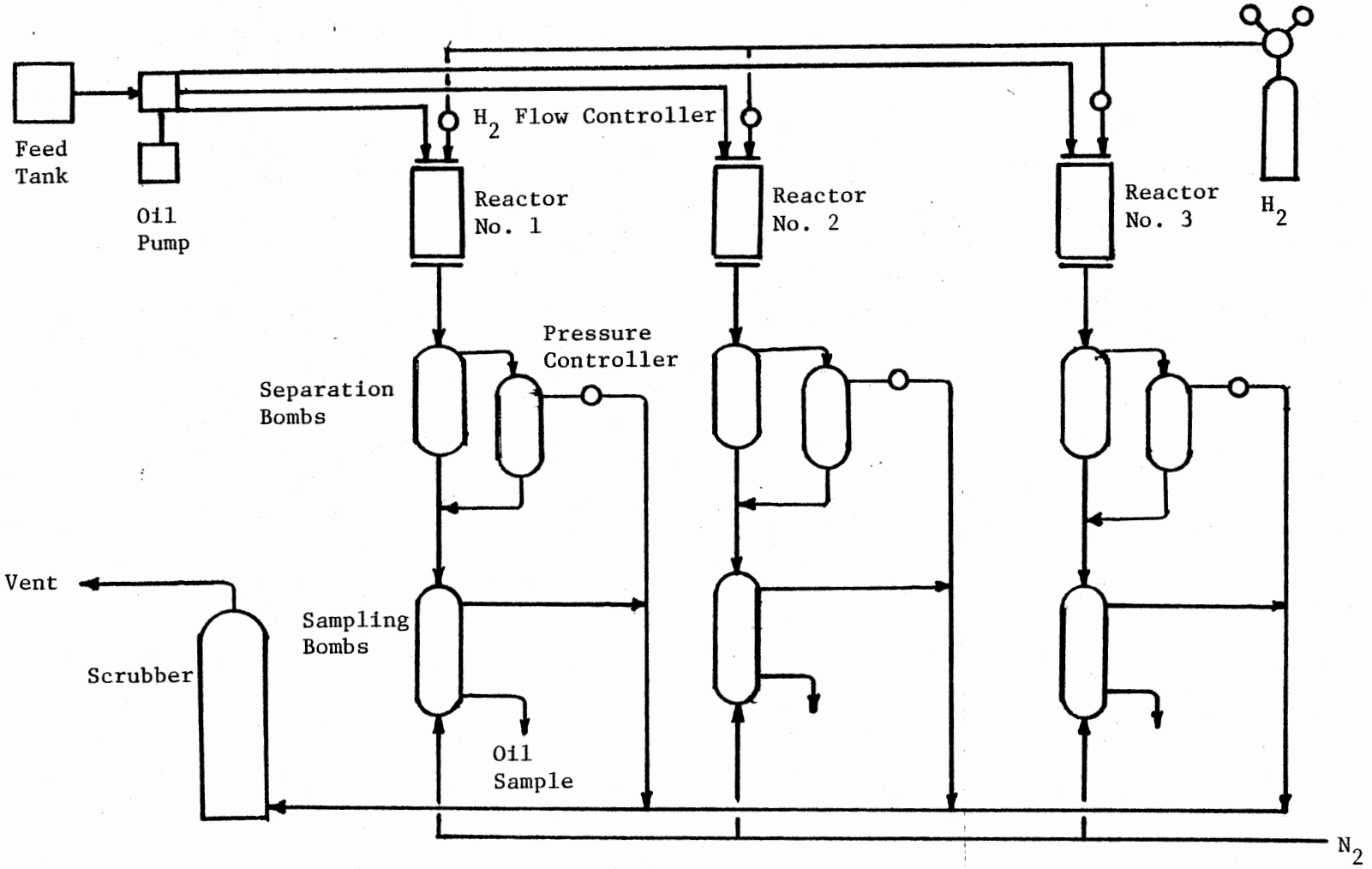

Figure 8. Schematic of the Catalyst Life Test Unit (CLTU)

from a storage tank, and then pumped to the reactors by a triple head plunger type metering pump capable of supplying oil to the three separate reactor units. Hydrogen on a once through basis meets the feed oil at top of the reactor and flows cocurrently down to the catalyst bed. Gas-liquid separation tanks and product oil sample bombs then follow the reactor. The effluent gases are scrubbed with a caustic solution before venting.

Details of the individual reactors are shown in Figure 9. The oil is fed at a preset rate and the hydrogen flow is controlled using a well calibrated micro-metering valve. The desired flat temperature profile in the reactor is maintained by encasing the tubular reactor within a massive copper cylinder wrapped with five electrical heating bands. The three central heaters are connected to an automatic temperature controller, while the top and the bottom heaters are manually regulated using variacs to counteract end heat losses. Separation of the reactor effluent into its gaseous and liquid components is accomplished in two consecutive separation tanks. Pressure control is accomplished through pneumatically operated air to open control valves located downstream of the separation tanks. The effluent gases from the separation tanks are scrubbed with 20 wt% caustic solution before venting. Product oil samples are collected at regular time intervals.

A list of the major equipments in the hydrotreatment system is given in Appendix A. For the sake of convenience the CLTU can be considered to consist of subsystems for oil feed, hydrogen feed, reactor, and product oils separation and pressure control. All these functions are under the supervision of a safety system. In the following sections, only important facts of the experimental equipment will be presented.

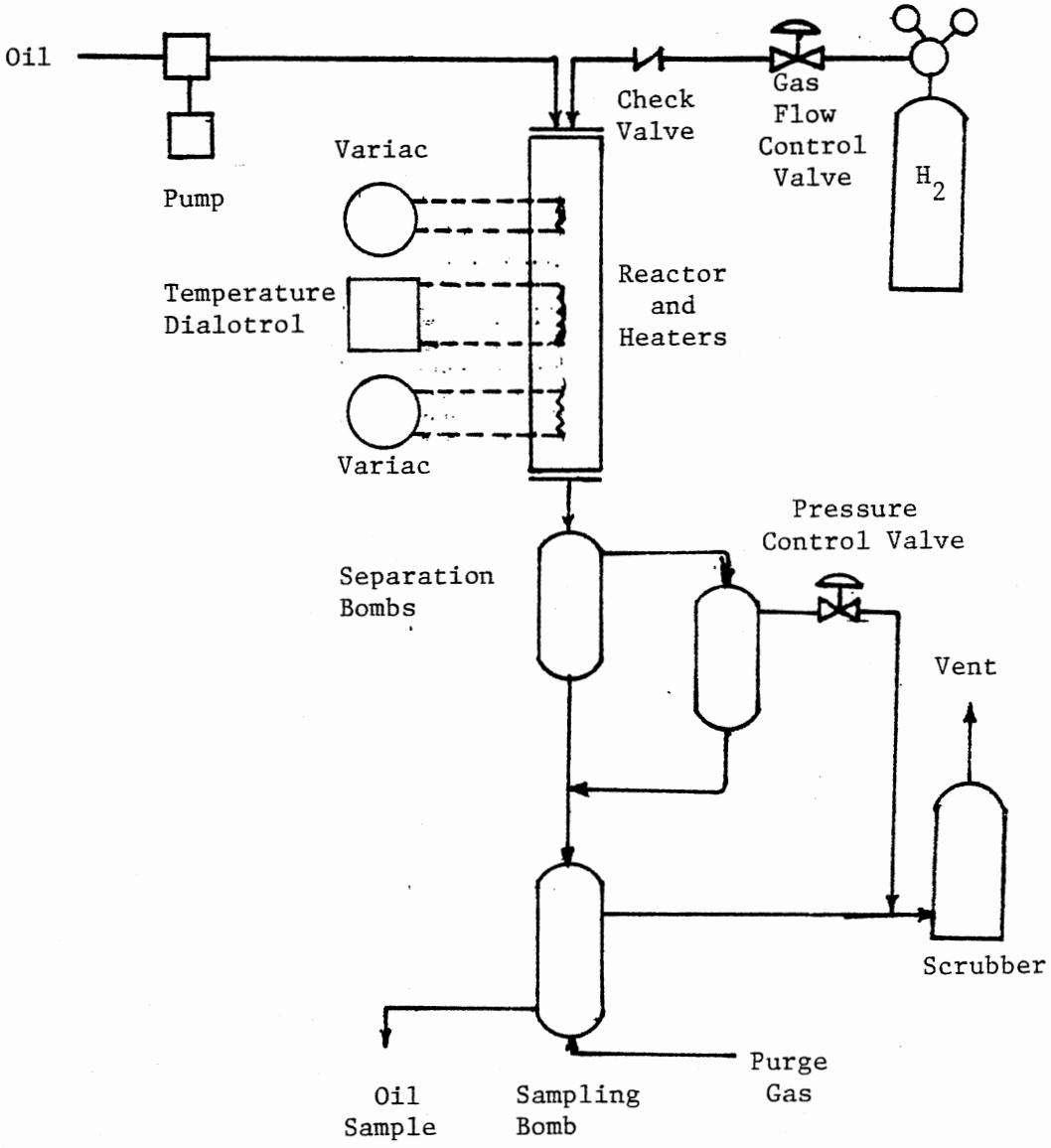

Figure 9. Individual Hydrotreating System

Equipment details are given in Appendix B.

Oil Feed System

As shown in Figure 10, oil is fed to the reactor by a Lewa metering pump at a preset rate. The pump consists of three plunger type heads totally independent of each other. These pump heads supply oil to the three reactors in parallel in the CLTU. The purpose of the high pressure feed tanks is to enhance the suction pressure for the pump heads and thus to leave the major pump duty to accurately control the liquid feed rate.

Pressure switch in the feed line is to activate the alarm, in case of overpressure, resulting in shut off of main power supply to the system and hence in shutdown of the system. The rupture disc is designed to blow out and thus to release the pressure in case of the pressure switch malfunctioning.

Hydrogen Feed System

In order to reduce the cost and prevent the possible delay associated with shipping of the high pressure hydrogen cylinders, a hydrogen pressure boost system has been designed and constructed. As shown in Figure 11, an air driven compressor is installed to boost the hydrogen from lower pressure to higher pressure cylinders. This boost system is independent of the hydrotreatment system, therefore can be operated any time to charge high pressure cylinders.

Hydrogen is fed to the reactor directly from high pressure cylinders. A manifold is constructed to allow switching of the hydrogen cylinders during the run as shown in Figure 12.

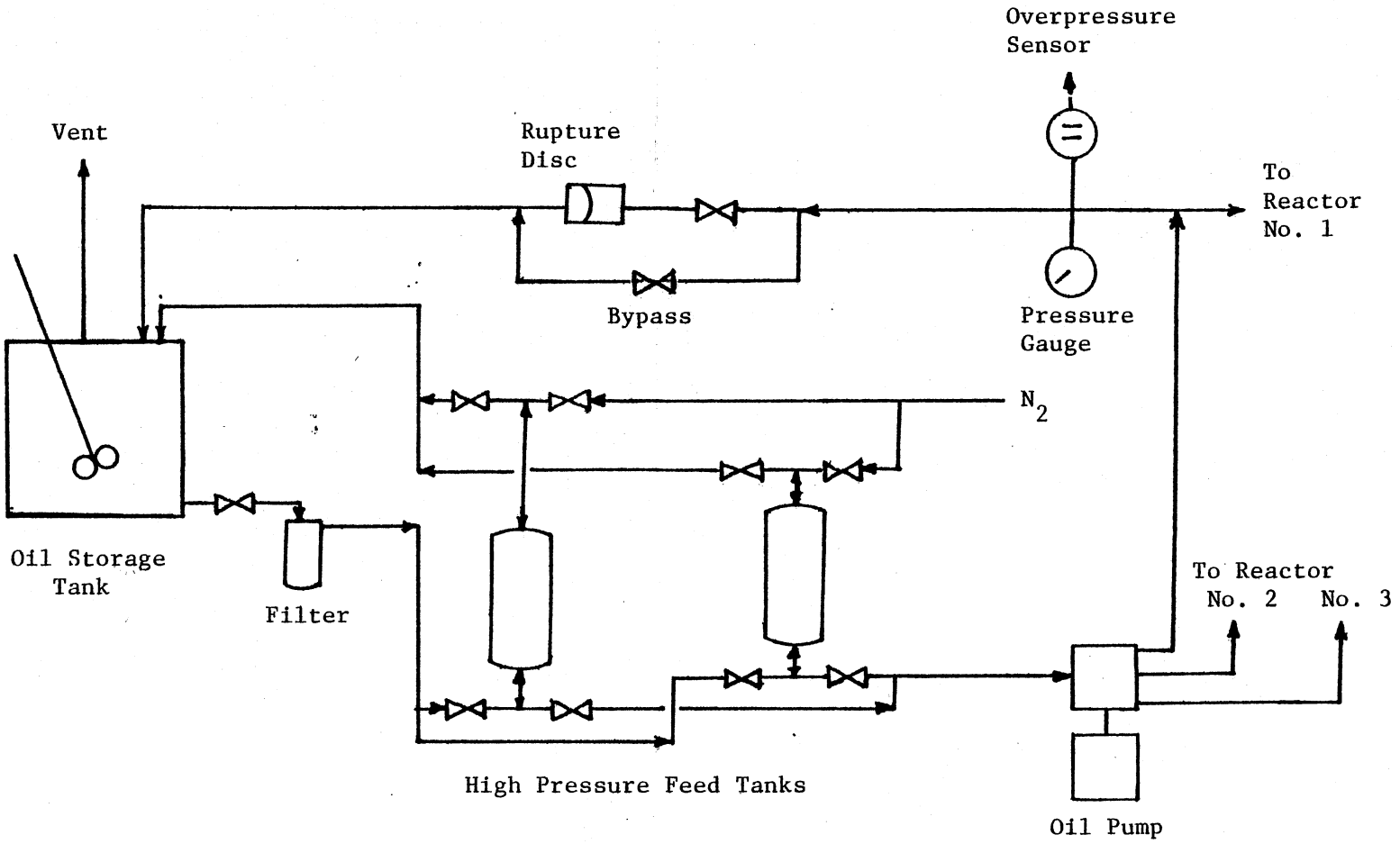

Figure 10. Oil Feed System

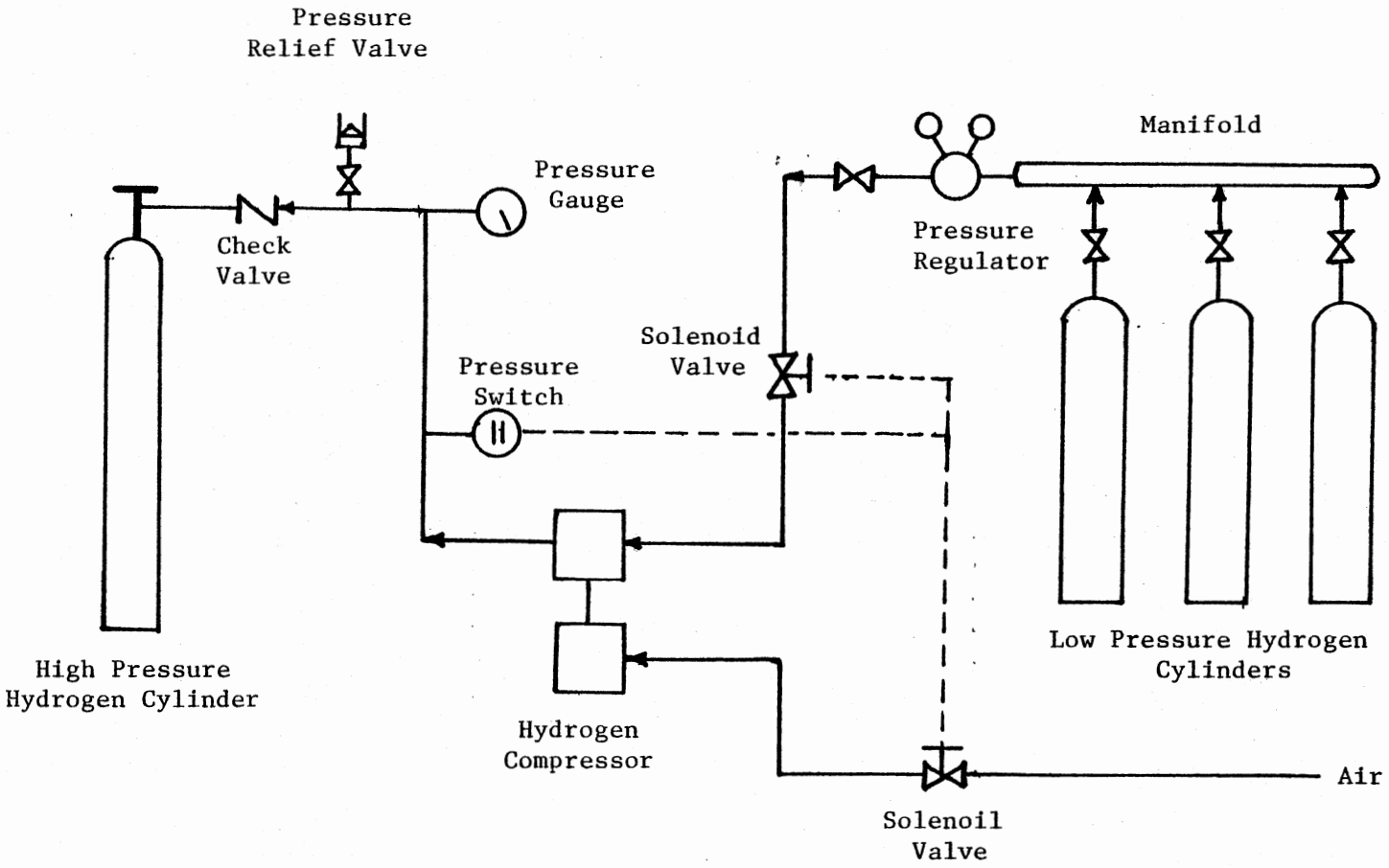

Figure 11. Hydrogen Pressure Boost System

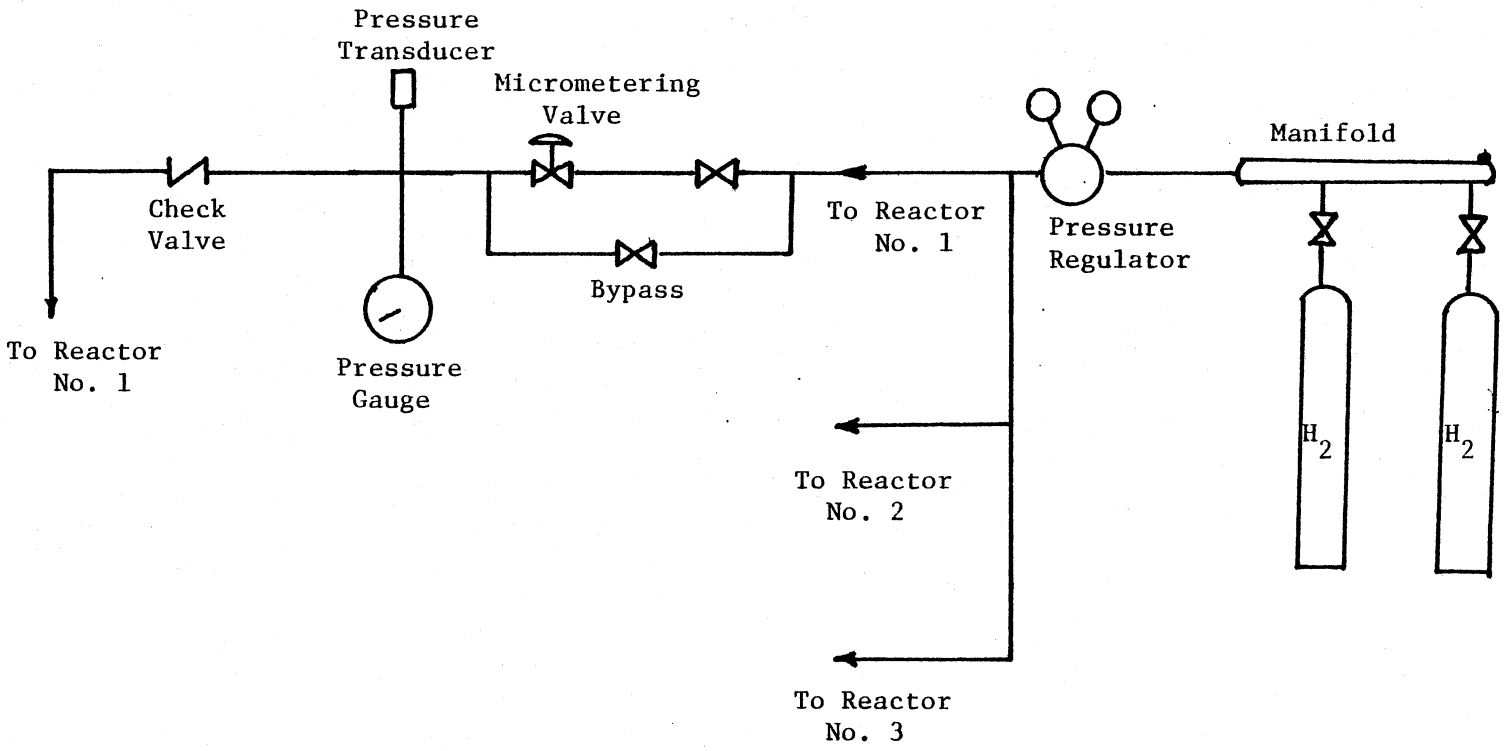

Figure 12. Hydrogen Feed System

Reactor System

The reactor system consists of three trickle bed reactors in parallel and a number of corresponding temperature controllers. Each reactor is a 0.868 m (34 inches) long, 13.08 mm (0.515 inch) I.D., 316 stainless steel tubing. An annular copper cylinder snugly fitting the reactor is wrapped with electrical heating bands to obtain a flat axial temperature profile along the reactor. The temperature in the middle of the reactor outer wall is used for control purposes and is supplied to a Honeywell three mode temperature controller. A thermocouple is installed at the center of the reactor to monitor the catalyst bed temperature. Except the one to the temperature controller, all other thermocouples are connected to a Doric temperature read-out as well as to a twenty-four point Honeywell strip chart recorder.

Separation and Pressure Control System

Gas-Liquid Separation

As shown in Figure 13, two-phase products from the reactor are separated in two consecutive separation bombs. Two separation bombs are necessary to provide proper separation and to avoid heavy product plugging the tubing carrying these two-phase products. Gases are released through a pneumatic pressure control valve. The released gases are scrubbed with a 20 wt% caustic solution before venting to the atmosphere. A water displacement type of wet test meter is installed in the gas line to the scrubber exit for measuring effluent gas flow rate.

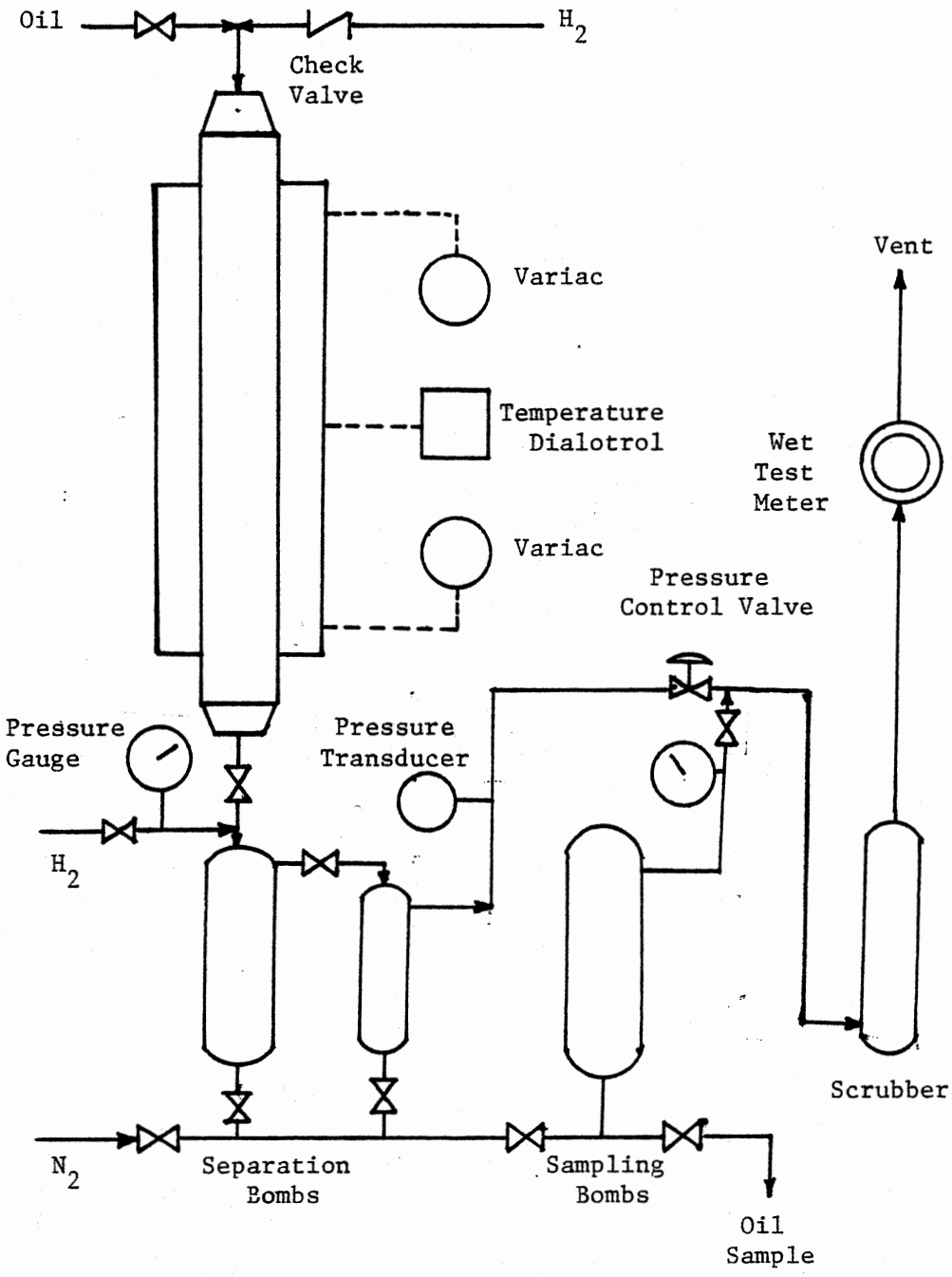

Figure 13. Reactor, Separation and Pressure Control System

Pressure Control

The reactor pressure is controlled by a penumatically operated air to open control valve located downstream of the second separation bomb. This pressure control valve has a specially designed p-14 tapered trim to handle high pressure drop and low hydrogen flow. This control valve is in turn controlled by a Dialotrol which accepts an input signal from a BLH pressure transducer located upstream or downstream of the reactor. If receives signal from upstream, the pressure controller can automatically release reactor downstream pressure and purge the reactor with hydrogen in case of partial plugging occurring within the reactor.

Safety System

The safety system is designed to detect following hazardous conditions: hydrogen leak, fire and smoke, overpressure in oil lines, low pressure in the gas line, and low liquid level in the feed tank. The first three are considered as alarm conditions, while the last two are considered as warning conditions. When alarm conditions occur, power supply to the system is shut off and the operators are informed by an automatic telephone dialer. If only warning conditions occur, the operators are informed while the system is still operating.

CHAPTER IV

EXPERIMENTAL PROCEDURE

The experimental procedure in this study consists of catalyst calcining and loading, catalyst presulfiding, startup, sampling, shut-down, product oil and catalyst sample analyses. In this chapter, basic principles of this procedure will be described and the properties of oils and catalyst used in this study will also be presented. More details of this experimental procedure are given in Appendix C; and gases and chemicals used in this study are listed in Appendix D.

Catalyst Calcining and Loading

Commercial $NiMo/Al_2O_3$ catalysts were calcined in a muffle furnace in air at 480$\pm$ 10 C (900 $\pm$ 18 F) for one hour before loading into the reactor. This procedure has been designed to remove moisture adsorbed on the catalyst surface.

The calcined catalyst was packed into the middle 0.5 m (20 inches) of the 0.86 m (34 inches) long reactor. The bottom of the reactor was left empty and the top was packed with glass beads to serve as a pre-heating and distribution zone. The reactor was then installed in place and the hydrotreatment system was pressure tested with hydrogen to assure that the system was free from potentially hazardous leaks.

Catalyst Presulfiding

After the hydrotreatment system was ready, the catalyst was presulfided with a mixture of 5 vol% H_2S and 95 vol% H_2. The sulfiding temperature was started at 204 C (400 F) and was stepwisely increased to 370 C (700 F). Large excess of H_2S has been charged into the catalyst bed during 5 hours of presulfiding.

This calcining and presulfiding procedure was suggested by catalyst manufacturers, Shell Chemical Company (1980) and Armak Company (1976). These companies have studied hydrodesulfurization of vacuum gas oils over $NiMo/Al_2O_3$ catalysts and reported that this activation procedure has given the best overall performance of the catalysts.

Startup Procedure

The reactor was pressurized to the operating pressure, then the oil flow was started when the reactor temperature was at 56 C (100 F) below the normal operating value. Special care was taken to avoid hot hydrogen flushing and damaging the presulfided catalyst during startup and before the contact of oil and catalyst. The reactor temperature was then gradually increased to the desired value after the catalyst bed was filled with oil. This lower than normal operating temperature startup was to minimize hot spot developing during the initial stage when the catalyst was undesirably active. The hot spot can result in uncontrollable reactions and excessive coke formation.

Sampling Procedure

Product oil samples were taken from the sampling bomb in a regular time period. Before collections, the liquid samples were purged with nitrogen to remove dissolved hydrogen sulfide and ammonia. Care has been taken to minimize disturbing the normal operation.

Shutdown Procedure

During shutdown the oil feed was cut off and the reactor heaters were shut off. Reactor pressure was maintained at the normal operating value and the hydrogen flow rate was increased to quench the reactor until ambient temperature was reached. The reactor was then disengaged from the system and the used catalysts were separated into five sections and taken out for analyses.

Product Oil Analyses

Product oil samples were routinely characterized, in terms of hydrogen and nitrogen contents, with a Perkin-Elmer Model 240B elemental analyzer. The Perkin-Elmer instruction manual describes details of the equipment and the analysis procedure.

This analyzer is designed to determine nitrogen, carbon and hydrogen contents in one oil sample, and consists of a combustion-reduction train and a scrubber-detector system as shown in Figure 14. The weighed oil sample in the combustion tube combusts over magnesium oxide and silver tungstate catalysts in an oxygen atmosphere. The sulfur oxides, halogens and ash so produced are removed by the packing in the combustion tube, and the resulting gases are carried to the reduc-

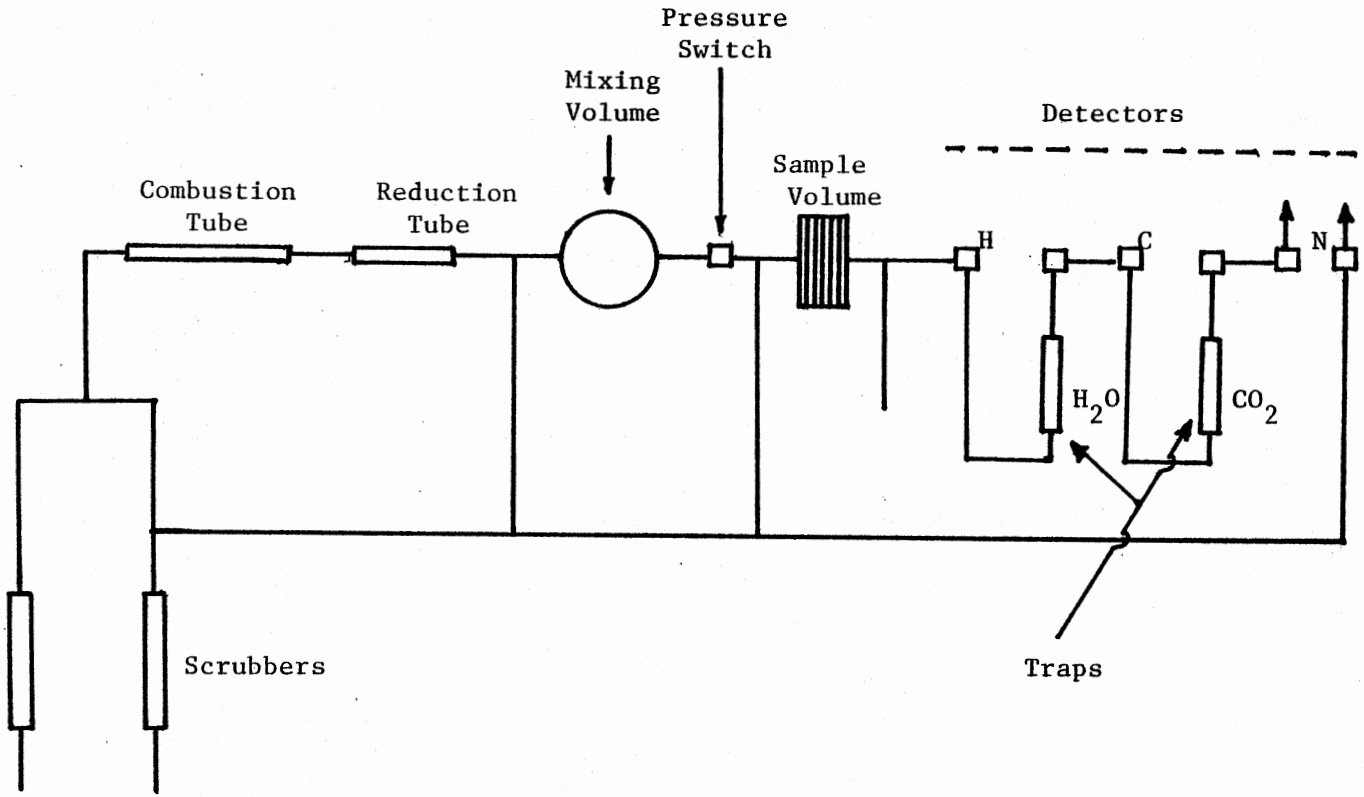

Figure 14. Schematic Diagram of the Elemental Analyzer

tion tube where the nitrogen oxides are reduced to molecular nitrogen by the cuprin packing. Gases coming out of the reduction tube contain H_2O, CO_2, N_2 and the carrier gas, Helium. These gases collect and mix in a mixing volume. After equilibrium the sample mixture is allowed to sweep through an elongated sample volume and then through a series of scrubbers and thermal conductivity cells. In the first cell the sample mixture passes through a trap (Figure 14) containing magnesium perchlorate for dehydration. The difference in thermal conductivities of the sample before and after the trap gives the concentration of water and hence the hydrogen concentration in the sample. The gases are then allowed to pass through a CO_2 trap and a thermal conductivity difference gives the carbon content in the sample. The remaining gases containing nitrogen and helium then flow through a conductivity cell, the output of which is compared with that from another cell through which only pure helium is flowing. The difference in thermal conductivities gives the nitrogen content in the sample.

Catalyst Characterizations

The spent catalysts from each experimental run were separated into five sections. Catalyst from each section was characterized individually. These catalysts were extensively extracted with pyridine using Soxhlet apparatus to remove soluble material. The 0.15 liter of solvent generally became clear after 24 hours of extraction; otherwise a new batch of solvent was used. The catalysts were then dried at 121 C (250 F) under vacuum for overnight.

The washed and dried catalysts were characterized in terms of coke content, surface area, pore volume, pore size distribution, and elemental profiles in a single catalyst pellet.

Coke Content

Coke contents of spent catalysts were determined by the loss of combustion in a muffle furnace. The catalyst samples can adsorb a significant amount of moisture on their surface; this moisture can badly mask the values of true coke content. The disturbance of the adsorbed moisture was avoided by drying the sample in a vacuum oven and sealing in a helium atmosphere before each weighing. Thus, the coke content in this study is defined as pyridine insolube and moisture free combustible carbonaceous material.

Surface Area

The surface areas of fresh and spent catalyst samples were determined using a micromeritics Model 2100D ORR Surface Area - Pore Volume analyzer. This analyzer is designed to obtain nitrogen adsorption isotherms at liquid nitrogen temperature, and thus, to obtain the B.E.T. plots. In the adsorption/equilibrium pressure ratio range of 0.05 - 0.30, the B.E.T. plot is linear and can be used to determine the surface area.

As shown in Figure 15, the instrument is capable of degassing four samples at a time. This degassing was necessary to remove the adsorbed gases and was achieved by evacuating the sample at 300 C for overnight under high vacuum. Helium, an inert gas, was used to measure the dead space in the sample flask. The amount of nitrogen adsorbed by the

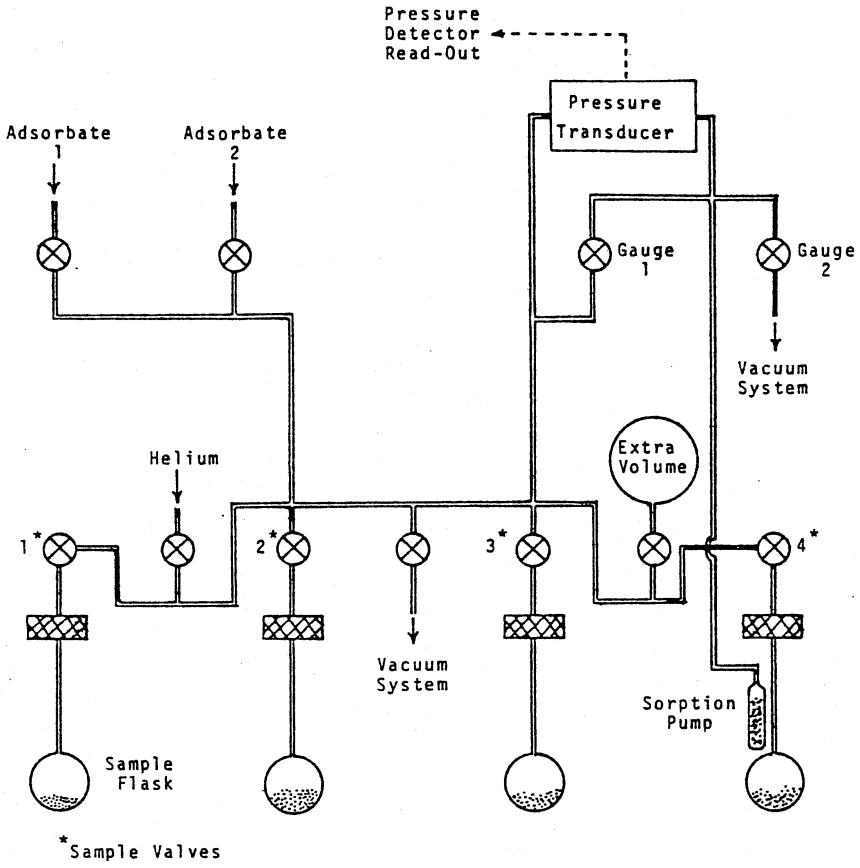

Figure 15. Schematic Diagram of the Surface Area Analyzer

catalyst was measured from the pressure decrease due to adsorption, and was used to calculate the surface area according to the B.E.T. plot.

Pore Size Distribution and Pore Volume

A Micromeritics Model 900/910 Series mercury penetration porosimeter was used to determine catalyst pore size distribution and pore volume in this study. A general schematic of the instrument is shown in Figure 16.

In this analysis, the mercury was forced into catalyst pores by pressure and the volume of mercury penetrated into pores was measured from the distance the movable probe travelled. Pore sizes and their distribution were calculated according to the following relationships.

$$PD = 4\ \sigma\ \cos\theta/p$$

and

$$D(PD) = \frac{d(V)}{d(\ln\ PD)}$$

where

PD = pore diameter

σ = surface tension of mercury

θ = contact angle, equal to 130° in this study

p = applied pressure

D(PD) = pore size distribution

V = cumulative pore volume

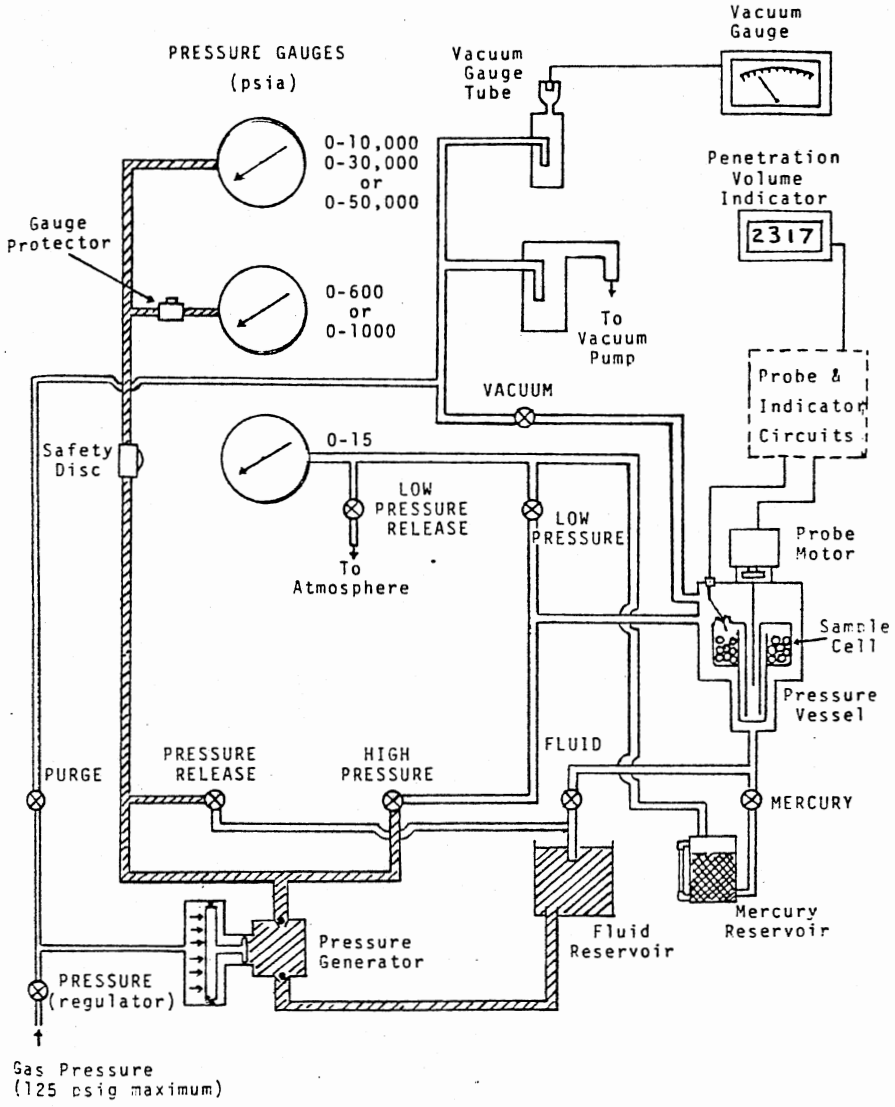

Figure 16. Schematic Diagram of the Mercury Penetration Porosimetry

Elemental Profiles in Catalyst Pellets

Scanning Auger Microscopic analyses for elemental profiles in the catalyst pellets were performed in a commercial laboratory, SCR Laboratory located in Houston, Texas. The scanning Auger microscopic analyses employed an energy source of 4 KeV and 1 μa, and could scan over the range of 0-2000 eV. Severe charging effect was encountered with the catalysts having high carbon contents (10-20 wt%). This charging effect can shift the output signal and may make the analysis impossible.

Properties of Fresh Catalyst and Feedstocks

Fresh Catalyst

The commercial Shell 324 $NiMo/Al_2O_3$ catalyst has been used because it is one of the most active commercial catalysts for coal oils hydrotreatment ever been reported (Berg, 1980; Bowman et al., 1980; Potts et al., 1978). Properties of this catalyst are given in Table II. This catalyst has a relatively high MoO_3 content of 19.3 wt%, a NiO content of 3.4 wt% and a Mo/Ni atomic ratio of 3. This high molybdenium content can result in both high activity and activity maintenance in coal oils hydrotreatment, as discussed in Chapter II.

The cumulative pore volume for the catalyst is plotted as a function of mercury penetration pressure up to 345 MPa (50,000 psig) in Figure 17. The pore size distribution is plotted in Figure 18 as a function of pore diameter. Clearly that the catalyst has well defined micropores with a most frequent pore diameter centering at 11.8 nm (118 Å) and most of the pore volume laying in the pore size

TABLE II

CATALYST PROPERTIES

Catalyst Code	Shell 324
Chemical Composition, wt%	
NiO	3.4 (3.4)*
MoO_3	19.3 (19.8)
Physical Properties	
Geometry	1.6mm (1/16") extrudate
Reactor density, kg/m^3	0.790×10^3
Surface area, m^2/kg	146×10^3 (150×10^3)
Pore volume, m^3/kg	0.43×10^{-3} (0.48×10^{-3})
Most frequent	
Pore diameter, nm	11.8 (118 Å)
Pore size distribution,** % pore volume in pore diameter, nm	%
3.5-7.0	12
7.0-10.0	21
10.0-15.0	57
15.0-20.0	2
20.0-40.0	1
40.0-60.0	1
>60.0	6
Total	100

* Values in the parentheses are vendor's data.

** See Figures 17 and 18 for more details.

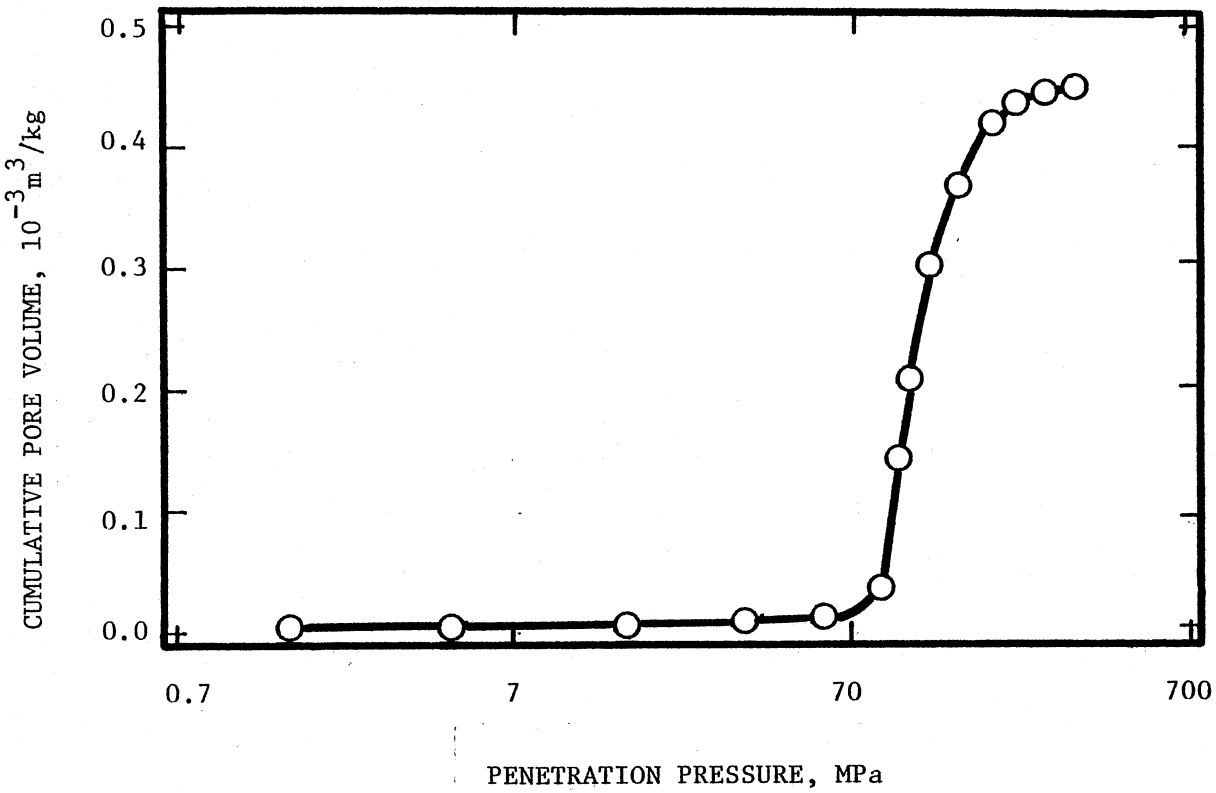

Figure 17. Cumulative Pore Volume for Fresh Shell 324 Catalyst

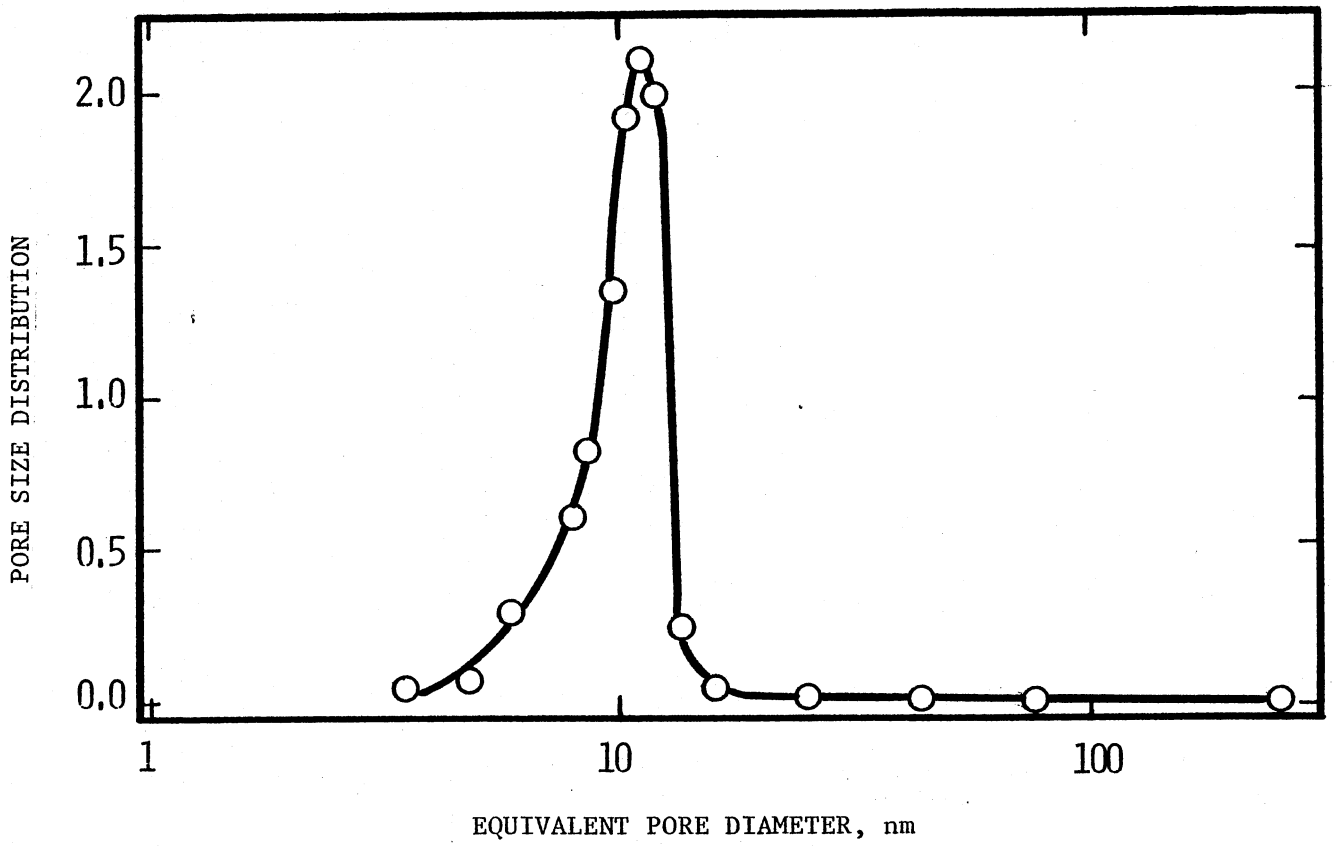

Figure 18. Pore Size Distribution for Fresh Shell 324 Catalyst

range of 7.0 to 15.0 nm. As mentioned, this median micropore size catalyst has been observed to give the best performance in coal liquids and petroleum residuum hydrotreatment.

Feedstocks

Two coal oil feedstocks have been used: EDS process oil and SRC process oil. The EDS oil is a mixture of 40 wt% vacuum gas oil and 60 wt% raw solvent, both derived from the EDS coal liquefaction process. The SRC oil is a mixture of 30 wt% SRC-I and 70 wt% SRC-I process solvent. The properties of these feedstocks are given in Table III. Although not shown in the table, the biggest difference between the two feedstocks is that the vacuum gas oil has a boiling point range of 371-538 C (700-1000 F) while SRC-I is a residue having boiling points higher than 454 C (850 F) without an end point. From Table III, one can see that the EDS oil has higher hydrogen and sulfur contents and lower nitrogen content than the SRC oil. The table also reveals that both oils are hydrogen deficient, low in ash and that the heteroatoms are more concentrated in higher boiling fractions. The low ash content is required in this study since the main objective is to investigate coking deactivation mechanism without the disturbance of metal deposition.

TABLE III

PROPERTIES OF FEEDSTOCK

Feedstock	SRC[a]		EDS[b]	
Total liquid density @ 20 C, kg/m^3	1129		1050	
Normal boiling point[c],	C	F	C	F
IBP	242	(468)	216	(411)
5 vol.%	258	(497)	224	(435)
10	273	(523)	231	(448)
20	288	(550)	245	(473)
30	303	(578)	283	(541)
40	322	(612)	321	(610)
50	344	(652)	388	(731)
60	382	(719)	451	(843)
70	439	(823)	-	-
End point	454	(850)	454	(850)
Recovery, wt%	67		56	
Residue, wt%	32		43	
Loss, wt%	1		1	
Elemental composition, wt%				
Total liquid				
C	87.25		88.21	
H	6.73		7.66	
N	1.40		0.72	
S	0.50		0.70	
H/C atom	0.93		1.04	
Ash	0.097		0.086	
454 C^+ (850 F^+)				
C	87.91		85.89	
H	5.41		6.63	
N	2.27		1.40	
S	0.65		1.29	
H/C atom	0.74		0.93	
454 C^- (850 F^-)				
C	87.92		89.16	
H	7.51		8.85	
N	0.88		0.36	
S	0.31		0.12	
H/C atom	1.03		1.19	

a. A mixture of 30 wt% SRC-I in 70 wt% process solvent.
b. A mixture of 40 wt% EDS vacuum gas oil in 60 wt% EDS raw solvent.
c. Determined from ASTM D1160 at 2.67kPa (20 mm Hg) vacuum.

CHAPTER V

EXPERIMENTAL RESULTS

The experiments were designed to study coking deactivation during hydrotreatment of coal-derived liquids. In order to investigate this catalyst decay mechanism within a reasonable run duration, a suitable combination of catalyst and feedstocks were chosen. The properties of these catalyst and feedstocks were given in Chapter IV. In the following sections, experimental results including experimental runs, oil analyses and catalyst characterizations will be presented.

Experimental Runs

All experimental runs in this study were conducted in a trickle bed reactor, CLTU no. 2 reactor under essentially the same nominal operation conditions. These operation conditions along with the run durations and shut down conditions are presented in Table IV. Note that the liquid volume hourly space time (LVHST) is defined as the volume of the catalyst used divided by the hourly volumetric flow rate of the feedstock.

EDS Oil Feedstock

Experimental run series LTB with the EDS oil feedstock has been designed to generate results for use as a reference to determine the durations of the succeeding runs used to investigate short-term catalyst

TABLE IV

EXPERIMENTAL RUN CONDITIONS

Reactor	CLTU II
Catalyst	Shell 324 (Table II)
Temperature	400 C (750 F)
Pressure	13.9 MPa (2000 psig)
Hydrogen Flow	1781 Std. m^3 H_2/m^3 Oil (10,000 SCF/bbl)

Run Series	Feedstock[1]	LVHST	Hours on Oil	Remark
LTY	SRC	1.88	153	
LTV	SRC	2.16-2.43	97	
LTW	SRC	2.93	30	
LTG	SRC	2.50	19	Plugged[2]
LTX	SRC	2.50	6	
LTZ	SRC	2.50	1	
LTB	EDS	2.26	261	

(1) See Table III.
(2) Shut down due to plugging.

decaying mechanisms. Run LTB was shut down on schedule at 261 hours on stream. The operation of this run was essentially continuous, except that the gas and oil flows were cut for one hour at 152 hours on stream to clean out a white crystal material which plugged the gas line right before the pressure control valve. The crystal material has been found to melt, become yellowish and have very strong ammonia and hydrogen sulfide smelling at room temperature. Material balance analyses using Perkin-Elmer Model 240B elemental analyzer and Leco sulfur analyzer showed that the plugging material has an elemental ratio of nitrogen, hydrogen and sulfur of 1, 5 and 1; this corresponds to a molecular formula of NH_4HS, ammonia hydrogen sulfide, which has a melting point of 20 C (68 F). This ammonia hydrogen sulfide plugging problem has also been encountered in a reactor effluent gas heat exchanger during hydrotreatment of petroleum residuum (Ehmke, 1975).

The temperature distribution along the reactor outer wall was excellent; a variation of no more than 1 C with respect to both position and time has been observed. However, a temperature difference of 11 C between the center of the catalyst bed and the outer wall of the reactor was observed whenever the oil was charged into the reactor at reaction temperature. This temperature differential was caused by exothermic hydrogenation reactions, and was difficult to control in the current reactor system.

The results from sample analyses are listed in Appendix E. The hydrogen contents are typically 3.4 wt% higher in product oils than in the feedstock, and greater than 80 wt% nitrogen removal was achieved at 400 C (750 F). at 427 C (800 F) operation, essentially all the nitrogen was removed. The weight percents of nitrogen and hydrogen

in product oil versus time on stream are plotted in Figure 19. The figure shows that the hydrogenation and hydrodenitrogenation activities of the catalyst do not decay during the entire 261 hours on stream.

The EDS oil feedstock used in this experimental run was relatively easily hydrotreated. Because the catalyst demonstrated no activity decay over a 261 hours' run, another feedstock, SRC oil mixture was used instead.

SRC Oil Feedstock

Experimental run series LTG, LTV, LTW, LTX, LTY and LTZ were made with the SRC oil feedstock. The objective of these runs were to generate data at various run durations for the investigation of catalyst deactivation which the EDS oil feedstock did not fulfill. The operating conditions of these experimental runs are shown in Table IV.

Run LTG was the first one made with this new feedstock. This run was shut down at 19 hours on stream due to plugging downstream of the reactor. The plugging material was taken out for analyses and found to be soluble in pyridine and has essentially the same elemental compositions as those of the residue in the feedstock. This may be because that after the solvent fraction is hydrogenated, the residue fraction becomes incompatible with the solvent and precipitate out at the reactor outlet where the temperature is considerably lower than the reaction temperature. Similar plugging problems have been observed in other coal oils hydrotreatment study (Stein et al., 1978).

The plugging problem was later solved by moving the first separation bomb directly under the reactor and maintaining the reactor exit

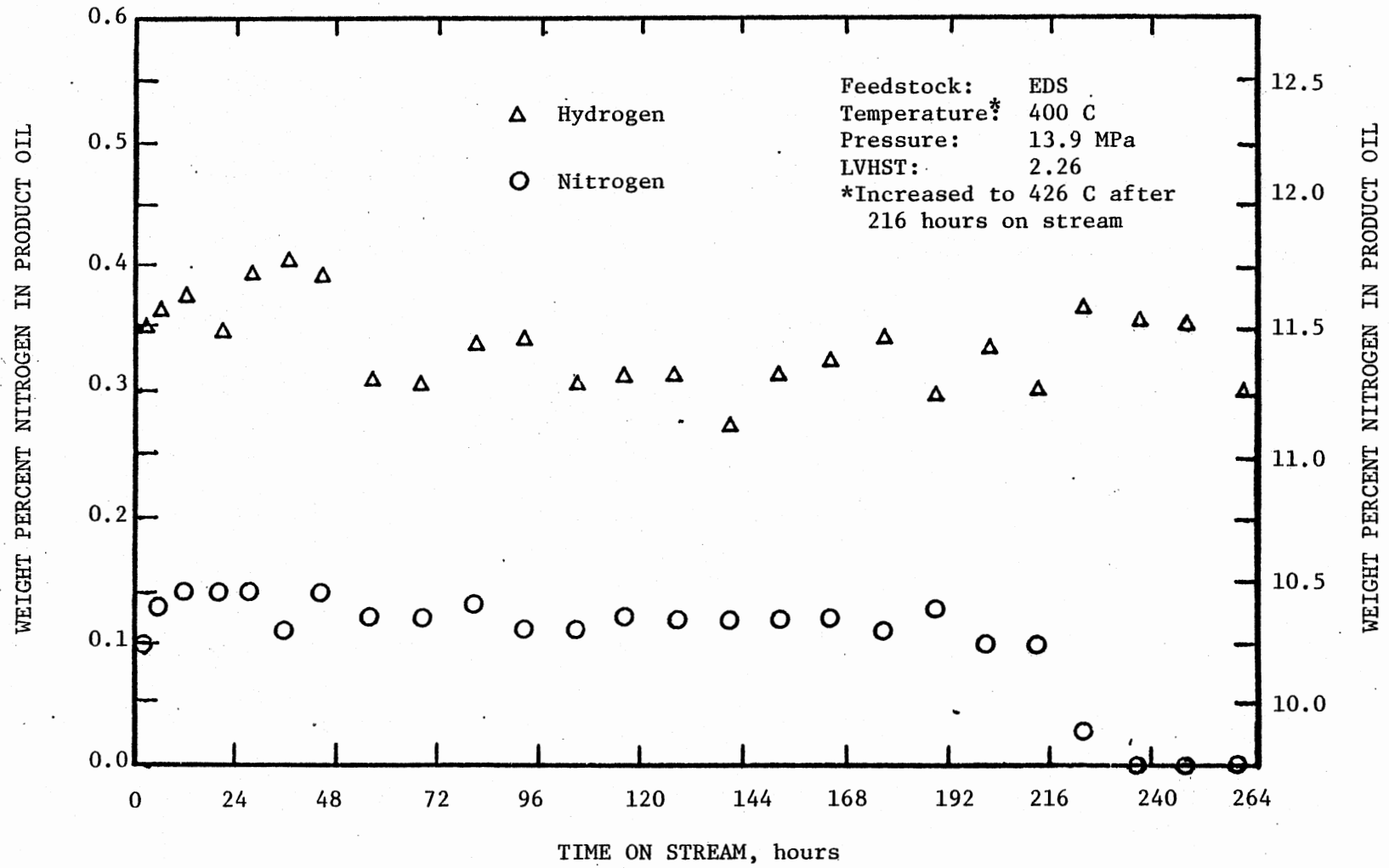

Figure 19. Hydrogenation and Hydrodenitrogenation Activity Responses for Run LTB

line heated. Runs LTV, LTW, LTX, LTY, and LTZ were made successfully with this modified system.

The duration of Run LTZ was one hour which is shorter than the liquid volume space time (2.50 hours). However, because of the start-up method, the catalyst in the reactor would have already been wetted by oil. No analysis was made on oil sample from Run LTZ since during its entire one hour on stream, the reactor was in transient stage while catalyst activity changed so fast that sample analyses could not reveal the true activity.

The results from sample analyses are listed in Appendix E. The hydrogen and nitrogen contents in the oil samples were analyzed with a Perkin-Elmer model 240B automatic elemental analyzer. All samples, including those from the run with the EDS oil feedstock have been analyzed at least three times to determine the analytical precision. The pooled standard deviations were 0.12 wt% and 0.04 wt% for the coal oil samples containing 6-12 wt% hydrogen and 0-2 wt% nitrogen respectively. The analytical precisions are high in terms of relatively low deviations.

The hydrogenation and hydrodenitrogenation activity responses for Runs LTG, LTV, LTW, LTX and LTY are plotted in Figures 20 and 21 respectively. In these figures, the elemental contents of the samples resulting from different liquid volume hourly space time (LVHST) have been normalized to a LVHST of 2.50 hours according to the liquid hold-up model proposed by Henry and Gilbert (1973) for a pseudo first order reaction, as shown in Eq. (2) in Chapter II. An equilibrium hydrogen concentration of 12.2 wt% in product oil has been assumed to normalize the hydrogenation activity. Figures 20 and 21 have demon-

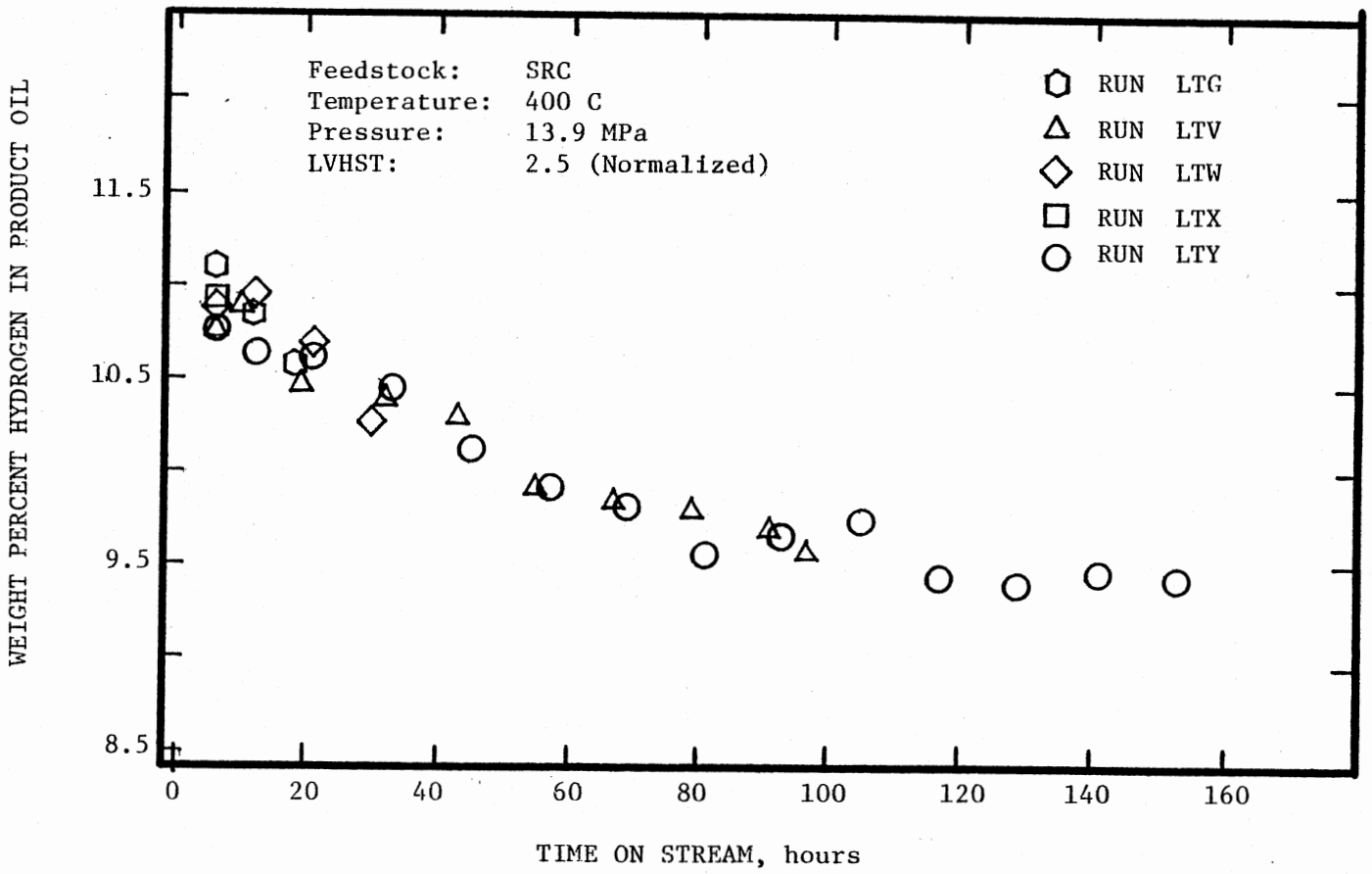

Figure 20. Hydrogenation Activity Response for the Runs with SRC Feedstock

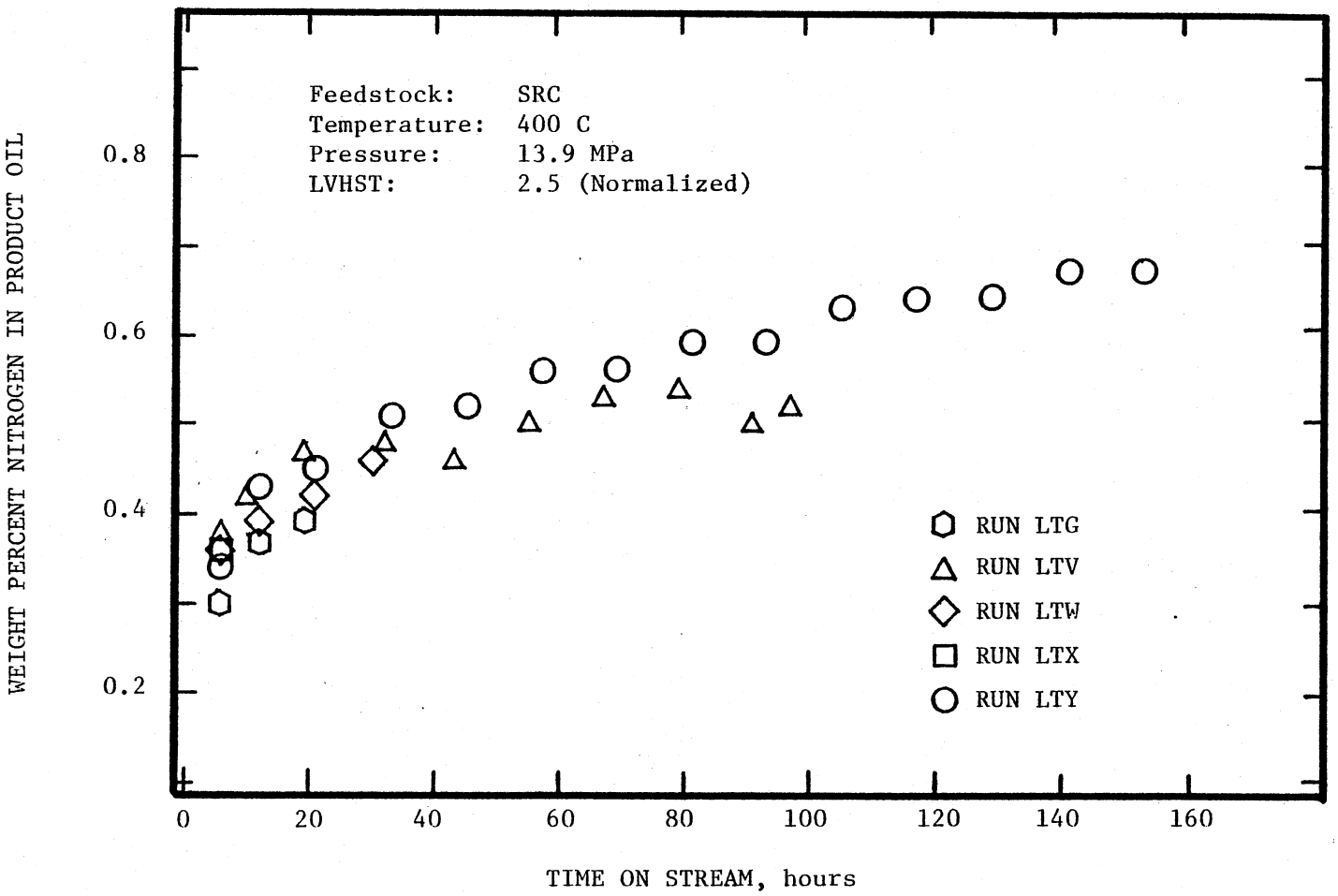

Figure 21. Hydrodenitrogenation Activity Response for the Runs with SRC Feedstock

strated good data reproducibility. As shown in these figures, the catalyst activity decayed rapidly initially, half of the activity was lost during the first 40 hours on stream, and then it demonstrated a reduced decay rate. This activity decay phenomenon provided an ideal situation for the study of catalyst deactivation mechanisms.

Reactor Radial Temperature Differentials

The radial temperature differentials of the reactor bed have been carefully investigated. This temperature differentials were definitely caused by the exothermic reactions, since they were observed to disappear whenever the oil feed was terminated. Figure 22 shows the temperature differentials versus time on stream for the runs with the SRC feedstock. At the first moment of catalyst-oil contact, the temperature of the catalyst quickly increased to 25 C (45 F) higher than the preset value and then leveled off at around 5 C (9 F) after 40 hours operation. This decreasing temperature differential with time seems to parallel the catalyst hydrogenation activity, which is shown on Figure 20. This would be expected since the hydrogenation reactions are highly exothermic. Therefore, the temperature differential across the reactor bed can be taken as an indication of the catalyst activity.

The temperature differential in Run LTW was further studied. Figure 23 shows this differential profile in the reactor bed at the first sampling time (2 hours on stream). The temperature is the highest at the catalyst bed entrance where the oil first contacts the catalyst, the differential then moves toward the reactor exit. This decending profile means that the most severe hydrogenation reactions occur at the reactor top at the initial stage. Figure 23 also shows

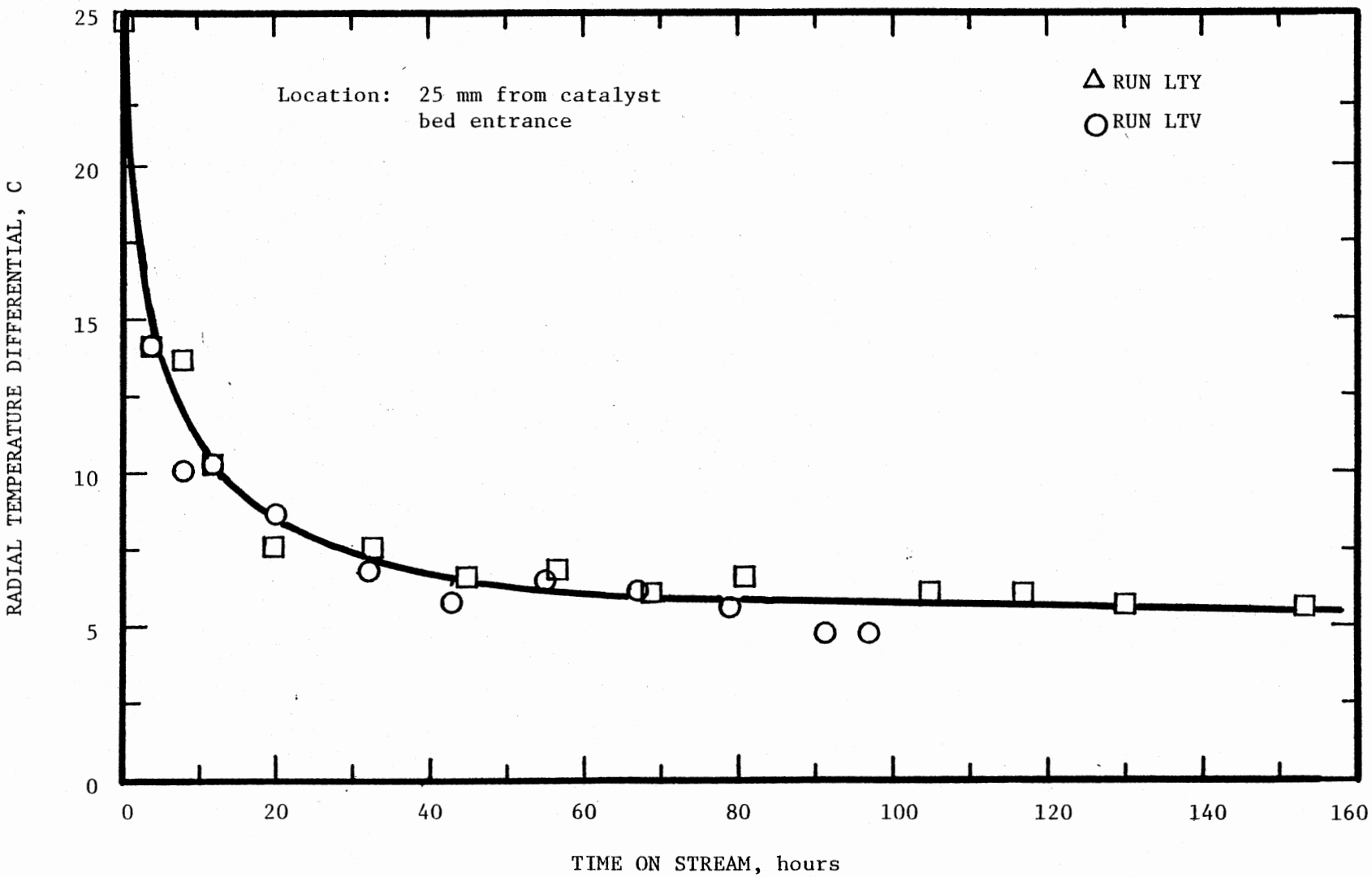

Figure 22. Reactor Radial Temperature Differential Versus Time on Stream

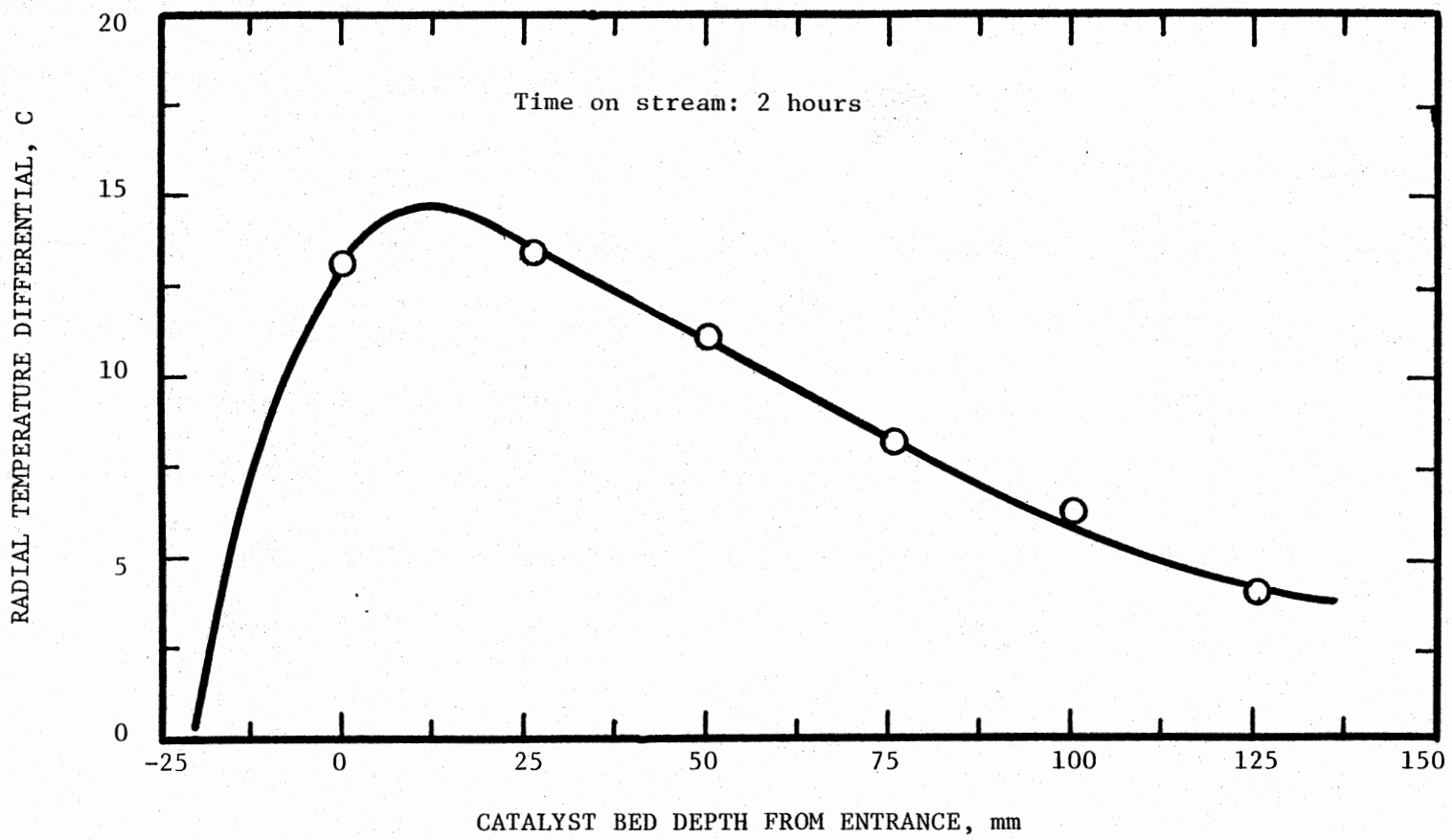

Figure 23. Reactor Radial Temperature Profile for Run LTW

that the radial temperature differential at reactor downstream was lower than 4 C; this means that the temperature differential across the reactor tube wall was 4 C or less, and the rest of the differential was across the catalyst bed itself.

Results of Catalyst Analyses

The aged catalysts were taken out of the reactors section by section, and washed with pyridine and dried. These washed and dried aged catalysts were anlayzed for coke contents, pore size distributions, pore volumes, surface areas and pellet elemental profiles using the equipment and procedure discussed earlier. Results of these analyses are corrected to a freshly sulfided catalyst basis and are presented in Table V.

In order to determine the analytical precisions, coke contents of the used catalysts from Run LTV were analyzed thrice using the established procedure. A satisfactory result has been obtained (11.30, 12.30, 11.76, and the average 11.80 $\pm$ 0.50 wt%). The fresh Shell 324 catalyst has been analyzed seven times and the deviations were determined. The results are 146 $\pm$ 5 x 10^3 m^2/kg for surface area, 11.8 $\pm$ 0.1 nm for the most frequent pore diameter and 0.43 $\pm$ 0.02 x 10^{-3} m^3/kg for pore volume. These low deviations along with the consistency with the vendor's data indicate that the analytical procedure is highly reliable.

Coke Profiles in the Reactor Beds

Figure 24 shows coke profiles in the reactor beds with time on stream for the runs with the SRC feedstock. Linear regression lines

TABLE V

RESULTS OF CATALYST ANALYSES

Run Series	Reactor Position[a]	Wt% Coke[c]	Pore Volume[d] (10^{-3} m^3/kg catalyst)	Pore Diameter (nm)	Surface Area[d] (10^3 m^2/kg catalyst)
Fresh		0	.430	11.8	150
Fresh Sulfided		0	.430	11.0	160
LTV	Average[b]	11.79	.267	7.7	158
LTG	Average	7.13	.336	7.6	177
LTY	1	12.35	.275	7.6	163
LTY	2	13.28	.241	6.3	159
LTY	3	11.61	.234	6.8	143
LTY	4	12.38	.276	8.0	154
LTY	5	12.04	.311	8.2	156
LTW	1	11.86	.293	7.7	177
LTW	2	9.16	.304	8.0	165
LTW	3	8.11	.309	8.4	173
LTW	4	7.19	.344	8.4	166
LTW	5	6.18	.356	8.4	164
LTX	1	8.44	.333	8.4	174
LTX	2	6.30	.351	8.4	167
LTX	3	6.28	.357	8.0	167
LTX	4	4.98	.364	8.0	166
LTX	5	4.58	.389	8.0	169

TABLE V (Continued)

Run Series	Reactor Position[a]	Wt% Coke[c]	Pore Volume[d] ($10^{-3}m^3$/kg catalyst)	Pore Diameter (nm)	Surface Area[d] (10^3m^2/kg catalyst)
LTZ	1	7.42	.283	8.8	179
LTZ	2	5.69	.336	8.4	176
LTZ	3	5.05	.355	8.8	168
LTZ	4	4.03	.385	8.8	164
LTZ	5	4.49	.364	9.3	160
LTB	1	9.06	.317	8.0	144
LTB	2	7.92	.339	8.4	154
LTB	3	13.75	-	8.0	142
LTB	4	15.26	.283	8.0	160
LTB	5	16.58	.294	8.6	149

a. Catalysts in reactor were separated into five sections, 0.1 meter per section. Number increases from reactor top to bottom.

b. Overall average; catalysts were not separated into sections.

c. Based on freshly sulfided catalyst.

$$\text{Wt\% coke} = \frac{L-S}{1.0 - L}$$

where L = percent weight loss upon combustion based on the extracted and dried spent catalyst.
S = percent weight increase from fresh catalyst after sulfiding. S = 1.75 wt% according to the presulfiding procedure.

d. By Perken-Elmer model 240 B elemental analyzer. Results are also based on freshly sulfided catalyst.

e. Based on fresh sulfided catalyst.

have been used in this figure to show the trends. The steepness of the line increases as time increases, reaches a maximum then tends to level off. This indicates that the fastest coke formation rate starts from the top of the reactor. When the coke content at reactor top approaches an equilibrium level, the area of the fastest rate of formation gradually moves down along the reactor. This type of coke profile seems to fall into the category of the parallel fouling model proposed by Froment and Bischoff (1961) as discussed in Chapter II. On the other hand, Figure 25 shows the opposite trend for Run LTB with the EDS feedstock. The feedstock clearly caused this difference in carbon profile responses.

Since no deactivation in catalyst activity was observed in Run LTB with EDS oil feedstock during its entire 261 hours on stream, the following discussions on pore volume, pore size and surface area will be concentrated on the catalysts from runs with the SRC feedstock only.

Average Coke Contents

The coke contents were averaged over all five sections for each run with the SRC feedstock. The averaged values are plotted versus time on stream; each point corresponds to a run at shut-down conditions, as shown in Figure 26. Half of the equilibrium coke has formed in less than 30 hours on stream. This type of coke buildup appears to be parallel to the catalyst activity.

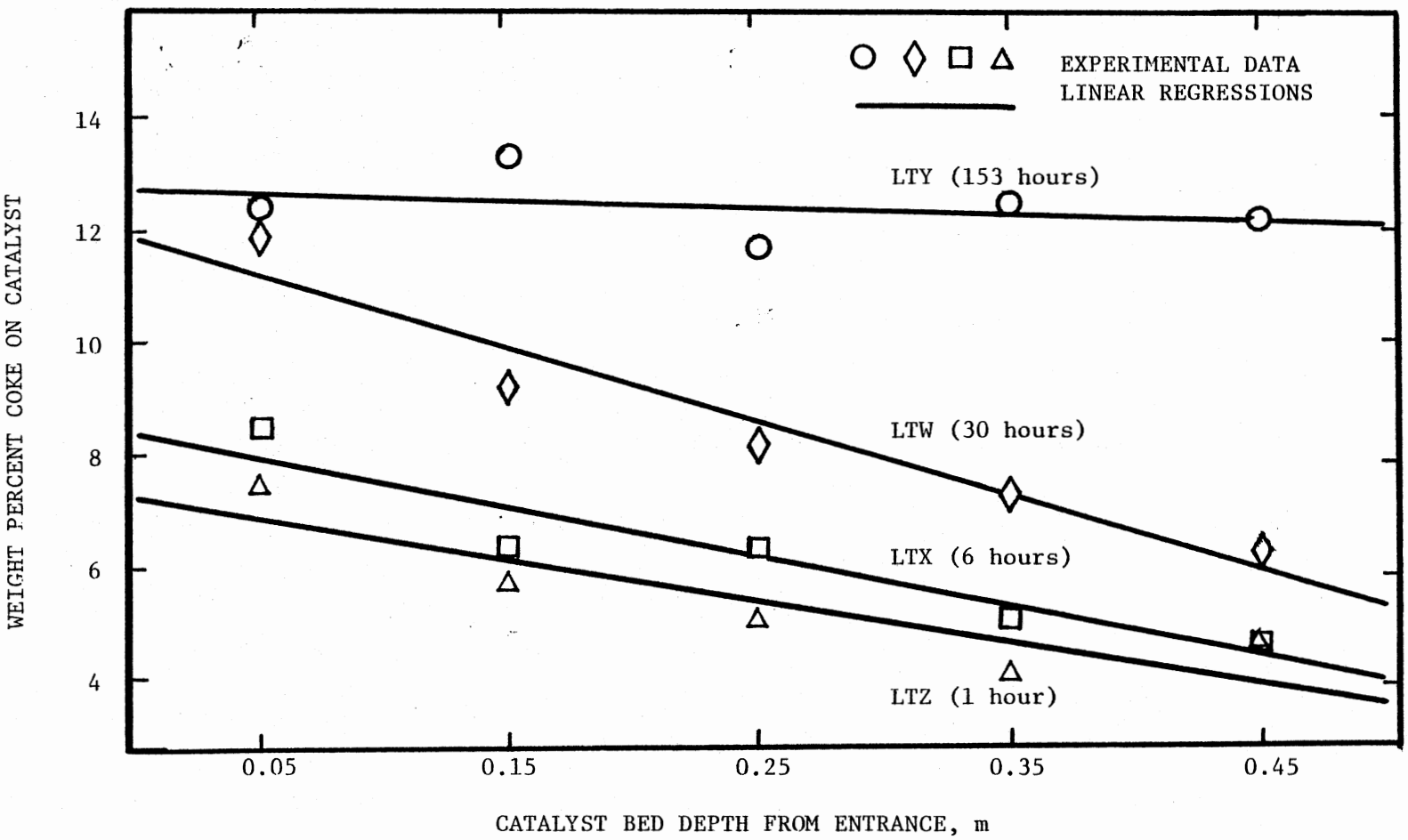

Figure 24. Coke Profiles in the Reactor Beds for the Runs with SRC Feedstock

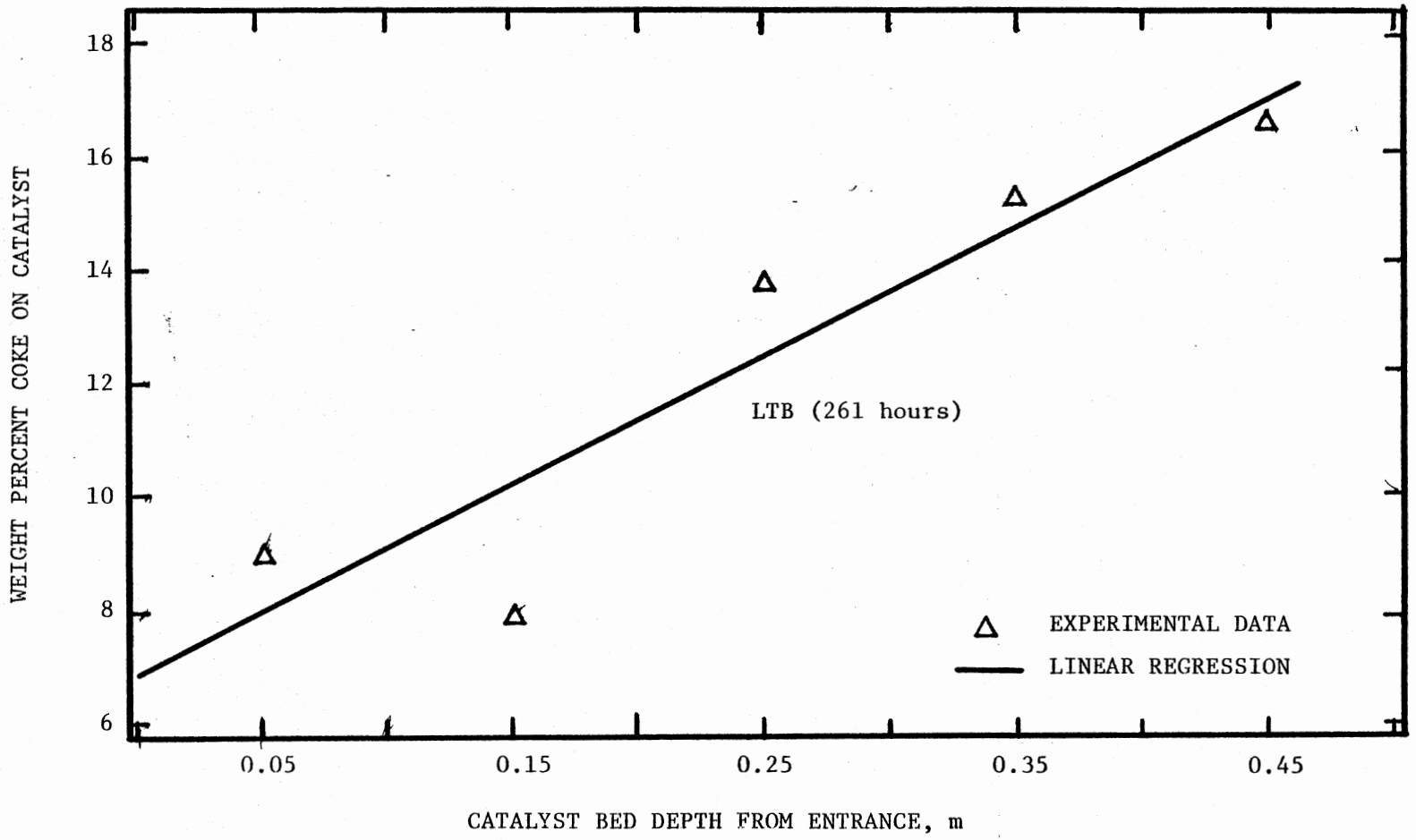

Figure 25. Coke Profile in the Reactor Bed for the Run with EDS Feedstock

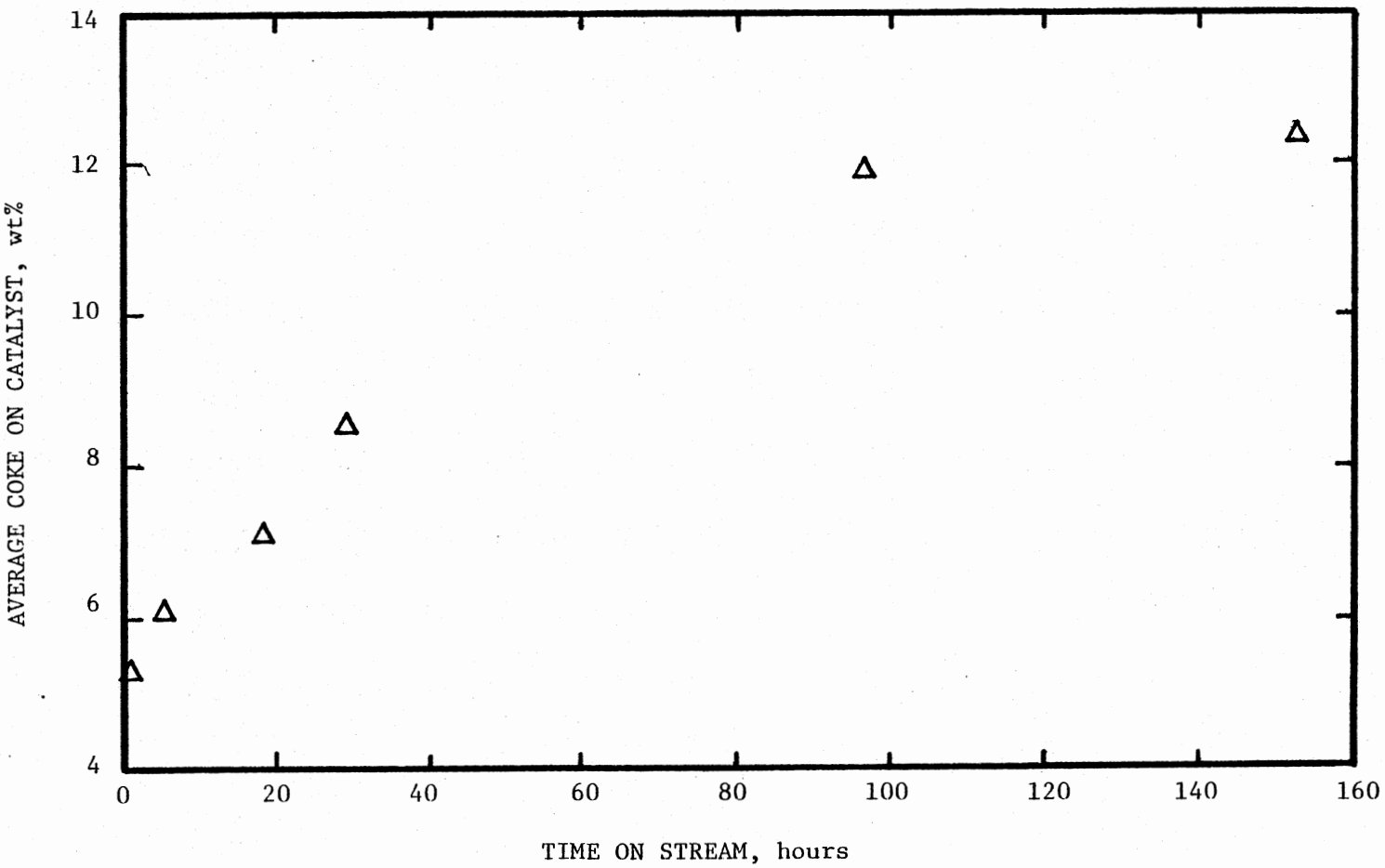

Figure 26. Average Reactor Coke Content Versus Time on Stream

Catalyst Activity Versus Coke Content

Excellent linear relationships between catalyst activites and coke content have been obtained for the runs with the SRC feedstock, as shown in Figures 27 and 28. All points fall within 95% confidence limits. In these two figures, the atom (nitrogen and hydrogen) contents in oil are obtained by averaging those atom contents of the samples having the same hours on stream from different runs. The atom contents are normalized to an LVHST of 2.5 hours according to the liquid hold up model proposed by Henry and Gilbert (1973) for pseudo first order reactions. This was discussed in Chapter II.

Pore Size Distributions

In order to know how the deposited coke affects the catalyst properties, pore size distributions, pore volumes and surface areas of the used catalysts were measured. Pore size distributions are given in Appendix F. As shown in Figure 29, although the most frequent pore diameters decrease, pore size distributions of the coked catalysts remain the same shape as fresh and freshly sulfided catalysts. Figure 30 shows most frequent pore diameters versus coke contents. A linear regressional line with 95% confidence limits is drawn. When linearly extrapolated to zero coke content, the most frequent pore diameter is 9.3 nm (93 Å), which is smaller than that of the freshly sulfided catalyst, 11.0 nm (110 Å). This may be due to the fact that most coke accumulates at the outer shell of the catalyst pellet, blocks the pore mouths and creates bottlenecks.

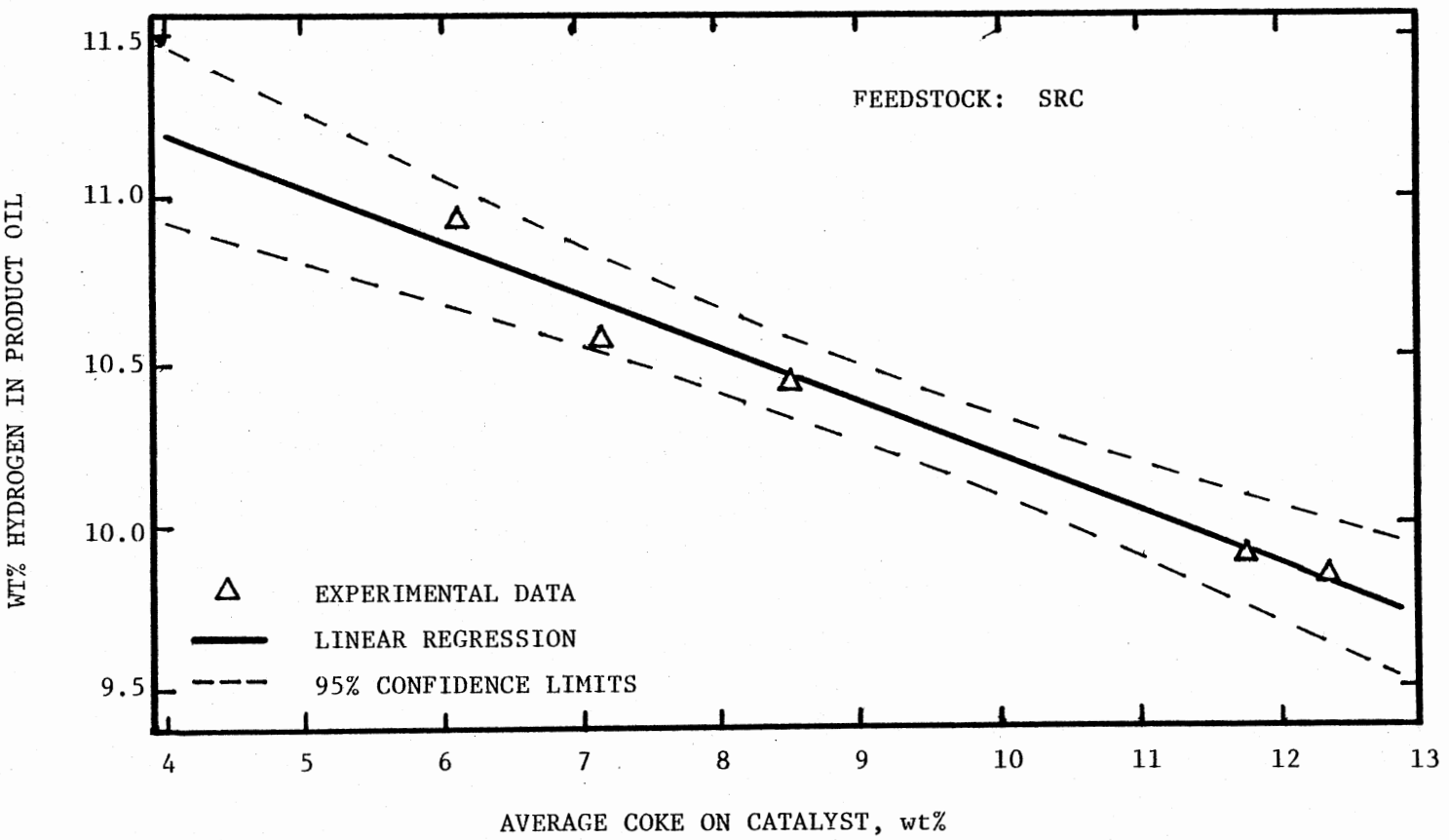

Figure 27. Catalyst Hydrogenation Activity Versus Reactor Coke Content

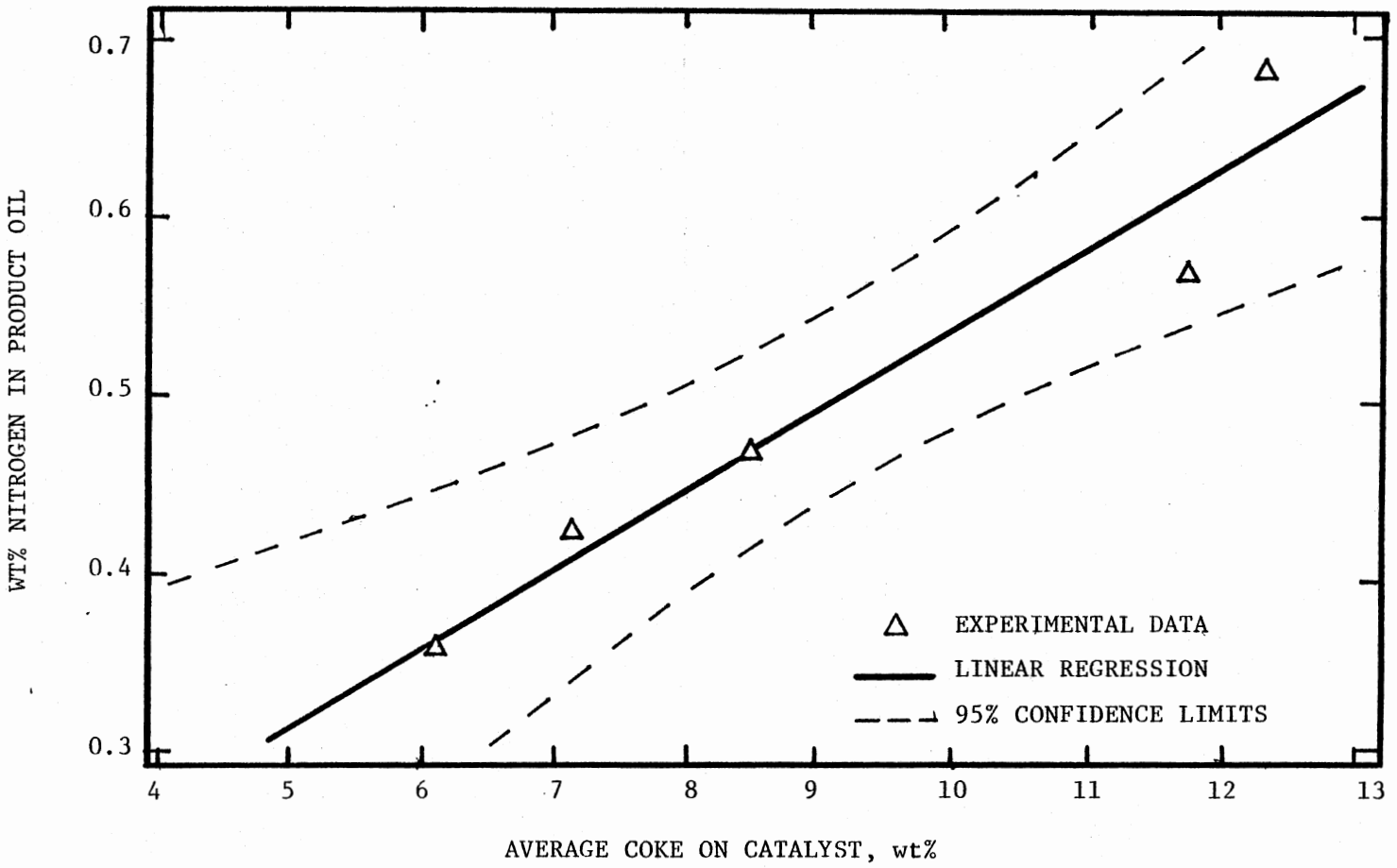

Figure 28. Catalyst Hydrodentirogenation Activity Versus Reactor Coke Content

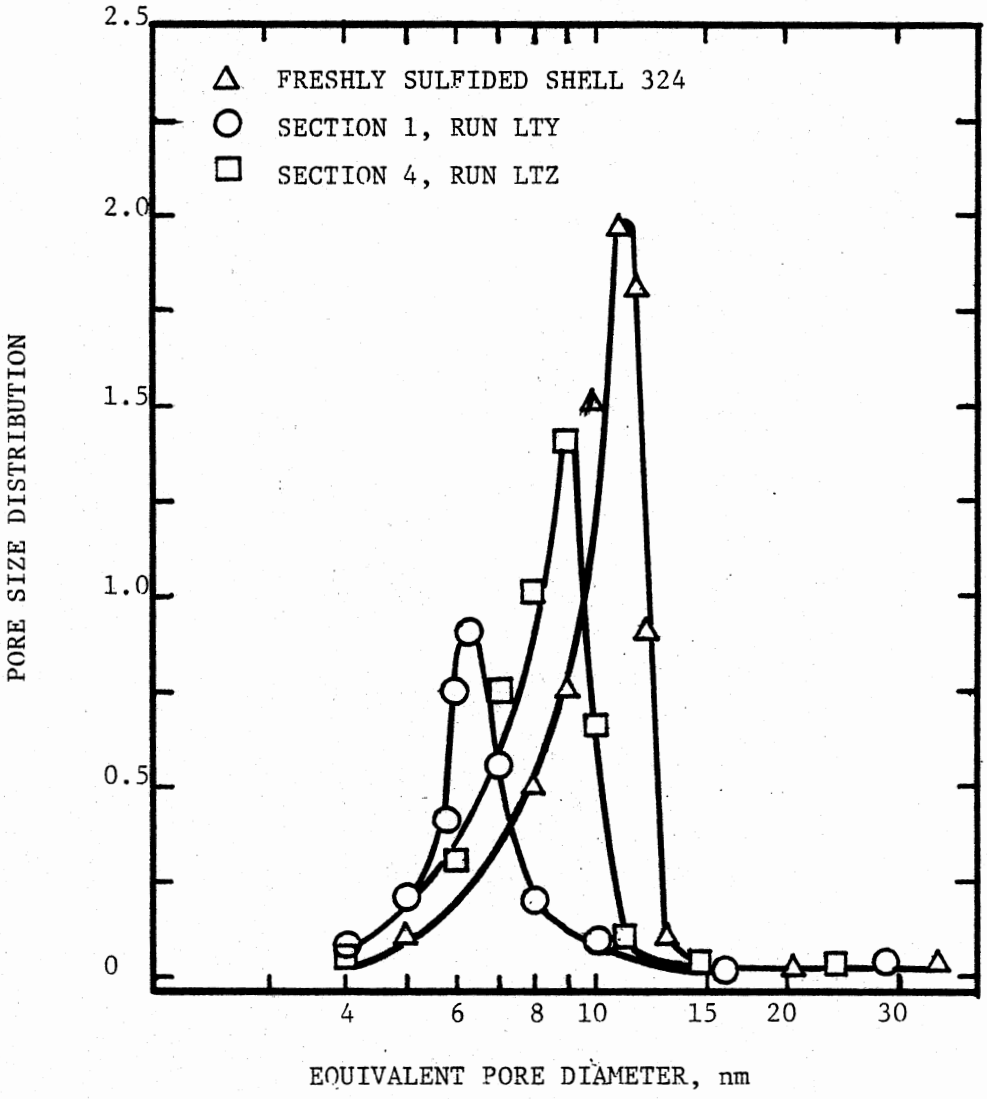

Figure 29. Pore Size Distribution of the Fresh and Spent Catalysts

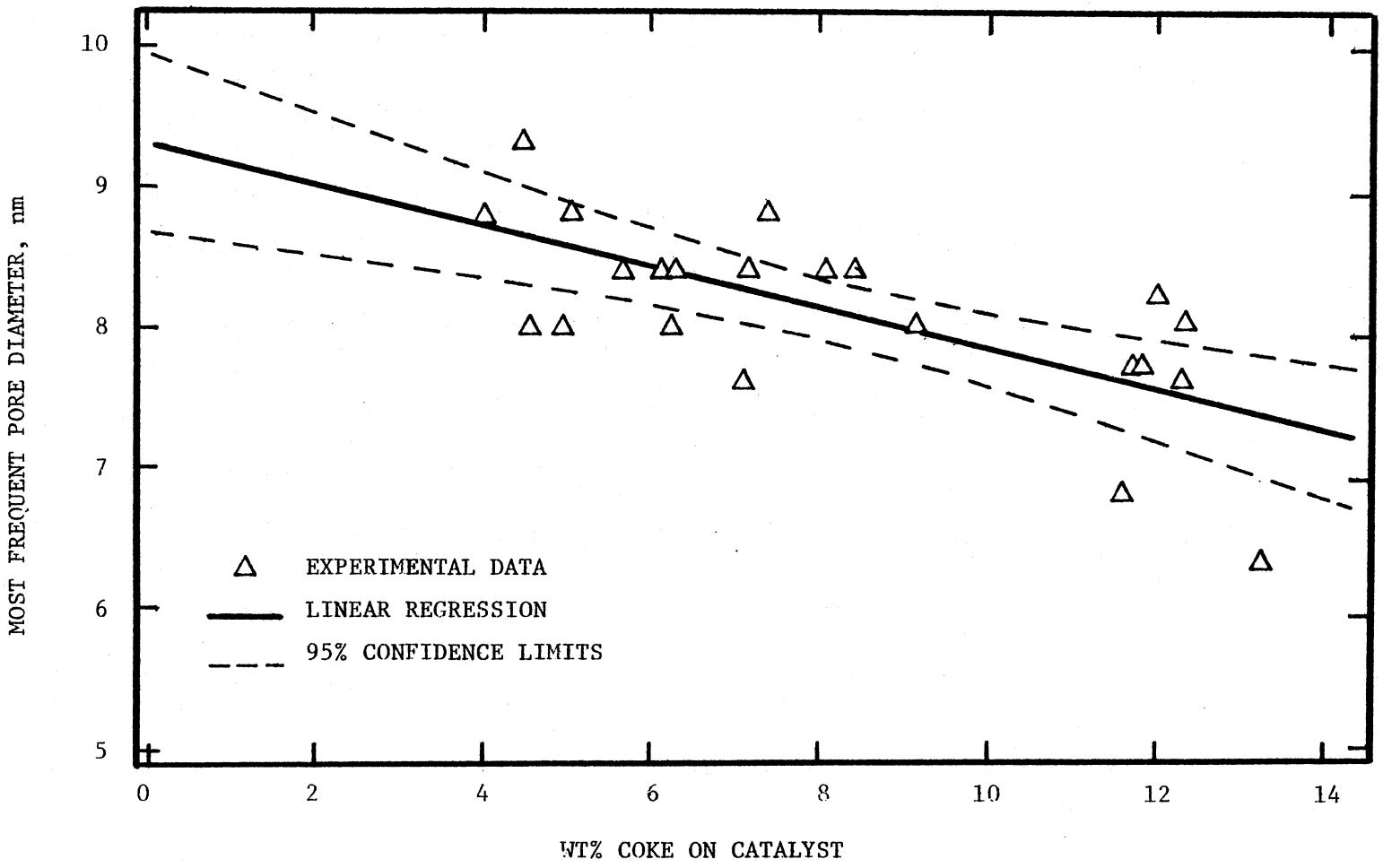

Figure 30. Most Frequent Pore Diameter Versus Coke Content

Pore Volumes

Pore volumes were determined by the amount of mercury penetrated up to 345 MPa (50,000 psig), which is equivalent to 3.3 nm (33 Å) diameter when a contact angle of 130 degrees is assumed. Figure 31 shows an excellent linear relationship between pore volume and coke content. Most of the points are within 95% confidence limits. When linearly extrapolated to zero coke content, the pore volume is consistent with that of freshly sulfided catalyst, 0.43×10^{-3} m^3/kg.

Surface Areas

BET nitrogen adsorption was used to determine surface areas. The results versus coke content are shown in Figure 32 and are relatively scattered. Unlike that of fresh catalyst, the surface area analysis of the freshly sulfided catalyst has shown larger variation, ranging from 140 to 175 $\times 10^3$ m^2/kg, with an average of 160×10^3 m^2/kg. Linear extrapolation to zero coke content from Figure 32 shows that the surface area of the freshly sulfided catalyst is 175×10^3 m^2/kg compared to a measured value of 160×10^3 m^2/kg. The deviations of the surface area analyses of the freshly sulfided and spent catalysts may have been caused by the strong adsorption of moisture and oil on the active sites. The more active the surface is, the stronger is the adsorption, and hence the more variation in the analyses. The change of surface area with coke content is not significant. Since the coke density calculated from pore volume-coke content relationships (Figure 31) is 0.80×10^{-3} m^3/kg, this low density coke may be porous and may have confounded the true catalyst surface area analyses.

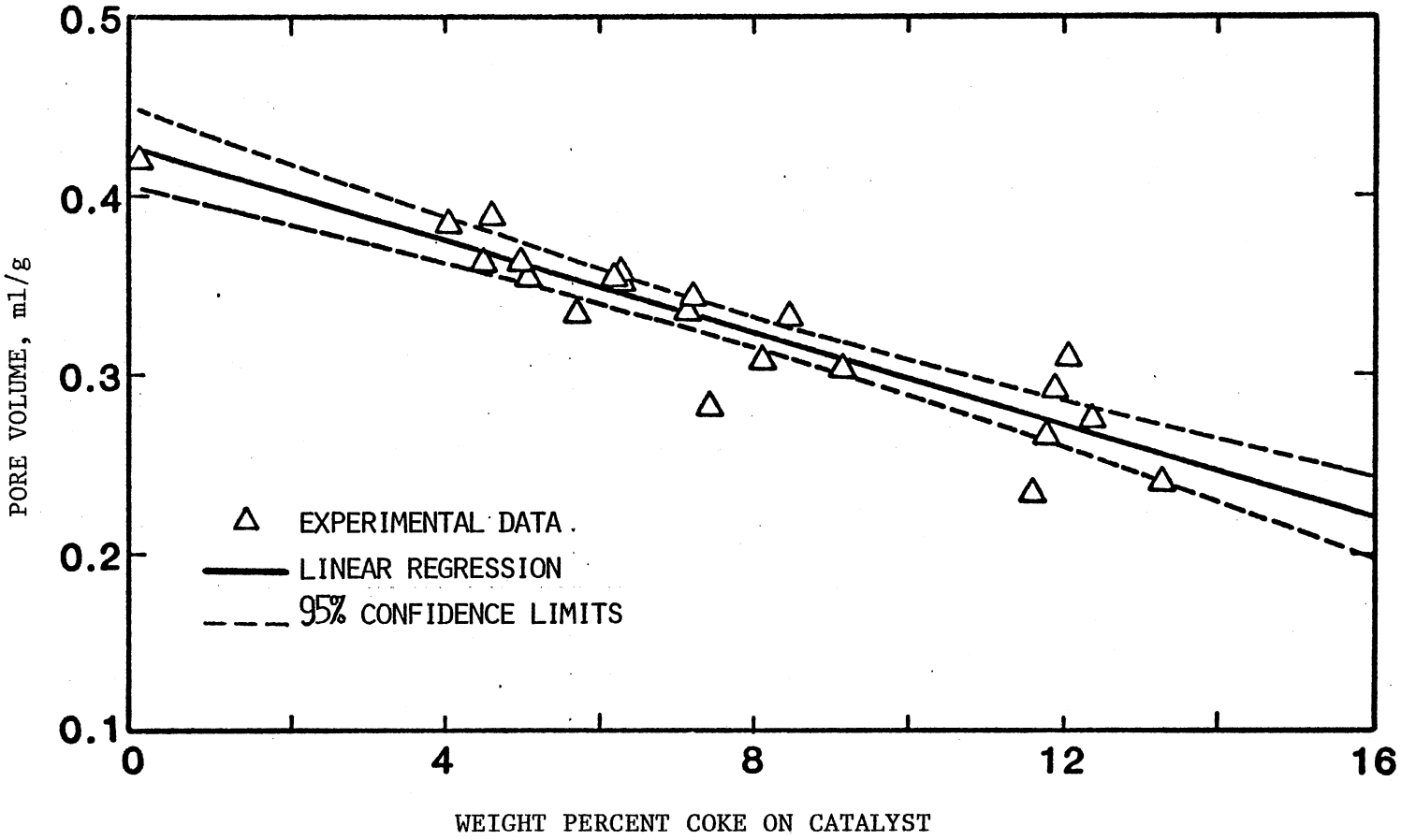

Figure 31. Pore Volume Versus Coke Content

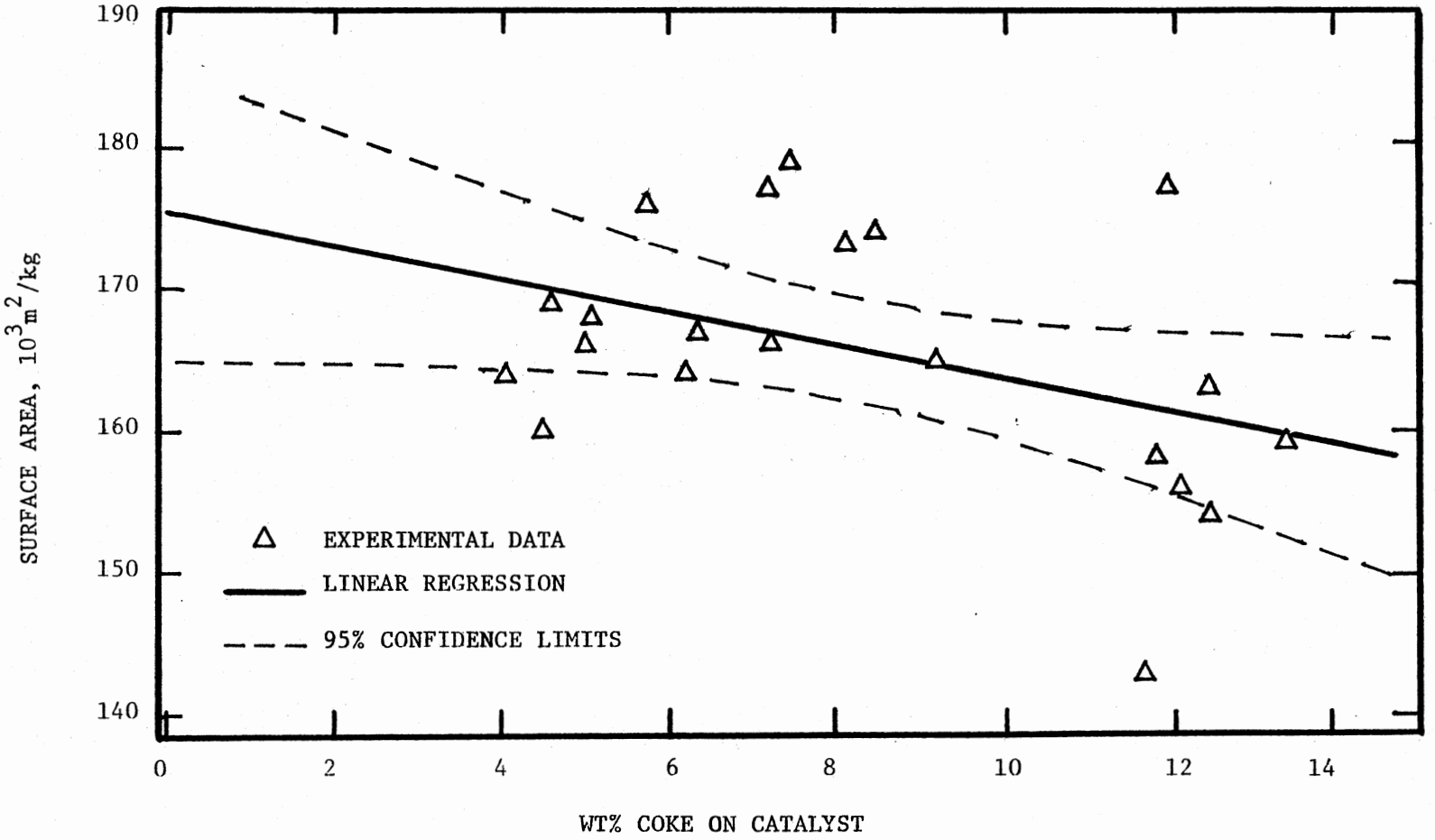

Figure 32. Surface Area Versus Coke Content

Carbon Profiles in Catalyst Pellets

Some spent catalysts were analyzed for carbon profiles within the pellets with a scanning Auger microscope (SAM) in a commercial laboratory. The complete results are listed in Appendix G. The highest carbon content is around 80 atom%, whereas essentially no nitrogen (not shown in the table) was detected; this means that the nitrogen content on the spent catalyst is lower than 1 atom%. Furthermore, all other elements not listed in Appendix G were not detected, not even the nickle in the freshly sulfided catalyst.

Figure 33 presents the precisions of the SAM analyses over the catalyst pellets from the same section of a run. Note that the SAM analyses should be regarded as qualitative results only because: 1) SAM is a very surface sensitive instrument, it can only detect the atoms within the depth of 1 to 4 nm from the surface, this exaggerates the contents for the deposited atoms; and 2) catalysts are heterogeneous in nature and may be different from pellet to pellet, as Figure 33 shows. Additional results from SAM analyses will be discussed in the next chapter.

Summary

The experimental results can be summarized as follows:

1. The run with the EDS feedstock demonstrated no catalyst deactivation during the entire 261 hours on stream; whereas the runs with the SRC feedstock showed rapid catalyst deactivation during the first 40 hours on stream, and then tended to level off.

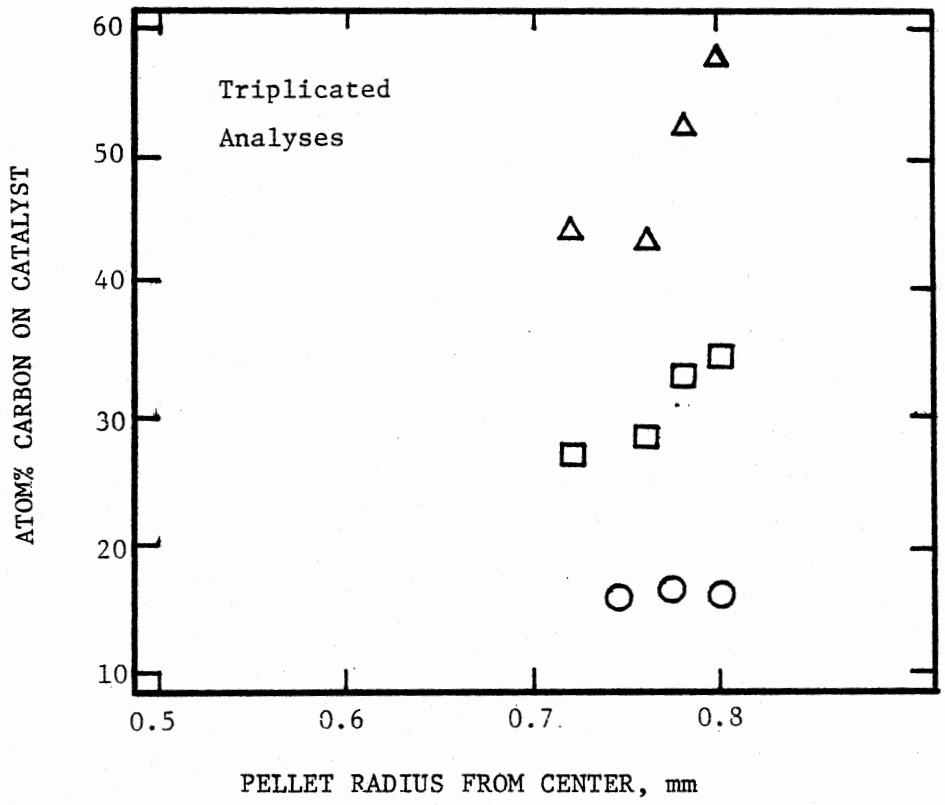

Figure 33. Precisions of the Carbon Profile Analyses

2. The pattern of coke profiles in the reactor beds follows parallel fouling mechanism for runs with the SRC feedstock, whereas it follows series fouling mechanism for the run with the EDS feedstock.

3. Hydrogenation and hydrodenitrogenation activities of the catalyst decreased linearly with increasing average coke content in the reactor bed.

4. Pore volumes and most frequent pore diameters decreased with increasing coke content.

5. Surface area may not be a good measure of the catalyst activity since coke may have a large surface area to confound the true catalyst surface area analysis.

6. Scanning Auger microscopic analyses qualitatively showed that coke was the only significant deposit on the catalyst surface; and most of this deposit was on the outer shell of the catalyst pellet.

These experimental results imply that: catalyst activity is parallel to the coke content; and coke on catalyst can block the pore mouths and severely reduce the effective diffusivity of the reactants in the catalyst pellet. In the next chapter, the catalyst deactivation mechanism will become clear through the study of a model which is based on a parallel fouling and incorporates intrinsic reaction rate and reactants effective diffusivity as functions of coke content.

CHAPTER VI

DISCUSSION

The loss in catalyst activity during hydrotreatment operations can be due to carbonaceous and inorganic depositions, inhibitive adsorption and sintering as discussed in Chapter II. In general the active life of the catalyst can be defined as the period during which the desired conversion with minimum undesirable side reactions can be obtained. This period is an important factor in determining the commercial feasibility of a catalyst, and hence, a given process.

In hydrotreatment operations the hydrogen and nitrogen concentrations in the product oils can be taken as a measure of the hydrogenation and hydrodenitrogenation activities, respectively, of the catalyst. The objectives of this study include the assessment of the factors responsible for the loss of hydrogenation and hydrodenitrogenation activities of the catalyst. The success and usefulness of any research work depend on the reproducibility of its results. These can be affected by variations of the operational conditions in the reactor and the performance of the trickle bed reactor used.

Reproducibility and Precision

All experimental runs in this study have been conducted at 13.9 MPa (2000 psig), and a variation of 34 KPa (5 psi) was observed during

normal operation. However, occasionally a maximum pressure differential of 6.9 MPa (1000 psi) occurred due to partial plugging in the reactor. In this situation the reactor was either shut down or purged with a high hydrogen flow promptly to clear the restriction. As discussed in this literature review, an increase in pressure beyond 7.0 MPa (1000 psig) has no significant effect on the heteroatom removal from petroleum as well as coal-derived liquids. Therefore, the effect of the temporary pressure fluctuation in this study is not expected to be significant.

The oil in the storage tank was agitated continuously to maintain homogeneity. A positive displacement pump has been used for feeding the oil to the reactor. This pump can deliver a constant preset oil rate with little variation so long as the suction pressure is kept constant. The hydrogen gas flow was controlled by a micrometering valve at reactor upstream and monitored by a wet test meter after the scrubber. At normal operational mode, the hydrogen flow rate was essentially stable without observable variations.

Temperature distributions along the reactor outer wall were excellent. The maximum variation both with position and with time were less than 1 C. There were significant temperature differentials across the reactor radial direction, especially at the reactor top and during the first oil-catalyst contact. These differentials were highly reproducible from run to run. Therefore, the reproducibility of the results of this study, in terms of temperature, pressure, liquid flow rate and hydrogen-to-oil feed ratio, should be within appropriate ranges. Figures 20 and 21 which present product hydrogen and nitrogen contents,

respectively, from different runs have provided further solid evidence that the experimental runs in this study are highly reproducible.

The analytical precisions for the oils and catalysts analyses have been discussed in Chapter V under each related section. Except for the scanning Auger microscopic results, which will be used for qualitative reference only, the low deviations of the analyses have shown that the analytical results should be highly reliable.

Performance of the Trickle Bed Reactor

The analysis of data obtained with chemically reacting flow systems requires the consideration of the interactions between momentum, heat and mass transfer processes. The fluid dynamic aspects to be considered in trickle bed reactors include the flow distribution, fluid-solid contacting (wettability), liquid holdup and backmixing effects.

This particular study was not designed to investigate the effect of fluid dynamic parameters on the performance of trickle bed reactors. However, an attempt here will be made to analyze the influence of these parameters on the results, and hence the conclusions. In the case of fixed bed reactors operating in the trickle flow mode, the gas flows as the continuous phase with liquid as the dispersed phase. This particular flow pattern can result in efficient contacting of the gas and liquid phases with negligible mass transfer resistance across the gas-liquid interface. Transition from gas continuous to pulsing flow is also possible in trickle bed reactors.

In hydrotreating operation, the reactor is designed to bring the reactants, hydrogen (gas phase) and oil species (liquid and some vapor) in contact in the presence of a catalyst (solid phase). In packed bed

reactors even though the liquid is dispersed in the continuous gas phase, the catalyst particles are covered with a thin film of the liquid. Thus the reaction mechanism involves the diffusion of hydrogen through this film to the catalyst surface. In the case of pulsing flow (slug flow) the possible hydrogen deficient in the liquid slug can result in undesirable thermal cracking reactions leading to coke formation.

The above discussion indicates that liquid-solid contacting can play a major role in the performance of trickle bed reactors. In the case of small diameter laboratory reactors, as well as large commercial units, the liquid can migrate to the wall as well as follow a channeling pattern through the catalyst bed. This will result in an inefficient utilization of the catalyst in the reactor. At this stage two aspects need to be considered: namely liquid flow pattern and liquid-solid contacting. The liquid flow pattern consideration is also needed to establish the backmixing effects.

Liquid Flow Pattern

Consideration of the tube diameter to particle diameter ratio (D_t/D_p), liquid flux, and gas flux can give an insight to the flow distribution effects. In this study the D_t/D_p ratio was 6.5. Sooter (1974) and Satchell (1974) in their hydrotreatment studies with raw anthracene oil on a similar reactor used a D_t/D_p ratio of 4.0 and varied the liquid flux in the range of 0.09-0.38 $kg/m^2/s$ and observed no significant effects on heteroatom removal. The liquid flux used in this study was in the range of 0.06-0.08 $kg/m^2/s$. This suggests that

the effects of flow distribution in the radial direction in the present study may be of little importance. In the case of trickle bed reactors, plug flow of liquid has been found to be a good approximation (Paraskos et al., 1975). Radial velocity gradients can contribute to flow non-idealities in the trickle bed reactor. The study of Koros (1976) has indicated that the ratio of liquid flow through an inner core to that through an annular core in a trickle bed reactor was of the order of 5-6 for liquid fluxes less than 0.1 $kg/m^2/s$ and about four for 0.1-8.0 $kg/m^2/s$. However, he observed no significant differences in conversion (decomposition of H_2O_2 to H_2O and O_2) between inner and annular cores, and concluded that the liquid flows in the plug flow pattern with a high rate of radial mixing.

In the present study hydrotreatment of coal-derived liquids were carried out in a trickle bed reactor. These liquids have a high tendency towards coking. Hydrogen deficiency in the liquid phase can enhance the rate of undesirable reactions leading to the formation of coke in the catalyst bed interstices and can result in increased resistance to flow due to bed plugging. Slug flow pattern compared to the homogeneously dispersed liquid in continuous gas phase flow pattern (trickle flow) is prone to enhance coking. In the present study the liquid and gas fluxes are such that the operation is highly likely to be in the trickle flow mode based on the mapping of the flow patterns reported in the literature (Morsi et al., 1978).

Axial Dispersion

An axial dispersion effect can contribute to the non-ideal behavior even though radial variations in liquid flow have insignificant effects on the conversion. Assuming the axial dispersion to be dominant, Mears (1971) suggested the following criteria for assessing the backmixing effects:

$$\frac{L}{D_p} > \frac{20n}{B_o} \ln\left(\frac{C}{C_o}\right) \qquad (1)$$

where

L = catalyst bed height

D_p = catalyst pellet diameter

n = reaction order

C, C_o = inlet and outlet concentrations of the reactant

B_o = Bodenstein number, vD_p/D_b

v = superficial velocity of the fluid

D_b = bulk diffusivity

Hochman and Effron (1969) in their studies with nitrogen-methanol system in cocurrent gas-liquid operation in a packed bed correlated the liquid Reynolds number and the Peclet number. Mears (1971) using this correlation suggested a L/D_p equal to 350 for less than 5% deviation at 90% conversion for first order kinetics in hydrotreating gas oils. The L/D_p ratio in the present study was between 250 and 320, almost meeting the Mears criterion. Considering the question associated with Mears' criterion, there probably exists no significant backmixing effects and the operation approaches, very nearly, plug flow. Reproducibility of data, previous studies in our laboratory (Satchell, 1974) support this observation.

Liquid Holdup and Solid-Liquid Contacting Efficiency

In this section, literature observations on solid-liquid contacting efficiency and liquid holdup effects will be presented first, and the reactor used in this study will be compared and evaluated.

Armak Company (1976), a catalyst manufacturer has tested hydrodesulfurization of vacuum gas oils in a trickle bed reactor over diluted or undiluted catalysts. The catalysts were diluted with equal volumes of various sizes of 0.23-0.85 mm inert carborundum. The dilution significantly improved the reactor performance. The improvement in conversion increased with increasing catalyst extrudates, the dilution could double the conversion if the extrudate length was 4 mm; whereas, no improvement in conversion could be made if the length was 2 mm or shorter.

van Klinken and van Dongen (1980) studied hydrodenitrogenation of a vacuum distillate over diluted and undiluted 1.5 mm spherical $NiMo/Al_2O_3$ catalyst using a trickle bed reactor. The catalyst performance was significantly improved by diluting with an equal volume of 0.2 mm silicon carbide. Meanwhile they observed that the dilution has doubled the liquid retention time and thus increased the total liquid holdup.

The work on coal liquid hydrotreatment in the trickle bed reactor by Berg and McCandless (1977) has shown that the H_2/oil feed ratio had an optimal value at 1800 ± 360 std. 1/1 ($10,000 \pm 2,000$ scf/bbl) due to the reactor hydrodynamics.

The above discussions suggest that the laboratory trickle bed reactor may have poor performance due to insufficient liquid holdup

and solid-liquid contact. In the present study, the 1.6 by 4.0 mm (1/16 inch by 1/6 inch) catalyst extrudates have been diluted with 0.8-1.0 mm spherical glass beads during packing. Meanwhile, the reactor has been operated at a hydrogen to oil feed ratio of 1800 std. 1/1. This combination would have reduced the reactor non-ideality to a minimum, and yielded the data valuable for kinetic study and for scale up.

Effectiveness Factor and Pore Diffusion

In heterogeneously catalyzed reactions several mass transfer steps are involved. The first condition in the case of hyrotreatment reactions is the presence of a liquid phase saturated with hydrogen around the catalyst pellet. The next step is the transport of the reactants to the active sites. These reactants then adsorb to form intermediate activated complexes with the active sites. This is followed by the formation of reaction products and their desorption while regenerating the active sites. The products then must diffuse back into the fluid phase surrounding the catalyst pellet. The transport of reactants to and the products from the active sites is a diffusional process and the global reaction rate controlling factors can lie within one of the following steps: 1) reactants and/or products diffusional processes, 2) adsorption-desorption phenomenon and 3) surface reaction. This of course assumes that bulk phase mass and heat transfer limitations are absent.

In hydrotreatment supported catalysts are used and the surface area, hence the active sites, lie mostly within the catalyst internal

porous structure. An increase in surface area with the most frequent pore diameter remaining the same should result in an increased rate of reaction in the case of surface reaction being the rate determining step. This increase may or may not be observed in the presence of pore diffusional limitations. However, if the pore size distribution is changed such that there is a decrease in the most frequent pore diameter then the reaction rate will decrease for these pore diffusion limited cases. Based on similar arguments, keeping the pore size distribution the same but processing heavier liquids (containing larger molecules) should also result in a decrease in the rate of reaction in pore diffusion limited cases.

Effectiveness Factor

The pore diffusional effects are accounted for in terms of an effectiveness factor which is a function of Thiele modulus. For the pseudo power law model of nth order reaction, the rate can be expressed as follows:

$$\frac{-dC}{dt} = kC^n\eta = k_{obs}C^n \qquad (2)$$

where

C = reactant concentration in the oil

k = intrinsic reaction rate constant

η = effectiveness factor, function of Thiele Modulus

k_{obs} = observed reaction rate constant

n = order of reaction

The effectiveness factor η can be expressed as a function of Thiele modulus as shown by Wheeler (1955). The Thiele modulus, h, for

arbitrary geometric shapes can be written as:

$$h = 2\frac{V}{S}\sqrt{\frac{kC}{\bar{r}D_{eff}}} \qquad (3)$$

where

V = geometrical volume of the pellet

S = external area of the pellet

$\bar{r}$ = average pore radius

D_{eff} = effective diffusivity

Effective Diffusivity

In order to know the diffusional limitations, the effective diffusivities of the reactants in the solvent must be estimated first; the kinetic constant can be derived from the reaction data. In general, structures of the heteroatom containing and non-heteroatom containing compounds in various coal liquids are more or less the same and the major difference lies in the amount present and in the distribution of various compound types. Therefore for simplicity the diffusivity can be referred to that of the overall average, not to any specific species.

Correlations of predicting the effective diffusivities for restricted diffusions in hydrocarbon liquids within fine pores of alumina supported catalysts have been proposed by several investigators (Satterfield et al., 1973; Prashel et al., 1978). These correlations take into account the effect of the ratio of the critical solute molecular diameter to pore diameter and of preferential solute adsorption on the surface of the porous solid. The mathematical form for predicting effective diffusivity, D_{eff}, for the system with critical

solute to pore diameter ratio in the range of 0.1-0.5, as in the case of this study, was given by Satterfield et al. (1973) as:

$$D_{eff} = \frac{D_A \varepsilon e^{-4.6\lambda}}{\tau K_p} \qquad (4)$$

where

D_{eff} = effective diffusivity

D_A = bulk diffusivity of A

ε = catalyst porosity

$\lambda = \frac{\text{critical solute diameter, SD}}{\text{pore diameter, PD}}$

K_p = adsorption equilibrium constant of the diffusing molecule on the catalyst surface

τ = tortuosity factor of the catalyst

Bulk Diffusivity

The estimation of bulk diffusivity, D_b can be made using the semiempirical correlations proposed by Wilke and Chang (1955), and the Strokes-Einstein equation (Bird et al., 1963). These equations are given as follows:

Strokes-Einstein equation:

$$D_A = 1.05 \times 10^{-9} \frac{T}{\mu V_b^{1/3}} \qquad (5)$$

Wilke and Chang's correlation:

$$D_A = \frac{7.4 \times 10^{-10} \, T(XM)^{1/2}}{\mu V_b^{0.6}} \qquad (6)$$

where

D_A = bulk diffusivity of A, cm^2/sec

T = reaction temperature, °K

X = association parameter for the coal liquid, for aromatic compounds like benzene, toluene, X=1

M = molecular weight of the solvent (coal liquid)

μ = viscosity of the coal liquid, gm/cm/sec

V_b = molar volume of the heteratom containing compound (solute), ml/gm-mole

As discussed by Satterfield and Sherwood (1963), the lower value calculated from either equation should be used as bulk diffusivity. In order to estimate the bulk diffusivity, the viscosity, molecular weight and molar volume of the oil at the desired temperature must be known first. These quantities were not measured in this study, however, can be estimated from the available data in literature. Stein et al. (1978) have used gel permeation chromotography to determine the molecular weights of coal oils which are mixtures of SRC-I and its various solvent from various coal origins. The results were well correlated with the oxygen contents in coal liquids. Using this correlation, the molecular weight of the SRC feedstock in the current study is estimated to be around 400. Peppas (1981) reported the weight average molecular weight of the pyridine soluble portion of a coal liquid to be 500. The molecular weight of currently used SRC feedstock can also be roughly estimated using the method for petroleum fractions given in the Engineering Data Book (1975); this results in a value of 300. Therefore, the average molecular weight of the SRC feedstock in this study should be in the range of 300-500.

No viscosity data of coal liquids at a reaction temperature of 400 C are available. However, values can be extrapolated from lower temperature data. Given et al. (1977) have measured the viscosities of

SRC-I mixtures with different proportions of solvent at various temperatures up to 204 C. Using their data and extrapolating to 400 C, the viscosity is 0.002 Pa·s for the 30% SRC-I/process solvent mixture. Stein et al.(1971) used the following correlation (Reid et al., 1977) to fit their viscosity data of SRC-I and its porous solvent mixtures:

$$\ln (KV) = X_{sol} [A_{sol} + E_{sol}/(T + B_{sol})] + X_{SRC} [A_{SRC} + E_{SRC}/(T + B_{SRC})] \quad (7)$$

where

KV = kinematic viscosity

T = temperature

X = weight fraction of solvent or SRC-I

A, B, E = constants

Using the regression values by Stein et al. (1978) for the constants the viscosity of the SRC feedstock in this study is 0.002 Pa·s at 400 C. Kershaw et al. (1980) also measured the viscosity of a hydrogenated oil, when extrapolated to 400 C, it has a value of 0.001 Pa·s. Note that the oil viscosity does not change as significantly with different oil at high temperatures as at low temperatures.

From the above available molecular weight and viscosity information, the bulk diffusivity of the current SRC feedstock was estimated to be between 0.45 and 5.0 10^{-9} m^2/s. This diffusivity range will be compared to the model results next.

Mechanisms of Catalyst Deactivation

As discussed in Chapter II, catalyst deactivation can be due to sintering, poisoning, inorganic and carbonaceous deposits. Sintering is caused by high temperature and/or long oil-catalyst contact time, and can result in loss of surface area and increase in pore size due to the agglomeration of the support. In the previous study (Ahmed, 1979), the regenerated catalysts from hydrotreating a Synthoil feedstock were observed to have essentially the same most frequent pore size as fresh catalyst. Some decreases in surface area were noted, however, it was due to the metal deposits. In this study, the most frequent pore sizes of the spent catalysts decreased significantly whereas the surface areas remained essentially the same as those of the fresh catalysts. All these facts indicate that sintering effects in this study is insignificant if any. In any case, sintering occur at much higher temperature than in this study.

Poison deactivation is mainly caused by the adsorption of basic nitrogen compounds in coal liquid, as discussed in Chapter II. Scanning Auger microscopic analyses on the pyridine washed spent catalysts showed that the nitrogen-to-carbon atom ratios were lower than 1:40 which is in the range of the heavy end of the feedstock. These facts indicate that concentrations of nitrogen compounds were not especially high on the catalyst surfaces. Therefore, the basic compounds poisoning should not be a major concern in this catalyst deactivation study.

Metal deposition were not a primary catalyst deactivation mechanism either in this study. This is judged from the facts the oil feedstocks had low ash content and the run durations were short (less

than 153 hours for those with the SRC feedstock). Moreover, scanning Auger microscopic analyses showed no detectable inorganic deposits on the aged catalysts.

Coke deposits on the spent catalyst were as high as 14 wt% based on the freshly sulfided catalyst as Table V shows. These high coke contents can occupy up to one half of the pore volume in the fresh catalyst, and can block the pore mouths as the results of the porosimetric and scanning Auger microscopic analyses revealed. The effects of coke on catalyst are further confirmed by comparing the physical properties of the fresh, spent and regenerated catalysts. Table VI and Figures 34 and 35 show that although the pore volumes and most frequent pore diameters of the spent catalysts have been reduced by more than one third, these pore volumes and pore diameters were recovered to the values of the fresh catalyst after regeneration. Surface areas were also recovered as shown in Table VI. All of these facts indicate that the property changes in spent catalysts are mainly caused by coke or carbonaceous depositions. Therefore, such depositions on the catalysts in this study is the primary deactivation mechanism with inorganics depositions, basic nitrogen adsorption and sintering the secondary mechanisms.

Model Development

In this section, an attempt will be made to develop a reaction-deactivation model to represent the experimental observations in this study. Only coke deposits will be considered since the other three decay mechanisms were not significant. And since Run LTB with the

TABLE VI

PHYSICAL PROPERTIES OF THE FRESH, THE SPENT AND THE REGENERATED CATALYSTS

	Surface Area ($10^3 m^2/kg$)	Pore Volume ($10^{-3} m^3/kg$)	Most Frequent Pore Diameter (nm)
Fresh Shell 324	146	0.430	11.8
Freshly Sulfided	160	0.430	11.0
Section 2, Run LTZ			
Spent	176	0.336	8.4
Regenerated	142	-	-
Section 2, Run LTX			
Spent	167	0.351	8.4
Regenerated	146	-	-
Section 2, Run LTW			
Spent	165	0.304	8.0
Regenerated	145	0.425	11.1
Section 2, Run LTY			
Spent	159	0.241	6.3
Regenerated	143	0.408	11.3

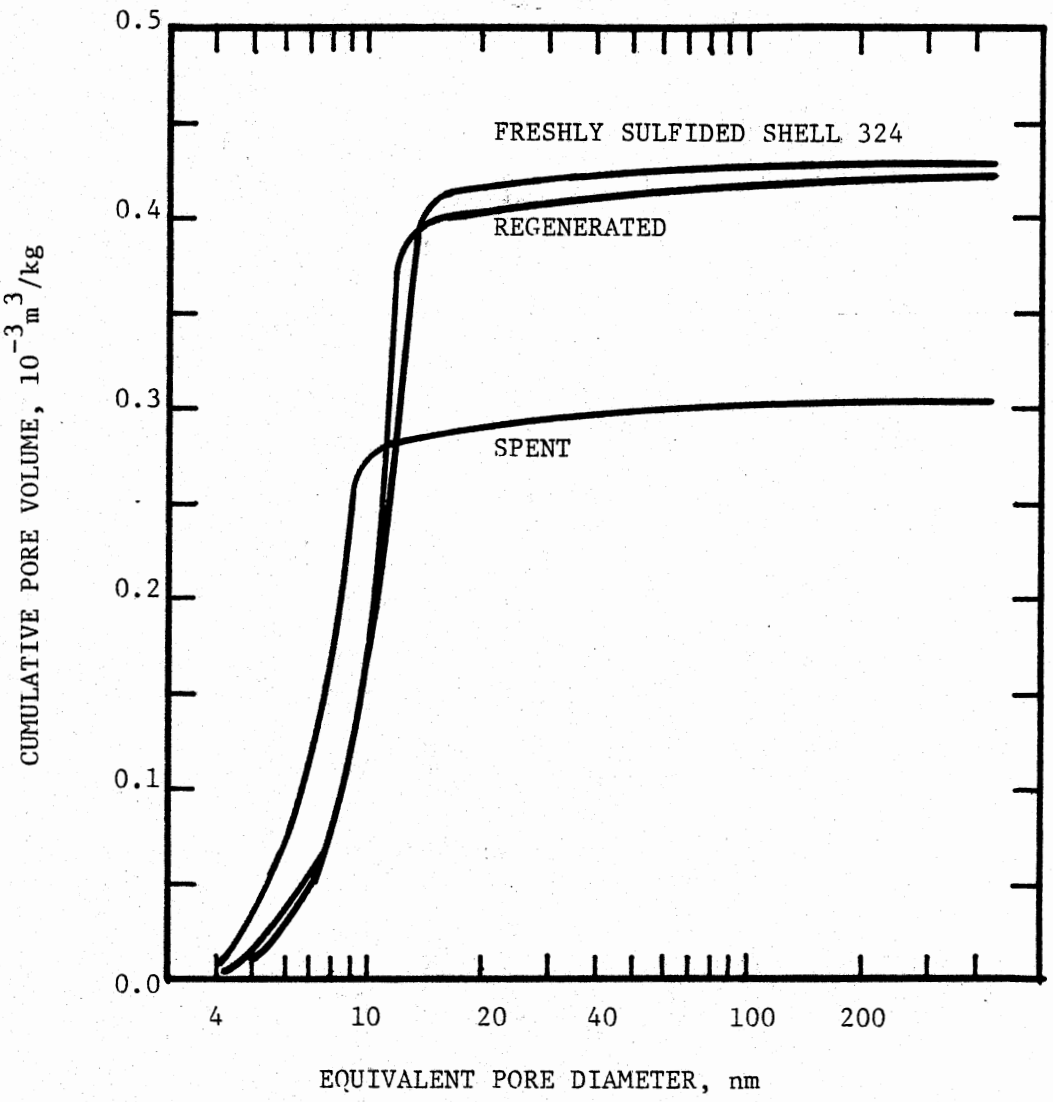

Figure 34. Cumulative Pore Volumes of the Catalyst from Section 2, Run LTW

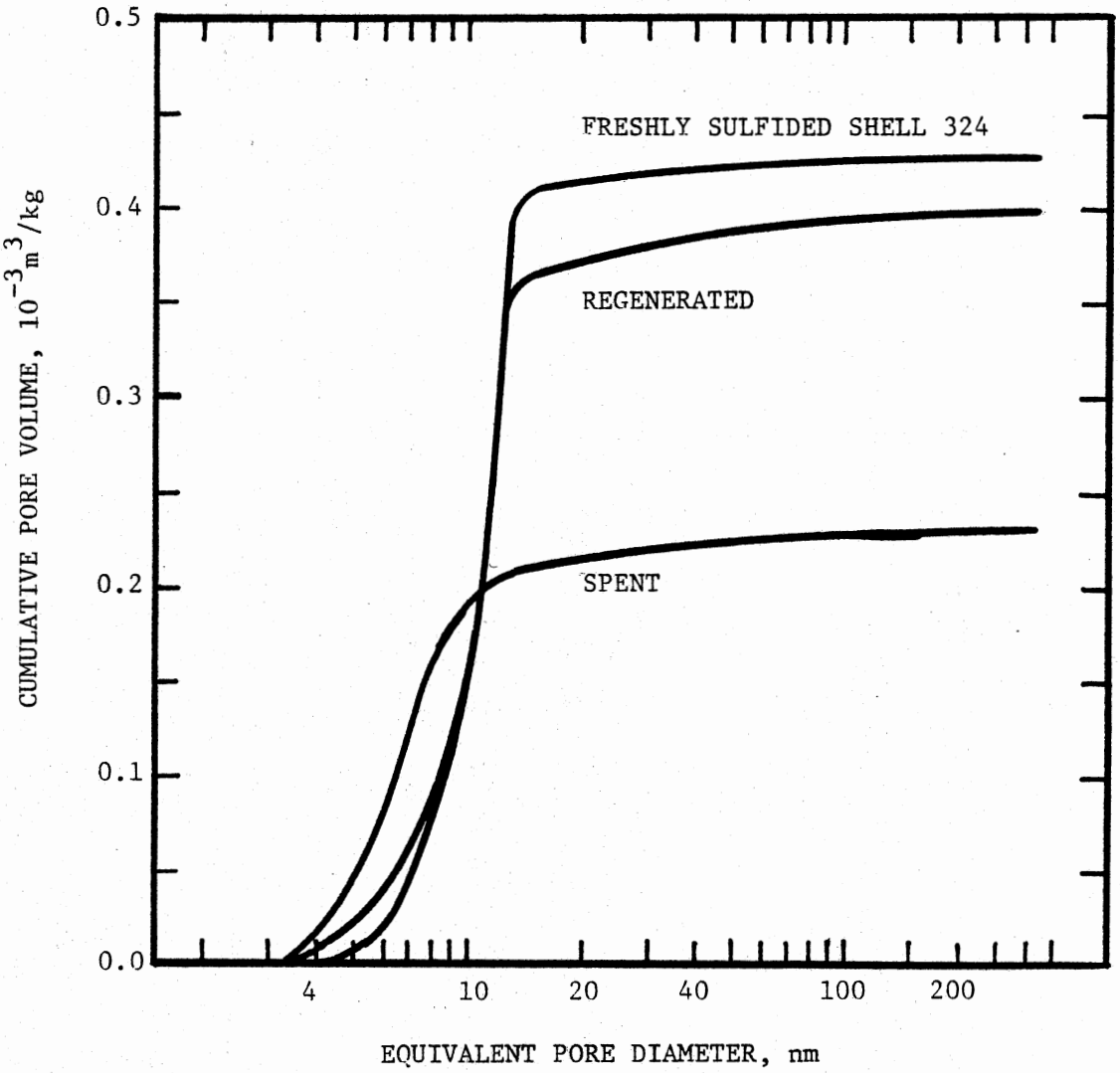

Figure 35. Cumulative Pore Volumes of the Catalyst from Section 2, Run LTY

EDS oil feedstock did not show any activity decay, only those runs with the SRC oil feedstock will be used for modeling.

Assumptions and Approaches

As discussed in the literature review, in the case of parallel fouling, the reactor catalyst coke profile decreases from the entrance to the exit, and the coke on catalyst pellet profile decreases from the periphery toward the center. The experimental results of the coke on catalyst profiles in reactor beds from combustion analyses and the profiles in single pellets from scanning Auger analyses consistently shown that the coke formation in this study is via a parallel route.

A deactivation model based on parallel fouling and catalyst coke content, a true deactivation parameter, was developed to represent the experimental observations, including activity-time profile, coke-time profile, coke-space profiles in reactor beds and catalyst pellets, and the pore size-coke relationship. For modeling purposes the conditions in the hydrotreatment operations were assumed to be as follows:

1. The catalyst pellet is surrounded by a liquid film. Earlier discussions on the reactor liquid holdup and solid-liquid contacting efficiency justify this assumption.

2. A large excess of hydrogen is available for reactions in the liquid phase. This implies that the hydrogen solubility is high and no mass transfer limitation exists between gas and liquid phases. At temperatures between 100 and 400 C (212-750 F) and hydrogen pressures between 3.5 and 20.7 MPa (500-3000 psig), the solubility of hydrogen in creosote oil was reported to increase linearly with hydrogen pressure (Prather et al., 1977). However, increasing the hydrogen

pressure beyond 6.9 MPa (1000 psig) while hydrotreating raw anthracene oil and Synthoil liquid has been observed to have less significant effect on the heteroatom removal activity of a $CoMo/Al_2O_3$ catalyst (Soni, 1977; Sooter, 1974). This means that in the present study, at the reaction pressure of 13.9 MPa, excess hydrogen in the liquid phase was available and bulk pahse transfer limitations were negligible.

3. Catalyst pores are filled with coal-derived liquid. Ketkar (1977) in his study with FMC oil observed complete pore filling of alumina supports at atmospheric pressure and 138 C (280 F). Under reaction conditions of 13.9 MPa (2000 psig) and 400 C (750 F) coal liquids can encounter lesser resistances due to lower viscous and surface tension forces, and hence, can be assumed to completely fill the pores.

4. Only those reactions catalyzed by catalyst surfaces are significant. Most of the surface area lies within the internal porous structure, as in the case for the high surface area catalyst as used in this study. The reactants must diffuse into the pores to utilize the internal surface area.

With the above assumptions, the approach in this model development consisted of the following:

5. The reactor is in ideal plug flow with negligible radial gradients and axial dispersion.

6. The reactor is isothermal throughout. Although this takes the risk of over simplification, this is still the best approach in this study. Any deviation caused by non-isothermality will be discussed later.

7. The main and coking reactions can be represented by two simple, pseudo, first order, parallel reactions (routes 1 of the coking scheme presented on Page 38):

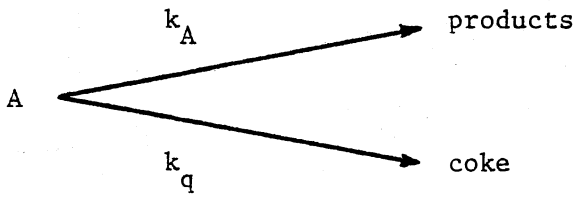

(8)

where k_A and k_q are intrinsic rate constants, $m^3/s/kg\text{-catalyst}$, for the main and the coking reactions respectively.

8. The coking rate is much slower than the main reaction rate, that is $k_q << k_A$. This assumption will be justified later.

9. The intrinsic reaction rate linearly decrease with increasing coke content on the catalyst. For first order reactions, these can be expressed as:

$$R_A = -k_A(1 - q_p)^M C_{Ap} \tag{9}$$

$$R_q = k_q (1 - q_p)^N C_{Ap} \tag{10}$$

where

M, N = orders of dependency of the activities on the active sites

R_A, R_q = surface reaction rates of the main and coking reactions, respectively, kg/s/kg-catalyst

q_p = dimensionless local coke content in the catalyst pellet, Q_p/Q_m

Q_p = local coke content in the catalyst pellet, kg-coke/kg-catalyst

Q_m = Maximum coke content can from on the catalyst, kg-coke/kg-catalyst

C_{Ap} = local concentration of the main reactant in the catalyst pellet, kg/m^3

k_A, k_q = intrinsic reaction rate constants for the main and the coking reactions, respectively, $m^3/s/kg\text{-catalyst}$

The last two equations show that, instead of relating to time directly, the activity decay is related to the coke content which is the true catalyst deactivation parameter in this study.

10. The catalyst porosity is reduced by the coke according to the equation:

$$\varepsilon_p = \varepsilon_{po} - Q_p \, (\rho_p/\rho_q) \tag{11}$$

where

ε_p = catalyst porosity at any time

ε_{po} = catalyst porosity at initial conditions

ρ_p = bulk density of the catalyst pellet, kg/m^3

ρ_q = coke density, kg/m^3

11. The catalyst pellet consists of cylindrical pores which are parallel to each other. The diameter of these pores are uniform initially and are uniform at the same cross face at any time. Thus the local pore diameter can be expressed as:

$$PD = PD_o(\varepsilon_p/\varepsilon_{po})^{1/2} \tag{12}$$

where

PD = local pore diameter, nm

PD_o = pore diameter at initial conditions, nm

12. Effective diffusivity of the reactant in the porous catalyst, D_{Ae} follows the correlation (Satterfield et al., 1973):

$$D_{Ae} = \frac{D_A \varepsilon_p}{\tau} \; e^{-4.6\lambda}$$

where

D_A = bulk diffusivity of species A, m^2/s

τ = tortuosity of the catalyst pore

λ = ratio of the critical solute diameter to pore size, SD/PD

SD = critical solute diameter, nm

As discussed earlier in this chapter, this equation is valid for values in the range of 0.1-0.5. This λ value along with D_A, τ and SD will be further discussed following the model development. The equilibrium adsorption coefficient, K_p does not appear in the equation since it will be automatically incorporated in the reaction term in the equation for overall mass balance.

Mass Balance Over the Catalyst Pellet

Mass balance over a spherical catalyst pellet for the main reactant A can be written as:

$$\frac{1}{r^2} \frac{\partial}{\partial r} \left(r^2 D_{Ae} \frac{\partial C_{Ap}}{\partial r} \right) - \rho_p k_A (1 - q_p)^M C_{Ap} = \varepsilon_p \frac{\partial C_{Ap}}{\partial t} \qquad (14)$$

and for coke formation as:

$$\frac{\partial Q_p}{\partial t} = k_q (1 - q_p)^N C_{Ap} \qquad (15)$$

where

r = position in the pellet from the center, m

t = time on stream, s

D_{Ae} in the equation (14) can not be taken as a constant, since it is a function of coke content which in turn a function of time and position. Full derivation details are found in Appendix H.

Since the reactor was started up by filling with gas and liquid at lower than the normal reaction temperature, the void spaces in the catalyst pellet and in the reactor bed can be assumed to be filled with liquid initially. Thus the initial and boundary conditions can be written as follows:

initial conditions:

$$\text{at } t = 0 \text{ and } 0 \leq r \leq r_e,\ C_{Ap} = C_{Ab} \text{ and } Q_p = 0 \qquad (16)$$

boundary conditions:

$$\text{at } r = 0 \text{ and } t > 0,\ \frac{\partial C_{Ap}}{\partial r} = 0 \qquad (17)$$

$$\text{at } r = r_e \text{ and } t > 0,\ C_{Ap} = C_{Ab} \qquad (18)$$

where

r_e = equivalent radius of the catalyst pellet, m

C_{Ab} = concentration of reactant A in the bulk liquid surrounding the pellet, kg/m

The last boundary condition, equation (18), is derived from the assumption that diffusional resistances external to the pellet are negligible.

For convenience and broader application, the above equations are expressed in terms of dimensionless parameters as follows:

1. For the main and coking reactions (from equations (14) and (15)):

$$\frac{1}{x^2}\frac{\partial}{\partial x} Dx^2 \frac{\partial y_p}{\partial x} - h_A^2 (1 - q_p)^M y_p - h_q^2 \varepsilon \frac{\partial y_p}{\partial \theta_p} = 0 \qquad (19)$$

$$\frac{\partial q_p}{\partial \theta_p} = (1 - q_p)^N y_p \qquad (20)$$

2. For catalyst porosity and effective diffusivity (from equations (11) - (13)):

$$\varepsilon = 1 - \gamma q_p \tag{21}$$

$$\lambda = \lambda_o / \varepsilon^{1/2} \tag{22}$$

$$D = \beta \varepsilon e^{-4.6\lambda} \tag{23}$$

3. For initial and boundary conditions (from equations (16) - (18)):

at $\theta_p = 0$ and $0 \leq x \leq 1$,

$$y_p = 1,\ q_p = 0,\ \varepsilon = 1 \text{ and } D = 1 \tag{24}$$

at $x = 0$ and $\theta_p > 0$,

$$\frac{\partial y_p}{\partial x} = 0 \tag{25}$$

at $x = 1$ and $\theta_p > 0$, $y_p = 1$ (26)

where

x = dimensionless position in the pellet, r/r_e

θ_p = dimensionless catalyst age, $C_{Ab} k_q\ t/Q_M$

y_p = dimensionless reactant concentration in the pellet, C_{Ap}/C_{Ab}

h_A = Thiele modulus for the main reaction, $r_e \sqrt{\rho_p\ k_A / D_{Ao}}$

h_q = Thiele modulus for the coking reaction, $r_e \sqrt{C_{Ab} \varepsilon_{po}\ k_q / Q_M D_{Ao}}$

D_{Ao} = initial effective diffusivity, $(D_A\ \varepsilon_{po}/\tau) e^{-4.6\lambda}$

D = dimensionless effective diffusivity, D_{Ae}/D_{Ao}

λ_o = initial ratio of critical solute diameter to pore diameter, SD/PD_o

ε = porosity ratio, $\varepsilon_p/\varepsilon_{po}$

β = dimensionless constant, $\varepsilon_{po} D_A/D_{Ao}\tau$

γ = dimensionless constant, $Q_M \rho_p/\varepsilon_{po}\rho_q$

The other parameters which do not appear above have been defined earlier under appropriate equations.

Effectiveness factors for the main and coking reactions, η_A and η_q, defined as the ratios of the actual reaction rates at time θ_p to the maximum reaction rates on a clean catalyst without diffusional limitations can be calculated from the following equations:

$$\eta_A = \frac{\int_o^{r_e} k_A(1-q_p)^M C_{Ap}(4\pi r^2)dr}{\frac{4}{3}\pi r_e^3 k_A C_{Ab}} = 3\int_o^1 (1-q_p)^M y_p x^2 dx \qquad (27)$$

$$\eta_q = \frac{\int_o^{r_e} k_q(1-q_p)^N C_{Ap}(4\pi r^2)dr}{\frac{4}{3}\pi r_e^3 k_q C_{Ab}} = 3\int_o^1 (1-q_p)^N y_p x^2 dx \qquad (28)$$

These effectiveness factors are indications of the catalyst pellet performance under a coking environment and will be used in modeling the reactor bed performance as presented next. In the absence of deactivation, the effectiveness factor can be expressed as a function of Thiele modulus. In the presence of deactivation, the catalyst effectiveness factor can be expressed as a function of coke content and Thiele modulus when the coke is the only deactivation parameter. Alternatively, the effectiveness factor can be expressed as a function of Thiele modulus and time on stream since coke content is in turn a function of time on stream.

Mass Balance Over the Reactor Bed

The mass balance equations over the reactor bed for the pseudo first order main and coking reactions are:

$$\varepsilon_b \frac{\partial C_{Ab}}{\partial t} = - \frac{F}{S} \frac{\partial C_{Ab}}{\partial Z} - \rho_b \, k_A \, \eta_A \, C_{Ab} \tag{29}$$

$$\frac{\partial Q_b}{\partial t} = k_q \, \eta_q \, C_{Ab} \tag{30}$$

with initial conditions

at $t = 0$ and $0 \leq Z \leq L$,

$$C_{Ab} = C_{Af}, \text{ and } Q_b = 0 \tag{31}$$

and boundary conditions

$$\text{at } Z = 0 \text{ and } t > 0, \; C_{Ab} = C_{Af} \tag{32}$$

where

ε_b = porosity of the catalyst bed

F = volumetric oil feed rate, m^3/s

S = reactor cross section area, m^2

Z = longitudinal position from reactor entrance, m

ρ_b = packed density of the catalyst in the reactor bed, kg/m^3

Q_b = local coke content in the reactor bed, kg-coke/kg-catalyst

C_{Af} = concentration of the reactant A in the feed, kg/m^3

In terms of dimensionless form, equations (29) - (32) can be written as:

$$\frac{\partial y_b}{\partial \theta_b} + E \frac{\partial y_b}{\partial z} + G \, \eta_A \, y_b = 0 \tag{33}$$

$$\frac{\partial \psi_b}{\partial \theta_b} = \eta_q \, y_b \tag{34}$$

at $\theta_b = 0$ and $0 \leq z \leq 1$,

$$y_b = 1 \text{ and } q_b = 0 \tag{35}$$

at $z = 0$ and $\theta_b > 0$,

$$y_b = 1 \tag{36}$$

where

y_b = dimensionless reactant concentration in the reactor bed, C_{Ab}/C_{Af}

θ_b = dimensionless reactor age, $C_{Af}\ k_q\ t/Q_M$

z = dimensionless reactor position, Z/L

E = dimensionless constant, $Q_M/C_{Af}\ k_q\ T$

G = dimensionless constant, $k_A\ \rho_b\ Q_M/C_{Af}\ k_q$

q_b = dimensionless local coke content in the reactor bed, Q_b/Q_M

L = total reactor length, m

T = Liquid volume space time, s

Full, detailed derivations are contained in Appendix H. This model is significant because it incorporates a variable diffusivity as a function of coke deposition, activity is related to coke content, time and space profiles for coke can be predicted within both pellet and reactor, and the effects of diffusional resistances on the catalyst life can also be predicted.

Methods of Solutions

The above differential equations have coupled dependent variables, therefore these are non-linear, partial differential equations which in general must be solved numerically. Masamune and Smith (1966) and

Froment and Bischoff (1961) used a finite difference method to solve the reaction-deactivation problems similar to those in this study. They assumed pseudo steady states which mean that the rate of concentration change is slow with respect to that of the main reaction; this assumption resulted in savings of computer time. Recently Broghi et al. (1976), Dudukovic (1976), and Lamba and Dudukovic (1978) have developed integral transform techniques to transform non-linear coupled differential equations into a single non-linear diffusion-reaction equation which can be solved more readily by numerical techniques.

Some approximate solutions have also been presented. Tai and Greenfield (1978) developed approximate analytical expressions for a time-dependent effectiveness factor for the cases of a spherical catalyst. Their method of solution involves describing the activity profile within the catalyst by one or more functions which are linear in radial position.

In this study, such advanced or elegant approaches in solving these non-linear partial differential equations have not been attempted due to the lengthy time involvement and the uncertainty in saving computer time. Instead, a commonly used finite difference method was employed without any further simplification, such as pseudo steady state approach. Although, compared to other methods, this method of solutions may require more computer time to accomplish, this takes less time to develop and can maintain all of the characteristics of the original equations. The development of the finite difference equations is given in Appendix I. The computer programs for solving these equations over a catalyst pellet and a reactor bed are listed in Tables XII and XIII, respectively, in Appendix I.

Before solving the differential equations, the required physical constants must be determined first. These constants are presented in Table VII. The coke density was calculated from the pore volume-coke content relationship shown in Figure 31. The maximum coke content is taken as the maximal coke the porous structure can tolerate, which is equal to the pore volume multiplied by the coke density. The spherical approach is used for the 1.6 by 4.0 mm extrudate and the equivalent pellet diameter is calculated according to the spherical volume to external surface area relationship. The initial pore diameter is taken as the most frequent pore diameter of the freshly sulfided catalyst.

Although the critical solute diameter and oil bulk diffusivity can be determined experimentally with considerable difficulty, these values could still be uncertain at the hydrotreatment conditions. Therefore, in solving the differential equations, the critical solute diameter, oil bulk diffusivity, orders of catalyst active site dependency and intrinsic kinetic constants were varied to obtain the best data fit. Of course their range of values must be consistent with reasonable and physcially dictated limits.

Since the model is expected to generate the information of activity-time profiles, coke profiles in reactor beds and in catalyst pellets, coke-time profiles and pore size-coke profiles, experimental data on those profiles have been used in the regression to obtain the parameters. A regression technique was used to obtain the data fit. Since there were so many parameters to vary and so many data to be fitted, mathematical method of minimizing the error was not attempted The goodness of fit was judged by graphically comparing to the experimental data.

TABLE VII

CONSTANTS* USED IN MODEL CALCULATIONS

Feedstock density:	$\rho_A = 1.13 \times 10^3$ kg/m^3
Catalyst bulk density:	$\rho_p = 1.42 \times 10^3$ kg/m^3
Catalyst packed density:	$\rho_b = 0.78 \times 10^3$ kg/m^3
Coke density:	$\rho_q = 0.80 \times 10^3$ kg/m^3
Catalyst pellet porosity:	$\varepsilon_p = 0.60$
Catalyst bed porosity:	$\varepsilon_b = 0.78$
Feedstock hydrogen content:	$C_{Ao,H} = 6.73$ wt%
Feedstock nitrogen content:	$C_{Ao,N} = 1.40$ wt%
Maximum coke content:	$Q_M = 0.34$ kg-coke/kg-catalyst
Equivalent radius of the catalyst pellet:	$r_e = 1.0 \times 10^{-3}$ m
Initial pore diameter:	$PD_o = 11.0$ nm
Reactor length:	L = 0.5 m

* Experimentally determined.

Convergence of the Solutions

Convergence is of critical importance in solving complex simultaneous equations numerically. In this study an explicit finite difference method has been used to obtain numerical solutions for the model. A shortcoming of this technique is the slow convergence, especially in the case of higher order partial differential equations. In numerical calculations, the pellet and the reactor were divided into 20 and 40 increments respectively. The dimensionless time increment was 0.00004 for solving the pellet equations, and 0.001 for the reactor bed equations. A dimensionless time increment of 0.001 corresponds to a real time increment of 66 seconds. This time increment was small compared to a nominal space time of 2.50 hours and run durations of 1-153 hours. Note that the very small time increment for solving the pellet equations was needed due to the nature of the second order differential equation involved. In order to check the convergence, time and space increments were decreased several folds to see if there were any convergence problems and to see if reasonable accuracy had been obtained. Figures 36 and 37 show the effects of decreasing stepsize on the product oil concentration and coke content from the trickle bed calculations. In Figure 36 the top line is a result of using double stepsizes and the bottom line is a result of using half of the normal stepsizes. As can be seen the change in the resulting concentration would not be any more significant if the stepsizes were further reduced. Figure 37 shows no change in coke content as a result of decreasing stepsizes. Therefore, the normal stepsizes which resulted in the middle line in

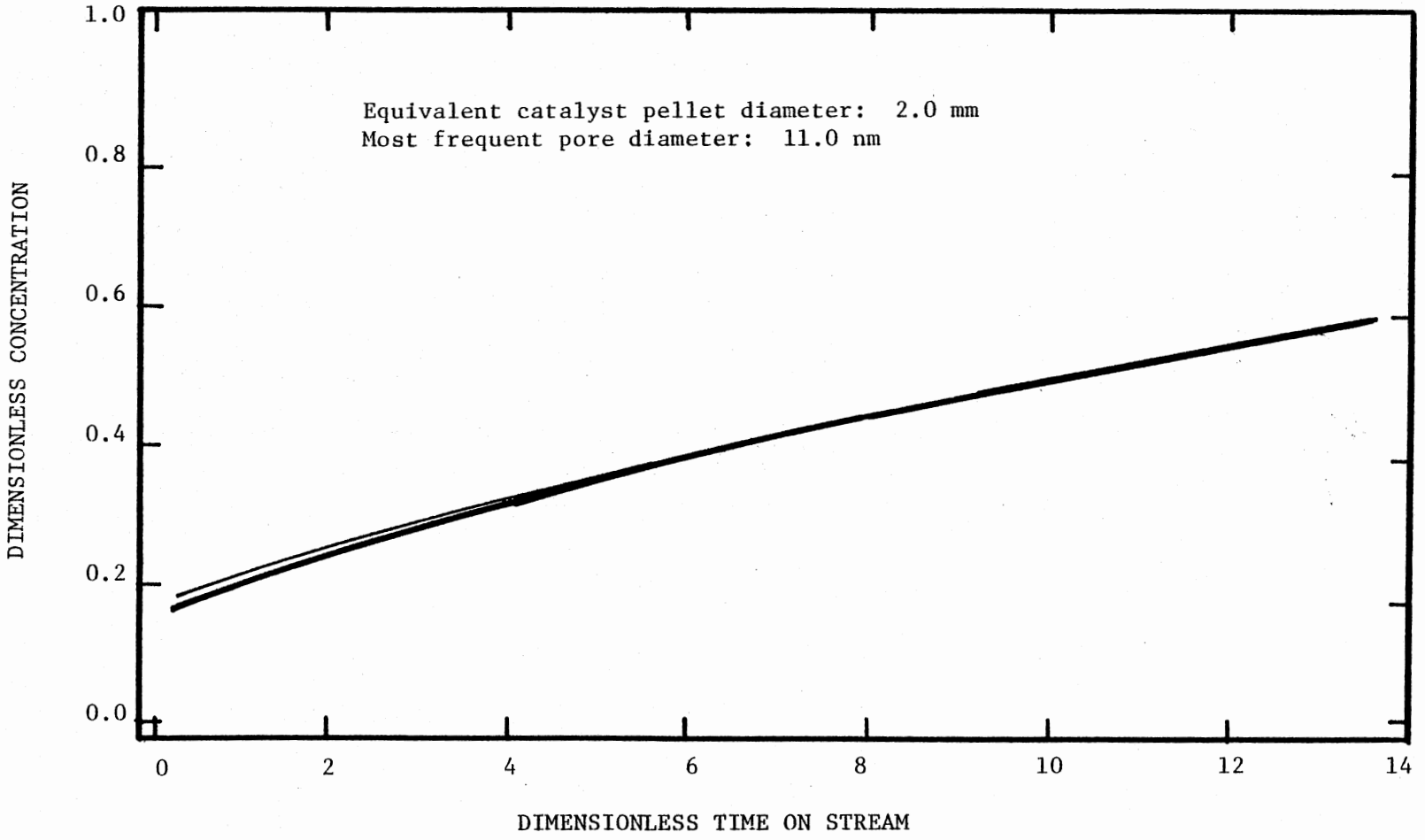

Figure 36. Effect of the Stepsize on the Resulting Concentration

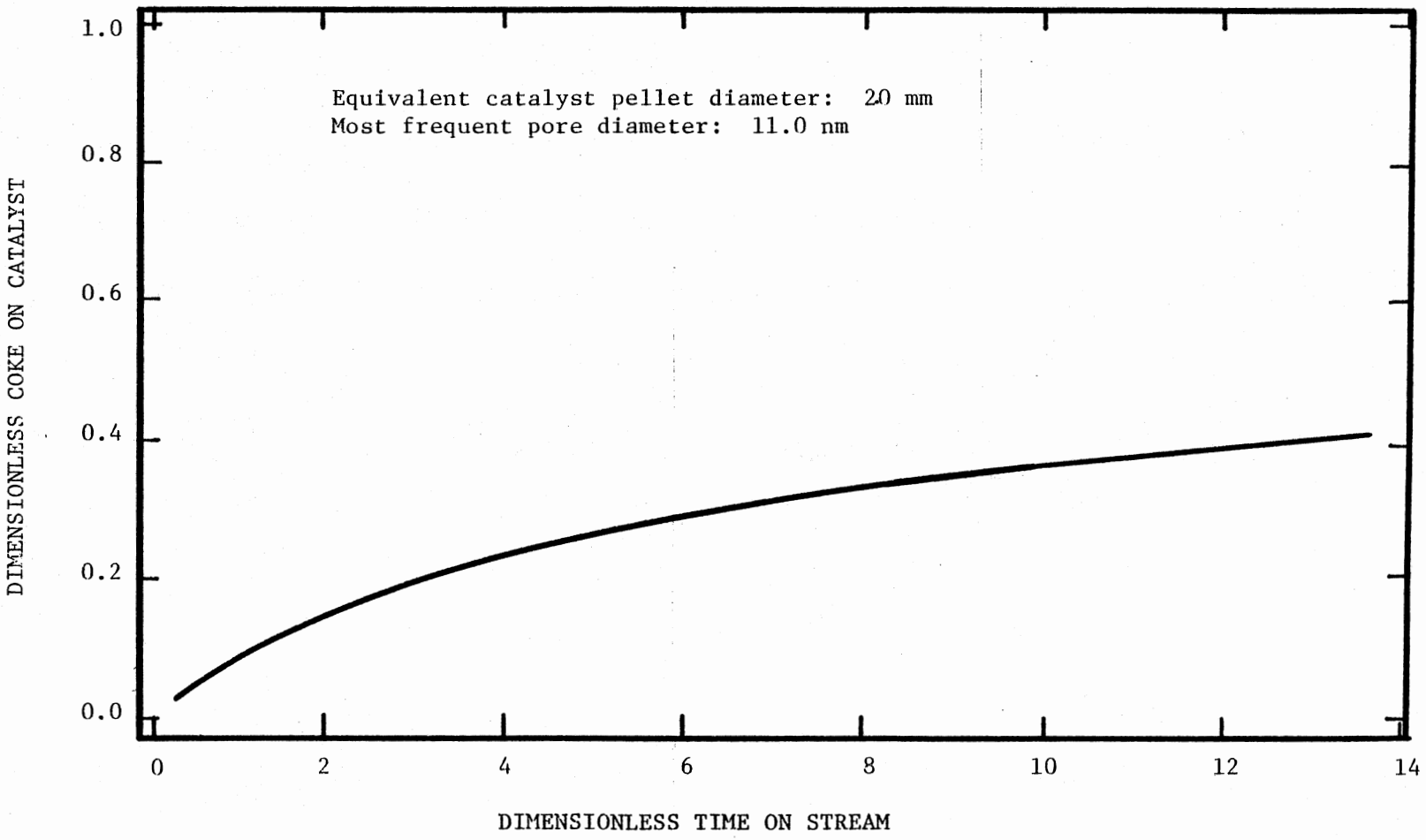

Figure 37. Effect of the Stepsize on the Resulting Coke Content

Figure 36 were small enough and were used in the data fitting.

Results of Regression

From the data fit, the resulting parameters are listed in Table VIII. The order of dependency of coke formation on the uncovered, active catalytic sites is 2 meaning that the coke formation takes dual sites. This higher order dependency makes the rate of coke accumulation decrease rapidly with time on stream. While the order of dependency of the main reaction on the clean active site is one half meaning that some of the smaller molecules are still able to utilize the covered active sites. That the coke covered sites are accessible for the reactants becomes clear when one investigates the results from Run LTB with the EDS oil feedstock. In Run LTB no catalyst activity decay was observed even though the coke on the catalyst had accumulated up to a level of 17 wt% (Table V), which should cover a significant fraction of the active surface. This high coke level and yet high activity may have been due to the possibility that the coke does not further restrict molecular diffusion and moreover, the molecules of coal oil may still be able to utilize the covered sites for reactions. Note that the EDS oil feedstock was a mixture of solvent and vacuum gas oil containing negligible residue of boiling point higher than 538 C (1000 F). Thus molecules of the EDS oil feedstock should be much smaller than those of the SRC feedstock, and should be less subjective to form large micelles which are sterically hindered from reaction sites.

The intrinsic kinetic rate constants for the coking reactions in terms of hydrogen and nitrogen contents are 0.95 and 3.70 10^{-9} $m^3/s/$

TABLE VIII

RESULTING PARAMETERS FROM DATA FITTING

Variable	Description	Value
	Intrinsic kinetic rate constants, $m^3/s/kg$-catalyst	
k_A	Main reaction	1.13×10^{-6}
	Coking reaction in terms of	
$k_{q,H}$	Hydrogen Content	0.95×10^{-9}
$k_{q,N}$	Nitrogen Content	3.70×10^{-9}
	Order of Catalytic site dependency	
m	Main Reaction	1/2
n	Coking reaction	2
SD	Critical solute diameter, nm	3.3
D_A	Bulk diffusivity, m^2/s	0.19×10^{-9}
h_A	Thiele modulus for the main reaction at clean catalyst conditions	11.4
n_A	Effectiveness factor for the main reaction at clean catalyst conditions	0.25

kg-catalyst respectively. These rate constants are small compared to that of the main reaction, 1.13 x 10^{-6} m^3/s/kg catalyst and thus justifies the earlier assumption (P. 131). Note that the rate constant of hydrogenation is equal to that of hydrodenitrogenation; this is resulted from the model fit and is supported by literature (Chu and Wang, 1982; Gates, et al., 1979). Previously in the hydrotreatment of Synthoil liquids, the observed first order rate constants for hydrodenitrogenation at temperatures between 370-450 C were reported to be between 0.036 and 0.25 10^{-6} m^3/s/kg-catalyst (Ahmed, 1979). In considering an effectiveness factor of 0.25 in this study, the currently used Shell 324 catalyst has higher activity than the catalyst previously studied (Ahmed, 1979). This higher activity is expected since the Shell 324 catalyst has been reported to be one of the most active catalysts in coal liquid hydrotreatment.

A critical solute diameter of 3.3 nm has been generated from the model fit. Whitehurst (1979b) has reported that the average molecular sizes of SRC coal oil were between 2.0 and 4.0 nm. A value of 3.3 nm falls in this range. Note that the solute diameter obtained from data fit is relative to the pore diameter which was determined by mercury porosimetry.

As discussed in Page 123, the SRC oil feedstock has a bulk diffusivity in the range of 0.5 - 5.0 10^{-9} m^2/s. The regressional result shows a value of 0.19 x 10^{-9} m^2/s which is well below the estimated value; however, it is still reasonable, since the properties of coal oils may vary widely with coal origin and process conditions.

The intrinsic rate constants, bulk diffusivity, critical solute diameter, intrinsic rate dependencies on catalyst site, Thiele moduli

and effectiveness factors all fall within reasonable ranges as discussed above. Therefore, the model assumptions, approaches and method of solutions are reasonable and reliable.

Comparison of Model Results and Experimental Data

Average Coke Contents

With the constants and parameters listed in Tables VII and VIII, the model results will be compared to the experimental data. Figure 38 shows excellent consistency has been obtained between model prediction and experimental data for the average catalyst coke content in the reactor bed versus time on stream. Note that within the time period of reactor startup plus one hour of operation, the average catalyst coke content in reactor bed is already at about 5 wt%. The model can not be applied to this startup and initial period with the rapid transients of temperature and activity 'spike'. This transient behavior is beyond the scope of this study. However, compensation for this interval was made by a time translation of the model: a model time of 36 hours is fixed at an experimental time of zero. As discussed earlier in Chapter V, reactor radial temperature differential of more than 25 C in the startup stage has been observed. About four-fifths of this difference were across the catalyst bed itself. High temperature has apparently resulted in excess coke formation. Startup of the reactor at reasonably lower temperatures in order to control coke formation and to better maintain the catalyst activity is, therefore, important. The successfulness of this time translation strongly indicates that coke is a true catalyst deactivation parameter, i.e.,

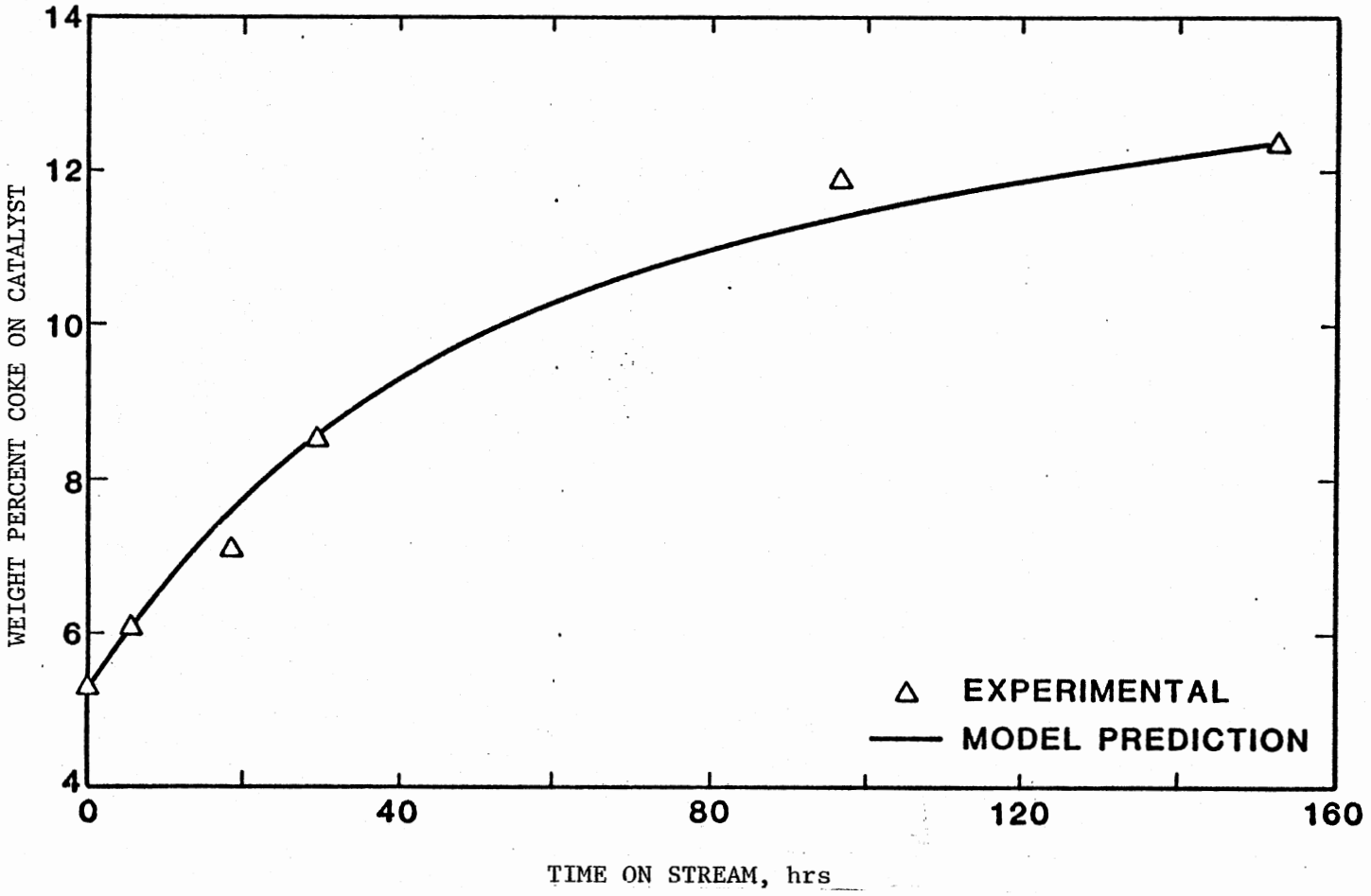

Figure 38. Average Catalyst Coke Content Over the Reactor Versus Time on Stream

catalyst activity can be related to coke on catalyst. This 36 hours time translation will stay valid whenever the model predictions are compared to the experimental data on a time on stream basis.

Catalyst Activity Versus Time on Stream

Figure 39 and 40 show the catalyst activity in terms of hydrogen and nitrogen contents, respectively, in product oil versus time on stream. Satisfactory data fits have been obtained. Note that the experimental data from different runs with different space times have been normalized to a liquid volume space time of 2.50 hours according to a pseudo, first order, power law and plug flow model which are two of the assumptions made earlier in model development. This normalization method was discussed on page 86. An equilibrium hydrogen concentration of 12.2 wt% is assumed in this normalization of hydrogenation activity responses. This is a reasonable assumption because: the aromatic compounds favor complete hydrogenation at hydrotreating conditions of 400 C and 13.9 MPa (Kobe and McKetta, 1963); and the hydrogen contents of the completely hydrogenated 3 to 5 ring aromatic compounds are 12.5 to 12.0 wt% respectively. The SRC feedstock was estimated earlier in this chapter to have a molecular weight between 300 and 500 which indicates that this SRC oil contained a significant fraction of high molecular weight aromatic compounds.

Coke Profiles in the Reactor Beds

Coke profiles in the reactor bed are also well represented by the model as shown in Figure 41. Although not very explicit, the profile becomes flatter as time proceeds. A flatter profile means

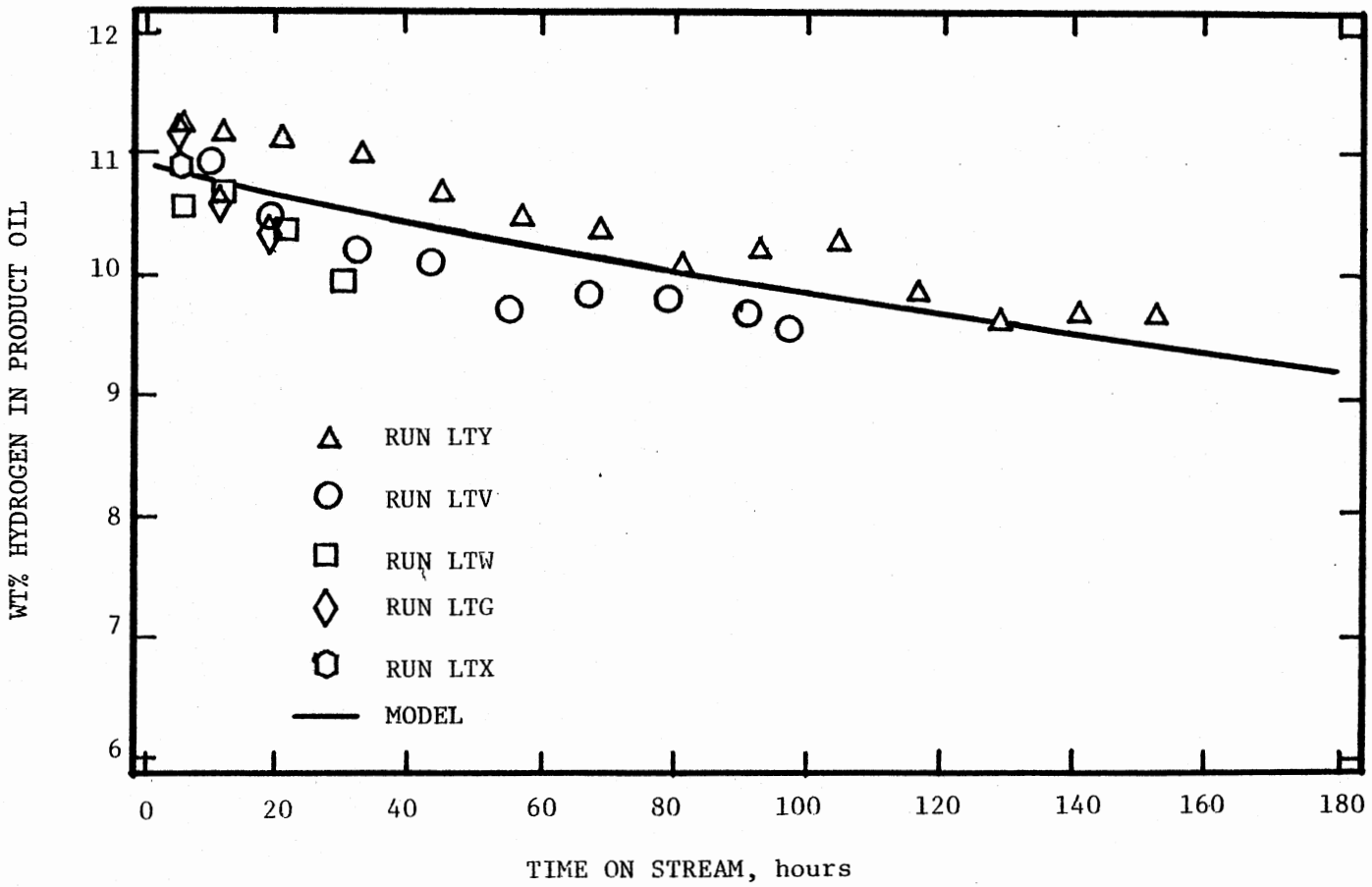

Figure 39. Catalyst Hydrogenation Activity Versus Time on Stream

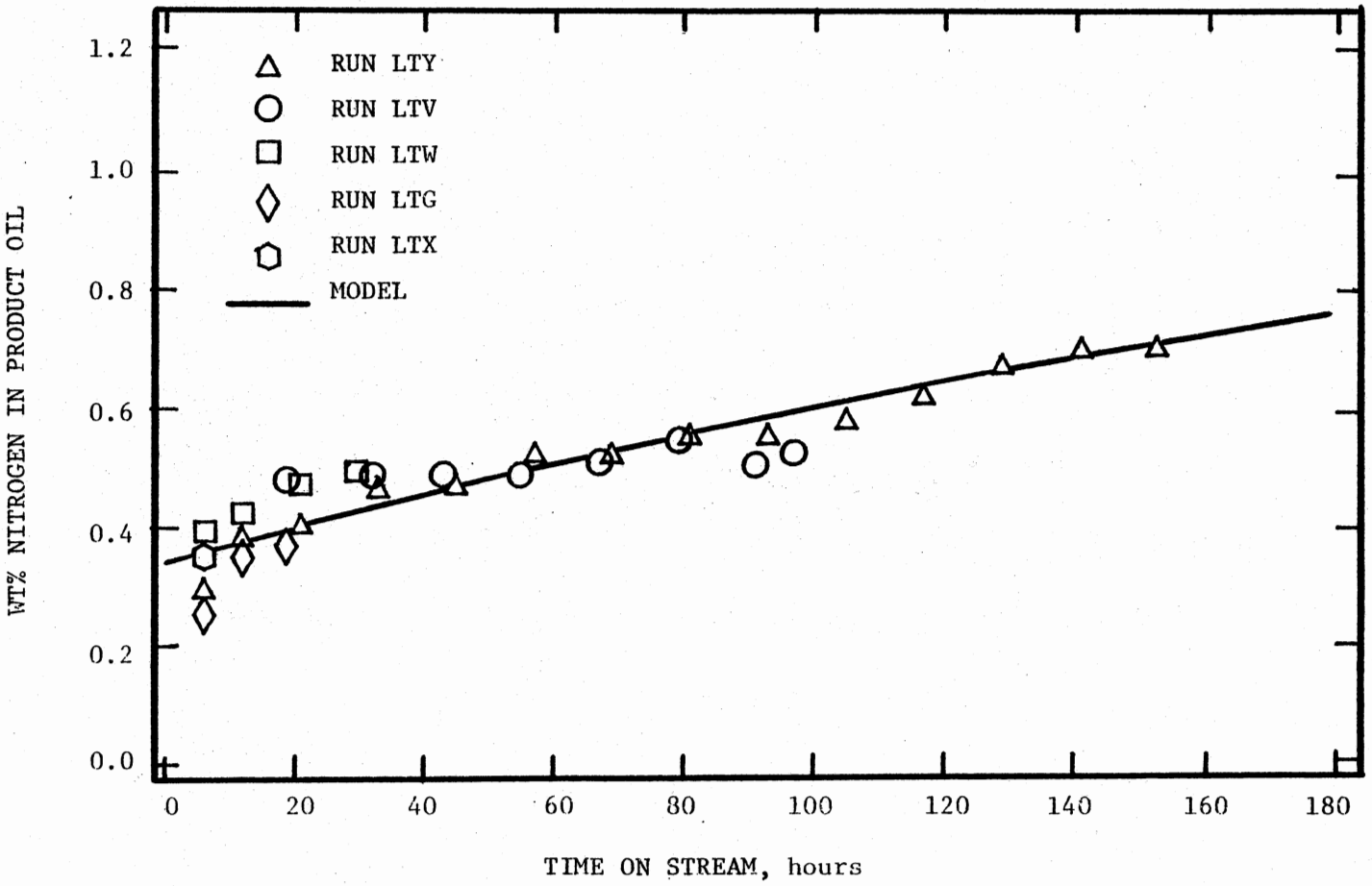

Figure 40. Catalyst Hydrodenitrogenation Activity Versus Time on Stream

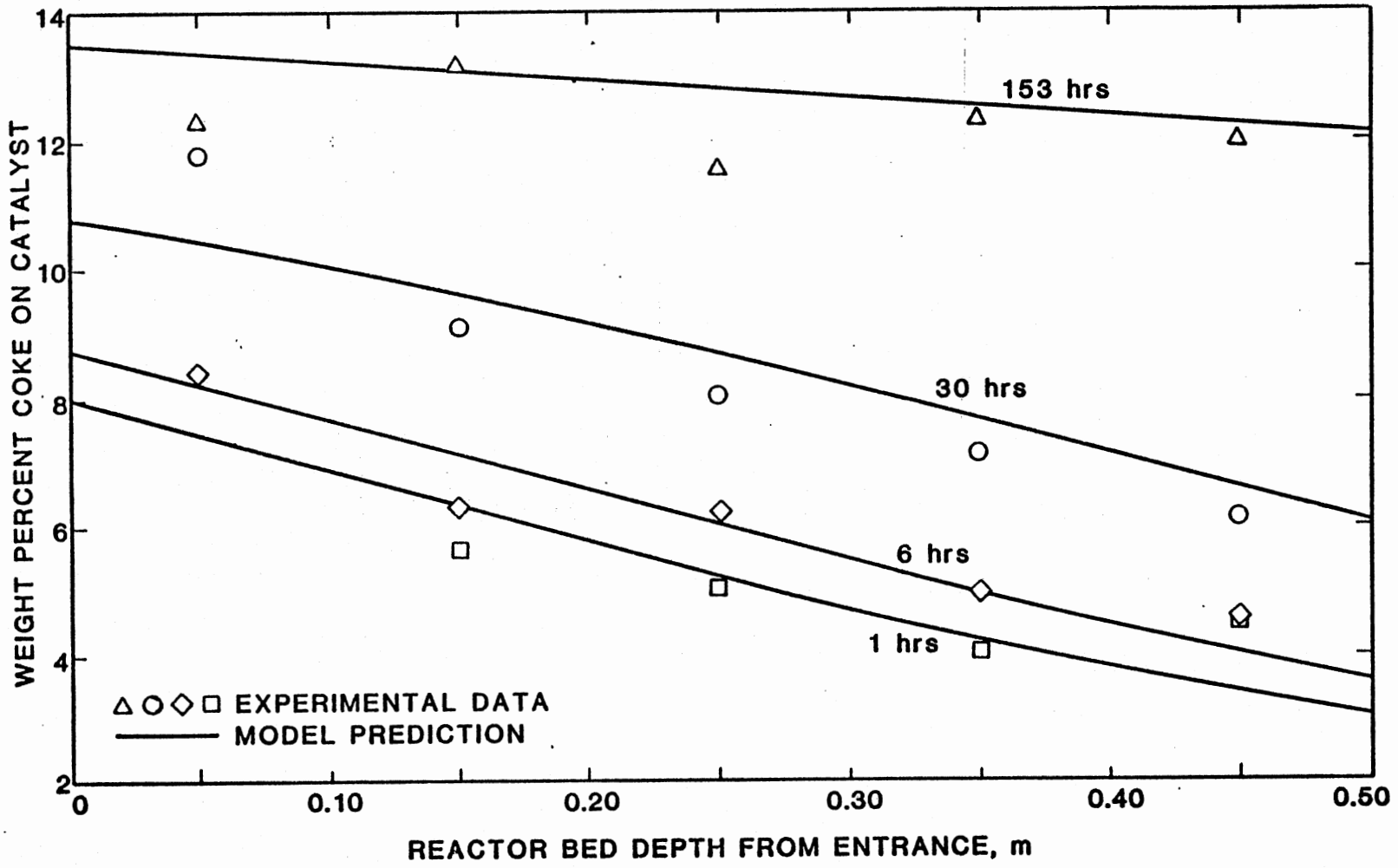

Figure 41. Coke Profiles in the Trickle Bed Reactor

the catalyst is more deactivated, so that more reactants and more coke precursors utilize downstream catalysts for reactions.

Catalyst Activity Versus Coke Content

The model predicts that the dependencies of hydrogenation and hydrodenitrogenation activities on the average catalyst coke content in the reactor are stronger than linear, and are satisfactorily supported by the experimental data as shown in Figures 42 and 43. The non-linear dependencies are expected, since the coke can not only cover the active sites, but can also block the pore mouth and restrict pore diffusion.

Pore Size Versus Coke Content

The predicted pore size-coke content relationship is shown in Figure 44. The trend is consistent with the experimental data, although data at high coke loading lie above the predicted line. Two reasons may have contributed to this: 1) Value of the calculated pore size from mercury porosimetry depends on the assumed contact angle between the mercury and the material analyzed. In this study, the mercury contact angle in coked catalysts were assumed to be the same as that of the fresh catalyst, 130 degrees. However, the real contact angle may vary with coke content on the catalyst, and has to be determined experimentally. 2) The pore sizes of heavily coked catalysts have approached the limit of the mercury porosimeter. High mercury pressure may have modified the coke structure on the catalyst. Further details on the mercury porosimetric method is beyond the scope of this study.

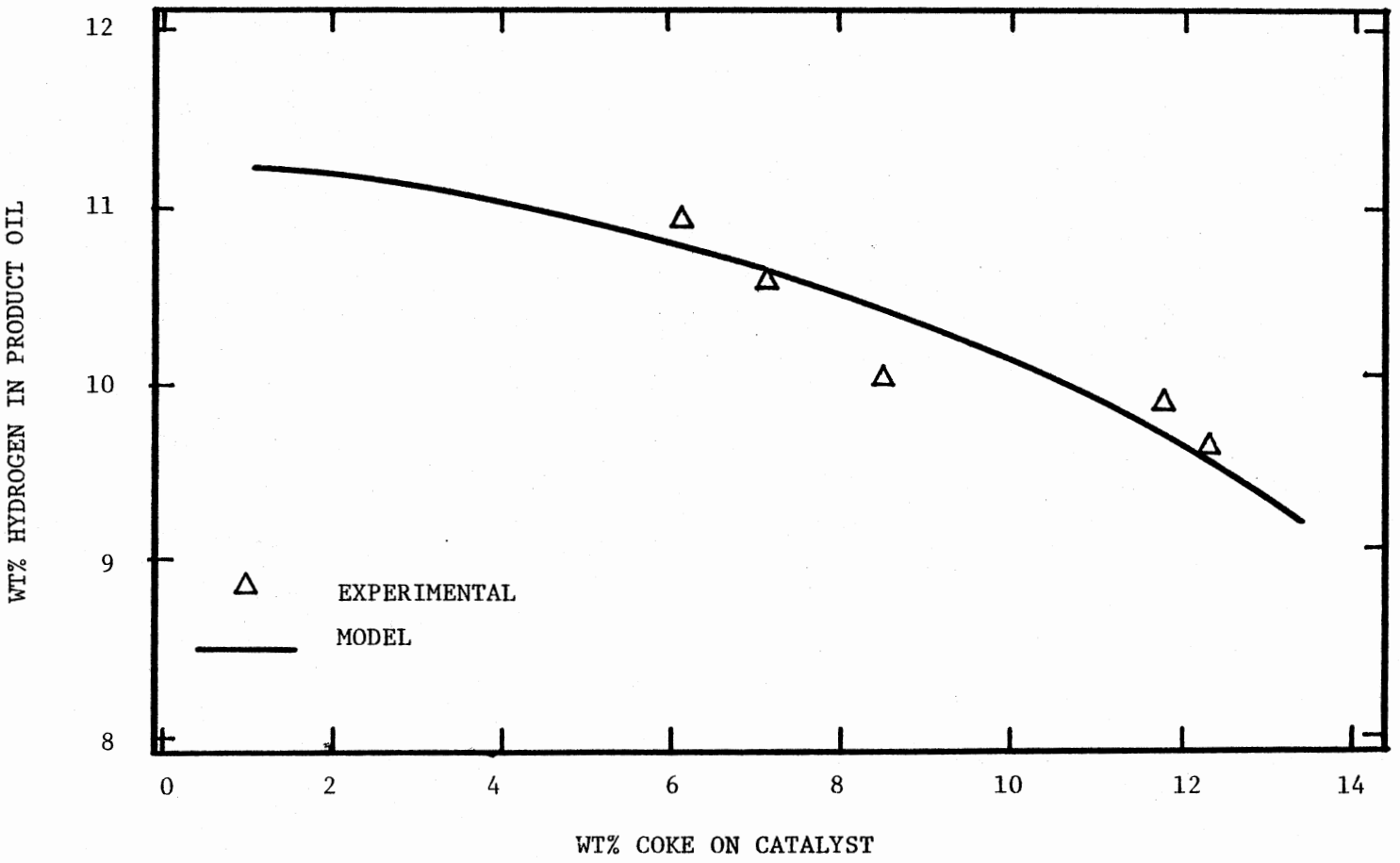

Figure 42. Catalyst Hydrogenation Activity Versus Coke Content Over the Reactor

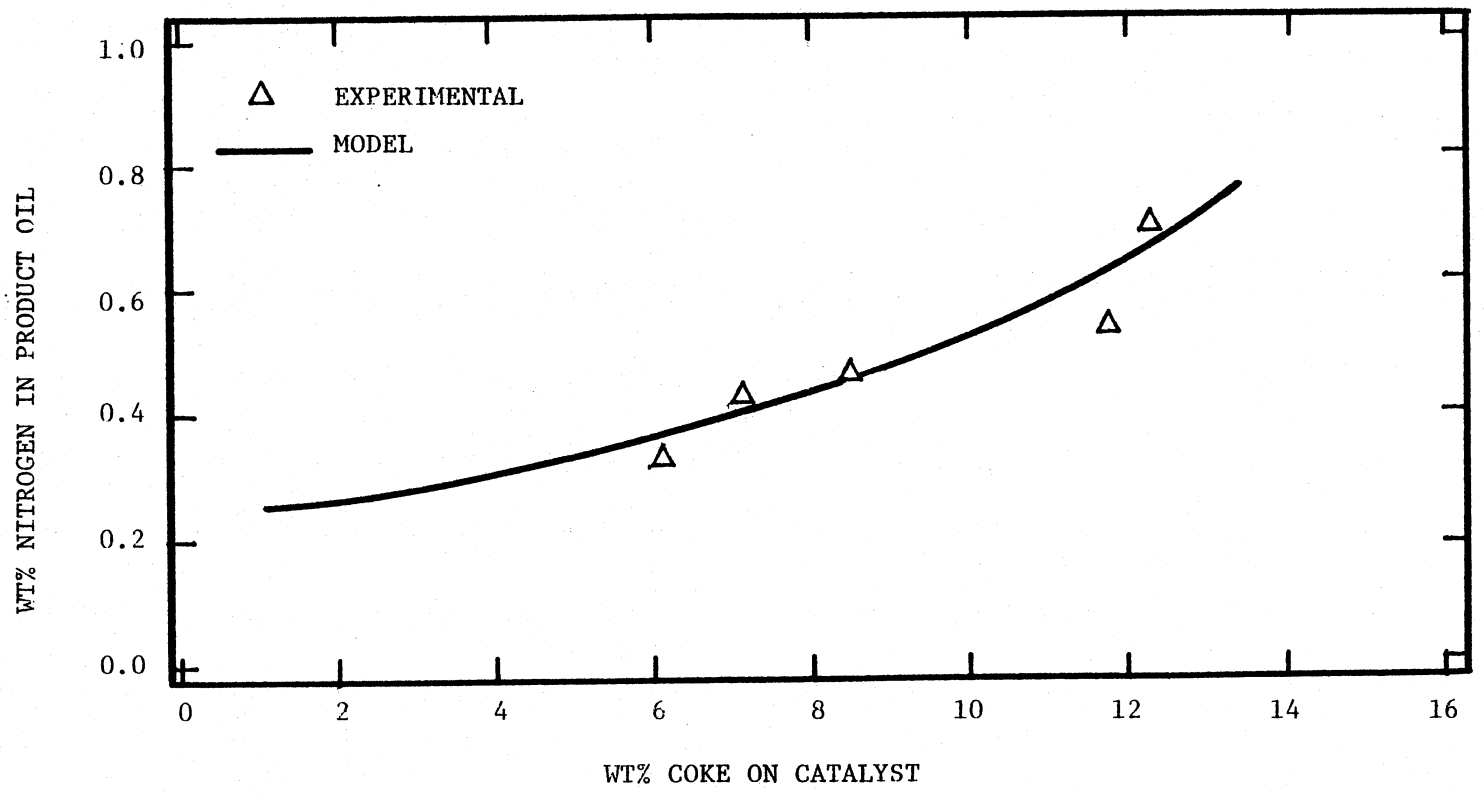

Figure 43. Catalyst Hydrodenitrogenation Activity Versus Coke Content Over the Reactor

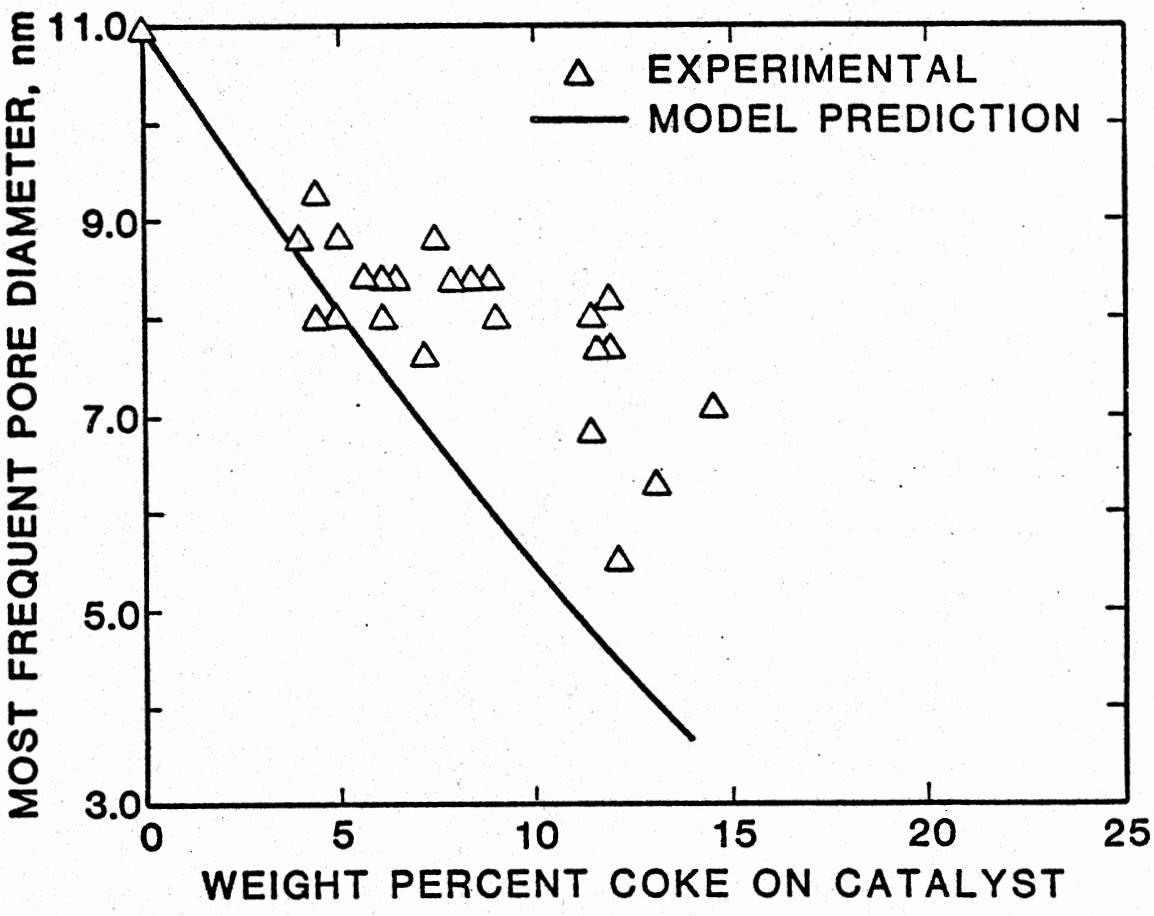

Figure 44. Most Frequent Pore Diameter Versus Catalyst Coke Content

Coke Profiles in the Catalyst Pellets

Figures 45-49 show the coke profiles within catalyst pellets from scanning Auger microscopic analyses for five representative samples. The relative dimensionless ages, θ_p's for these catalyst samples, LTZ-5, LTW-5, LTX-1, LTW-1, and LTY-3 are 0.60, 1.28, 2.12, 3.32, and 8.00 respectively. The profiles predicted by the model are also presented for comparison. The trends are consistent even though the experimental Auger data are qualitative and somewhat scattered.

Figure 50 summarizes coke profiles predicted by the model for the catalysts shown in Figures 45-49 to demonstrate the responses of coke buildup in catalyst pellets to time on stream. The figure shows that coke depositions become heavier starting from outside of the catalyst pellets as time on stream increases until the pore mouth is blocked and the reactants can never diffuse into the pellets for reactions. Note that the maximal coke content the catalyst porous structure can take is 0.34 g-coke/g-catalyst. The central half of the catalyst pellet is left unused even when the pore mouth is almost completely blocked by coke, as Figure 50 shows.

Model Predictions

This catalyst deactivation study is one of the broader research program aimed at tailoring better catalysts for upgrading coal derived liquids. The SRC is one of the currently active coal liquefaction processes. In the meanwhile, SRC product oils are also among the most troublesome oils to upgrade by hydrotreatment. Catalysts, especially

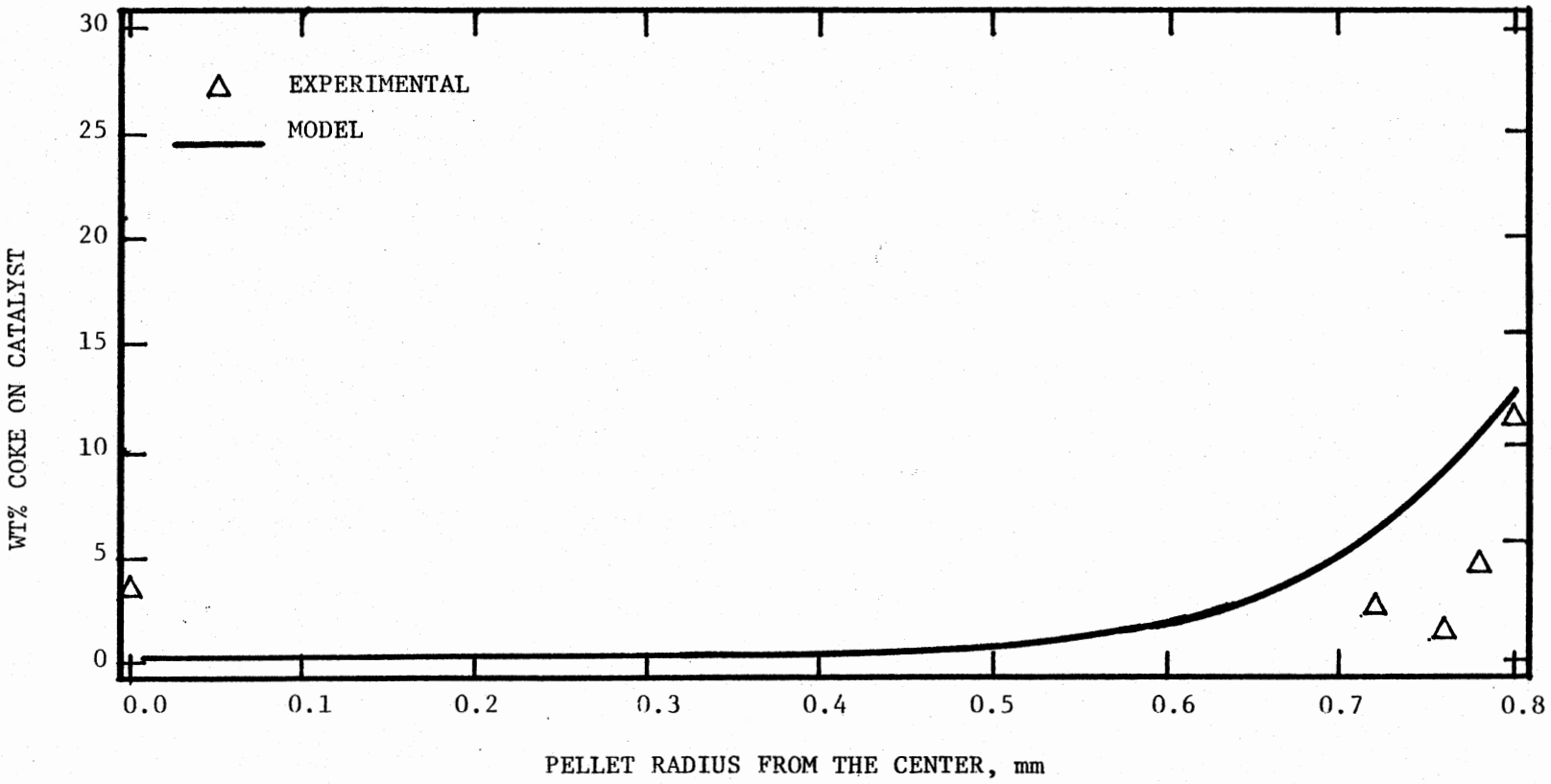

Figure 45. Coke Profile in the Catalyst Pellet from Section 5, Run LTZ

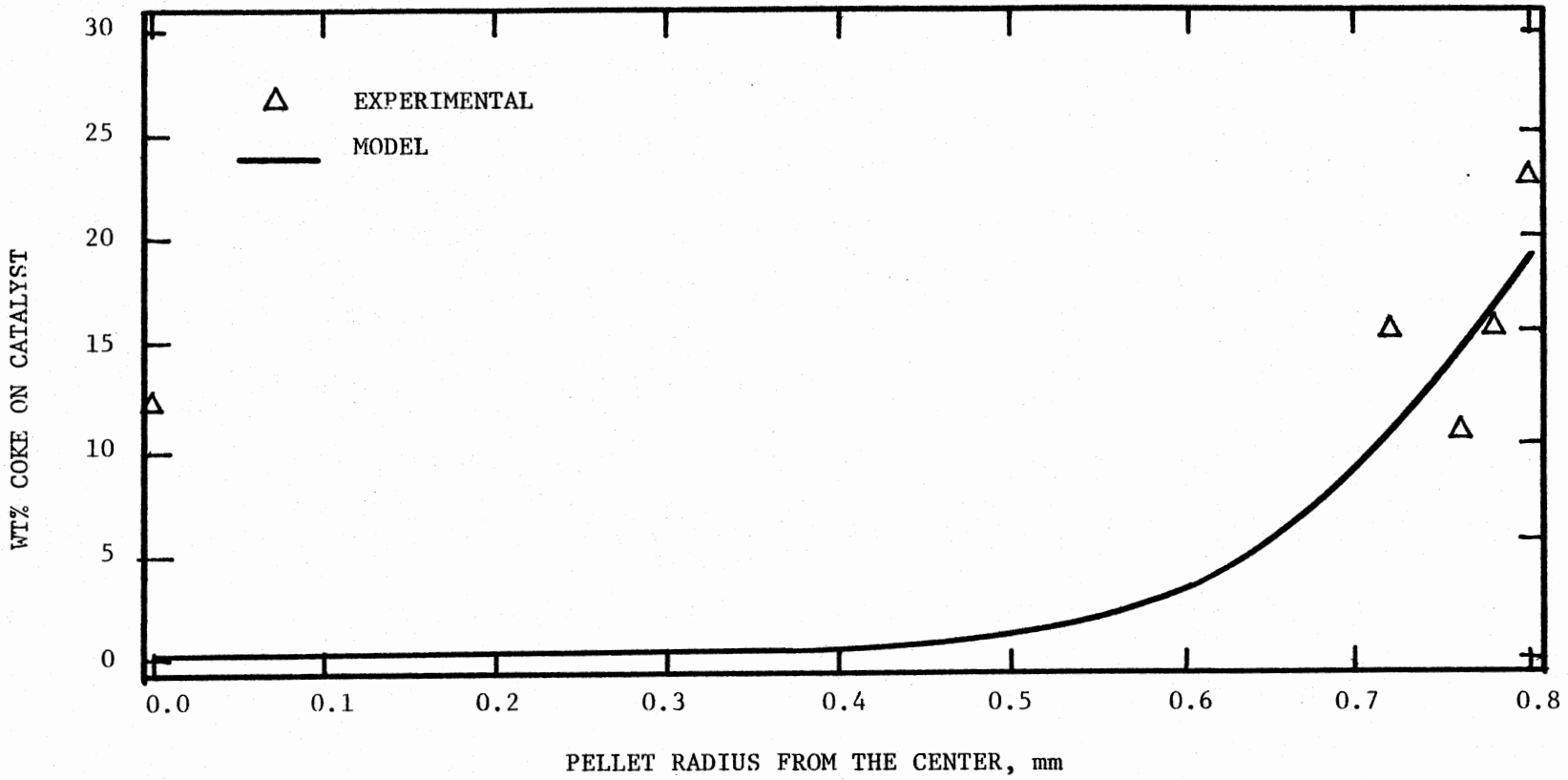

Figure 46. Coke Profile in the Catalyst Pellet from Section 5, Run LTW

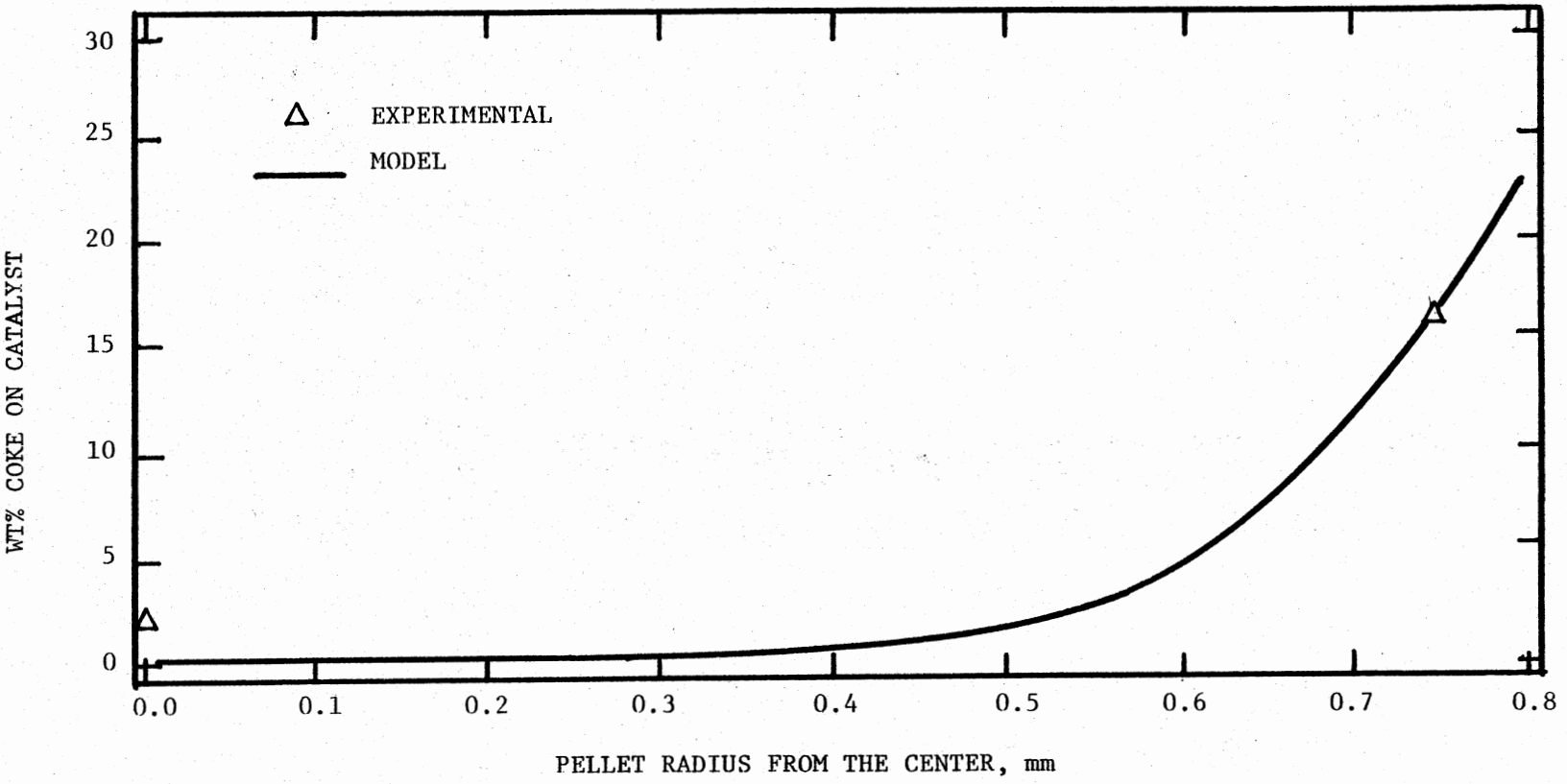

Figure 47. Coke Profile in the Catalyst Pellet from Section 1, Run LTX

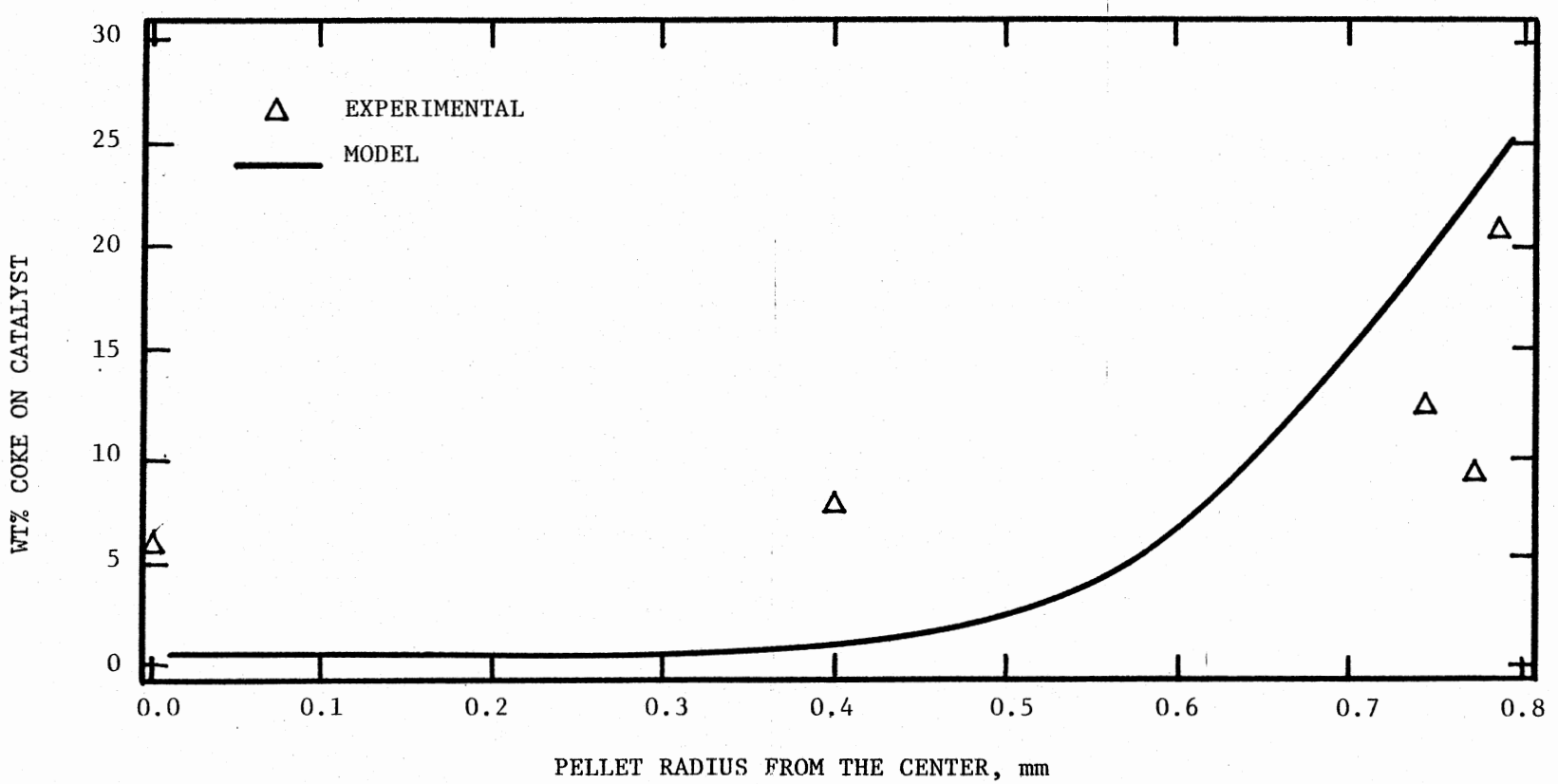

Figure 48. Coke Profile in the Catalyst Pellet from Section 1, Run LTW

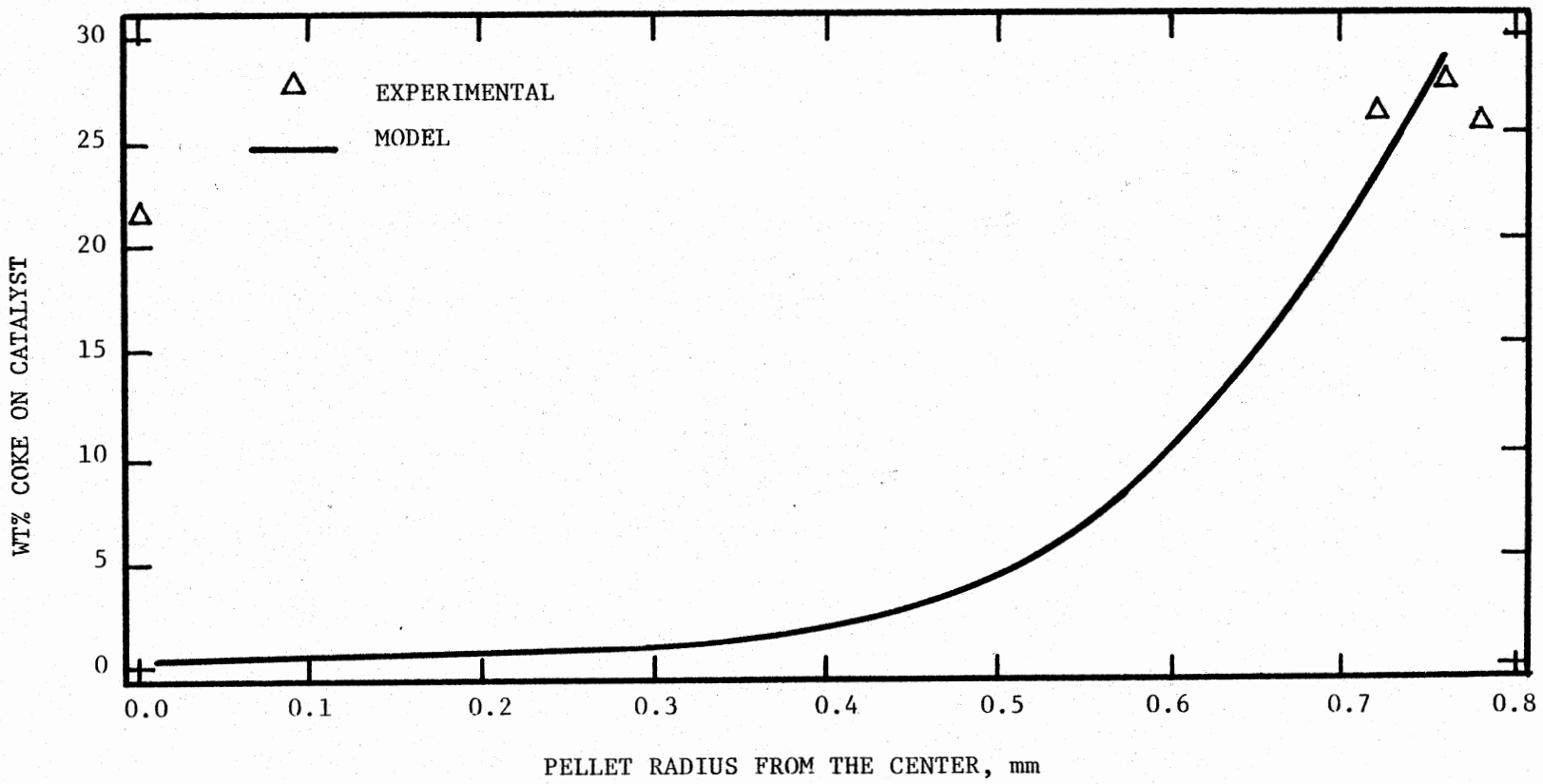

Figure 49. Coke Profile in the Catalyst Pellet from Section 1, Run LTW

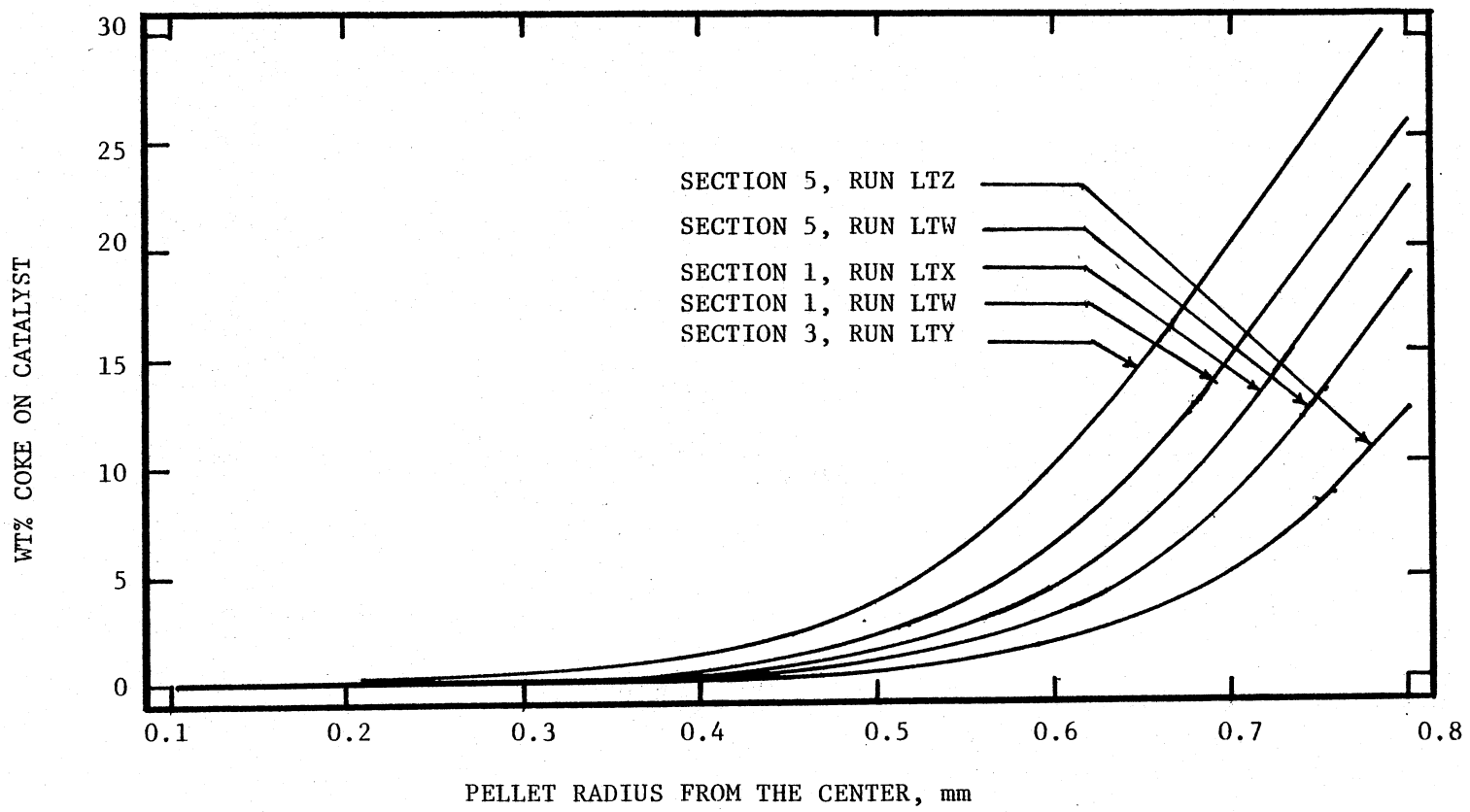

Figure 50. Coke Profiles in the Catalyst Pellets

catalyst support properties play a critical role in the successfulness of hydrotreating these oils.

In this section, the effects of catalysts support properties on the performance of hydrotreating SRC oil will be assessed based on the model and the experimental data generated from this study. For comparison purposes, following assumptions are made in predicting the effects of catalyst physical properties.

1. The same SRC oil feedstock is used, which means that the feedstock properties were held fixed (bulk diffusivity and critical solute diameter as shown in Table VIII, and elemental contents as shown in Table III).

2. The hydrotreatment is conducted under fixed operating conditions as shown in Table IV.

3. When this SRC feedstock is hydrotreated, the catalyst used has the same orders of intrinsic rate dependencies on the clean catalyst sites and the same first order intrinsic kinetic rate constants based on the unit catalyst weight as shown in Table VIII.

With these basic conditions fixed, the effects of important catalyst physical properties, pore size and pellet size, on hydrotreatment performance can be predicted based on the model's calculations. For the convenience sake, dimensionless concentrations and time will be used in the following discussions.

Effect of Catalyst Pore Size

Figures 51-56 present the effects of pore diameter on the hydrotreating performance. The equivalent pellet diameter is 2.0 mm which is the same as that used in this experimental study, Shell 324 catalyst.

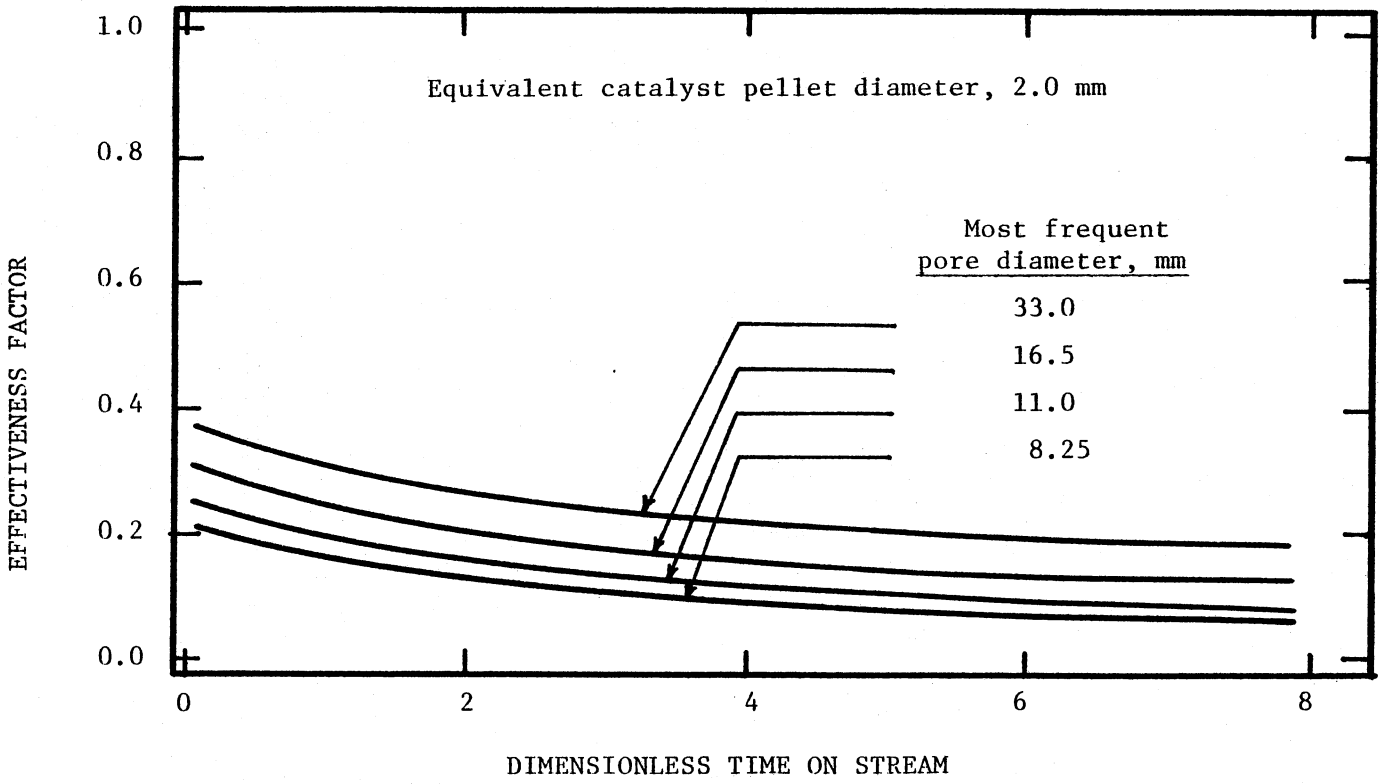

Figure 51. Effect of Catalyst Pore Diameter on Catalyst Activity Decay - Effectiveness Factor Versus Time

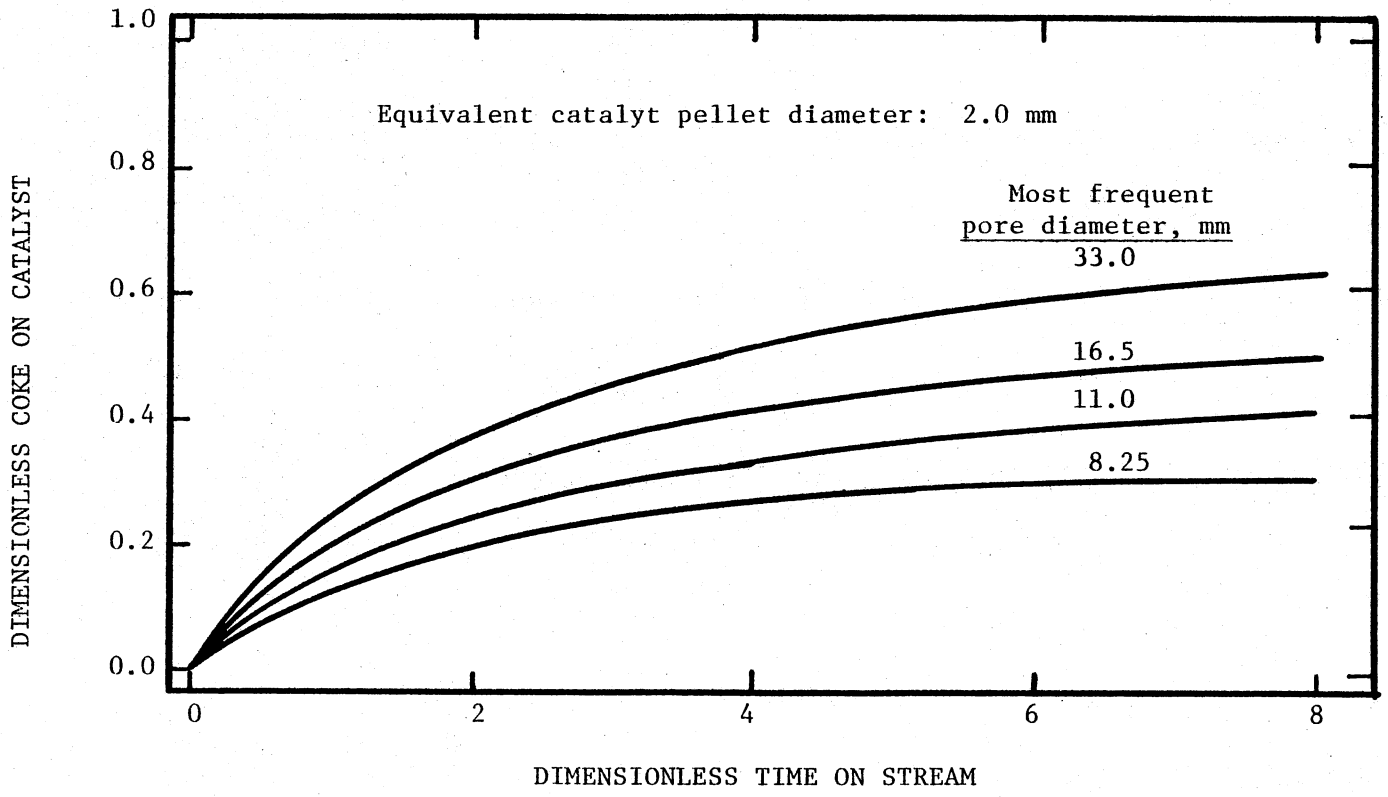

Figure 52. Effect of Catalyst Pore Diameter on Catalyst Activity Decay - Coke Content Versus Time

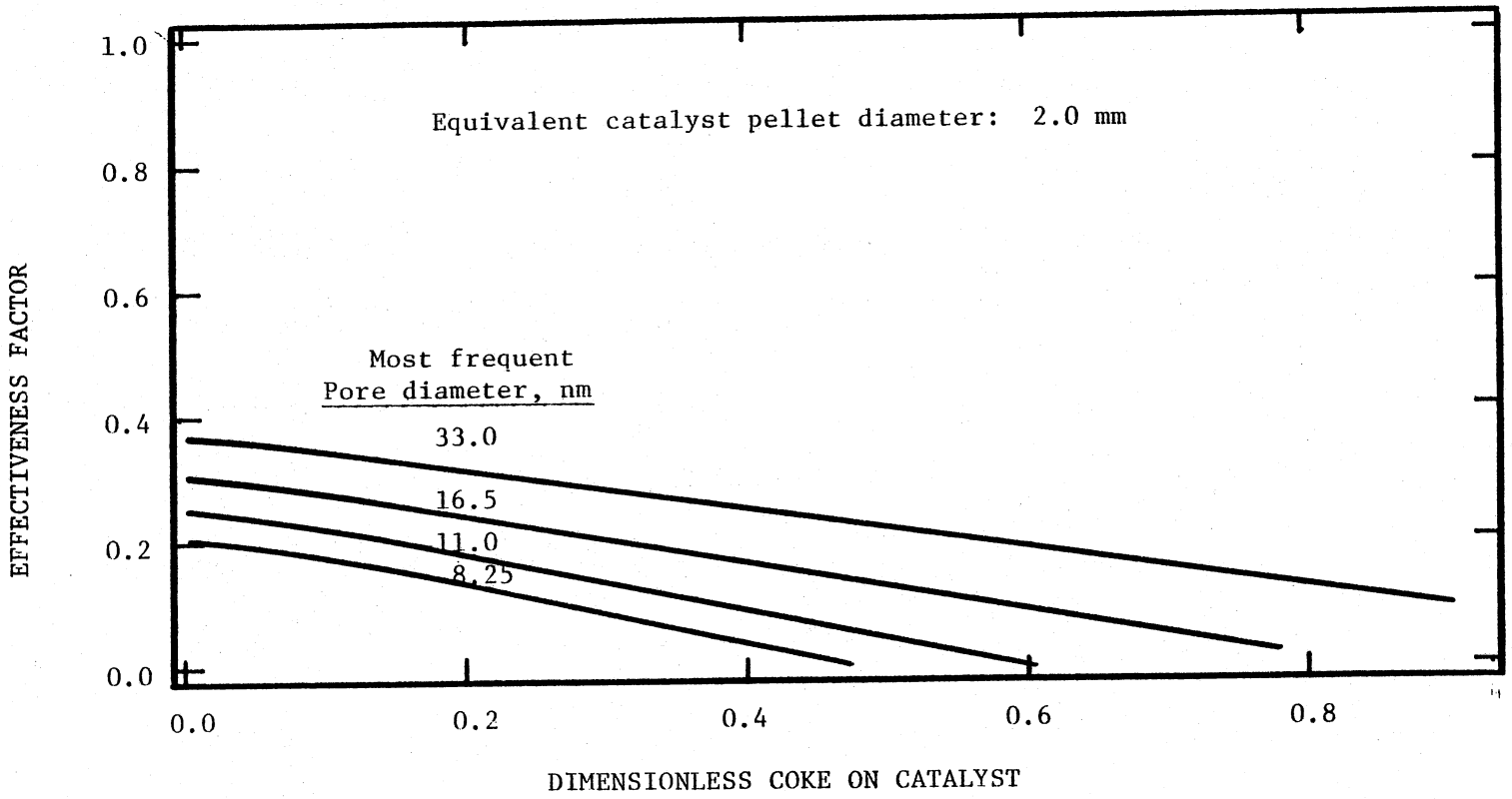

Figure 53. Effect of Catalyst Pore Diameter on Catalyst Activity Decay - Effectiveness Factor Versus Coke Content

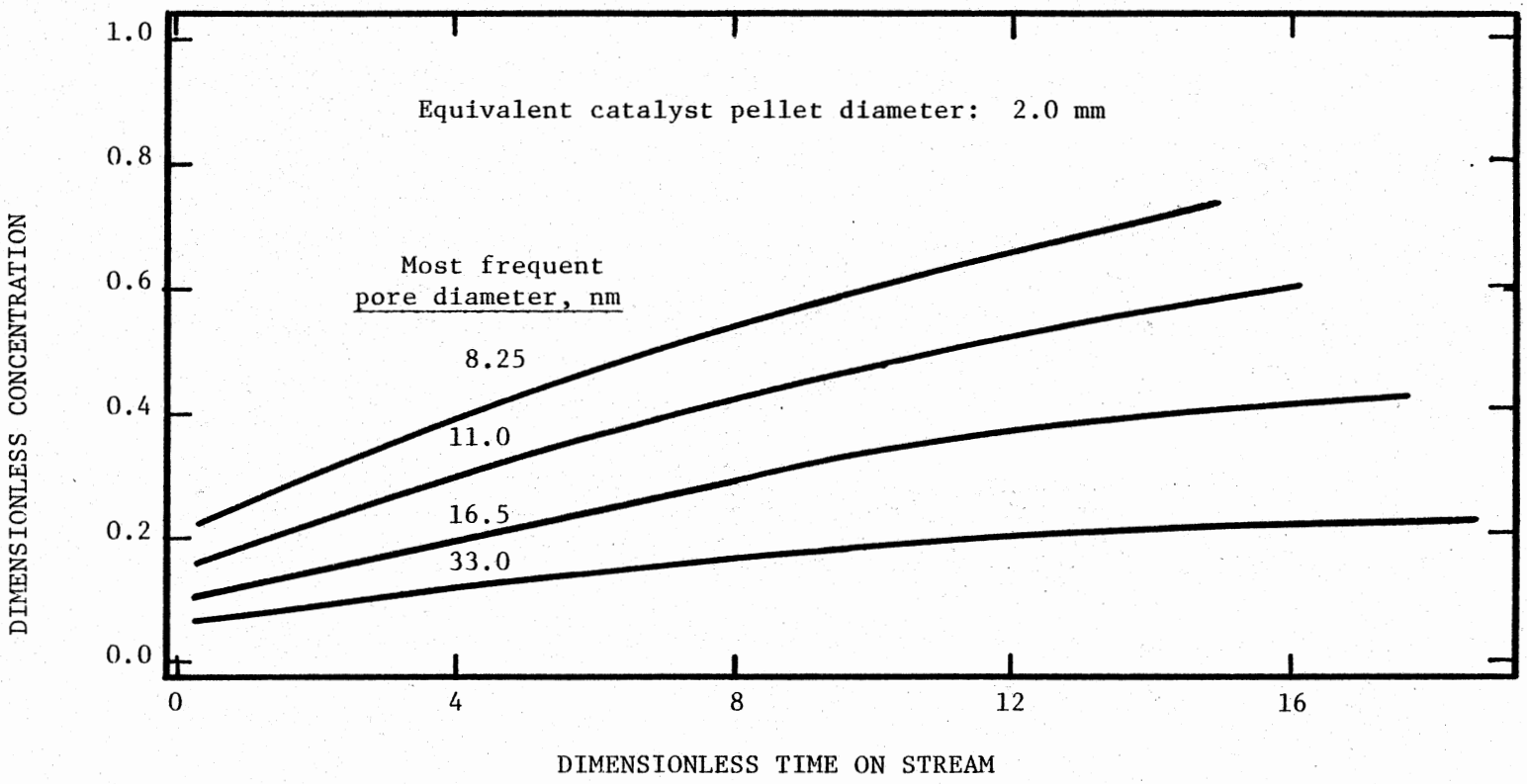

Figure 54. Effect of Pore Diameter on the Trickle Bed Reactor Performance - Concentration Versus Time

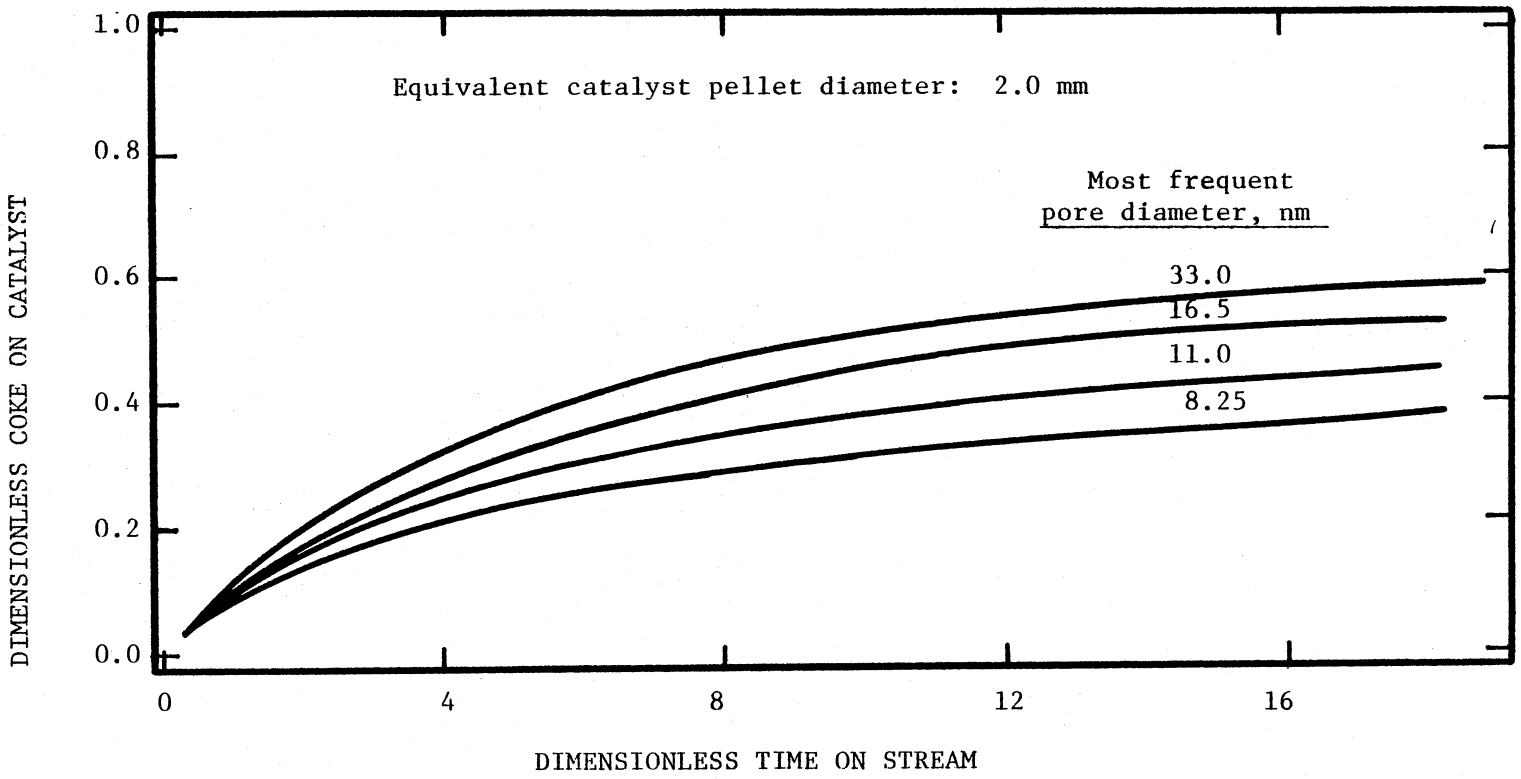

Figure 55. Effect of Pore Diameter on the Trickle Bed Reactor Performance - Concentration Versus Coke Content

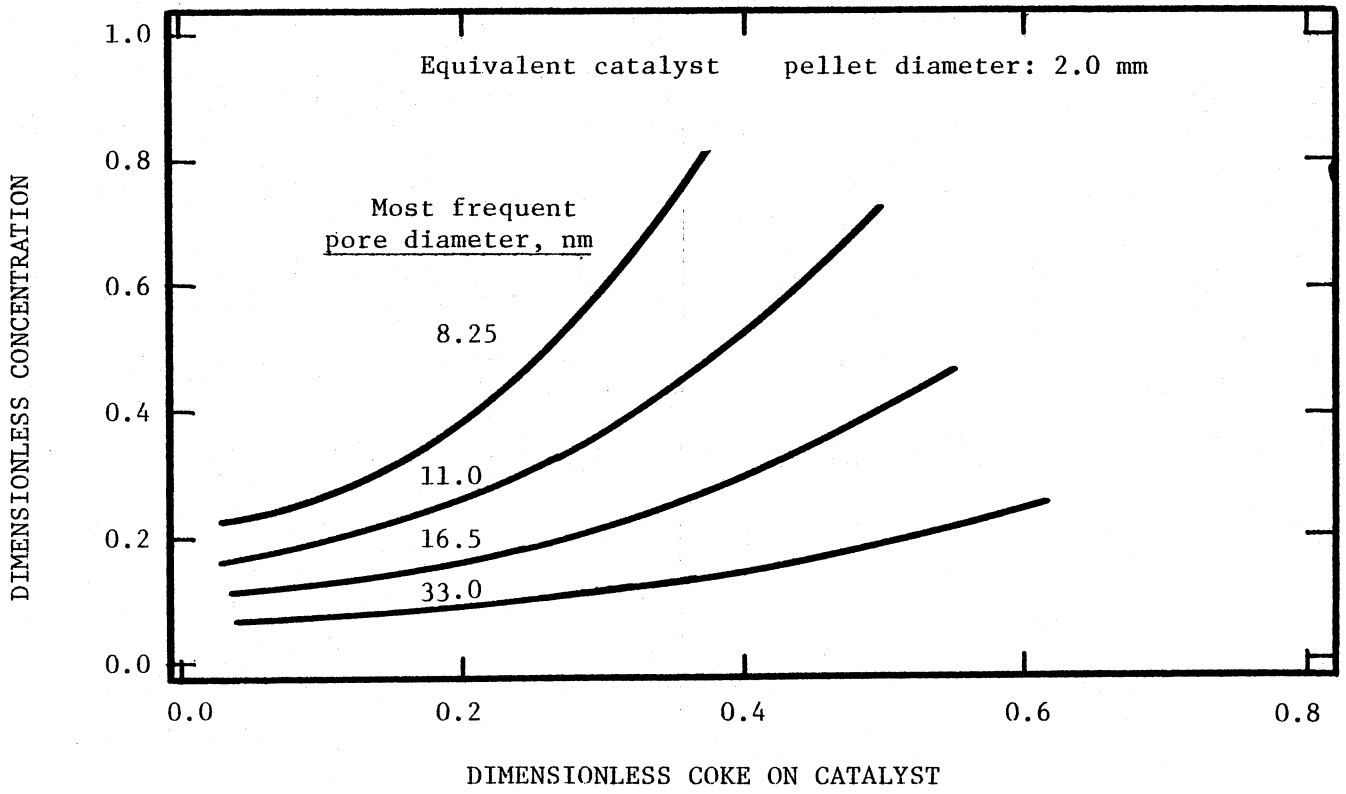

Figure 56. Effect of Pore Diameter on the Trickle Bed Reactor Performance - Concentration Versus Coke Content

As shown in Figure 51, the catalyst activity (in terms of effectiveness factor) increases with increasing pore diameter. In the meanwhile, the larger pore catalyst also causes higher coke accumulation, as shown in Figure 52, but the coke accumulation quickly levels off. The equilibrium coke levels are parallel to each other without showing any tendency to crossover. Although the larger pore catalyst produces more coke deposits, it can accomodate more coke as well, as Figure 53 shows. As a result, the larger pore catalyst can not only give higher initial activity but also give better stability. Accordingly, the same trends also exist in the trickle bed reactor performance as Figures 54-56 show.

Effects of Catalyst Pellet Diameter

The effects of decreasing catalyst pellet diameter at a fixed pore diameter are parallel to those of increasing pore diameter at a at a fixed pellet diameter, as shown in Figures 57-62. Note that equivalent pellet diameters of 1.0, 2.0 and 3.4 mm correspond to the pellets of 1/32, 1/16 and 1/8 inch extrudates, respectively. These parallel effects are expected, since both decreasing pellet size and increasing pore size result in decreasing diffusional restrictions.

Summary

Therefore, in hydrotreating the SRC coal oils as used in this study, decreasing internal diffusional resistance of the catalyst is beneficial to both initial activity and life of the catalyst. This prediction is consistent with that made by Newson (1975) who

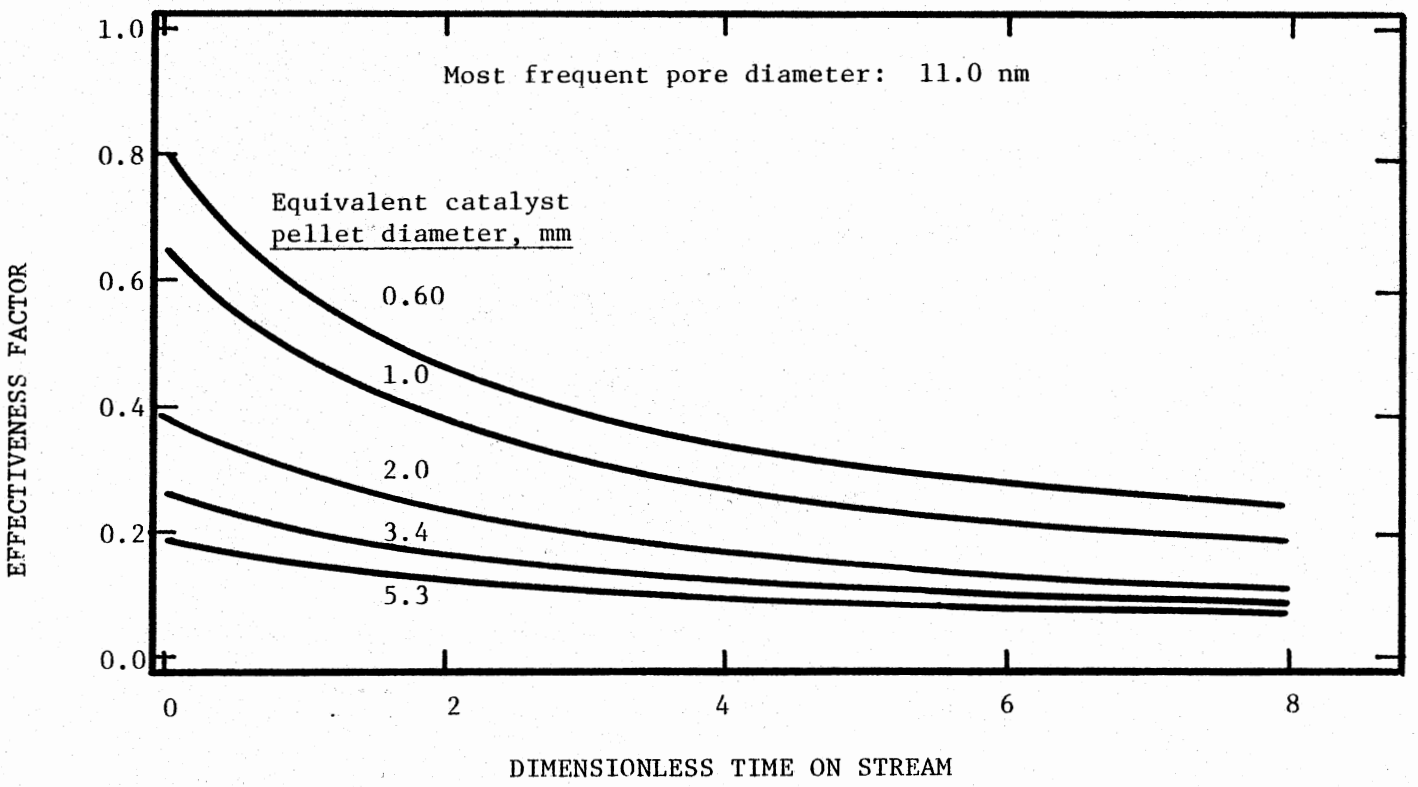

Figure 57. Effect of Catalyst Pellet Size on Catalyst Activity Decay - Effectiveness Factor Versus Time

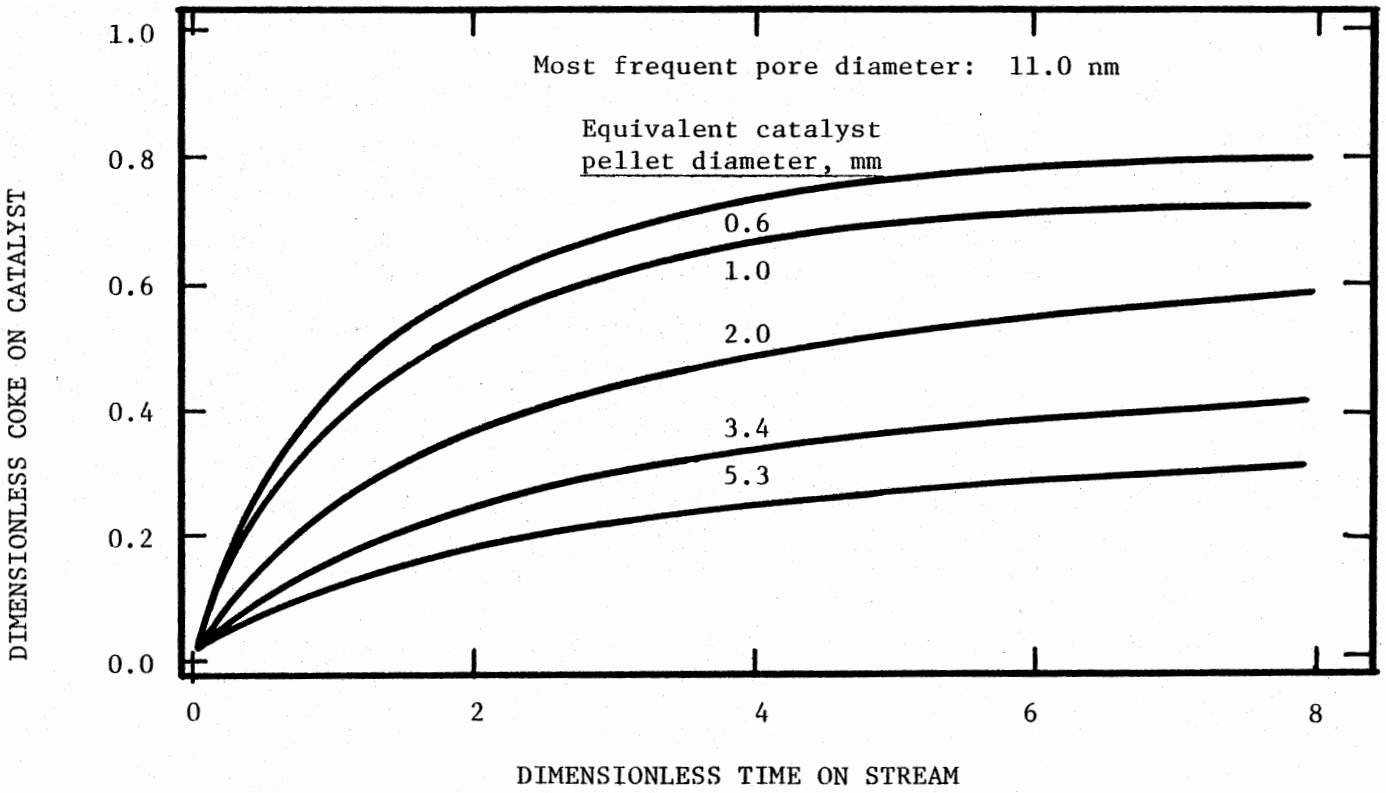

Figure 58. Effect of Catalyst Pellet Size on Catalyst Activity Decay - Coke Content Versus Time

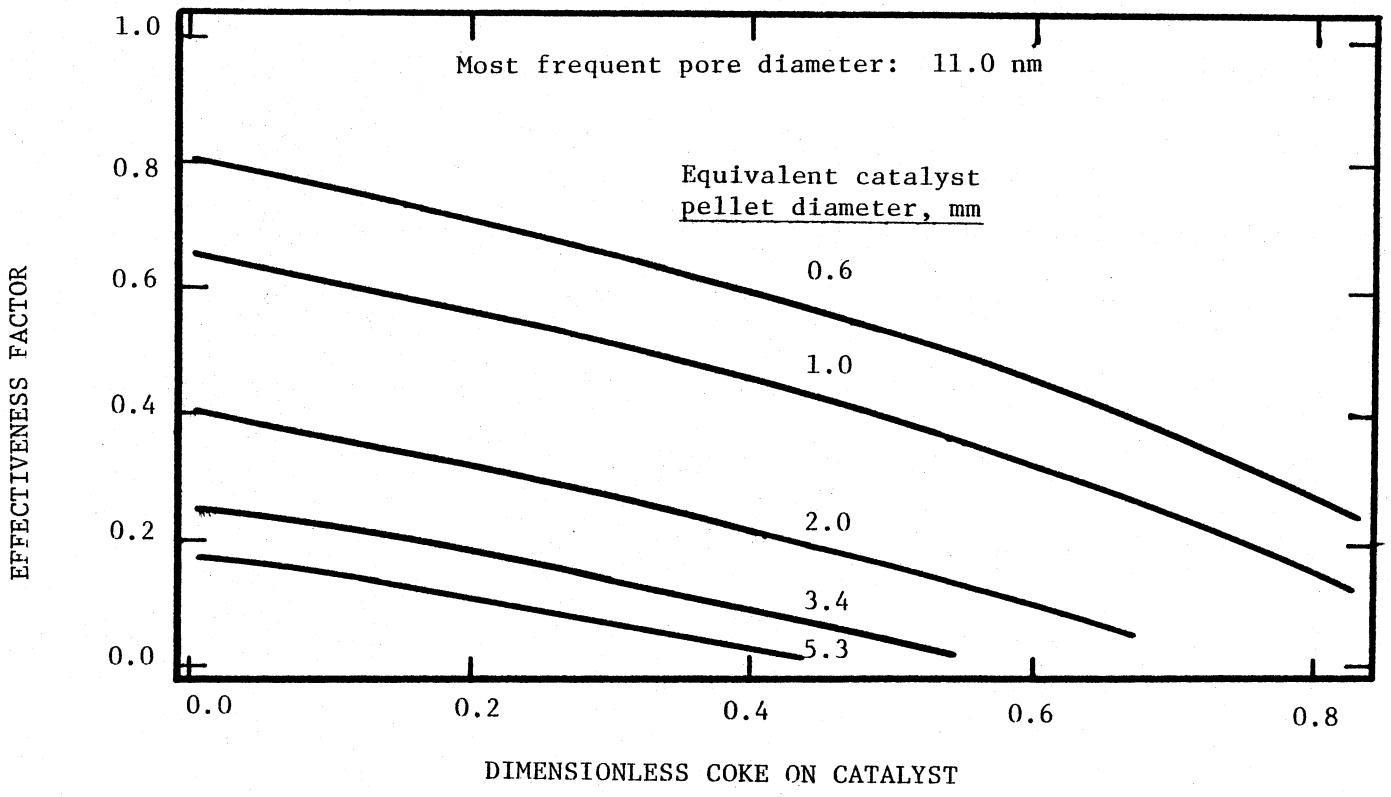

Figure 59. Effect of Catalyst Pellet Size on Catalyst Activity Decay - Effectiveness Factor Versus Coke Content

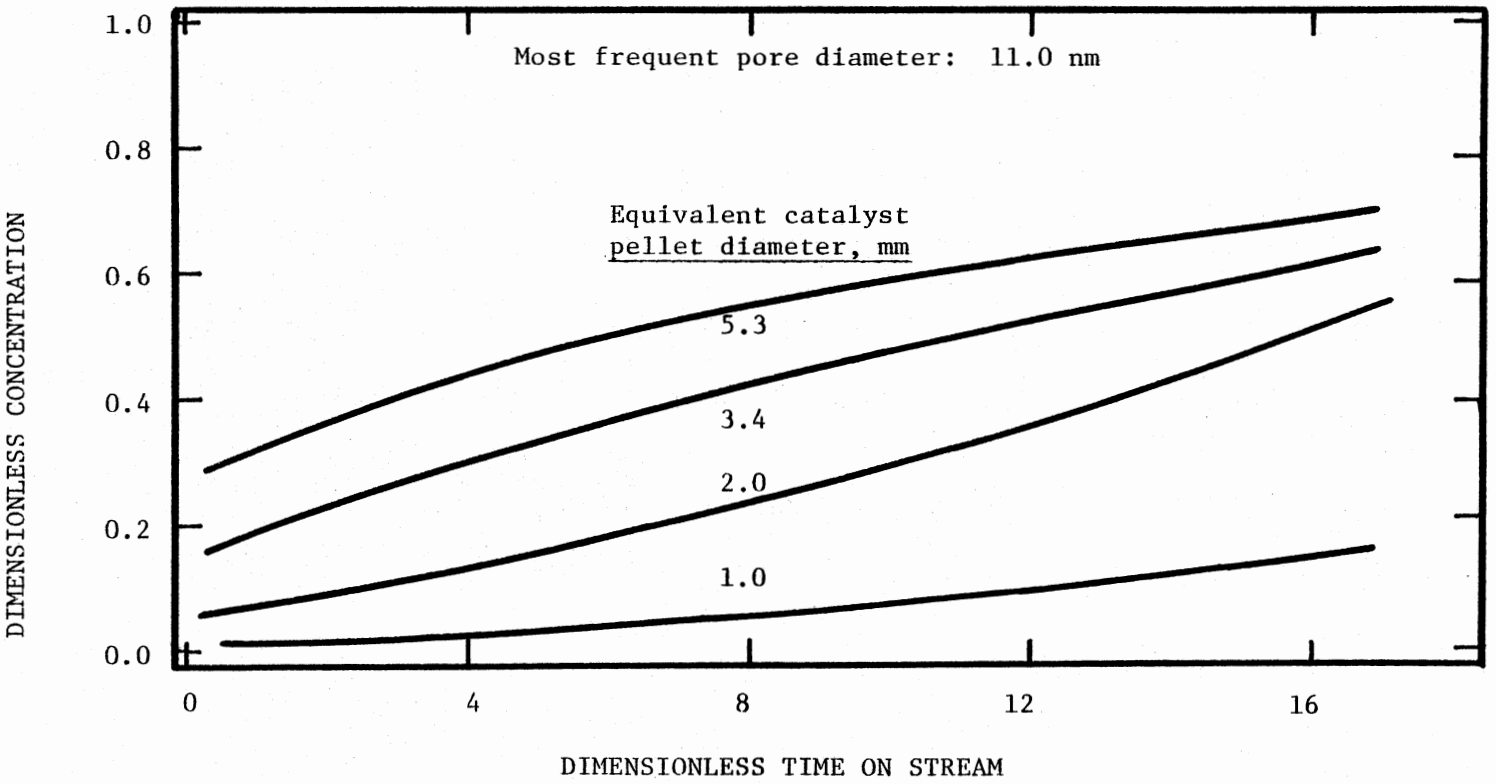

Figure 60. Effect of Catalyst Pellet Size on the Trickle Bed Reactor Performance - Concentration Versus Time

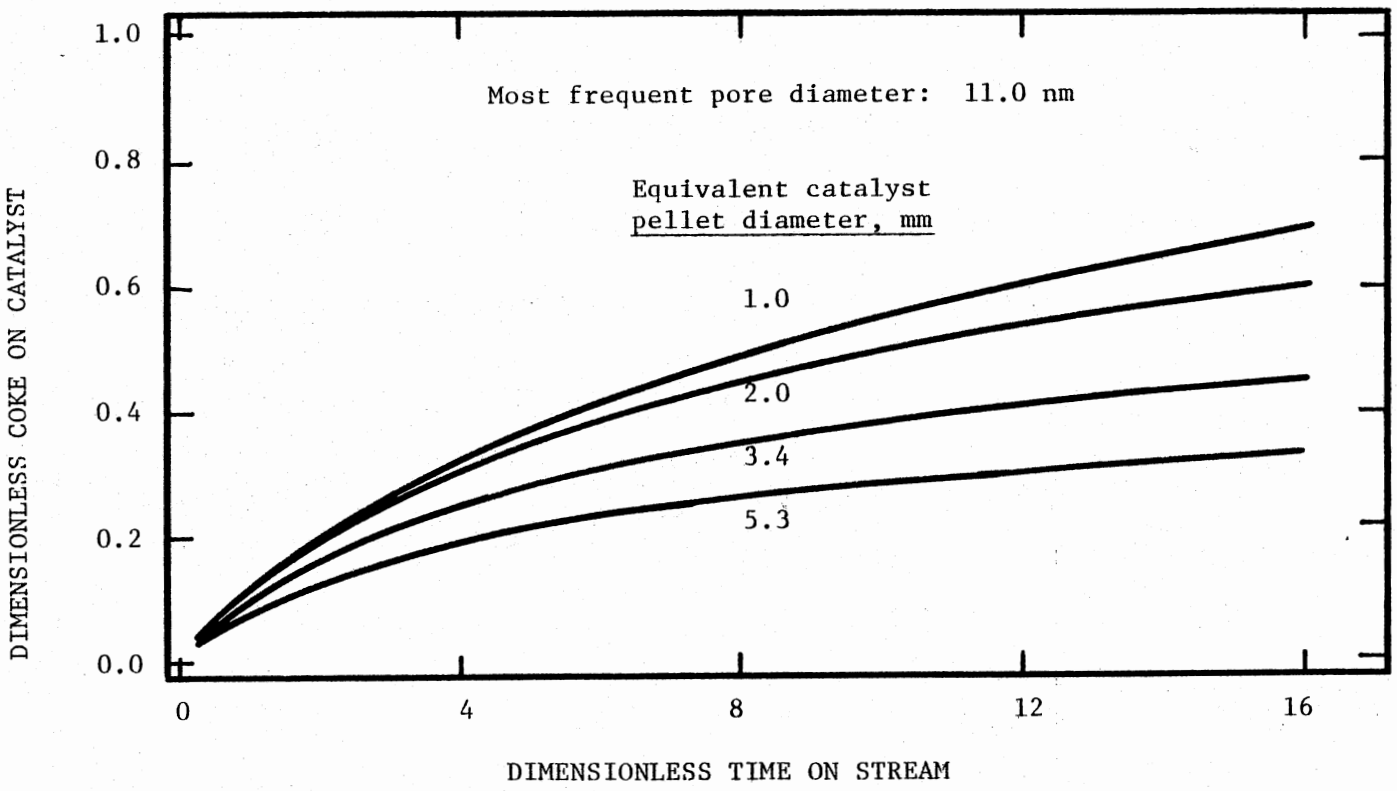

Figure 61. Effect of Catalyst Pellet Size on the Trickle Bed Reactor Performance - Coke Content Versus Time

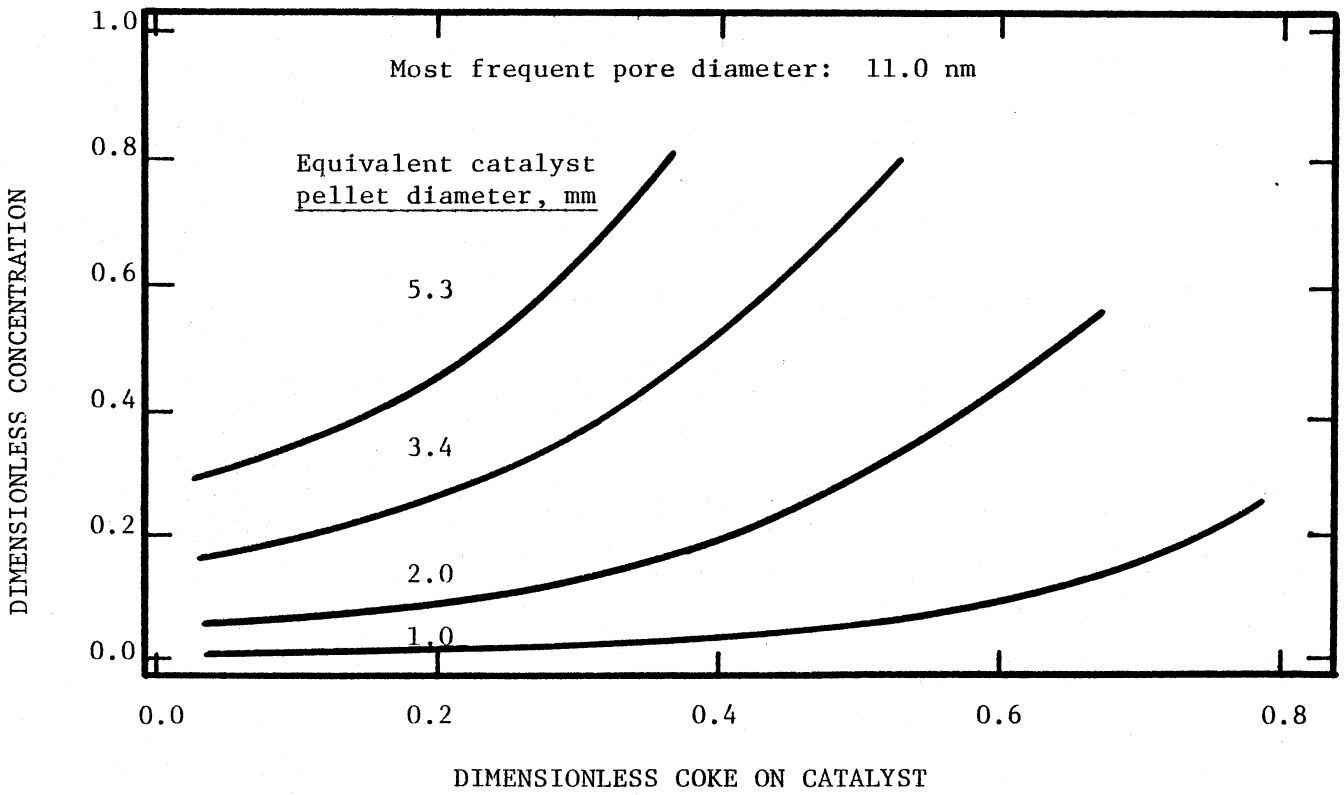

Figure 62. Effect of Catalyst Pellet Size on the Trickle Bed Reactor Performance - Concentration Versus Coke Content

in proposing a pore plugging model incorporated with available experimental data, concluded that pore diffusional limitations in heavy oil hydrotreatment can shorten the catalyst life. More details of Newson's work has been presented in this literature review. On the other hand, Masamune and Smith (1966), Murakami et al. (1968), Lee and Butt (1973) and Polinski et al. (1981) have reported that the catalyst with some degree of diffusional limitations can have better stability and longer life. These differences may have resulted from the different systems investigated. In the studies by Masamune and Smith (1966), Murakami et al. (1968) and Lee and Butt (1973), they assumed that the coking and main reaction activities have the same order of dependency on the coke content, and that the effective diffusivity is not affected by the coke accumulation. In this study, a more realistic approach based on broad experimental observations has been taken. This approach concludes that the dependency of the activity of the main reaction on coke content is half order, and that the effective diffusivities of the reactants decrease with increasing coke content. Thus the catalyst activity decay caused by coke is mainly via pore mouth plugging. This type of deactivation mechanism can completely destroy the catalyst even though much of its internal surface is still active.

Care must be taken in predicting catalyst deactivation behavior. In some situations, diffusional limitations are beneficial to catalyst life, whereas such limitations are disastrous in others. The situation depends on whether pore mouth blocking or surface active site covering is more critical in deactivating the catalyst, and this in turn depends on the nature of the hydrotreatment system, a combination of the

catalyst, the feedstock and the operating conditions.

The larger pore and/or smaller pellet catalysts are more resistant to deactivation in hydrotreating the SRC-I oil. However, larger pore catalysts have relatively lower surface areas and thus give lower initial activity, and small pellets may result in excess pressure drop in the reactor bed. The choice of the proper catalyst is, therefore, dependent on the process conditions and the product requirements.

CHAPTER VII

CONCLUSIONS AND RECOMMENDATIONS

Conclusions

A trickle bed reactor has been successfully used to study catalyst deactivation during hydrotreatment of a coal derived oil. A parallel fouling model has been developed to represent the experimental observations. This model is significant because it incorporates a variable diffusivity and intrinsic activties as functions of coke content, and is developed consistently from a single pellet to the reactor bed itself. This model has successfully predicted coke profiles with time and reactor position, and hydrogenation and hydrodenitrogenation activities as functions of coke content. This model has also suggested better catalysts for hydrotreating SRC oils. The following conclusions can be drawn from this study.

1. The catalyst life test unit used in this study operated satisfactorily in terms of stabilities of temperature, pressure and flow rates controls. Large temperature differentials across the radial direction of the reactor bed have been observed. This was due to exothermal chemical reactions and was repeatable throughout the study.

2. The experimental run with EDS vacuum gas oil and solvent mixture showed no deactivation during the entire 261 hours on stream.

This EDS feedstock contained 0.72 wt% nitrogen and 0.70 wt% sulfur, essentially all these heteroatoms were removed at 400 and 426 C. The ammonia and hydrogen sulfide in the product gas stream reacted to form ammonia hydrogen sulfide which solidified at ambient winter temperature (below 20 C) and plugged the reactor gas exit line.

3. A plugging problem was encountered downstream of the reactor during the runs with SRC feedstock. This plugging was caused by severe hydrogenation of the solvent fraction which left the heavy residue incompatible with the solvent. The residue precipitated out at lower temperatures.

4. Significant activity decay and significant amounts of coke deposits on catalysts were observed in the runs with the SRC feedstock. More than half of the catalyst activity loss and coke buildup occured during the first 40 hours on stream. Coke profiles in the reactor bed showed that the coking reactions were parallel to the main reactions.

5. Mercury porosimetric analyses revealed that pore volumes and pore sizes of the spent catalysts were linearly reduced by the coke on the catalyst. BET nitrogen adsorption showed surface areas of the spent catalysts slightly increased. All of the catalysts recovered their original surface areas, pore volumes and pore sizes after regeneration. Thus all of these changes in physical properties were the results of coke deposits.

6. Scanning Auger microscopic analyses showed no detectable nitrogen and metal depositions on the spent catalyst surfaces. Moreover, most carbonaceous material deposited within one fifth depth of a catalyst pellet.

7. Among the four possible deactivation mechanisms, i.e., poison adsorption, sintering, and metal and coke depositions, only coke depositions were found to be the primary deactivation mechanism in this study.

8. A parallel fouling model was developed to represent the experimental observations. This model incorporates a variable diffusivity and intrinsic activities as functions of coke deposition, both time and space profiles for coke are predicted within pellet and reactor. The model is broadly supported by experimental data, and is able to predict catalyst lifes based on pore size and pellet size of the catalyst.

9. Catalyst coke content is a good measure of activity. Both hydrogenation and hydrodenitrogenation can be related to coke content which in turn is a function of time on stream.

10. Poorly controlled high temperatures during startup can result in excess coking reactions and catalyst deactivation. It is, therefore, important to startup the reactor at reasonably low temperatures in order to better maintain the catalyst activity.

11. Catalytic coking reactions require dual catalyst sites, whereas small size reactants which are less subjective to coking may be able to access the sites restricted by coke.

12. Coke on the catalyst severely reduced pore sizes and restricted reactants diffusions in the catalyst. These diffusional restrictions are dominant over the active sites coverage in coking deactivation during hydrotreating the SRC oil.

13. With reasonable range of surface area, the better catalyst, in terms of higher activity and longer life, for hydrotreating SRC oil

is the one that has lower diffusional restrictions, which can be achieved by increasing the pore size and/or decreasing the pellet size, but preferably both.

14. In hydrotreating some light oils, catalyst deactivation characteristics may be different from hydrotreating the SRC oil as in this study, and some diffusional restrictions may be desirable in better catalyst life maintenance.

Recommendations

With increasing interest in coal conversion and heavy oils refining, research on improving hydrotreating catalysts are playing a major role. However, many questions still remain unanswered with respect to hydrotreating coal and heavy oils. As a continuity of this work, the following recommendations are made based on the results and the experience gathered from this study:

1. This coke deactivation study should be extended to different reaction temperatures; this is to obtain the activation energies of the coking and the main reactions for the design and optimization purposes. This information can also be used to investigate and to minimize the initially rapid coking formation.

2. Model prediction of deactivation responses of the SRC oil hydrotreatment on varying the catalyst pellet size and pore size should be experimentally verified. Care should be taken to isolate the hydrodynamic effects from the diffusional effects.

3. Activities of fresh, aged and regenerated catalysts of this study should be compared using a well characterized coal oil. This is to gain further confidence on the effects of coke deposits on the

catalyst activity.

4. Since the scanning Auger microscopic analyses for carbon profiles in catalyst pellet was only marginally successful, other methods such as thermal gravimetric analytical technique should be developed to verify the coke profiles in catalyst pellets quantitatively.

5. Other reactor configurations, such as batch reactor should also be used to enhance the observations from trickle bed reactor studies. Batch reactor can give simpler mathematics in modeling the reaction-deactivation kinetics as observed in this study.

6. In order to gain more confidence in scaling up the trickle bed reactor using experimental data, reactor hydrodynamics should be further studied. The comparison on the performance of up and down flow reactors, diluted and undiluted catalyst beds, and various flow rates are necessary.

7. Characteristics of temperature differentials across the reactor radial direction require further study for the scaleup purposes. Methods of minimizing temperature differentials should be developed in order to get better isothermal data. This may include reactor bed dilution with inert material and the use of low activity catalyst at reactor top.

8. Plugging in the hydrotreatment system, either caused by ammonia hydrogen sulfide or by heavy residue should be throughly investigated in order to guarantee the smoothness of the future experimentations. This may include solubilities study of ammonia hydrogen sulfide in gas phase and heavy residue in liquid phase at various operation conditions.

9. Characteristics of coke resulted from different oils and from different preparation methods should be studied. Properties of the coke such as porosity, pore size and surface area should also be determined. These may help understand why in some cases, the catalyst activity is sensitive to the coke deposits, whereas it is not in other cases.

10. Effective diffusivities of oils in fresh and coked catalysts should be experimentally verified to enhance this model predictions.

SELECTED BIBLIOGRAPHY

Ahmed, M., "Coal-Derived Liquids Hydrotreatment - Catalyst Deactivation Study", Ph.D. Thesis, Oklahoma State University, Stillwater (1979).

Akhtar, S., S. Friedman, and P. M. Yavorsky, AIChE Symp. Ser., 70 (137), 106 (1974).

Angevine, P. J., et al., EPRI Report No. AF-1255 (1979).

_____, Armak Company, Catalyst Division, Product Data Bulletin No. 76-4 (1976).

Appleby, W. G., J. W. Gibson, and G. M. Good, Ind. Eng. Chem. Proc. Des. Dev., 1, 102 (1962).

Badilla-Ohlbaum, R., and D. Chadwick, Fuel, 58, 834 (1979a).

Badilla-Ohlbaum, R., K. C. Pratt, and D. L. Trimm, Fuel, 58, 309 (1979b).

Baker, R. T. K. et al., J. Catal., 26, 51 (1972).

Baker, R. T. K., and P. S. Harris, Chemistry and Physics of Carbon, 14, 83 (1978).

Beeckman, J. W., and G. F. Froment, Ind. Eng. Chem. Fundam., 18, 245 (1979).

Beeckman, J. W., and G. F. Froment, Chem. Eng. Sci., 35, 805 (1980).

Berg, L., and F. P. McCandless, U.S. DOE Report No. FE-2034-6 (1977).

Berg, L., and F. P. McCandless, U.S. DOE Report No. FE-2034-20, June 13 (1980).

Bird, R. B., W. E. Stewart, and E. N. Lightfoot, "Transport Phenomena", John Wiley and Sons, New York, (1960), p. 514.

Bodzek, D., and A. Marzec, Fuel, 60, 47 (1981).

Borghi, M. D., J. C. Dunn, and K. B. Bischoff, Chem. Eng. Sci., 31, 1065 (1976).

Bouwman, R., and L. H. Toneman, J. Catal., 61, 146 (1980).

Bowman, R. M., B. J. Jody, and G. Jarvi, U.S. DOE Report No. DOE/SF/10760-2 (1980).

Brinkman, D. W., M. L. Whismam, and J. N. Bowden, U.S. DOE Report No. BETC/RI-78/23 (1979).

Butt, J. B., Adv. Chem. Ser., 109, 286 (1972).

Caldwell, R. D., and S. M. Everman, Prep. Div. Pet. Chem. Am. Chem. Soc., 22, 984 (1979).

Carberry, J. J., "Chemical and Catalytic Reaction Engineering", McGraw-Hill, New York (1976).

Carberry, J. J., and R. L. Gorring, J. Catal., 5, 529 (1966).

Carnahan, B., H. A. Luther, and J. O. Wilkes, "Applied Numerical Methods", Wiley, New York (1974).

Caspers, J., R. P. Van Driesen, K. Hastings, and S. Morris, Coal Processing Technology, 7, 43 (1981).

Chiou, M. J., and J. H. Olson, Prep. Div. Pet. Chem. Am. Chem. Soc., 23, 1421 (1978).

Chu, C., and I. Wang, Ind. Eng. Chem. Proc. Des. Dev., 21, 338 (1982).

Chun, S. W., U.S. DOE Report No. DOE/PETC/QTR-81/1 (1981).

Cocchetto, J. F., and C. N. Satterfield, Ind. Eng. Chem. Proc. Des. Dev., 20, 49 (1981).

Comolli, A. G. et al., Proceedings of the EPRI Contractor's Conference on Coal Liquefaction, Palo Alto, May 8-10 (1979).

Crynes, B. L., "Chemistry of Coal Utilization", (Editor: Elliott, M. A.), John Wiley and Sons, Inc. (1981a), p. 1993.

Crynes, B. L., U.S. DOE Report No. DE-14876-6 (1981b).

Curtis, C. W., et al., Prep. Div. Fuel. Chem. Am. Chem. Soc., 26, 23 (1981).

Daly, F. P., J. Catal., 41, 221 (1978).

Dautzenberg, F. M. et al., ACS Symp. Ser., 65, 254 (1978).

Davidson, R. M., Report No. ICTIS/TR08, IEA Coal Research, London (1980).

DePauw, R., and G. F. Froment, Chem. Eng. Sci., 30, 789 (1975).

deRosset, A. J., U.S. DOE Report No. FE-2001-01 (1976).

deRosset, A. J., G. Tan, and Gatsis, Adv. Chem. Ser., 179, 109 (1979).

Dickie, J. P., and T. F. Yen, Anal. Chem., 39, 1847 (1967).

Doelman, J., and J. C. Vlugter, Sixth World Pet. Cong., 3, 247 (1963).

Doraiswamy, L. K., Catal. Rev., 10, 177 (1975).

Dudukovic, M. P., AICHE J., 22, 945 (1976).

Duraiswamy, K., "Effect of Coke Formation on the Kinetics of Hydrocracking of Heavy Oil", Ph.D. Thesis, University of Utah, Salt Lake City, Utah (1973).

Eberly, P. E. Jr., C. N. Kimberlin, Jr., W. H. Miller, and H. V. Drushel, Ind. Eng. Chem. Proc. Des. Dev., 5, 193 (1966).

_____, Engineering Data Book, Gas Processors Suppliers Association, Tulsa (1977).

Ehmke, E. F., Materials Performance, 14(7), 20 (1975).

Epperly, W. R., U.S. DOE Report No. FE-2893-45 (1980).

Fant, B. T., and W. J. Barton, Proceedings, Refining Dept., API, 224 (1978).

Finseth, D., M. Hough, J. A. Queiser, and H. L. Retcofsky, Prep. Div. Pet. Chem. Am. Chem. Soc., 24, 979 (1979).

Froment, G. F., Proc. 6th Int. Cong. Catal., 1, 10 (1976).

Froment, G. F., "Catalyst Deactivation", (Editors: Delmon, B., and G. F. Froment), Elsevier Scientific Publishing Company, New York (1980), p. 1.

Froment, G. F., and K. B. Bischoff, Chem. Eng. Sci., 16, 189 (1961).

Frumkin, H. A., R. F. Sullivan, and B. E. Stangeland, ACS Sym. Ser., 156, 75 (1981).

Furimsky, E., Ind. Eng. Chem. Prod. Res. Dev., 17, 329 (1978).

Furimsky, E., AIChE J., 25, 306 (1979).

Gary, J. H., J. O. Golden, and R. L. Bain, U.S. DOE Report No. FE-2047-10 (1978).

Garg, D. A. et al., Fuel Processing Technology, 3, 263 (1980).

Garg, D. A., A. R. Tarrer, and J. A. Guin, ACS Symp. Ser., 156, 191 (1979).

Garg, D. A. et al., ACS Sym. Ser., 156, 191 (1981).

Gates, B. C. et al., U.S. DOE Report No. FE-2028-15 (1979).

Given, P. H., Fuel, 39, 147 (1960).

Given, E. N. et al., U.S. DOE Report No. FE-2003-27 (1977).

Given, E. N., M. A. Collura, R. W. Skinner, and E. J. Greskovich, Adv. Adv. Chem. Ser., 179, 121 (1979).

Greskovich, E. J., E. N. Given, and M. A. Collura, U.S. DOE Report No. FE-2003-21 (1977).

Haldeman, R. G., and M. C. Botty, J. Phy. Chem., 63, 489 (1959).

Hausler, D. W. et al., Fuel, 60, 40 (1981).

Heck, R. H., and T. R. Stein, Prep. Div. Pet. Chem. Am. Chem. Soc., 22, 948 (1977).

Heck, R. H., Proceedings of EPRI Contractor's Conference on Coal Liquefaction, Palo Alto, CA, May 8-10 (1977).

Heck, R. H., Proceedings of EPRI Contractor's Conference on Coal Liquefaction, Palo Alto, CA, May 10-11 (1978).

Henry, H. C., and J. B. Gilbert, Ind. Eng. Chem. Proc. Des. Dev., 12, 328 (1973).

Hildebrand, R. E., DOE Contractor's Conference, Richmond, CA, May 7-8 (1979).

Ho, B., and E. Briggs, AIChE New Orlean Meeting, November 10 (1981).

Hochman, J. M., and E. Effron, Ind. Eng. Chem. Fundam., 8, 63 (1969).

Holloway, P. H., and G. C. Newson, Prep. Div. Pet. Chem. Am. Chem. Soc., 22, 1352 (1977).

Huang, C. S., K. C. Wang, and H. W. Haynes, "Liquid Fuel From Coal", (Editor: Ellington, R. T.), Academic Press, New York (1977), p. 63.

Hughes, C. C., and R. Mann, ACS Sym. Ser., 65, 201 (1978).

Huntington, M. G., U.S. Patent No. 3,244,615 (1966).

Jacob, H. E., J. F. Jones, and R. T. Eddinger, Ind. Eng. Chem. Proc. Des. Dev., 10, 558 (1971).

Johnson, C. A., et al., Chem. Week, 114, 549 (1974).

John, T. M., R. A. Pachovsky, and B. W. Wojciechowski, "Chemical Reaction Engineering, II" (1974), p. 422. .

Karn, F. S., F. R. Brown and A. G. Sharkey, Prep. Div. Fuel Chem. Am. Chem. Soc., 19, 2 (1974).

Katzer, J. R., B. C. Gates, J. H. Olson, and A. B. Stiles, U.S. DOE Report No. FE-2028-7 (1976).

Katzer, J. R., and R. Sivasubramanian, Catal. Rev. Sci. Eng., 20, 155 (1979).

Kershaw, J. R., B. Gordon, I. C. Dupreez, and D. Gray, Fuel Processing Technology, 3, 115 (1980a).

Kershaw, J. R., B. Gordon, I. C. Dupreez, and D. Gray, Fuel Processing Technology, 3, 131 (1980b).

Ketkar, R., Special Report Submitted to Dr. B. L. Crynes, Oklahoma State University, Stillwater (1977).

Kobe, K. A., and J. J. McKetta Jr., "Advances in Petroleum Chemistry and Refining", Vol. 7, Interscience Publishers, New York (1963).

Koros, R. M., Fourth ISCRE, Heidelberg, April (1976).

Krishnamurthy, S., S. Panvelker, and Y. T. Shah, AIChE J., 27, 994 (1981).

Laine, J., K. C. Pratt, and D. L. Trimm, Ind. Eng. Chem. Prod. Res. Dev., 18, 329 (1979).

Lamba, H. S., and M. P. Dudukovic, The Chem. Eng. J., 16, 117 (1978).

Lee, H. C., and J. B. Butt, J. Catal., 49, 320 (1977).

Lee, W. J., and J. B. Butt, The Chem. Eng. J., 6, 111 (1973).

Levenspiel, O., J. Catal., 25, 265 (1972).

Lewis, H. E., U.S. DOE Report No. FE-2270-74 (1981).

Lewis, I. C., and T. Edstrom, J. Org. Chem., 18, 2050 (1963).

Lin, Y. Y., L. L. Anderson, and H. H. Wiser, Prep. Div. Fuel Chem. Am. Chem. Soc., 19, 2 (1974).

Lipsch, J. M., J. G., and G. C. A. Schuit, J. Catal., 15, 163 (1969).

Madison, J. J., and R. M. Roberts, Ind. Eng. Chem., 50, 237 (1958).

Masamune, S., and J. M. Smith, AIChE J., 12, 384 (1966).

McGinnis, E. L., Prep. Div. Pet. Chem. Am. Chem. Soc., 23, 1340 (1978).

McIlvried, H. G., Ind. Eng. Chem. Proc. Des. Dev., 10, 125 (1971).

McKinley, J. B., Catalysis, Vol. V, 405 (1975).

Mears, D. E., Chem. Eng. Sci., 26, 1361 (1971).

Mears, D. E., Adv. Chem. Ser., 133, 218 (1974).

Mehta, D. C., "Catalyst Aging Tests and the Role of Catalyst Wetting on Hydrodesulfurization of a Coal Derived Liquid", Ph.D. Thesis, Oklahoma State University, Stillwater (1978).

Mineav, V. Z. et al., Chem. Technol. Fuel Oils, 7, 436 (1975).

Mitchell, T. O., Coal Processing Technology, VI, 28 (1980).

Morsi, B. I., N. Midoux, and J. C. Charpentier, AIChE J., 24, 357 (1978).

Murakami, Y., T. Kobayashi, T. Hattori, and M. Masuda, Ind. Eng. Chem. Fundam., 7, 599 (1968).

Newson, E., Ind. Eng. Chem. Proc. Des. Dev., 14, 27 (1975).

Nokamura, M., O. Togari, and T. Ono, Proceedings Refining Dept., API, 201 (1979).

O'Rear, D. J., R. F. SUllivan, and B. E. Strangelan, Prep. Div. Fuel Chem. Am. Chem. Soc., 25, 78 (1980).

O'Rear, D. J., R. F. Sullivan, and B. E. Strangelan, ACS Sym. Ser., 156, 115 (1981).

Owens, P. J., and C. H. Amberg, Can. J. Chem., 40, 941 (1962a).

Owens, P. J., and C. H. Amberg, Can. J. Chem., 40, 947 (1962b).

Ozawa, Y., and K. B. Bischoff, Ind. Eng. Chem. Proc. Des. Dev., 7, 67 (1968a).

Paraskos, J. A., J. A. Frayer, and Y. T. Shah, Ind. Eng. Chem. Proc. Des. Dev., 14, 315 (1975).

Peppas, N. A. et al., U.S. DOE Contract No. DE-FG22-80PC30222 (1981).

Polinski, L. M., G. J. Siegel, and R. E. Tischer, U.S. DOE Report No. DOE/PETC/TR-81/2 (1981).

Potts, J. D., K. E. Hastings, and H. Unger, U.S. DOE Report No. FE-2038-25 (1978).

Potts, J. D., K. E. Hastings, R. S. Chillingworth, and H. Unger, ACS Sym. Ser., 156, 153 (1981).

Prasher, B. D., G. A. Gabriel, and Y. H. Ma, Ind. Eng. Chem. Proc. Des. Dev., 17, 266 (1978).

Prather, J. W. et al., Ind. Eng. Chem. Proc. Des. Dev., 16, 267 (1977).

Qadar, S. A., and G. R. Hill, Fuel, 51, 54 (1972).

Reid, M., J. M. Prausnitz and T. K. Sherwood, "The Properties of Gas and Liquid", 3rd ed., McGraw-Hill, New York (1977).

Riley, K. L., Prep. Div. Pet. Chem. Am. Chem. Soc., 23, 1104 (1978).

Ryan, D. F., DOE Contractor's Conference, Richmond, CA, May 7-8 (1979).

Rudershausen, C. G., and C. C. Watson, Chem. Eng. Sci., 3, 110 (1954).

Sapre, A. V., and B. C. Gates, Ind. Eng. Chem. Proc. Des. Dev., 20, 68 (1981).

Satchell, D. P., "Hydrogenation of a Coal Derived Liquid", Ph.D. Thesis, Oklahoma State University, Stillwater, Oklahoma (1974).

Satterfield, C. N., AIChE J., 21, 209 (1975).

Satterfield, C. N., C. K. Colton, and W. H. Pitcher, Jr., AIChE J., 19, 628 (1973).

Satterfield, C. N., A. A. Pelossof, and T. K. Sherwood, AIChE J., 15, 226 (1969).

Satterfield, C. N., M. Modell, and J. F. Mayer, AIChE J., 21, 1100 (1975).

Satterfield, C. N. and J. F. Cocchetto, Ind. Eng. Chem. Proc. Des. Dev., 20, 53 (1981).

Satterfield, C. N., M. Modell, and J. A. Wilkens, Ind. Eng. Chem. Proc. Des. Dev., 19, 154 (1980).

Satterfield, C. N., M. Modell, R. A. Hites, and C. J. Declerck, Ind. Eng. Chem. Proc. Des. Dev., 17, 141 (1978).

Satterfield, C. N., and T. K. Sherwood, "The Role of Diffusion in Catalysis", Addison-Wesley, Reading, Massachusetts (1963), p. 11.

Schiller, J. E., Hydrocarbon Processing, 57, 147 (1977).

Seapan, M., and B. L. Crynes, U.S. DOE Report No. DOE/BC/10306-11 (1981).

Shah, Y. T., "Gas-Liquid-Solid Reactor Design", McGraw-Hill, New York (1979).

_____, Shell Chemical Company, Houston, Texas, Personal Communication (1980).

Shih, S. S., J. R. Katzer, H. Kwart, and A. B. Stiles, Prep. Div. Pet. Chem. Am. Chem. Soc., 22, 919 (1977).

Shih, S. S. et al., ACS Symp. Ser., 156, 175 (1980).

Shultz, J. L., C. M. White, F. K. Schweighardt, and A. G. Sharkey, Jr., U.S. DOE Report No. PETC/RI-7717 (1977).

Sivasubramanian, R., "Effect of Catalyst Support Properties on Hydrodenitrogenation of a Coal Liquid", Ph.D. Thesis, Oklahoma State University, Stillwater (1977).

Sivasubramanian, R., and B. L. Crynes, Ind. Eng. Chem. Proc. Des. Dev., 18, 175 (1979).

Sivasubramanian, R., and B. L. Crynes, Ind. Eng. Chem. Prod. Res. Dev., 19, 456 (1980).

Sivasubramanian, R., J. H. Olson, and J. R. Katzer, Prep. Div. Fuel. Chem. Am. Chem. Soc., 25, 84 (1980).

Soni, D. S., "A Comparison of the Desulfurization and Denitrogenation Activities of Monolith Alumina Impregnated with Cobalt and Molybdenum and Nalcomo 474 Catalyst", M.S. Thesis, Oklahoma State University, Stillwater (1974).

Soni, D. S., and B. L. Crynes, ACS Symp. Ser., 156, 207 (1981).

Sonnemans, J., W. J. Neyens, and P. Mars, J. Catal., 34, 230 (1974).

Sooter, M. C., "Effect of Catalyst Pore Size on Hydrodesulfurization of Coal Derived Liquids", M.S. Thesis, Oklahoma State University, Stillwater (1974).

_____, Oil and Gas J., March 17, 85 (1975).

Stanulonis, J. J., B. C. Gates, and J. H. Olson, AIChE J., 22, 576 (1976).

Stein, T. R. et al., FPRI Report No. AF-873 (1978).

Stern, E. W., J. Catal., 57, 390 (1979).

Sternberg, H. W., R. Raymond, and F. K. Schwerghardt, Science, 188, 49 (1975).

Struck, R. T. et al., Ind. Eng. Chem. Proc. Des. Dev., 8, 546 (1969).

Sullivan, R. F., D. J. O'Rear, and B. E. Stangeland, Prep. Div. Pet. Am. Chem. Soc., 25, 583 (1980).

Sullivan, R. F., C. J. Egan, and G. E. Langlois, J. Catal., 183, 3 (1964).

Sullivan, R. F., B. E. Stangeland, and H. A. Frumkin, DOE Contractor's Conference, Richmond, CA, May 7-8 (1979).

Sullivan, R. F., U.S. DOE Report No. FE-2315-45 (1981).

Tai, N. M., and P. F. Greenfield, The Chem. Eng. J., 16, 89 (1978).

Takatsuka, T., H. Nitta, S. Kodama, and T. Yokoyama, Prep. Div. Pet. Chem. Am. Chem. Soc., 24, 730 (1979).

Tamm, P. W., H. F. Harnsberger, and A. L. Bridge, Ind. Eng. Chem. Proc. Des. Dev., 20, 262 (1981).

Ternan, M., E. Furimsky, and B. I. Parsons, Fuel Processing Technology, 2, 45 (1979).

Uchida, S., S. Osuda, and M. Shindo, Can. J. Chem. Eng., 53, 666 (1975).

van Klinken, J., and R. H. van Dongen, Chem Eng. Sci., 35, 59 (1980).

van Zoonen, D., Proc. 3rd Int. Cong. Catal., 1320 (1965).

Veluswamy, L. R., "Catalytic Hydrogenation of Coal-Derived Liquids and Related Polycyclic Aromatic and Heterocyclic Compounds", Ph.D. Thesis, University of Utah, Salt Lake City (1977).

Voorhies, A. Jr., Ind. Eng. Chem., 37, 318 (1945).

Weekman, V. W., Ind. Eng. Chem. Proc. Des. Dev., 7, 90 (1968).

Weisser, O., and S. Landa, "Sulfide Catalysts, Their Properties and Applications", Pergamon Press, New York (1973).

Wheeler, A., Adv. Catal., 3, 249 (1951).

Wheeler, A., Catalysis, 2, 105 (1955).

White, P. J., J. F. Jones, and R. T. Eddinger, Hydrocarbon Processing, 47(12), 97 (1968).

Whitehurst, D. D. et al., EPRI Report No. AF-1184 (1979a).

Whitehurst, D. D. et al., EPRI Report No. AF-1255 (1979b).

Whitehurst, D. D., M. Farcasiu, and T. O. Mitchell, EPRI Report No. AF-252 (1976).

Wilke, C. R., and P. Chang, AIChE J., 1, 264 (1955).

Wiser, W. H., U.S. DOE Report No. FE-2006-5 (1977).

Wiser, W. H., U.S. DOE Report No. FE-2006-11 (1978).

Wojciechowski, B. W., Catal. Rev. Sci. Eng., 9, 79 (1974).

Wu, W. L., and H. W. Haynes, ACS Sym. Ser., 20, 65 (1975).

Yovorsky, M. M. et al., Chem. Eng. Prog., 71, 79 (1975).

APPENDIX A

LIST OF MAJOR EQUIPMENTS

Following is a list of the major equipments used in this study. The stainless steel tubings and valves used are from either Autoclave Engineers or Parker Hanifin, rated to 5000 psi and are, however, not included in the list below.

Oil Feed System

1. Lewa Model FL-3 Triplex Plunger Type Metering Pump - pump equipped with three independent plunger pump heads, each having a flow of 0-160 cc/hr at a maximum back pressure of 5700 psig and 42 str/min; American Lewa, Inc., Natick, Massachusetts.

2. Storage Tank - 10 gallon stainless steel storage tank; McMaster Model #4146Y22, McMaster Carr, Chicago, Illinois.

3. Pressure Guages - Crosby pressure gauges, maximum 5000 psig, Model #BSH-5009.

4. Rupture Discs - 1/4-inch, bursting pressure 3000 psig, Frangilde Discs, Inc..

5. Pressure Switches - UE Series 110 explosion proof pressure switches, pressure range 500-6000 psi, 120V and 15 amp SPDT switch, internally adjustable; Economy Gauge and Instrument Supply Model #J110614.

6. Temperature Controllers - UE Series 110 explosion proof, external knob and dial, 120V and 15 amp SPDT switch, adjustable range - 125 to 500°F, style C bulb; Economy Gauge and Instrument Supply Model #E1103CS.

7. Storage Tank Heater - Ogden Band Heater, inside diameter 14 inches, width 4.5 inches, nominal watts 4000; Economy Gauge and Industrial Supply.

8. Liquid Level Controller - Rochester Model #6250 switch gauge with four inch float (2/5023S00778); Rochester Gauges, Inc., Dallas, Texas.

9. Feed Tanks - Matheson high pressure cylinders, model #4HDM500; Matheson Gas Products, LaPort, Texas.

Hydrogen Feed System

1. Gas Supply Manifold - Maximum pressure 7500 psi, Linde Specialty Gases Model #5RMS-3-6-350.

2. Pressure Regulator - Matheson Gas Products Model #3063B-677.

3. Pressure Switches - Economy Gauge and Instrument Supply Model #J110614.

4. Solenoid Valve - 2 way-2 position, normally closed, 6000 psi maximum, Circle Seal Model #SV21S2Nc4P; D and O Products Company, Wichita, Kansas.

5. Flow Control Valves - Badger Meter Flow Control Valves, air to open, P14 trim; Ken Batchelor Company, Tulsa, Oklahoma.

6. Heise Gauge - 16 inch dial, 5000 psig maximum, Heise-Bourdon tube gauge.

7. Diaphragm Gauge Separator - Ruska Instrument Corporation Model #2178-125-00.

8. Pressure Transducers - 0-5000 psig, 28V D.C. input, 0-5V output, BLH Model #4402-0186; BLH Electronics, Inc., Waltham, Massachusetts.

9. Hydrogen Compressor - 2 heads; compression ratio, 13; maximum pressure, 10,000 psig; Model #46-4035; American Instrument Company.

10. Pressure Relief Valve - 500-3500 psig release pressure, externally adjustable, Model #B5349T-4PP(L)-3500; Circle Seal, Anaheim, California.

11. Pressure Switch - UE Series 110 explosion proof pressure switch, pressure range 500-6000 psig, externally adjustable, Model #J110614; Ecomony Gauge and Instrument Supply.

12. Mity-Mite Dome Regulator - Model #94, 5000 psig maximum; Grove Valve and Regulator, Oakland, California.

Reactor System

1. Reactors - 316 stainless steel, 0.75 inch OD, 0.515 inch ID, 34 inches long, Autoclave Medium Pressure Nipples.

2. Heaters - R. T. type L Lead arrangement, 4 ft. lead, 3 inch ID, 6 inches/12 inches wide, 120V, 500/1000 watts; Watlow Electric, St. Louis, Missouri.

3. Pressure Control Valves - Badger meter pressure control valves, air to open, P11, tapered trip; Ken Batchelor Company, Tulsa, Oklahoma.

4. Pressure Transducers - BLH Model #4402-0186; BLH Electronics, Inc., Waltham, Massachusetts.

5. Pressure Gauges - 0-5000 psi Crosby Pressure Gauges, Model #BSH-5009.

Product Oil Separation and Sampling System

1. Solenoid Valves - 3 way-2 position, 4500 psi maximum, Circle Seal Model #SV41S32PSP; D and O Products Company, Wichita, Kansas.

2. Pressure Gauges - Crosby pressure gauges, 0-5000 psi; Model #BSH-5009.

3. Sample Bombs - Matheson high pressure sampling cylinders, Model #4HDM500; Matheson Gas Products, LaPorte, Texas.

4. Scrubber Tank - McMaster Carr Model #4120T1, six gallon 304 ss tank rated to 80 psi, McMaster Carr, Chicago, Illinois.

Miscellaneous

1. Doric Electronic Temperature Readout - Model #410-J-F with four manual switching units, Model #405; Doric Scientific Corporation, San Diego, California

2. Honeywell Dialotrols - Temperature Controllers - PID, J-type thermocouple input, 0-1000°F Range, Model #R7355C-1132; Honeywell, Inc., Oklahoma City, Oklahoma.

3. Honeywell Dialotrols - Pressure Controllers - PID, 0-50 mv input, 0-5000 psi range, Model #R7355C-1140, Honeywell, Inc., Oklahoma City, Oklahoma.

4. Honeywell Multipoint Strip Chart Recorder - 0-1000°F; J-type thermocouple input, Model #11240150-0602-0000-00-000-10-102-18-100, 204,205; Honeywell, Inc., Oklahoma City, Oklahoma.

5. Honeywell Twelve Point Strip Chart Recorder - 0-50 mv DC input, Model #11240180-46010-00000-00-00020-102-18-100,204,205; Honeywell, Inc., Oklahoma City, Oklahoma.

6. Power Supply to Reactor Heaters - SCR Burst-Fire power regulator, 120V, Honeywell Model #R7291A.

7. DC Power Supply - 0-10V, 0-1 amp, Hewlett Packard Model #6289A; Hewlett Packard, Oklahoma City, Oklahoma.

8. DC Power Supply - 0-50V, 0-1 amp, Hewlett Packard Model #6289A; Hewlett Packard, Oklahoma City, Oklahoma.

9. Twin Six Volt Emergency Lights - McMaster Carr Model #1639K15; McMaster Carr, Chicago, Illinois.

10. Moldable Felt Insulation Fabrics - One inch thick, sheet size 24 inch x 36 inch; McMaster Car Model #9326N5.

11. Air Compressor - Delivers 1.5 scfm air at up to 80 psi, McMaster Carr Model #4369K51.

12. Filter-Regulator - Combination designed for pneumatic systems, 5-125 psi range, McMaster Carr Model #5001K14.

13. Gas Detector - MSA Model #I-501 with two remote diffusion heads for hydrogen; M.S.A. Instrument Division, Pittsburgh, Pennsylvania.

14. Smoke Detector - Security Systems Model #209-9; Security Systems, Salisbury, Maryland.

15. Dialing Arrangement - Security Systems Model #1612 telephone dialer arm; Model #1616 dual purpose power supply; Model #1614 tape cartridge; Model #1617 coupler calde; Model #1618 programmer for dialer; Security Systems, Salisbury, Maryland.

16. Pneumatic Pressure Transducers - 0-25 milliamp input, 3-15 psi output, Honeywell Model #8700220-12-00-00-01-00-00; Honeywell, Inc., Oklahoma City, Oklahoma.

APPENDIX B

DETAILS OF HYDROTREATMENT EQUIPMENT

Details of the experimental equipment, including oil feed, hydrogen feed, reactor, separation and pressure control and safety systems of the hydrotreatment system will be given in this appendix.

Oil Feed System

The oil feed system basically consists of a feed oil storage tank, a filter in the feed line, two high pressure feed tanks, a Lewa Model FL-3 Triplex plunger type metering pump, oil feed lines to the reactors and rupture relief lines including rupture discs and pressure gauges as shown in Figure 10. The filter shown in the figure is installed in the line between the feedstock storage tank and the entrance of the feed tanks to prevent fine particles being carried into pump heads.

Oil is fed to the reactor by the Lewa metering pump at a preset rate. The feed rate can be varied in the range of 0.0-0.16 liter per hour by adjusting the pump stroke length. The pump consists of three plunger type pump heads totally independent of each other. These pumps heads supply oil to the three trickle bed reactors in parallel in the CLTU. The purpose of the high pressure feed tanks are to

enhance suction pressure for the pump heads and thus to leave the major pump duty to accurately control the liquid feed rate.

The possible pressure buildup while pumping liquid with a constant displacement type pump and the consequent damage in case of the clogging of a portion or portions of oil lines is avoided by installing rupture relief lines. Rupture discs designed to blow out at 20.7 MPa (3000 psig) are installed in these rupture lines (Figure 10). The pressure in the oil lines for each reactor is monitored by a 0 - 34.6 MPa (0 - 5000 psig) bourdon type pressure gauge. A pressure switch is also installed between the pump discharge end and the rupture discs to trip an alarm at 3.4 MPa (500 psig) higher than the normal operating pressure. The activation of the alarm results in shut off of the main power supply to the system and hence in shut down of the whole system. Thus there are two safety measures (pressure switch and rupture disc) installed in the system to take care of overpressure. The rupture relief lines terminate in the storage tank for dumping of the break-through oil.

The oil feed tank, filters, oil feed lines, rupture relief lines and the pump heads are all wrapped with electrical heating tapes and maintained at constant temperatures of up to 204 C (400 F) depending on the feed oil. The heat loads supplied by these tapes are regulated by on-off type controllers with thermocouples providing the feedback signals.

Hydrogen Feed System

Hydrogen Pressure Boost

As shown in Figure 11, an air driven compressor (American Instrument Company Model 46-4035) is installed to boost hydrogen from low pressure to high pressure cylinders. Two safety devices are incorporated: a pressure switch and a pressure relief valve. The former is designed to cut off of the air supply and the hydrogen source whenever the preset delivery pressure is reached. The latter is designed to release excess pressure in case the system malfunctions and the pressure builds up. This auxillary system is independent of the hydrotreatment system and therefore, can be operated at any time to charge high pressure hydrogen cylinders.

Hydrogen Feed

Hydrogen is fed to the reactor directly from high pressure cylinders. A manifold is constructed to allow switching the hydrogen cylinders during the run as shown in Figure 12. These cylinders are connected to the manifold through lines containing one-way check valves. A Mity-Mite regulator is used to regulate the reactor upstream hydrogen pressure.

A solenoid valve hooked to the safety system follows the Matheson pressure regulator. Except in the case of an alarm condition this solenoid valve can be operated while bypassing the safety system. A check valve provided after the solenoid valve takes care of sudden pressure losses by restricting the hydrogen flow. A pressure switch similar to the ones installed in the oil feed system provides the input

to the safety system regarding pressure losses in the hydrogen line. This switch is adjusted to activate at 17.4 MPa (2500 psig).

The pressure in the hydrogen line is monitored using a bourdon type pressure gauge as well as using a BHL pressure transducer. The pressure transducer operates on a 28 volts D.C. input and gives a linear output of 0-5 volts in the range of 34.6 MPa (0-5000 psig). The output signal is stepped down to 0-50 mv range and supplied as input to a twelve point Honeywell strip chart recorder for pressure recording. Most of the high pressure gas lines are of 0.3175 cm (1/8 inch) 316 stainless steel tubing.

Reactor System

The reactor system basically consists of three trickle bed reactors in parallel and a number of corresponding temperature controllers.

Reactors

The reactors are 0.868 m (34 inches) long, 19.05 mm (3/4 inch) O.D., 316 stainless steel autoclave nipples threaded on both ends. A thermowell of 3.175 mm (1/8 inch) O.D., 316 stainless steel tubing with one end welded shut is secured at the top of the reactor by Swagelok fittings. The closed end is at the bottom of the reactor and the 6.35 mm (1/4 inch) to 3.175 mm (1/8 inch) reducing union is drilled for easy sliding of the thermowell tubing.

The reactors are packed with inerts at the top with a catalyst bed placed in the middle and an empty tubing at the bottom. These catalyst or inert material are held in place by wedging 50 mesh screens between the fittings and the top and bottom ends of the catalyst bed.

A one-way check valve and an oil trap are provided just before the hydrogen inlet to the reactor to avoid oil flow into the gas lines. The reactors are rated to 69 MPa (10,000 psig) at room temperature.

Reactor Temperature Controls

A 0.61 m (24 inches) long, 76.2 mm (3 inches) O.D. annular copper cylinder snugly fitting the 19.05 mm (4/3 inch) reactor is wrapped with electrical heating bands to obtain a flat axial temperature profile. Two 76.2 mm (3 inches) long heater bands rated to 500 watts are provided at both ends and are regulated manually using variacs. Three 0.152 m (6 inches) long bands in the middle are hooked in parallel to a Honeywell SCR Burst Power regulator. These bands are each rated to 1000 watts and the SCR power regulator is of on-off type providing a maximum current of 25 amps to the heaters. The temperature in the middle of the reactor is used for control purposes and is supplied to a Honeywell three mode temperature controller which in turn sends a signal in the range of 4-25 ma to the SCR Burst Power Supply.

Iron-constantan (J-type) thermocouples with grounded tip sensor are used for monitoring the axial temperature along the reactor at seven locations outside the reactor wall and one location inside the catalyst bed. Thermocouple #5 at middle of the reactor supplies the input signal to the temperature controller, while, all other thermocouples are connected to a Doric temperature read-out as well as to a twenty-four point Honeywell strip chart recorder. The temperature controllers (Dialotrols), strip chart recorder, Doric digital read-out, SCR Burst power regulator are all installed in the CLTU control panel.

Felt fabric and fiber glass are used for making the insulation in the form of a cylinder which is split in the middle. The entire reactor is surrounded by insulation and the insulation is held in place by fiber glass strips. The electrical connections for the heaters are made through the break in the insulation while carefully packing the break with fiber glass to avoid unnecessary heat losses.

All the wiring for the heaters (power lines) and the thermocouples (sensor lines) are run through flex conduits to meet the 1975 national electric code for safety considerations. All the electrical connections are made in explosion proof boxes and the power and sensor lines are run through separate conduits to avoid interference.

Separation and Pressure Control System

Gas-Liquid Separation

As shown in Figure 13, the two phase product stream from the reactor flows into the separator vertically via a half inch tubing. The heavy product is disengaged in the first separator which is maintained at 204 C (400 F) to prevent heavy product precipitation. The half inch tubing only shortly intrudes into the tank to avoid plugging by heavy product. The light product and the gas stream flow to the second separator which is operated at ambient temperature. The gas is released through a pressure control valve in which the pressure is reduced to the ambient value.

The effluent gases from the pressure control valve are scrubbed with a caustic solution before venting to the atmosphere. The scrubber consists of a 7.57 liters (2 gallons) stainless steel tank containing

a 20 wt% caustic solution and is maintained at a temperature of about 38 C (100 F). The scrubber tank is rated to 2.52 MPa (350 psig) at room temperature.

The volumes of the first and the second separation bombs are 1 and 0.5 liter respectively. The heating devices for the first separation bomb and the scrubber consist of insulating fiber glass and electrical heating tapes controlled by on-off type controllers. J-type thermocouples are used to monitor the temperatures at various locations. These temperatures are displaced on a Doric digital readout as well as recorded on a twenty-four point strip chart recorder.

The pressure in the separation system is monitored by bourdon type gauges. A water displacement type of wet test meter is installed in the gas line to the scrubber exit for measuring the effluent gas flow rate.

Pressure Control

The reactor pressure is controlled by a pneumatically operated air to open control valve designed to handle a pressure drop of 13.9 MPa (2000 psig) and located downstream of the second separation bomb. The pressure control includes a BLH pressure transducer, a Honeywell three mode controller (Dialotrol) and an electropneumatic pressure transducer. The BLH pressure transducer is operated on a 28 VDC power, supplied by a Hewlett-Packard constant voltage DC power supply unit located on the control panel. The output of the pressure transducer (0-5 Volts) is stepped down to 0-50 mV and is supplied to the Dialotrol for control and to the twelve point strip chart recorder

for recording purposes. The Dialotrol supplies an output signal in the range of 4-25 ma to the electropneumatic pressure transducer which in turn supplies an air pressure of 120-200 KPa (3-15 psig) to the control valve.

Air to the electropneumatic transducer is supplied by an air or a nitrogen cylinder located outside the cell. The air or nitrogen pressure is reduced to 239 KPa (20 psig) with a Matheson pressure regulator before fed to the transducer. The pressure control valve is supplied by Badger Meter Inc., and has a specially designed P-14 tapered trim to handle high pressure drop and low hydrogen flow.

In general the reactor upstream pressure is monitored in the oil lines by a bourdon type gauge, in the gas lines by a bourdon type gauge and a BLH pressure transducer both at upstream and downstream of the reactor. The pressure dialotrol can accept an input signal from BLH pressure transducer located up or downstream of the reactor. If receives signal from upstream, the pressure controller can automatically release the reactor downstream pressure and purge the reactor with hydrogen in case of partial plugging occurs in the reactor.

Safety System

The CLTU test cell has been rated to be in a Class I, Divison 2, Group B area under the 1975 National Electric Code by the Safety and Security Personnel at Oklahoma State University. This classification requires the running of all electrical wires through flex conduits and making the connections in explosion proof (hazardous) boxes, commonly

known as hubs. The flex conduits are connected to a sealing fitting before passing into the hub, thus avoiding fire hazards due to sparking contacts. The safety system consists of an arrangement to detect the following hazardous conditions:

1. Hydrogen leak.
2. Fire and smoke.
3. Overpressure of oil lines.
4. Sudden hydrogen pressure loss or a low pressure in the gas line.
5. Low liquid level in the feed tank.

The various component of the safety system include a hydrogen gas detector, smoke and fire detectors, pressure sensors, liquid level detector and an electronic circuitry capable of terminating the main power to the test cell and the control panel, activating an auto dialer to summon help, switching on an audible alarm and simultaneously activating an emergency lighting system (battery operated) in the cell and in the control room.

In general the dangerous situations are considered under two classifications: 1) warning conditions and 2) alarm condition.

Alarm Conditions

1. Hydrogen leak: Two detector heads, one located inside the cell and the other inside the main building behind the control panel.

2. Smoke and fire: Two detectors, one placed inside the cell and the other behind the control panel.

3. Overpressurization in any one or more oil lines: In case of clogging of a portion or portions of the oil flow path, the pressure

will build up due to the presence of the constant displacement type pump. Pressure sensors (pressure switches) are installed between the pump discharge end and the reactor inlet and are adjusted to activate the alarm system at 3.4 MPa (500 psi) higher than the normal operating pressure. Three pressure sensors, one each in the oil feed line of the three reactors are present in the system. Rupture discs rated to blow out at 2.08×10^4 KPa (3000 psig) are also provided in the system to avoid rupture of the oil lines in case of the failure of the safety system.

Warning Conditions

1. Hydrogen pressure loss or low pressure in the gas line: Hydrogen is supplied to the reactors from 41.5 MPa (6000 psig) cylinders. During normal operation the pressure in the gas lines is maintained at 2 MPa (300 psi) above the operating pressure, however, the cylinder pressure goes down because of consumption and in case of a sudden pressure loss there exist a possibility that the cylinder pressure may go below the operating pressure. Under such conditions oil will start flowing in the gas lines and there will be no hydrogen supply to the reaction zone thus enhancing the rate of undesirable side reactions.

2. Low liquid level in the feed oil tank: The feed oil is stored in a tank from which it is being constantly pumped out. There exists a possibility that the oil lines can run dry because of no oil in the tank. This can rarely happen, however, as a safety measure the liquid level is constantly monitored.

The sensor lines for all the detectors go through a circuit consisting of switches and low energy diodes installed in the CLTU control panel. These switches allow bypassing of one or more of these detectors in case of their malfunctioning.

APPENDIX C

DETAILS OF EXPERIMENTAL PROCEDURE

In this appendix, detail experimental procedure will be described so that the experiments can be understood and can be reproduced by following this described procedure. This procedure consists of catalyst preparation and loading, catalyst presulfiding, startup, normal operation, sampling, shut down, product oil and catalyst sample analyses.

Catalyst Calcining and Loading

The commercial $NiMo/Al_2O_3$ catalyst extrudates (1.6 x 4.0 mm or 1/16 x 1/6 inch) were calcined in a muffle furnace in air at 480 $\pm$ 10 C (900 $\pm$ 18 F) for one hour. These catalysts were then cooled down to room temperature in a dessicator and stored there until loading. This procedure has been designed to remove moisture adsorbed on the catalyst surface.

The 0.86 m (34 inches) long reactor was packed with 0.18 m (7 inches) empty tubing at the bottom, five sections of catalyst with 0.1 m (4 inches) each in the middle and 0.18 m of 0.8-1.0 mm diameter spheric glass beads (R-70, from Thomas Scientific Apparatus) at the top according to the following procedure.

1. Reactor is cleaned and the 19.05 mm (3/4 inch) Autoclave fitting is locked at the bottom.

2. A half inch tubing of 0.18 m long is slided into the reactor bottom from the top.

3. A steel support and a fifty mesh screen are secured at the top of the half inch tubing.

4. A 3.175 mm (1/8 inch) thermowell is held centrally from the reactor top through the rest of the packing.

5. Amount of catalyst is determined by weight before packing.

6. Catalyst pellets and R-70 glass beads are loaded into the reactor alternately with a small scoop until 0.1 m height is reached, then a screen with a central hole is pushed down to the top of the packing along the thermowell.

7. Repeat procedure 6 until only 0.18 m of the reactor space is left at the top.

8. The screens in the catalyst bed are to redistribute the oil and for the easy separation of the catalysts between sections. Therefore, it is necessary to make sure that the screen can hold the catalyst by turning the reactor over after packing each section.

9. The rest portion of the reactor is packed with R-70 glass beads and a fifty mesh screen is wedged between the reactor and the Autoclave fitting.

The packed reactor was then placed in the annular copper cylinder (heating system) and secured in the system by connencting the half inch Swagelok tee at the top to the feedline by a half to quarter inch reducer. The half inch Swagelok cross at the bottom was connected to the bourdon type pressure gauge by a half to quarter inch reducer. A commercial compound, Silver Goop, was used on all Swagelok threads

to facilitate their tightening and loosening and also to prevent seizing. "Snoop" leak detector solution was used for detecting leaks. The system was pressure tested with hydrogen at room temperature at a maximum pressure of 17.4 MPa (2500 psig), 3.4 MPa (500 psig) higher than the desired operating pressure, for two hours. In case of any leaks, the system was depressurized and adequate measures were taken for their rectification. If the pressure drop during the two hours period was less than 345 KPa (50 psig) and no detectable leaks were observed, then the system was assumed to be free from potentially hazardous leaks.

All the safety devices were tested for their proper functioning, and all the electrical connections were checked for short circuiting. Thermocouples were inserted into thermowells to monitor the temperatures at the eight locations inside and around the reactor. The next step in the experimental procedure is the activation of the catalyst.

Catalyst Presulfiding

After reactor setup and pressure testing, the reactor pressure was released by manually opening the control valve. The pressure control valve was kept opened during the presulfiding. The reactor was then charged with a mixture of 5 vol. % H_2S and 95 vol. % H_2 at a rate of 42 std. l/h (1.5 scf/h). The reactor temperature was then quickly raised to 204 C (400 F) and was stabilized there for two hours. The temperature was again increased to 316 C (600 F) for two hours and to 371 C (700 F) for one more hour. The total H_2S charged into the

catalyst in these five hours period was four times more than enough to completely sulfide all the nickle and molybdenum oxides in the alumina supported catalyst in the reactor.

This calcining and presulfiding procedure has been suggested by catalyst manufacturers, Shell Chemical Company (1980) and Armak Company (1976). These companies have studied the hydrodesulfurizations of vacuum gas oils over $NiMo/Al_2O_3$ catalysts and found that the above activation procedure has given the best results.

Startup Procedure

After presulfiding, the H_2S/H_2 gas stream was cut off and the pressure control valve was shut manually. The reactor temperature was reduced to 56 C (100 F) below the normal operating value. The oil storage tank, high pressure feed tanks, pump heads, oil feed lines, separation bombs and the scrubber were heated to the preset temperatures. The reactor and the separation bombs were isolated from each others by a valve. The hydrogen was charged into the reactor up to the normal operating pressure through the gas line at the reactor top, while into the separation bombs through a gas line located at top of the first separation bomb, as shown in Figure 13.

The oil pump was started and was first set at a rate of 0.1 liter per hour so that the catalyst bed could be filled with oil within half an hour of startup. When the pressure gauge on the oil line started increasing (which means that the oil line has been filled with oil), the valve before the reactor entrance was opened to let the oil flow into the reactor. The pressure controller was then set at the normal operating pressure, the valve between the reactor and the

first separation was opened, and the normal hydrogen flow was started by setting the micro-metering valve. Thirty minutes after the oil flowed into the reactor, the pump stroke length was set to give the desired normal oil flow rate. The reactor temperature was then gradually increased to the normal operating value in half an hour. At this time the reactor was considered as at normal operating mode. This low temperature startup was to minimize hot spot developing during the initial stage when the catalyst is undesirably active. The hot spot can result in uncontrollable reactions and excessive coke formation.

The pump manufacturer recommends to start the pump with zero stroke length for its optimum performance. Hence during an operation if the system was shut down and was being brought back on stream then the pump stroke length was first reduced at zero. After starting the pump the stroke length was increased to give the desired feed rate.

Normal Operation

The system was considered to be at normal operation mode when the temperature, pressure and flow rate had stabilized. The temperature and pressure usually stabilized within one hour from the time both oil and hydrogen were brought on stream. A maximum deviation of 3 C in temperature and 345 KPa (50 psig) in pressure was considered acceptable during normal operation.

The temperature profile along the catalyst bed was continuously recorded on the twenty four point strip chart recorder. The pressure

in the system was also recorded continuously on the twelve point strip chart recorder mentioned earlier.

Sampling Procedure

The main objective was to collect liquid product samples without disturbing the normal operation. The valve under the reactor was temporarily closed to keep the reactor pressurized. The valve under the separation bomb was slowly open to let the oil flow into the sampling bomb until the pressure at the sampling bomb started increasing significantly. This pressure increase was caused by the gas from the separation bomb when the liquid was completely drained. The pressure in the sampling bomb was released, and the same procedure was repeated for the second separation bomb.

The separation bombs were repressurized with hydrogen and the valve under the reactor was opened to resume the normal operation. The liquid sample was then purged with nitrogen for thirty minutes before collection. The vent gas from the sampling bomb passed through the scrubbing tank and escaped into the atmosphere.

Shut-Down Procedure

First the stroke length of the pump head corresponding to the reactor being shut down was reduced to zero, and the reactor heaters were shut off. The reactor pressure was maintained at normal operating value and the hydrogen flow rate was tripled to quench the reactor. Part of the reactor insulation material was taken off to accelerate the cooling down. When the reactor reached the ambient

temperature, the hydrogen flow was cut and the system was depressurized by slowly changing the set point on the pressure controller.

The reactor was then disconnected from the system and the catalysts and inert materials inside were taken out section by section. If difficulty was encountered during the taking out of the catalysts, the reactor was cut into sections according to the screen positions inside the reactor.

Product Oil Analyses

The product oil samples were characterized in terms of hydrogen and nitrogen contents using a Perkin-Elmer model 240B elemental analyzer. Readers should refer to the operator's manual for details of the analytical procedure.

Catalyst Characterizations

The used catalysts from each experimental run were separated into five sections. Catalysts from each section were characterized individually. These catalysts were extensively extracted with pyridine using Soxhlet apparatus to remove soluble materials. The 0.15 liter of solvent generally became clear within 24 hours of extraction; otherwise a new batch of solvent was replaced. The catalysts were then dried at 121 C (250 F) under vacuum for overnight. The washed and dried catalysts were characterized in terms of coke content, surface area, pore volume, pore size distribution and carbon profile in a single catalyst pellet.

Coke Contents

Catalyst samples can adsorb a significant amount of moisture on their surface. The adsorbed moisture must be removed before accurate weight can be determined. This was accomplished by vacuum drying using a Micromeritics Model 2100D ORR Surface Area-Pore Volume Analyzer. The sample flask was evacuated, then filled with helium and weighed. The catalyst sample was then poured into the sample flask and evacuated to 0.01 Pa (0.0001 mmHg) by slowly increasing the temperature to 300 C. This can generally be achieved overnight. The sample was then cooled, sealed in helium atmosphere and weighed

The weighed catalyst sample was then transferred to a crucible and put into a muffle furnace. During the combustion, the oven temperature was gradually raised to 480 $\pm$ 10 C (900 $\pm$ 20 F) in 30 hours. The catalyst was allowed to stay at that temperature until no significant change in weight could be detected. The catalyst was then taken out, cooled down to the room temperature, degased and weighed according to the aforementioned procedure. Thus, the coke content in this study is defined as pyridine insoluble and moisture free combustible carbonaceous material.

Surface Areas

The reader should refer to the operator's manual of the Micromeritics Model 2100 D ORR Surface Area-Pore Volume Analyzer for details of the surface area analysis.

Pore Volume and Pore Size Distribution

The reader should refer to the operator's manual of the Micromeritics Model 900 Series Mercury Penetration Porosimeter for details of the pore volume and pore size distribution determination.

Carbon Profiles

Carbon profile analyses using scanning Auger microprobe were conducted in a commercial laboratory, SCR Laboratory located in Houston, Texas. Readers should consult Mr. Foster at (713) 682-6738 for details of the analyses.

APPENDIX D

GASES AND CHEMICALS USED

The gases and chemicals used in the hydrotreatment system, elemental analyzer and catalyst analyses instruments are listed in Table IX.

TABLE IX

LIST OF GASES AND CHEMICALS USED

Hydrotreatment System	
Hydrogen	Prepurified, 99.995%, 3500 psig, Matheson
Hydrogen	Prepurified, 99.95%, 6000 psig, Air Products
Hydrogen sulfide	5.0 % mixture in H_2, 2000 psig, Matheson
Inert packing	R 70, Thomas Scientific Apparatus
Elemental Analyzer	
Oxygen	Ultra high purity (99.99%), 2700 psig, Linde
Helium	High purity (99.995%), 2700 psig, Linde
Aluminum capsules	Perkin-Elmer, part no. 240-0642
Nickel capsules	Perkin-Elmer, part no. 240-0643
Platinum gauze	Perkin-Elmer, part no. 240-1147
Silver gauze	Perkin-Elmer, part no. 240-0092
Magnesium perchlorate	Reagent grade, Fisher Scientific Company
Silver vanadate	33-130 regent, Coleman Instruments
Tungstic anhydride	Purified, Fisher Scientific Company
Quartz wool	Perkin-Elmer, part no. 240-1118
Colorcarb CO_2 absorber	Perkin-Elmer, part no. 240-0115
Copper (60-100 mesh)	Perkin-Elmer, part no. 240-0017
Silver oxide-silver tungstate on chromosorb reagent	Perkin-Elmer, part no. 240-0113
Silver tungstate-magnesium oxide	Perkin-Elmer, part no. 240-1344
Acetanilide	Organic analytical standard, BDH Chemicals Ltd.
Quartz combustion Tube (9mm I.D. x 11.2 mm O.D.)	Thermal American Quartz
Quartz reduction tube	Perkin-Elmer, part no. 240-1573
Pyrex tube (9mm I.D. x 11.2mm O.D.)	Perkin-Elmer, part no. 240-1217
Catalyst Analyses	
Pyridine	Reagent grade, Fisher Scientific Company
Nitrogen	Prepurified, 99.995%, 2500 psig, Air Products
Helium	Prepurified, 99.995%, 2500 psig, Air Products

APPENDIX E

EXPERIMENTAL DATA

Results of sample analyses of the experimental runs are listed in Table X. Unless indicated, all these runs were made with the Shell 324 $NiMo/Al_2O_3$ catalyst and the SRC oil feedstock at a temperature of 400 C (750 F), a pressure of 13.9 MPa (2000 psig) and a hydrogen-to-oil feed ratio of 1780 std. m^3H_2/m^3 oil (10,000 scf H_2/bbl oil). Details of these catalyst properties, feedstock properties and experimental run conditions are presented in Tables II, III and IV respectively.

TABLE X

LIST OF EXPERIMENTAL DATA

Run Series	Sample Number	Volume Hourly[a] Space Time	Hours[b] on Oil	Wt% N[c]	Wt% N[d] Removal	Wt% H[c]
LTB[e]	Feed	2.26		0.72		7.66
LTB	1	2.26	2	0.10	86	11.25
LTB	2	2.26	6	0.13	82	11.32
LTB	3	2.26	12	0.14	81	11.36
LTB	4	2.26	20	0.14	81	11.23
LTB	5	2.26	28	0.14	81	11.45
LTB	6	2.26	36	0.11	85	11.52
LTB	7	2.26	44	0.14	81	11.44
LTB	8	2.26	56	0.12	83	11.06
LTB	9	2.26	68	0.12	83	11.03
LTB	10	2.26	80	0.13	82	11.19
LTB	11	2.26	92	0.11	85	11.20
LTB	12	2.26	104	0.11	85	11.03
LTB	13	2.26	116	0.12	83	11.06
LTB	14	2.26	128	0.12	83	11.07
LTB	15	2.26	140	0.12	83	10.82
LTB	16	2.26	152	0.12	83	11.08
LTB	17	2.26	164	0.12	83	11.12
LTB	18	2.26	177	0.11	85	11.21
LTB	19	2.26	189	0.13	82	10.97
LTB	20	2.26	201	0.10	86	11.18
LTB	21	2.26	213	0.10	86	11.00
LTB	22[f]	2.26	224	0.03	96	11.35
LTB	23[f]	2.26	237	0.00	100	11.27
LTB	24[f]	2.26	248	0.00	100	11.26
LTB	25[f]	2.26	261	0.00	100	10.99
LTG	Feed			1.40		6.73
LTG	1	2.50	2	--	--	--
LTG	2	2.50	6	0.25	82	10.50
LTG	3	2.50	12	0.35	75	10.00
LTG	4	2.50	19	0.37	74	9.68
LTV	Feed			1.40		6.73
LTV	1	2.50	2	--	--	--
LTV	2	2.50	6	0.38	73	10.77
LTV	3	2.50	10	0.42	70	10.90
LTV	4	2.50	19	0.47	66	10.47
LTV	5	2.79	32	0.37	74	10.40
LTV	6	2.79	43	0.42	70	10.30
LTV	7	2.79	55	0.39	72	9.92
LTV	8	2.16	67	0.58	59	9.83

TABLE X (Continued)

Run Series	Sample Number	Volume Hourly[a] Space Time	Hours[b] on Oil	Wt% N[c]	Wt% N[d] Removal	Wt% H[c]
LTV	9	2.50	79	0.54	61	9.78
LTV	10	2.50	91	0.50	64	9.68
LTV	11	2.50	97	0.42	63	9.56
LTW	Feed			1.40		6.73
LTW	1	2.93	2	--	--	--
LTW	2	2.93	6	0.31	78	10.86
LTW	3	2.93	12	0.34	76	10.93
LTW	4	2.93	21	0.39	72	10.68
LTW	5	2.93	30	0.41	71	10.25
LTX,	Feed			1.40		6.73
LTX	1	2.50	2	--	--	--
LTX	2	2.50	6	0.35	75	10.90
LTY	Feed			1.40		6.73
LTY	1	1.88	2	--	--	--
LTY	2	1.88	6	0.43	69	10.75
LTY	3	1.88	12	0.53	62	10.62
LTY	4	1.88	21	0.55	61	10.59
LTY	5	1.88	33	0.61	56	10.43
LTY	6	1.88	45	0.62	56	10.10
LTY	7	1.88	57	0.66	53	9.90
LTY	8	1.88	69	0.66	53	9.80
LTY	9	1.88	81	0.69	51	9.53
LTY	10	1.88	93	0.69	51	9.64
LTY	11	1.88	105	0.72	49	9.72
LTY	12	2.00	117	0.73	48	9.42
LTY	13	2.20	129	0.73	48	9.38
LTY	14	2.20	141	0.76	46	9.44
LTY	15	2.20	153	0.76	46	9.41

a. This is a volume hourly space time (volume of catalyst/volume of oil per hour).
b. Total hours which the catalyst has been contacted with oil at reaction temperature.
c. Percent of nitrogen or hydrogen in liquid product.
d. % Removal = 100 x (fraction in feed less fraction in product)/ (fraction in feed).
e. The feedstock used was EDS Oil (See Table III for more details).
f. The reaction temperature was raised to 426 C (800 F).

APPENDIX F

PORE SIZE DISTRIBUTIONS OF SPENT CATALYSTS

Figures 63-89 present pore size distribution of the spent catalysts, while that of the fresh catalyst are shown in Figure 18. Note that the pore size distribution function, D(PD), on the vertical axis has been defined on page 73.

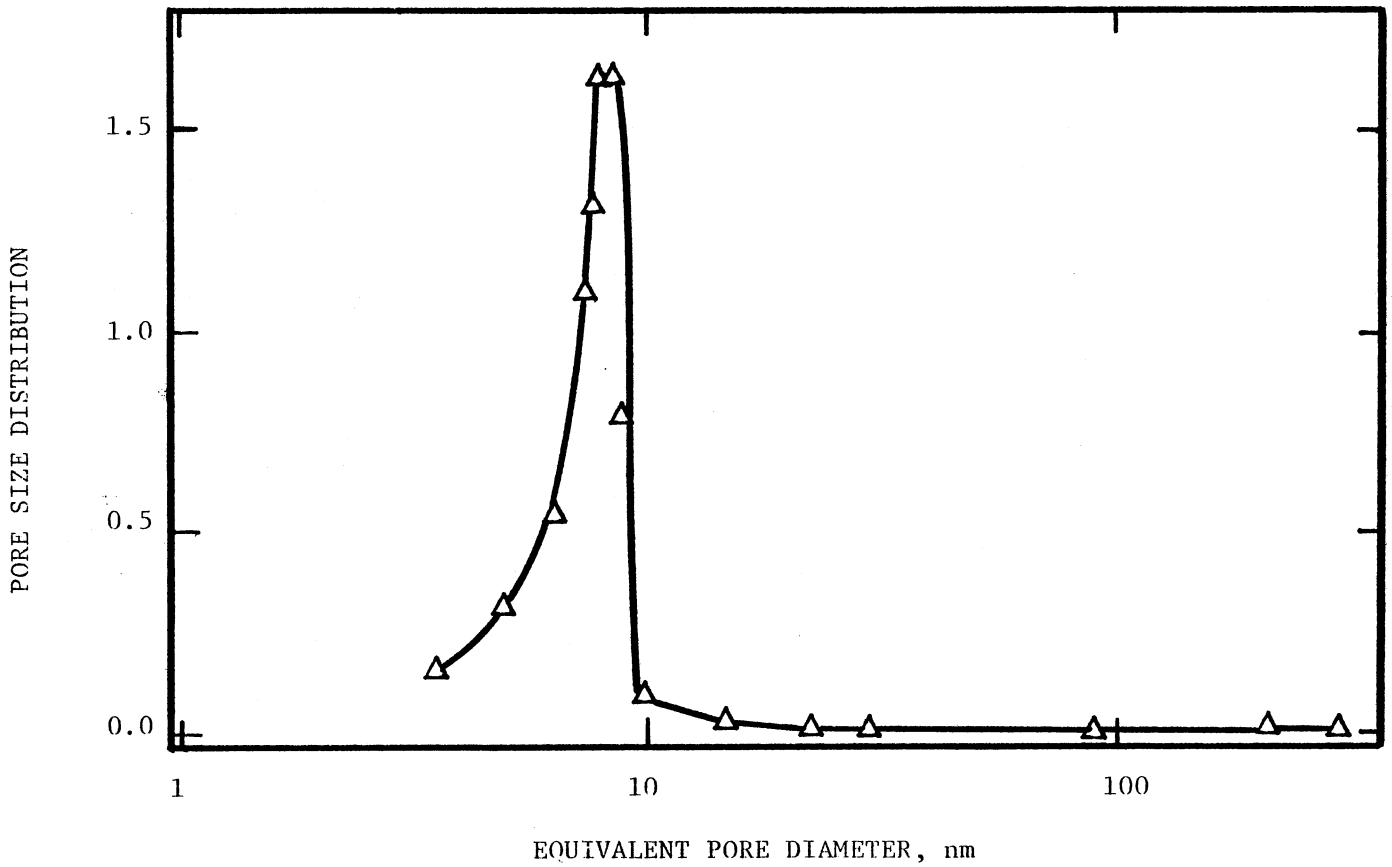

Figure 63. Pore Size Distribution of the Spent Catalyst from Section 1, Run LTB

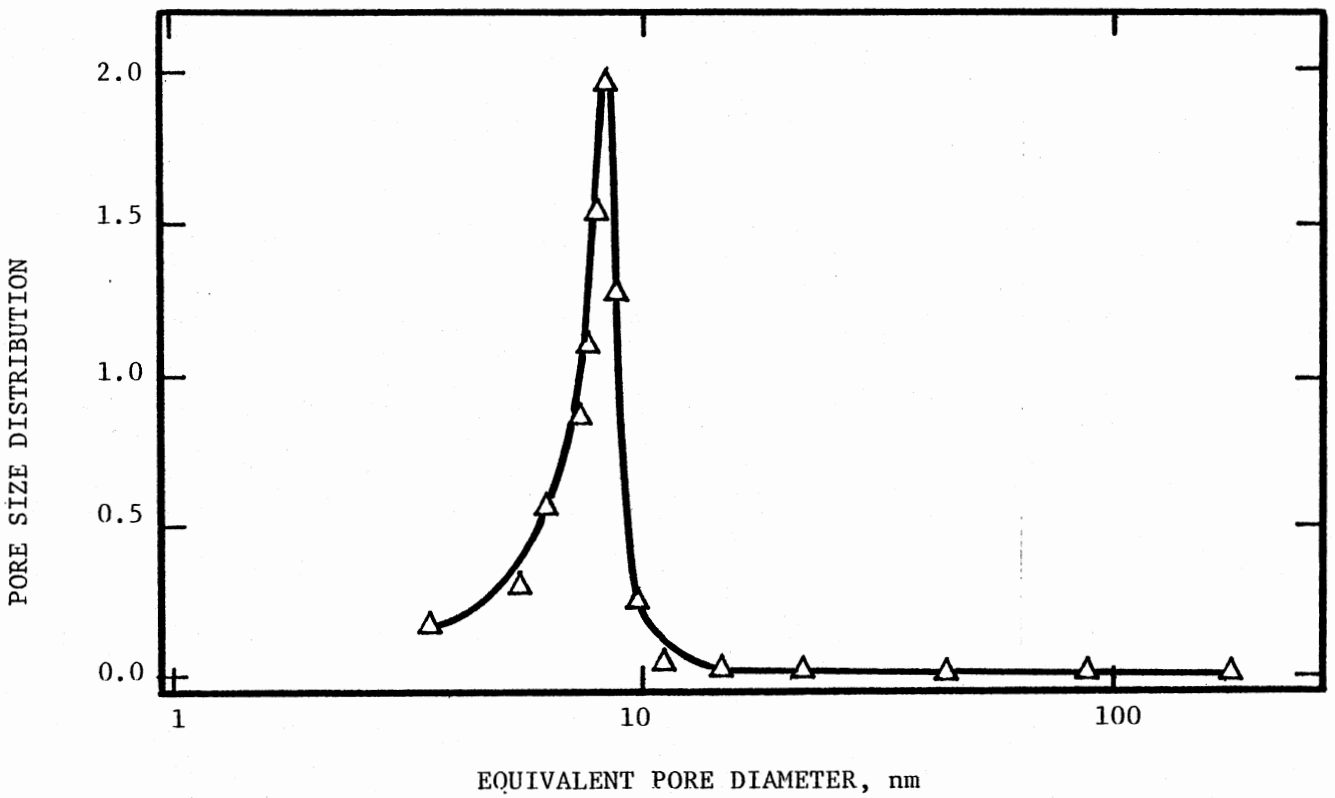

Figure 64. Pore Size Distribution of the Spent Catalyst from Section 2, Run LTB

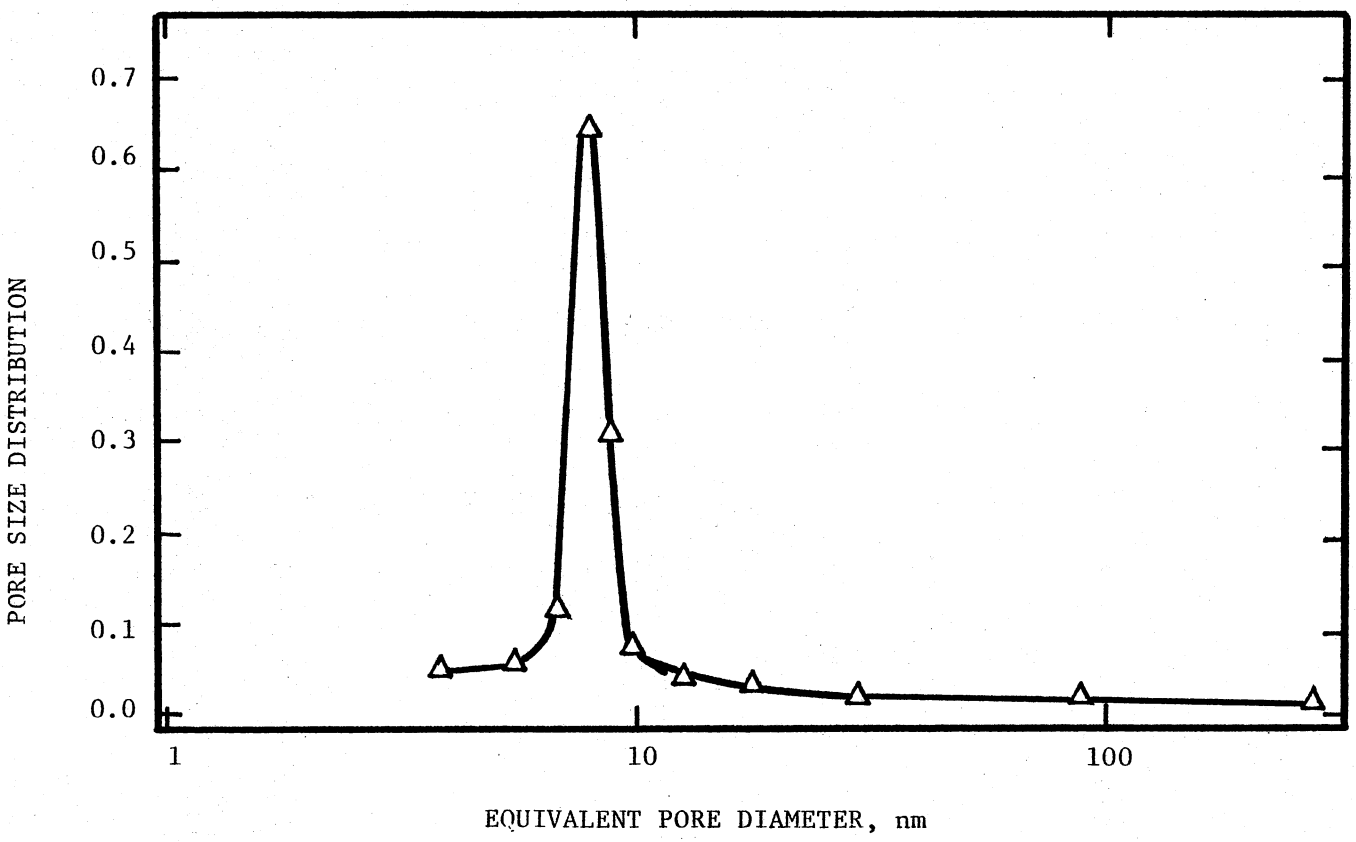

Figure 65. Pore Size Distribution of the Spent Catalyst from Section 3, Run LTB

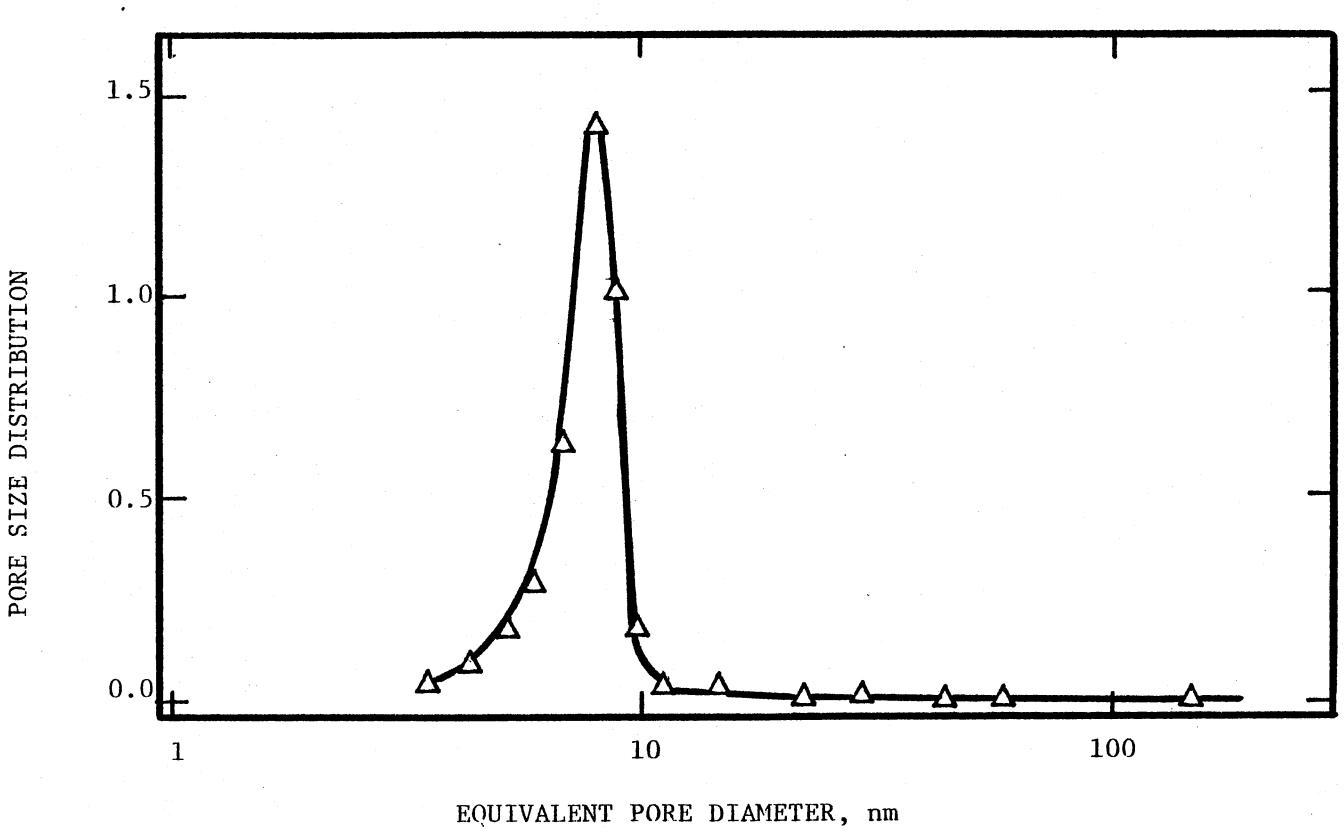

Figure 66. Pore Size Distribution of the Spent Catalyst from Section 4, Run LTB

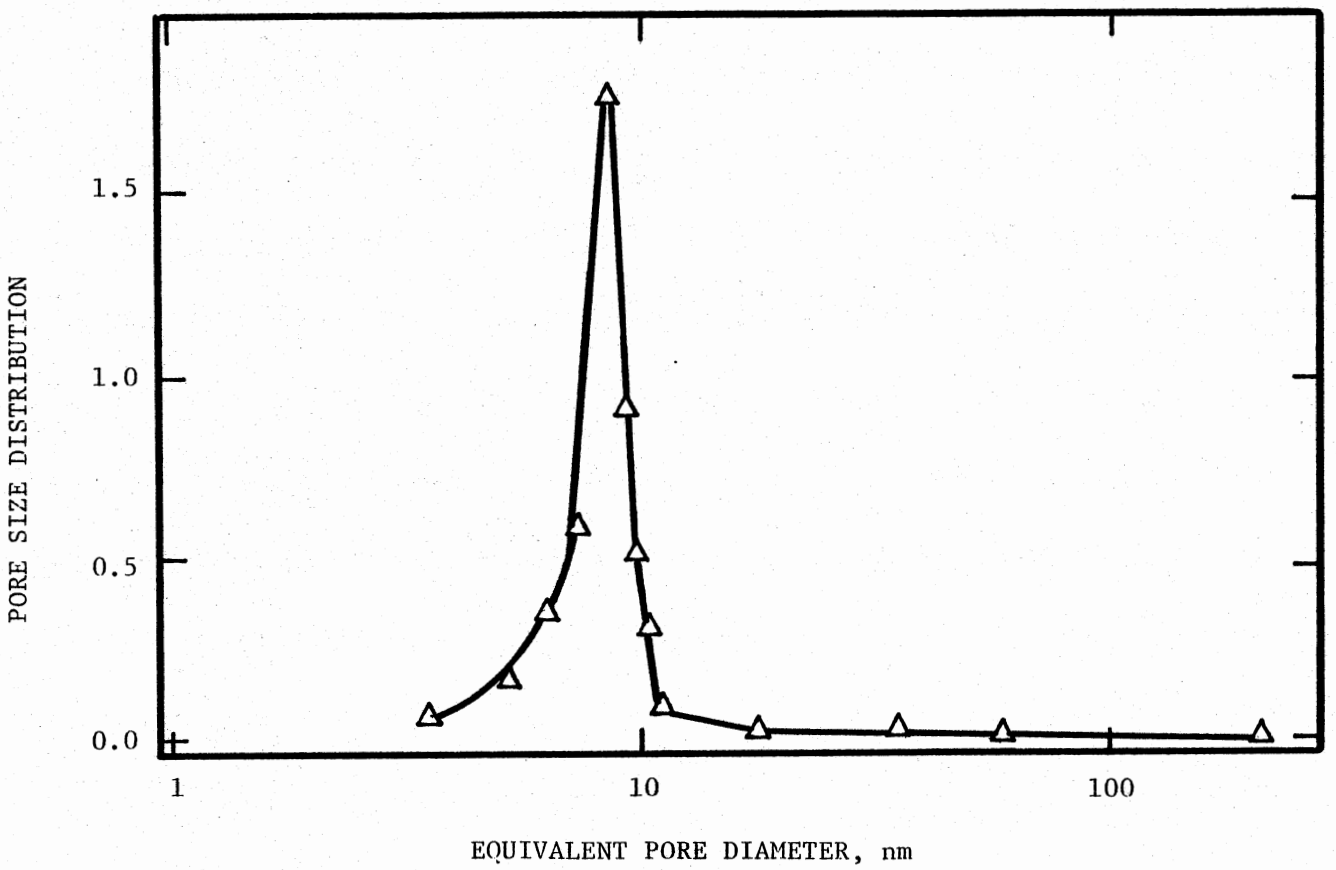

Figure 67. Pore Size Distribution of the Spent Catalyst from Section 5, Run LTB

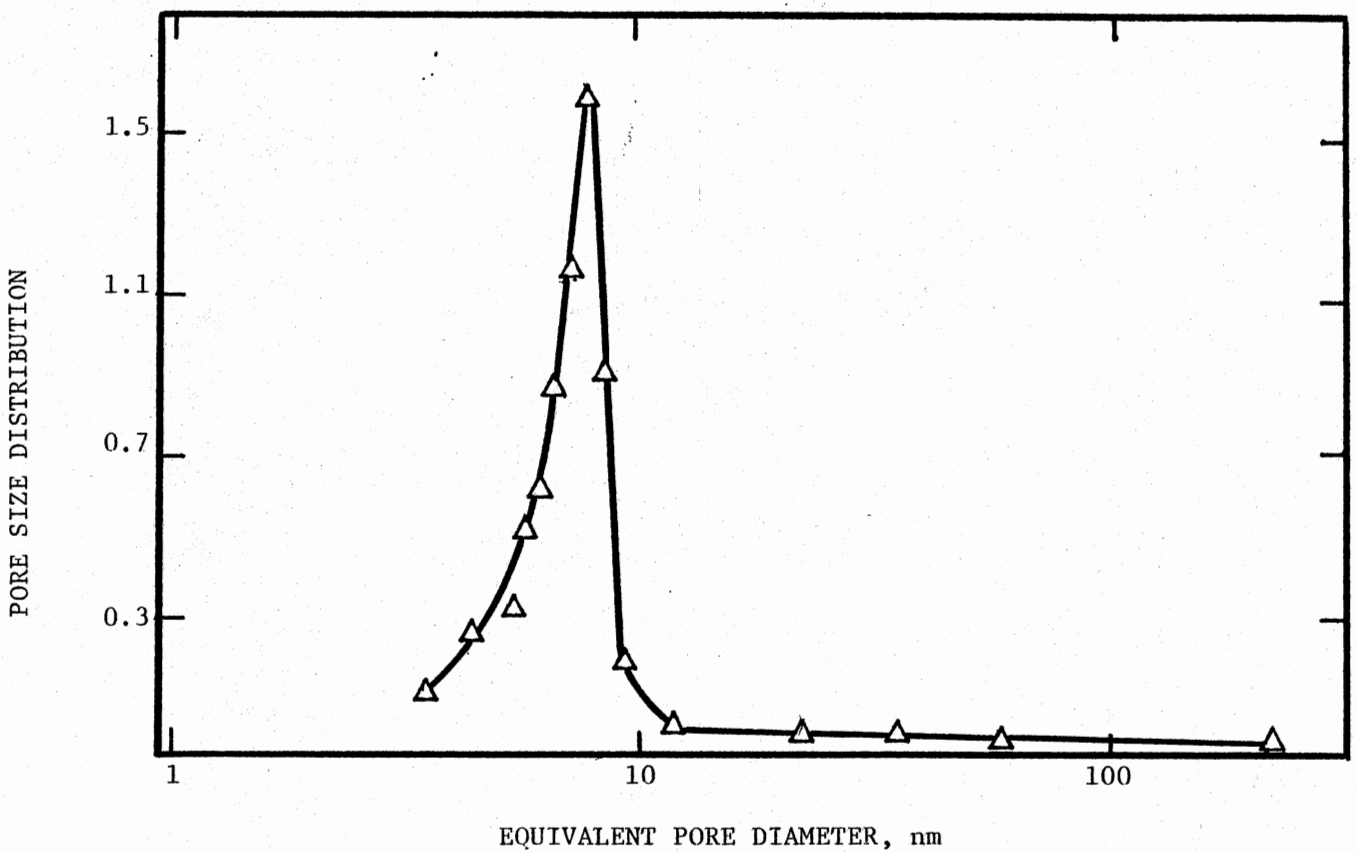

Figure 68. Pore Size Distribution of the Spent Catalyst from Run LTG

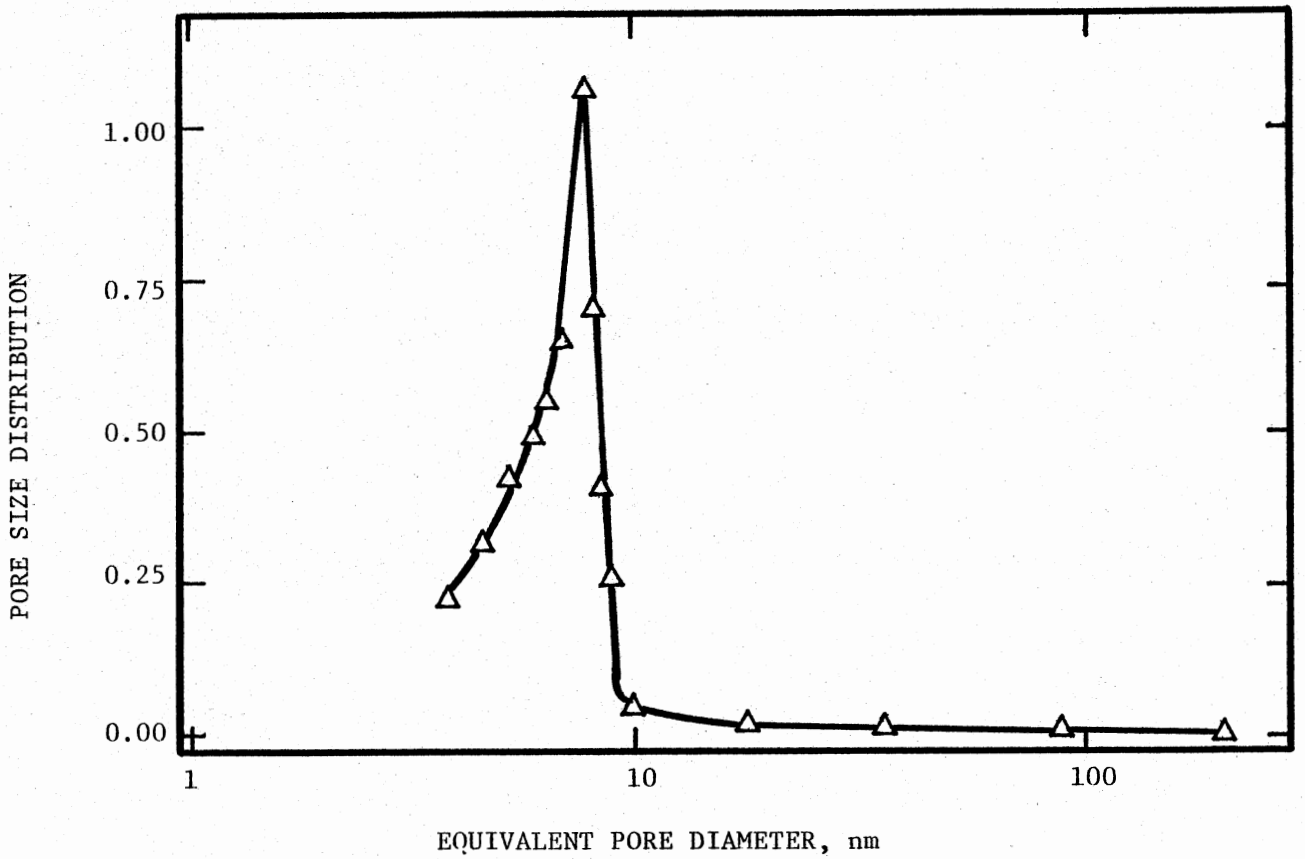

Figure 69. Pore Size Distribution of the Spent Catalyst from Run LTV

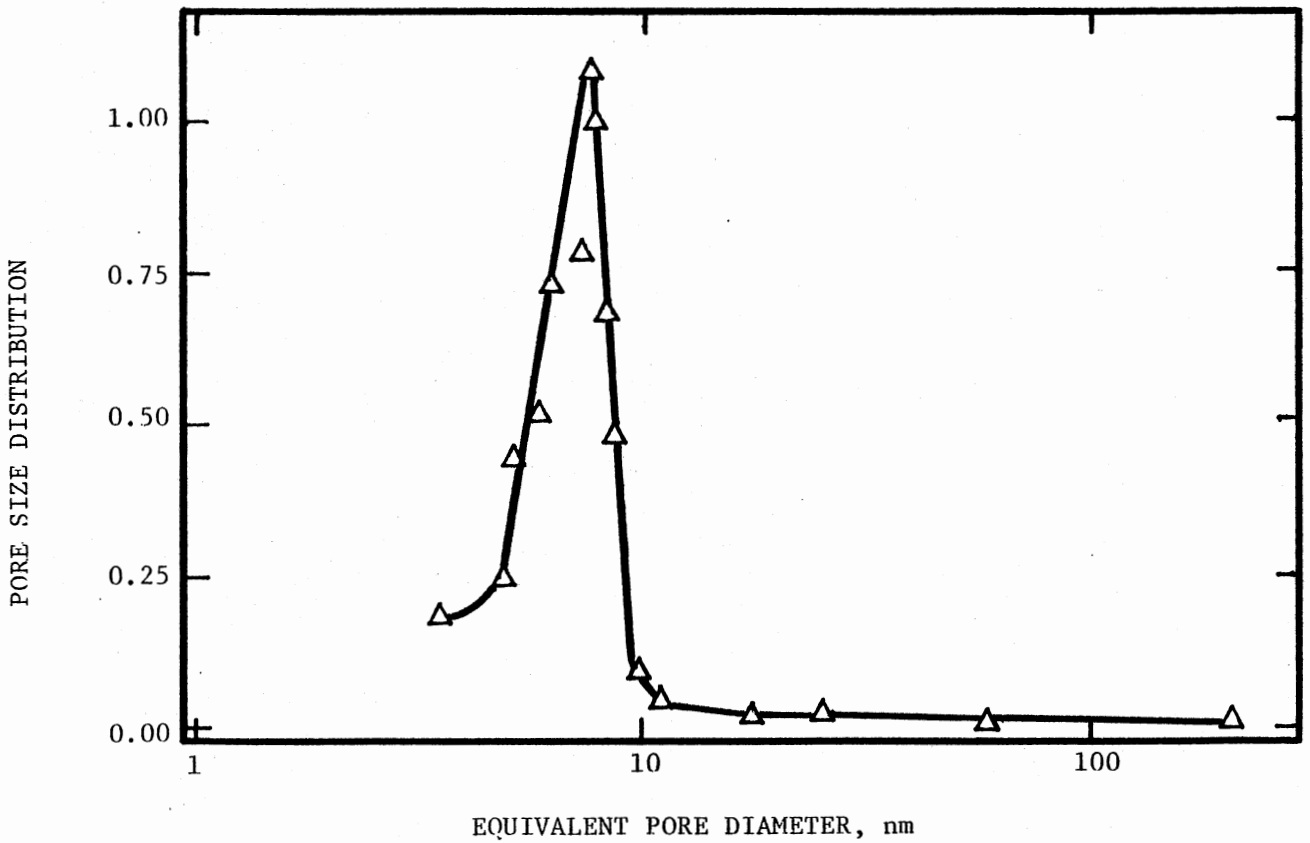

Figure 70. Pore Size Distribution of the Spent Catalyst from Section 1, Run LTW

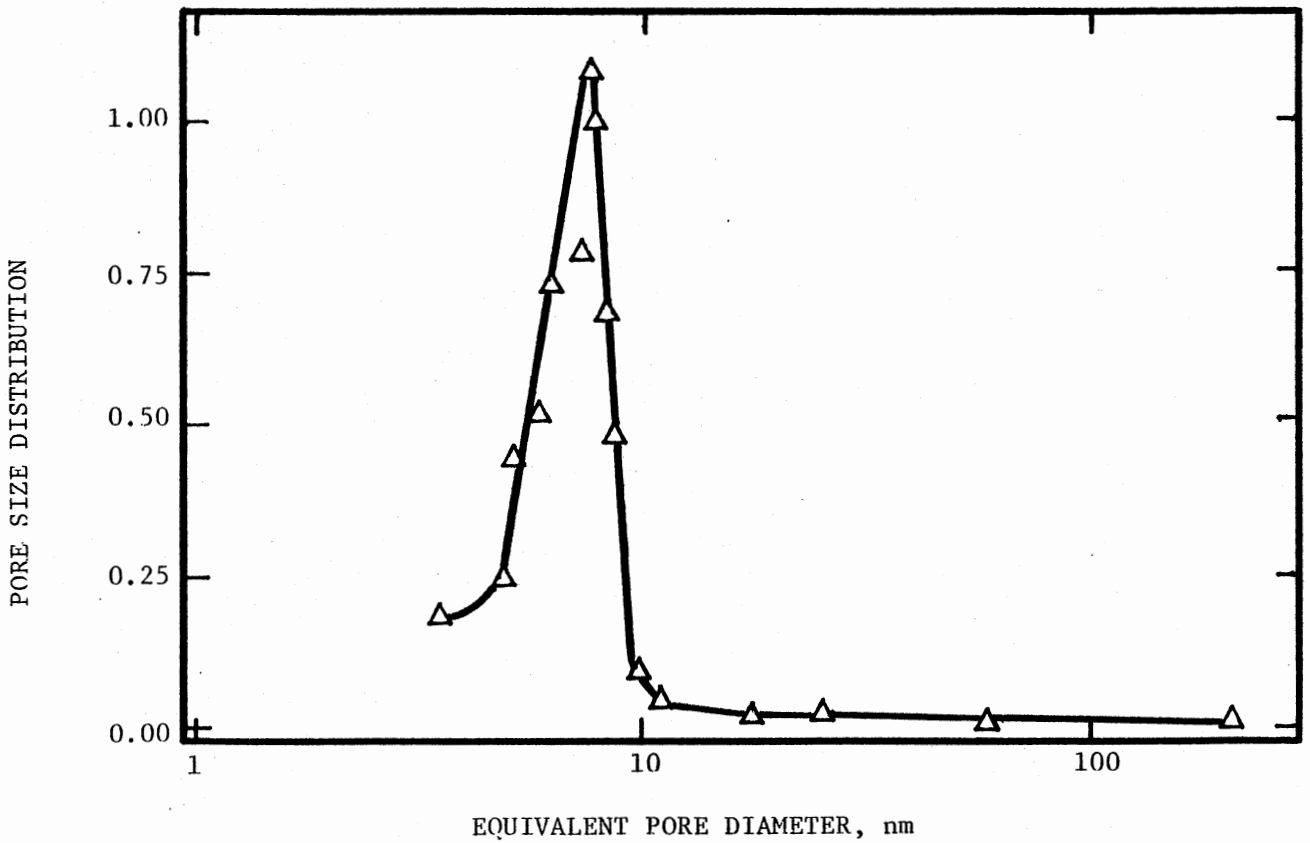

Figure 70. Pore Size Distribution of the Spent Catalyst from Section 1, Run LTW

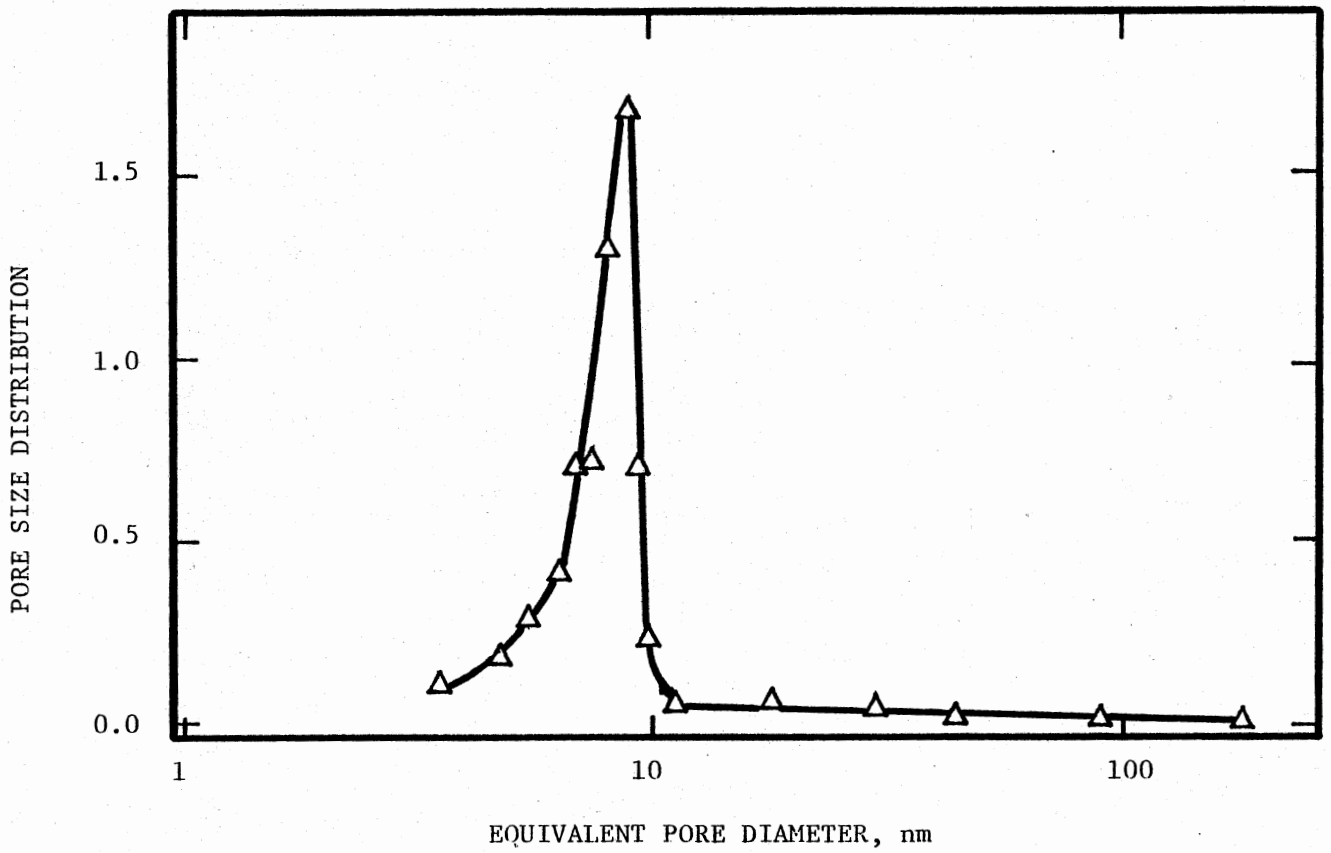

Figure 72. Pore Size Distribution of the Spent Catalyst from Section 3, Run LTW

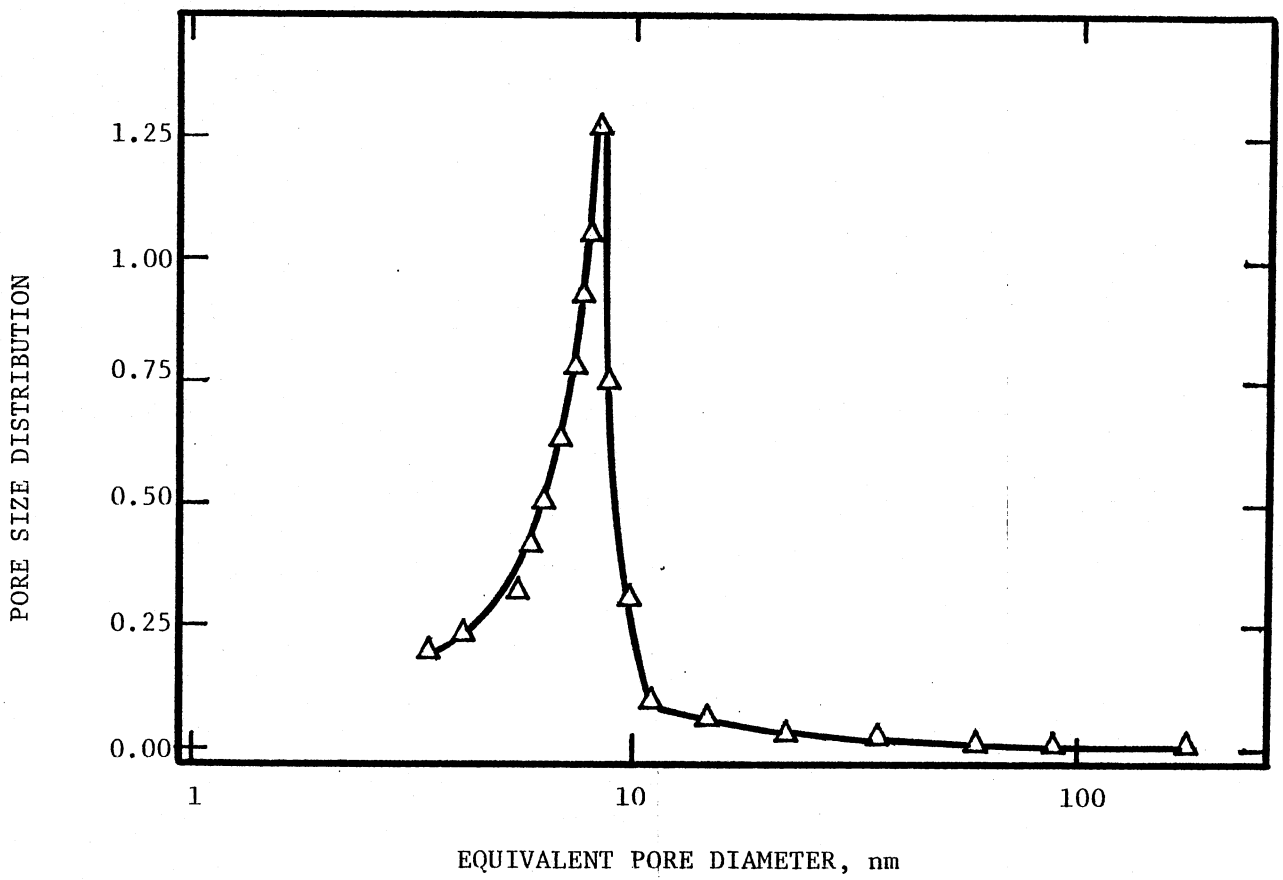

Figure 73. Pore Size Distribution of the Spent Catalyst from Section 4, Run LTW

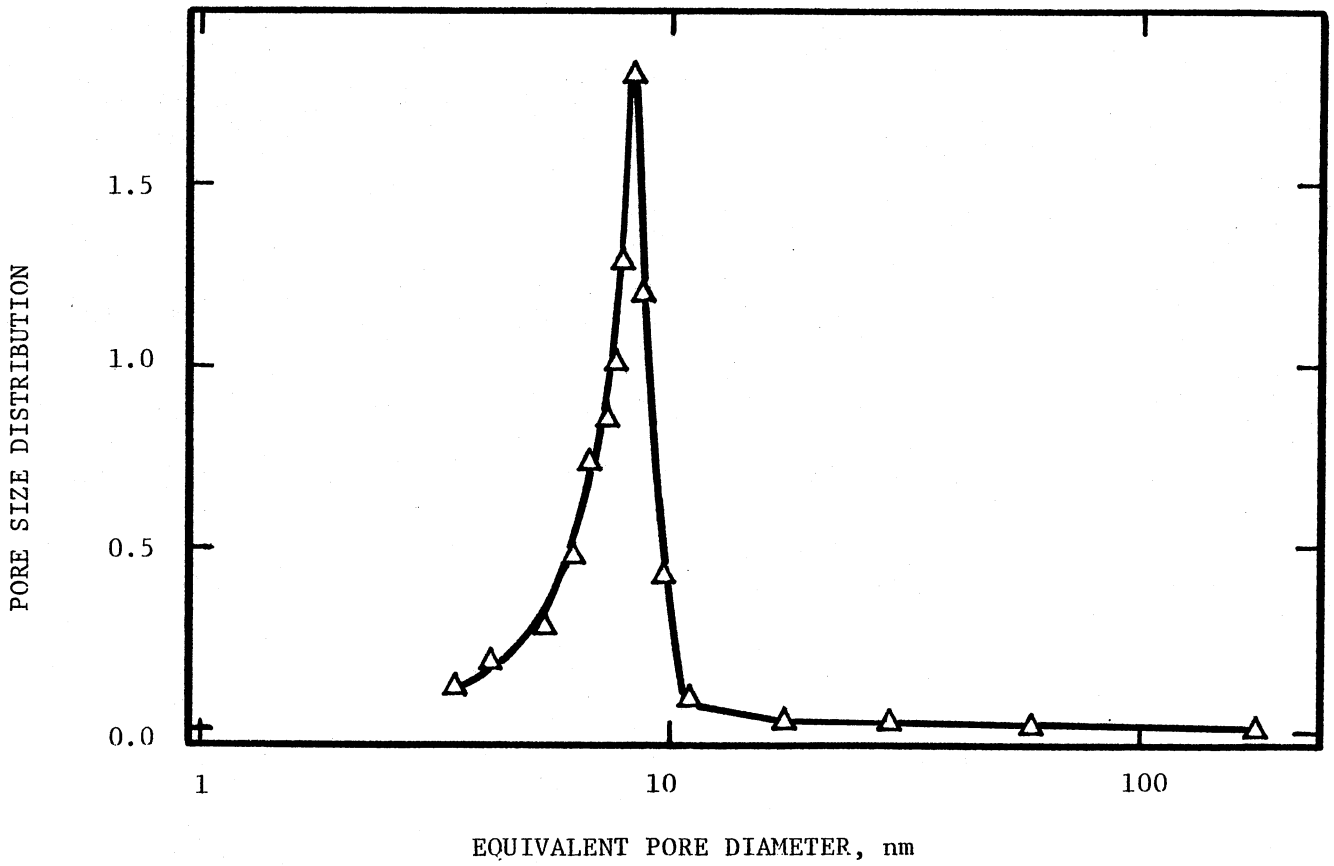

Figure 74. Pore Size Distribution of the Spent Catalyst from Section 5, Run LTW

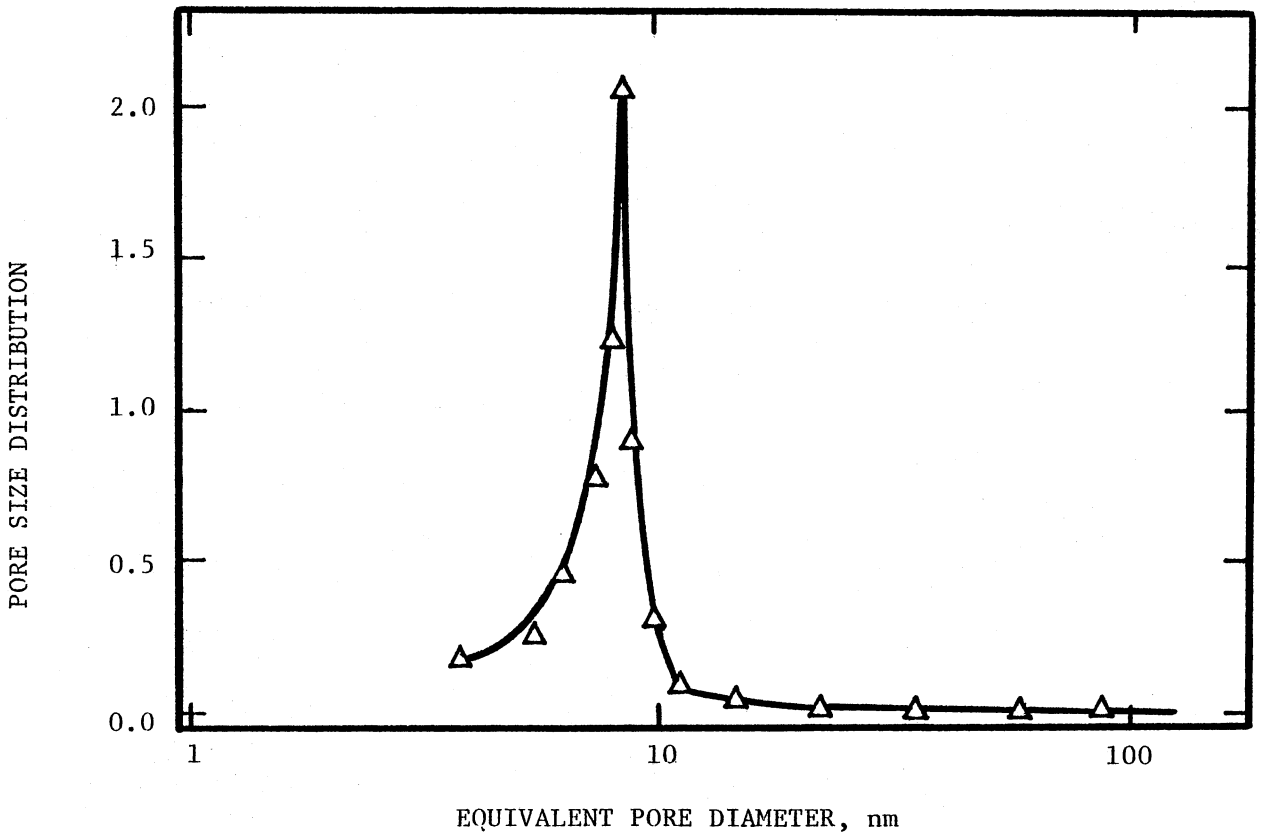

Figure 75. Pore Size Distribution of the Spent Catalyst from Section 1, Run LTX

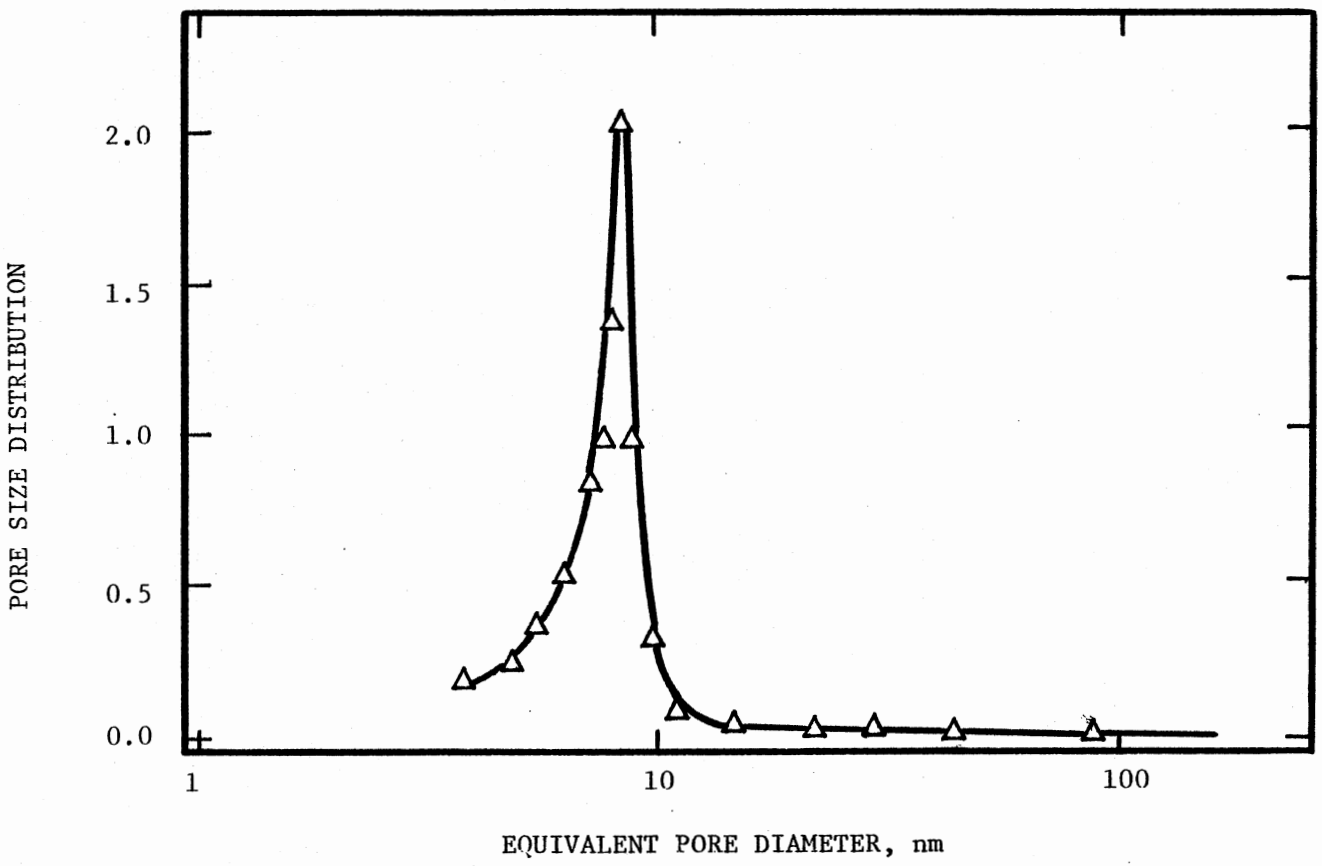

Figure 76. Pore Size Distribution of the Spent Catalyst from Section 2, Run LTX

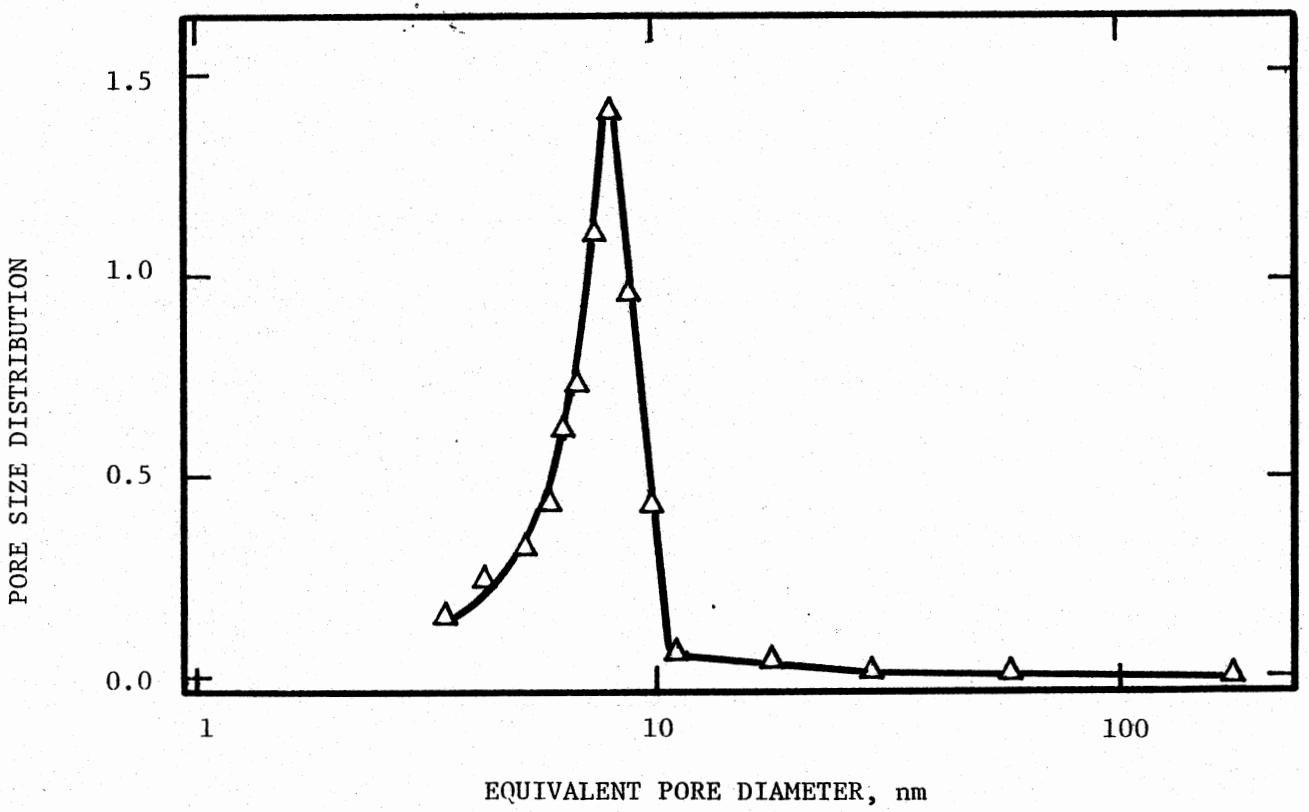

Figure 77. Pore Size Distribution of the Spent Catalyst from Section 3, Run LTX

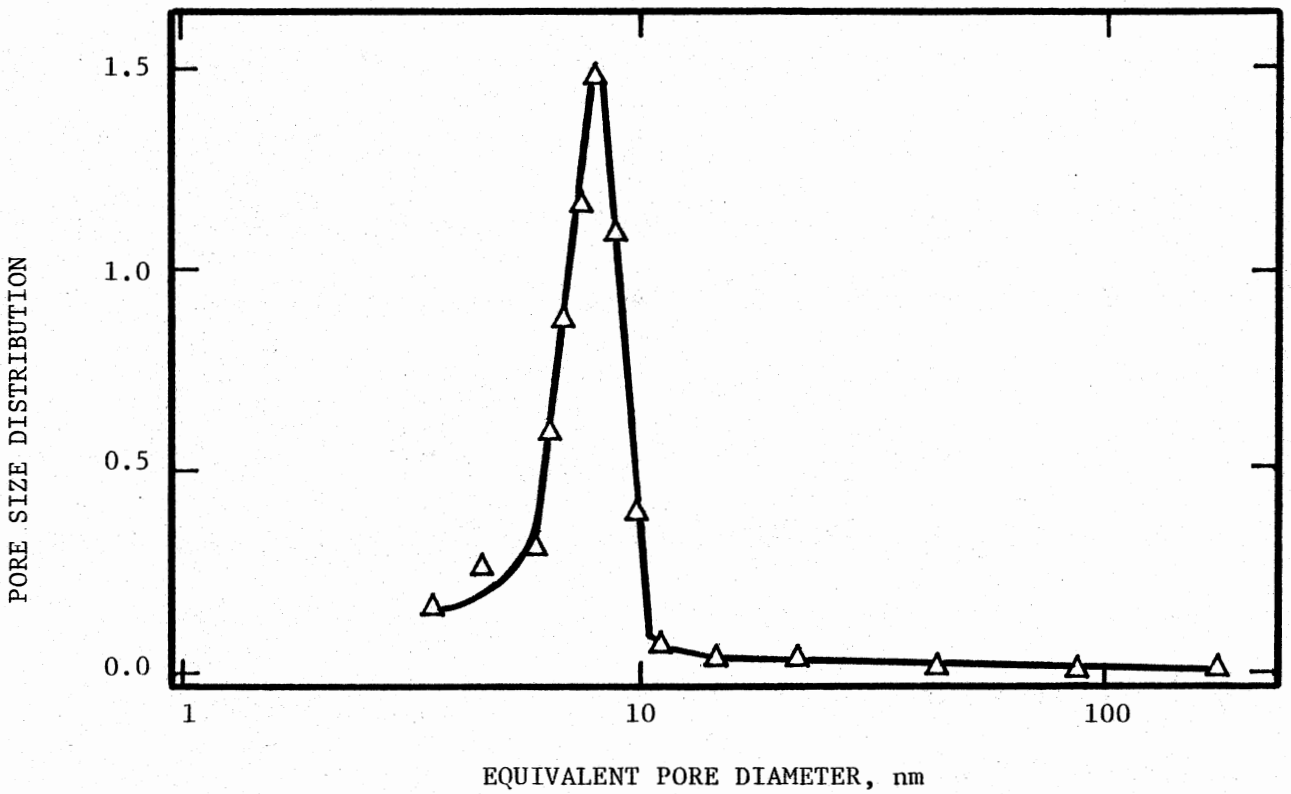

Figure 78. Pore Size Distribution of the Spent Catalyst from Section 4, Run LTX

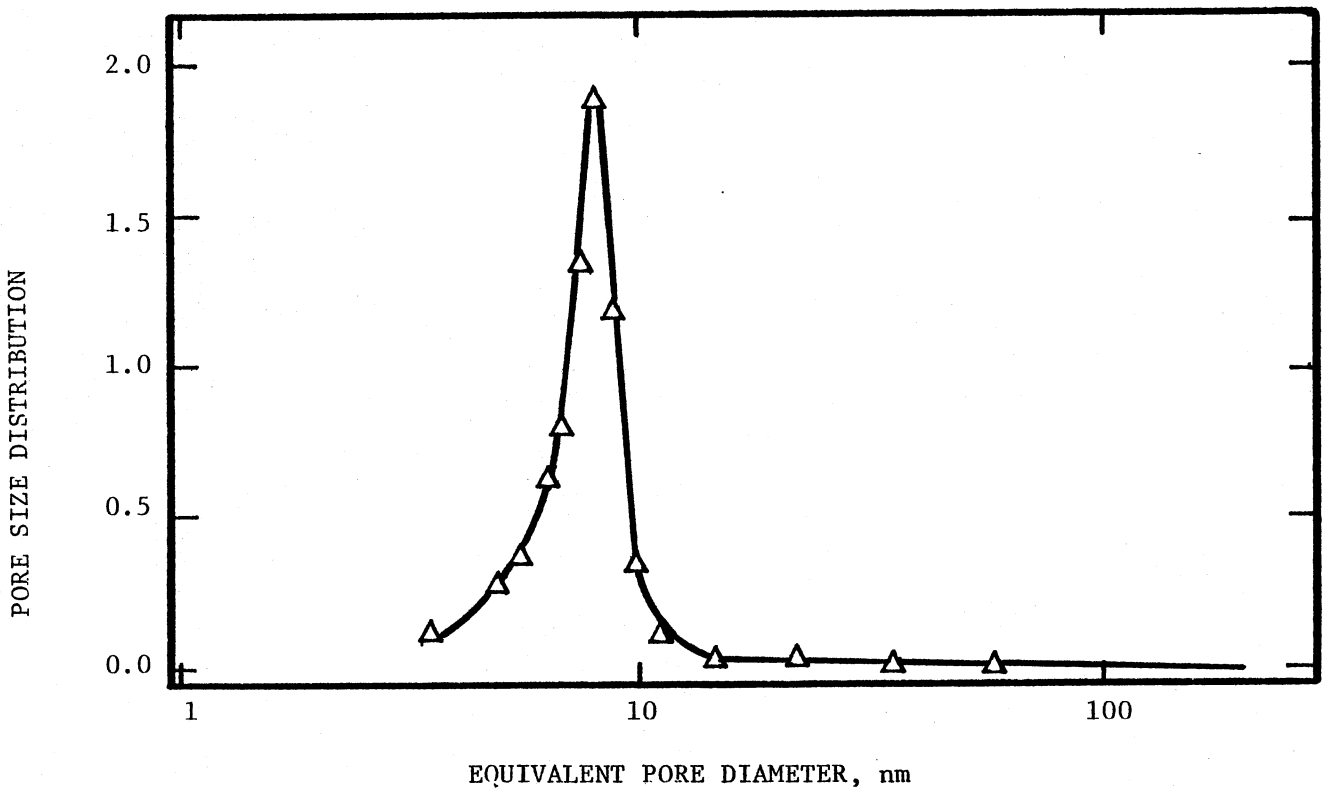

Figure 79. Pore Size Distribution of the Spent Catalyst from Section 5, Run LTX

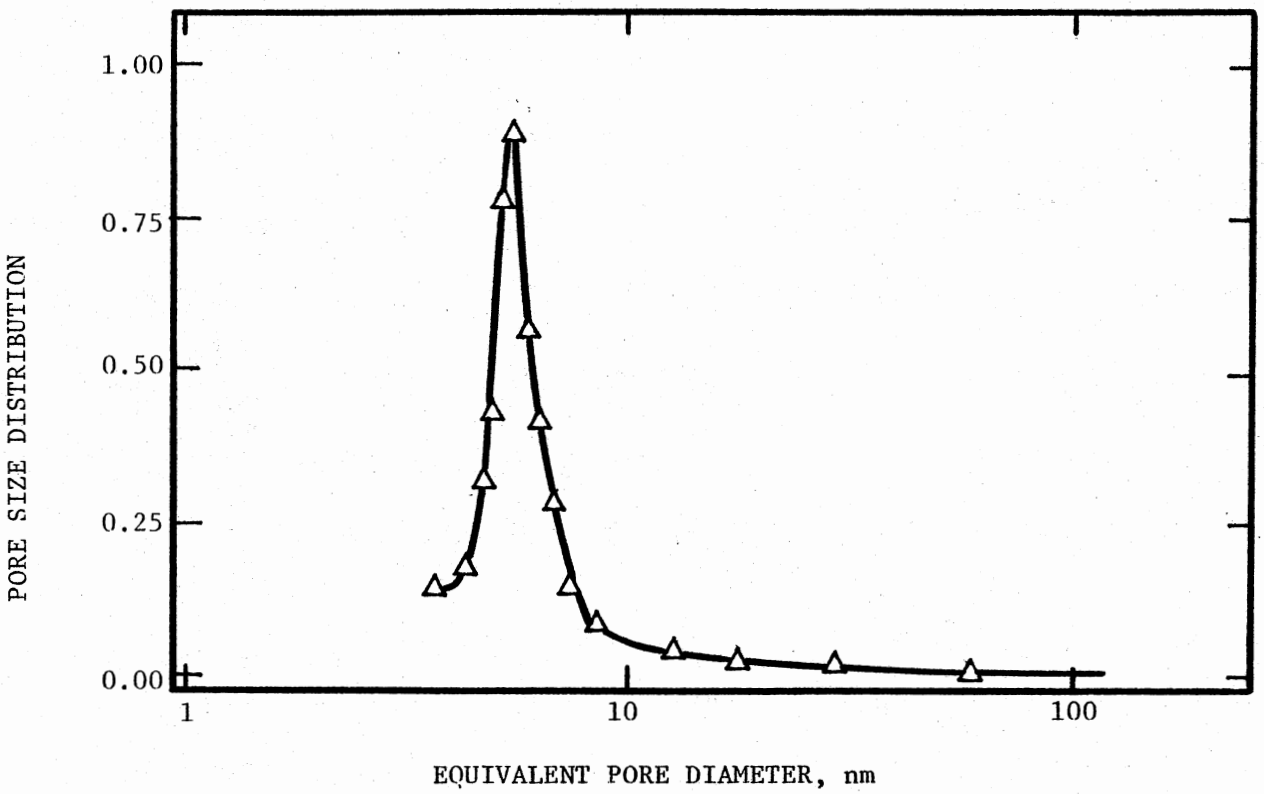

Figure 80. Pore Size Distribution of the Spent Catalyst from Section 1, Run LTY

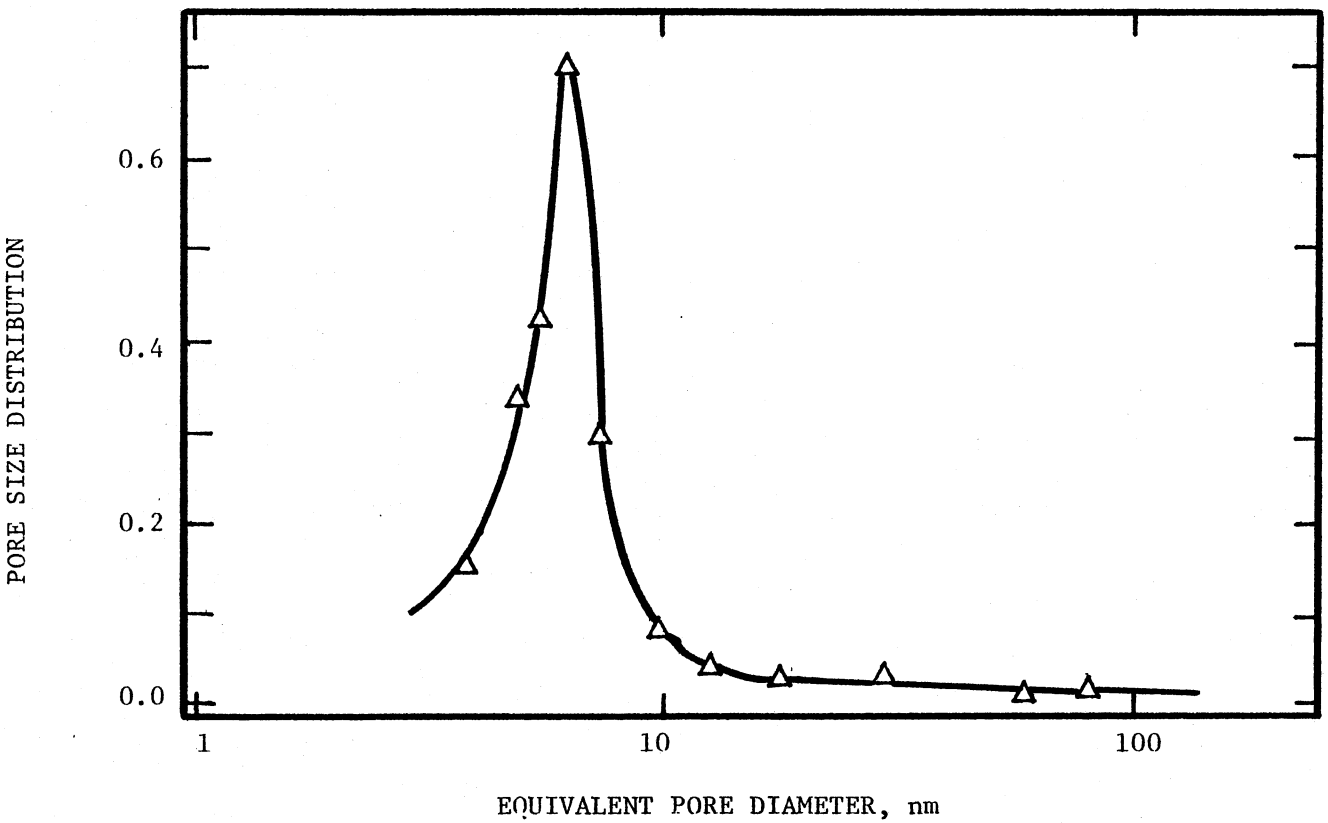

Figure 81. Pore Size Distribution of the Spent Catalyst from Section 2, Run LTY

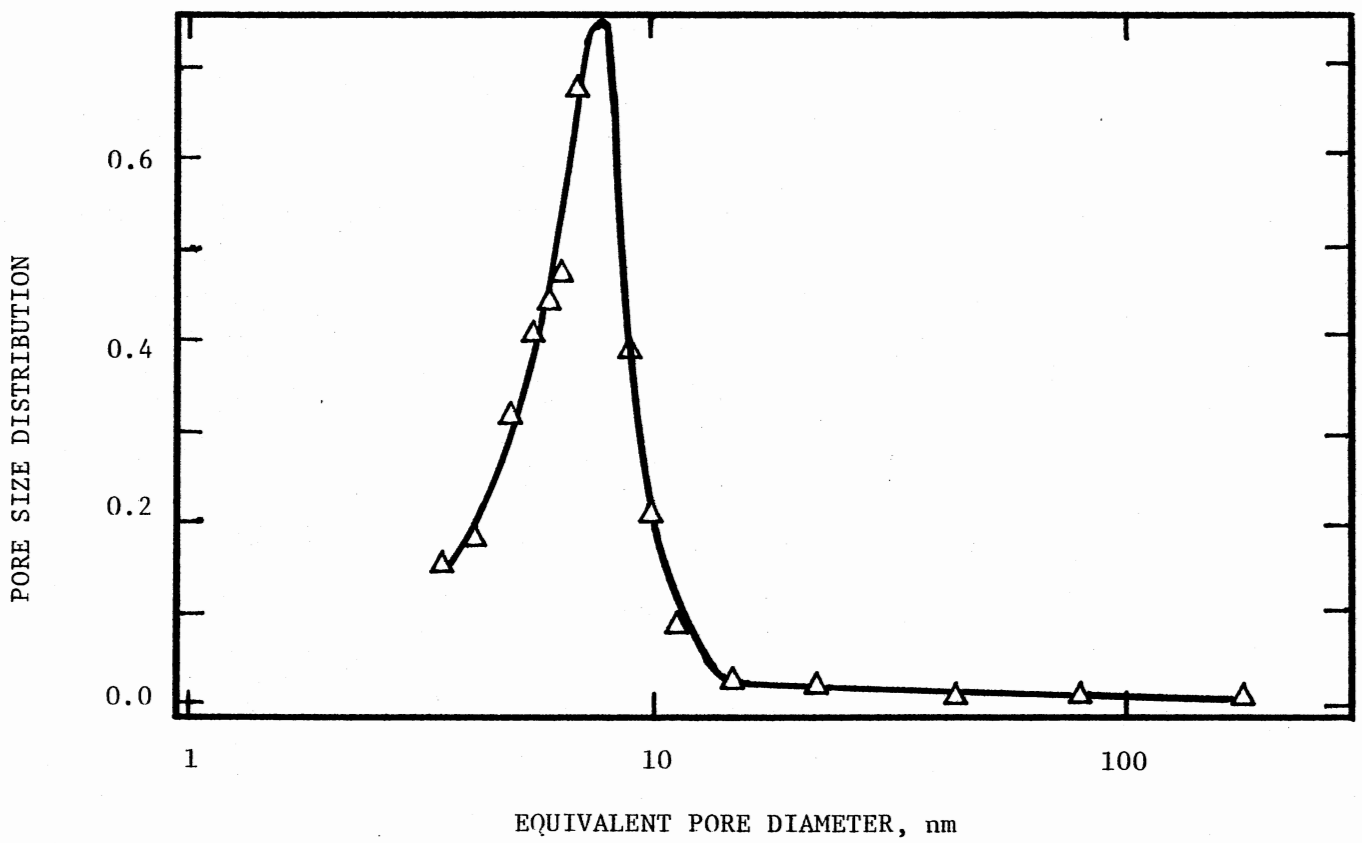

Figure 82. Pore Size Distribution of the Spent Catalyst from Section 3, Run LTY

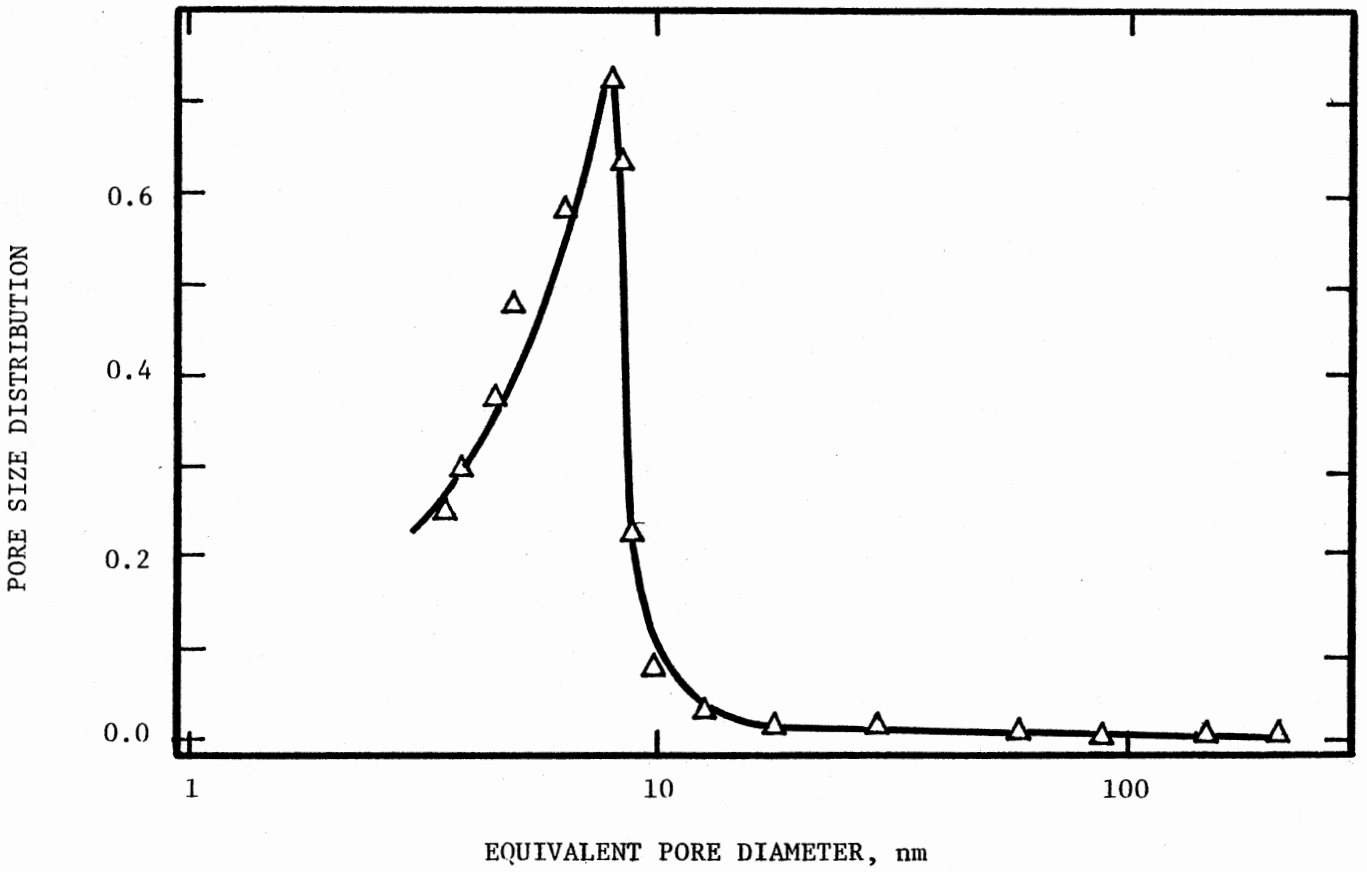

Figure 83. Pore Size Distribution of the Spent Catalyst from Section 4, Run LTY

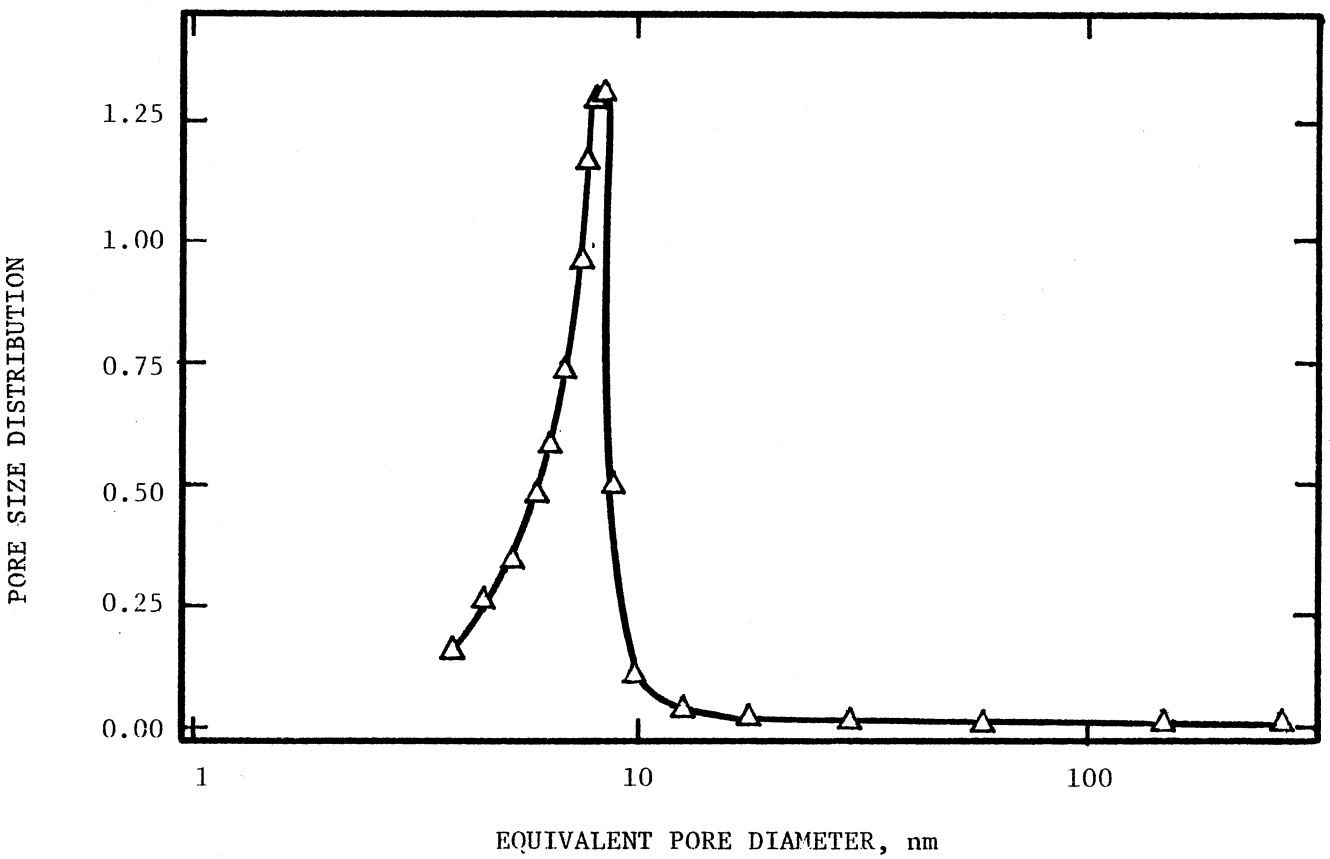

Figure 84. Pore Size Distribution of the Spent Catalyst from Section 5, Run LTY

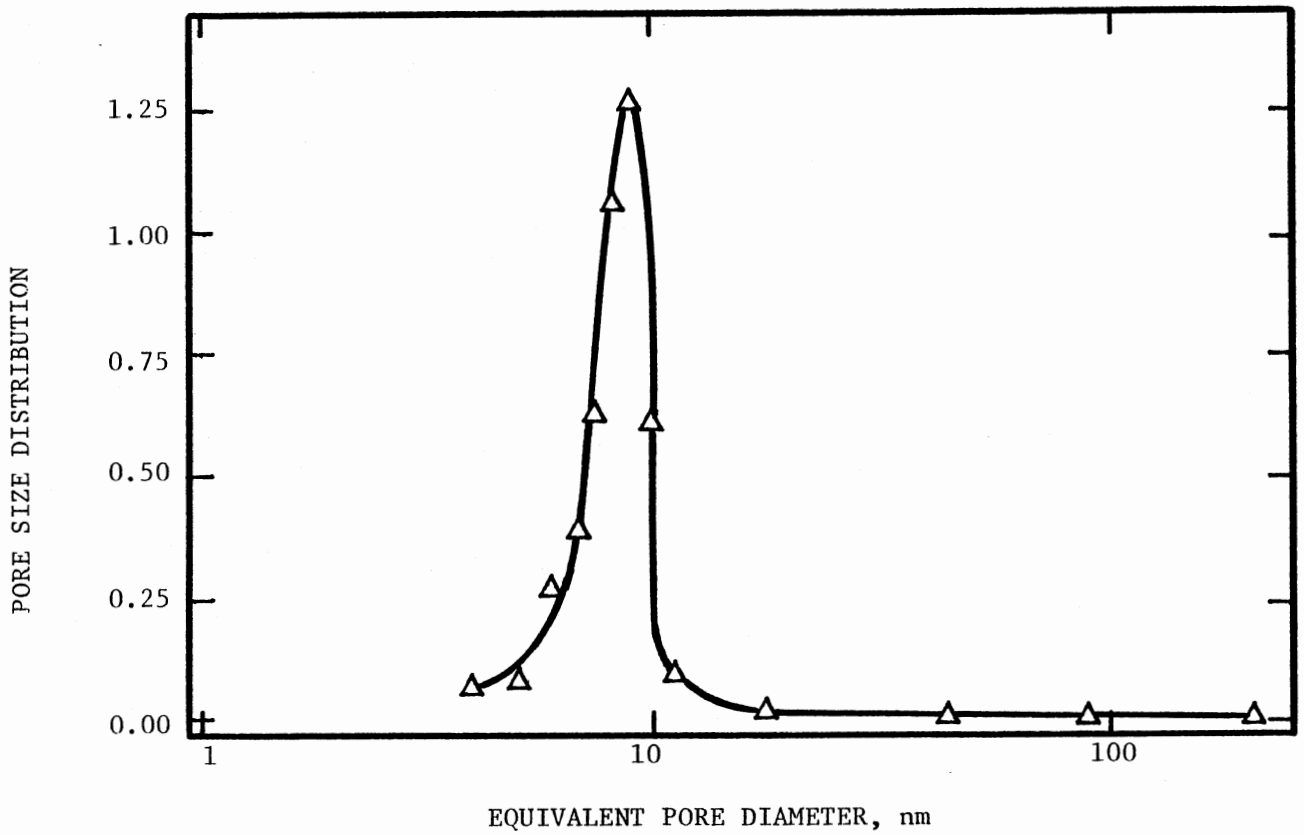

Figure 85. Pore Size Distribution of the Spent Catalyst from Section 1, Run LTZ

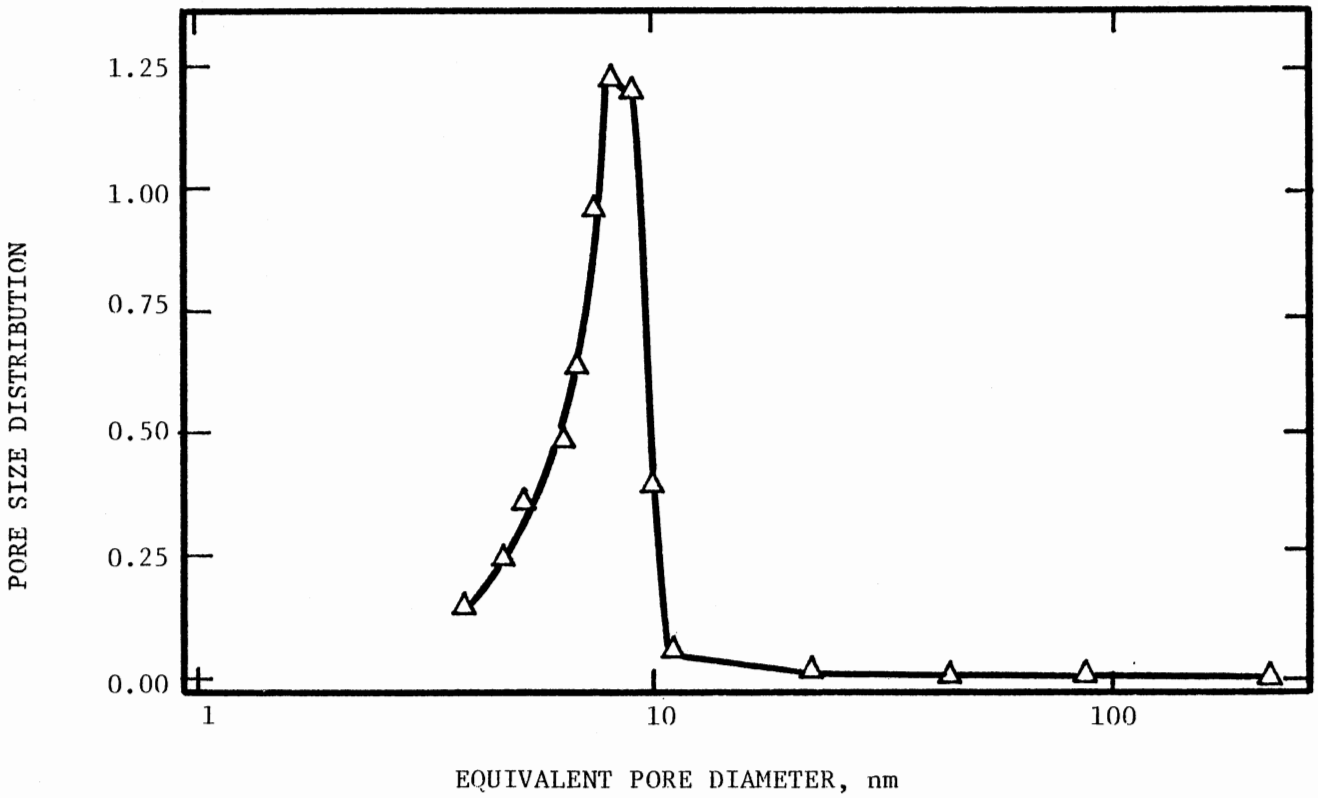

Figure 86. Pore Size Distribution of the Spent Catalyst from Section 2, Run LTZ

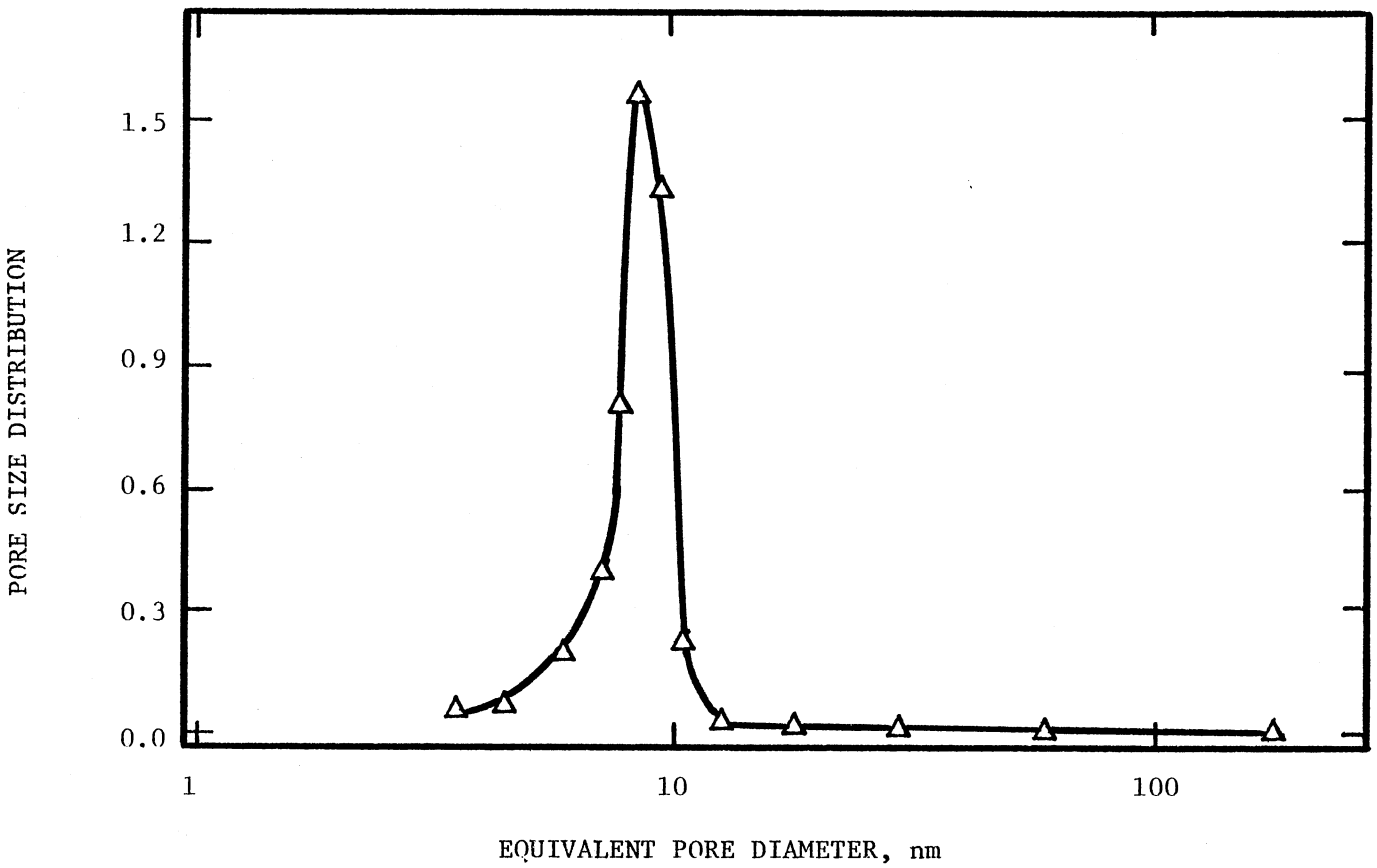

Figure 87. Pore Size Distribution of the Spent Catalyst from Section 3, Run LTZ

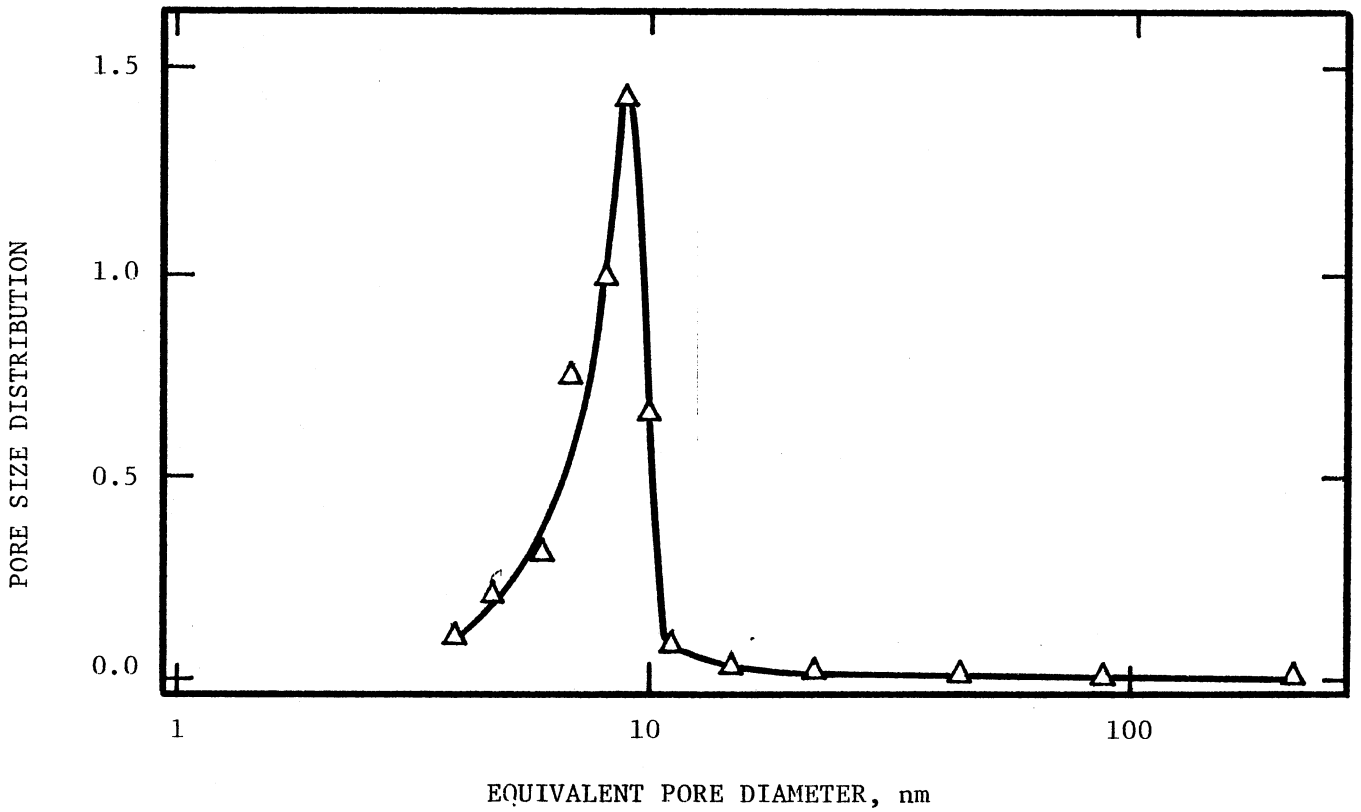

Figure 88. Pore Size Distribution of the Spent Catalyst from Section 4, Run LTZ

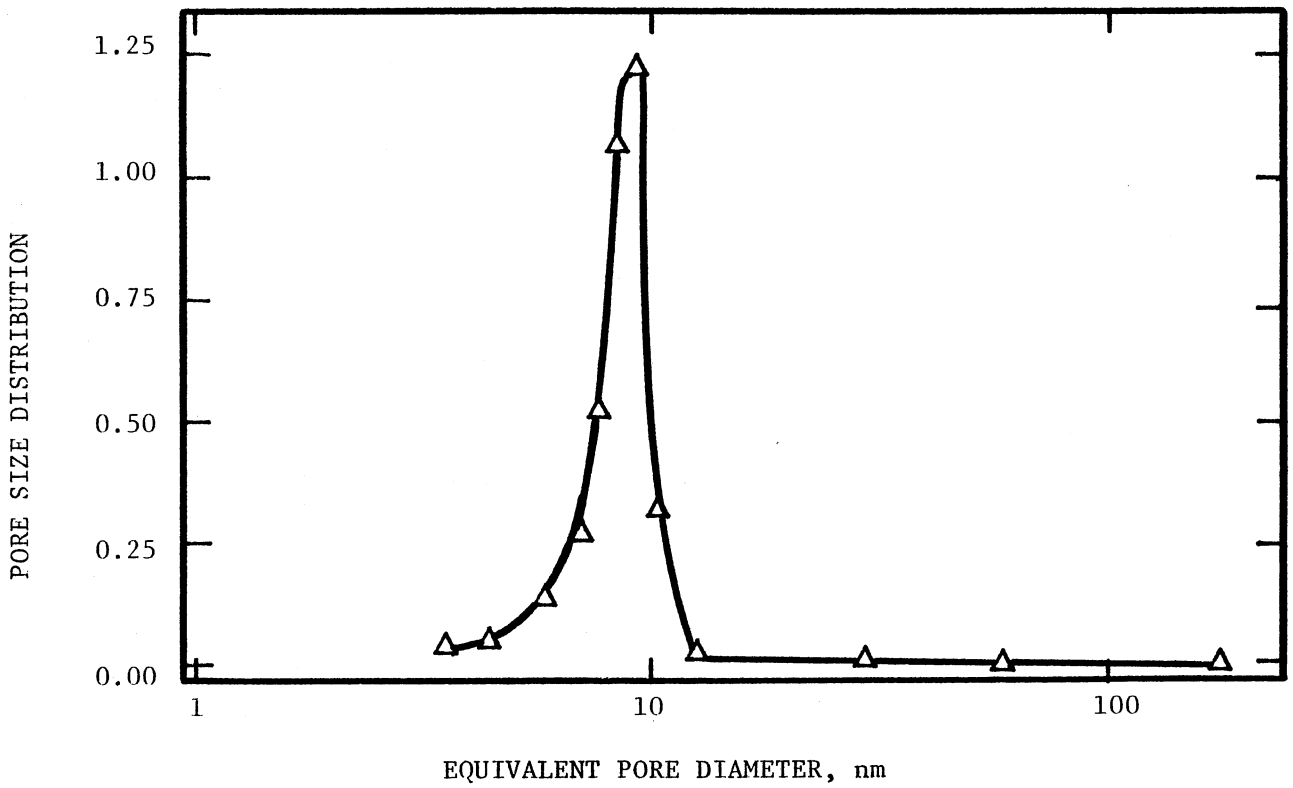

Figure 89. Pore Size Distribution of the Spent Catalyst from Section 5, Run LTZ

APPENDIX G

RESULTS FROM SCANNING AUGER MICROSCOPIC ANALYSES

Scanning Auger was used to analyze elemental profiles in catalyst pellets. The percentage of individual atom in one point was calculated based on the total atom detected at that specific point. The radial position was measured from the center of the pellet. The results in terms of atomic percentage are listed in Table XI.

TABLE XI

LIST OF RESULTS FROM SCANNING
AUGER MICROSCOPIC ANALYSES

Catalyst			Atom%				
Run	Sec.	Radius[a] mm	Sulfur	Moly.	Carbon	Oxygen	Aluminum
LTY	1	0.800	0.00	0.00	15.94	41.71	39.10
LTY	1	0.772	3.19	2.80	16.37	28.13	49.59
LTY	1	0.744	4.93	2.91	15.74	41.68	36.25
LTY	1	0.000	14.22	3.26	16.78	32.71	31.77
LTY	1	0.800	6.63	1.96	34.06	26.62	28.62
LTY	1	0.780	11.09	2.43	32.85	27.38	23.61
LTY	1	0.760	12.19	1.80	28.25	26.57	28.38
LTY	1	0.720	7.08	2.61	26.78	22.96	26.90
LTY	1	0.000	14.35	3.19	19.13	32.84	30.49
LTY	1	0.800	15.59	1.06	57.16	19.05	7.14
LTY	1	0.780	15.75	6.42	51.99	18.61	7.22
LTY	1	0.760	12.87	4.23	43.19	25.41	14.29
LTY	1	0.720	11.46	1.00	44.10	24.50	17.00
LTY	1	0.000	13.25	4.87	32.90	29.24	19.74
LTY	2	0.800	2.89	5.16	29.16	36.67	26.10
LTY	2	0.780	15.38	3.22	15.13	33.66	32.65
LTY	2	0.760	11.09	2.58	16.27	34.09	35.96
LTY	2	0.720	11.03	3.09	18.88	33.70	33.32
LTY	2	0.000	11.18	2.28	17.43	34.51	34.60
LTY	3	0.800	13.71	3.26	37.52	24.63	20.89
LTY	3	0.780	13.28	3.38	25.57	29.22	28.54
LTY	3	0.760	11.82	3.06	27.57	27.57	29.98
LTY	3	0.720	10.39	3.95	26.08	28.45	31.12
LTY	3	0.000	13.30	2.81	21.49	31.60	30.81
LTY	4	0.720	12.25	1.79	54.01	23.64	8.31
LTY	4	0.000	9.59	2.79	18.08	37.51	32.03
LTY	5	0.800	3.24	1.54	16.62	38.78	39.82
LTY	5	0.780	9.54	3.12	20.07	32.92	33.87
LTY	5	0.760	9.25	2.47	37.11	26.22	22.27
LTY	5	0.720	7.25	2.46	27.53	30.26	30.69
LTY	5	0.400	8.54	2.84	10.23	37.99	40.41
LTY	5	0.000	7.98	3.72	6.70	39.71	41.89

TABLE XI (Continued)

Catalyst			Atom %				
Run	Sec.	Radius[a] mm	Sulfur	Moly.	Carbon	Oxygen	Aluminum
LTW	1	0.800	8.44	0.00	64.96	17.32	0.00
LTW	1	0.786	11.58	3.47	20.85	29.89	34.21
LTW	1	0.772	11.97	2.85	9.22	37.56	38.41
LTW	1	0.744	10.19	2.64	12.39	36.46	38.34
LTW	1	0.400	14.36	4.34	7.81	35.27	38.22
LTW	1	0.000	16.49	3.21	5.77	38.47	36.07
LTW	5	0.800	12.30	3.63	22.86	32.65	28.57
LTW	5	0.780	13.87	4.65	15.71	36.31	29.46
LTW	5	0.760	16.59	5.33	10.79	39.18	28.11
LTW	5	0.720	13.36	4.35	15.67	37.22	29.39
LTW	5	0.000	12.82	5.14	12.34	41.13	27.95
LTX	1	0.800	4.38	0.00	78.75	16.89	0.00
LTX	1	0.786	6.65	0.00	71.72	21.63	0.00
LTX	1	0.772	6.18	0.00	39.04	28.47	26.31
LTX	1	0.744	7.90	2.46	16.60	39.47	33.72
LTX	1	0.000	12.28	3.68	2.22	43.48	38.35
LTX	2	0.800	4.82	1.65	26.72	29.69	37.12
LTX	2	0.786	6.37	2.22	23.93	30.48	36.64
LTX	2	0.772	6.63	1.10	16.07	35.30	39.89
LTX	2	0.744	6.67	2.50	19.83	32.14	38.86
LTX	2	0.400	7.63	2.66	10.41	35.15	44.18
LTX	2	0.000	10.31	3.27	3.36	39.76	43.31
LTX	3	0.800	9.10	2.36	31.14	26.89	30.52
LTX	3	0.786	12.02	2.98	6.04	39.36	39.61
LTX	3	0.772	12.37	3.24	2.19	41.13	41.07
LTX	3	0.744	13.60	3.61	3.25	39.23	40.32
LTX	3	0.000	13.15	4.17	3.75	42.53	38.09
LTX	3	0.000	13.15	4.17	3.75	42.53	38.09
LTX	3	0.744	11.71	3.60	2.77	39.45	42.47
LTX	3	0.772	9.49	2.88	7.26	36.63	43.74
LTX	3	0.786	8.69	4.13	8.36	39.63	39.19
LTX	3	0.800	7.58	1.80	18.65	33.79	35.74
LTX	4	0.800	7.30	2.52	6.82	48.45	38.32
LTX	4	0.786	3.69	2.34	3.16	48.40	42.42
LTX	4	0.772	6.08	2.41	3.47	44.19	43.86
LTX	4	0.744	9.48	3.38	6.08	39.02	42.04
LTX	4	0.000	11.49	3.83	2.95	43.93	37.80

TABLE XI (Continued)

Catalyst			Atom %				
Run	Sec.	Radius[a] mm	Sulfur	Moly.	Carbon	Oxygen	Aluminum
LTX	5	0.800	19.49	25.93	33.33	68.89	0.00
LTX	5	0.786	6.55	2.02	0.00	45.40	46.00
LTX	5	0.772	8.95	0.00	13.51	42.33	30.39
LTX	5	0.000	9.67	3.78	2.84	37.82	43.44
LTF	b	0.800	3.13	1.59	15.37	45.16	33.51
LTF	b	0.772	4.29	1.95	12.32	45.16	36.29
LTF	b	0.744	1.74	4.95	1.98	46.19	39.44
LTF	b	0.000	3.89	5.24	3.33	46.22	40.04
LTZ	1	0.800	10.82	4.02	6.04	40.64	38.48
LTZ	1	0.780	11.66	4.34	3.90	45.96	34.15
LTZ	1	0.760	11.73	4.18	2.51	45.14	36.44
LTZ	1	0.720	10.81	4.69	2.41	41.41	40.70
LTZ	1	0.000	11.75	4.51	2.31	44.46	36.97
LTZ	5	0.800	8.11	3.19	11.48	37.22	39.03
LTZ	5	0.780	9.79	2.70	4.86	41.61	41.04
LTZ	5	0.760	11.61	3.88	1.40	44.25	39.30
LTZ	5	0.720	11.31	4.40	2.64	40.47	39.59
LTZ	5	0.000	10.65	3.30	3.56	42.38	40.10
LTB	1	0.800	3.92	2.10	31.44	25.99	36.55
LTB	1	0.786	3.89	1.75	18.93	34.01	41.41
LTB	1	0.772	4.20	1.80	5.39	43.13	45.49
LTB	1	0.000	9.49	2.85	7.69	36.73	43.25
LTB	5	0.800	14.75	10.36	30.28	23.29	15.28
LTB	5	0.786	16.81	5.33	17.81	29.23	30.82
LTB	5	0.772	13.53	3.09	18.06	31.48	33.85
LTB	5	0.744	3.65	2.89	29.14	30.18	34.15
LTB	5	0.000	10.54	2.67	10.83	36.49	39.47
FRS	c	0.800	13.20	5.17	0.00	44.28	37.36
FRS	c	0.780	12.30	4.55	0.00	43.67	39.48
FRS	c	0.760	13.84	5.18	0.00	43.86	37.12
FRS	c	0.720	11.53	5.16	0.00	44.12	39.19
FRS	c	0.000	13.88	4.85	0.00	41.46	39.89
FRS	c	0.800	10.65	5.59	0.00	41.91	41.85
FRS	c	0.780	9.82	5.59	0.00	43.25	41.33
FRS	c	0.760	9.23	6.02	0.00	42.87	41.88
FRS	c	0.720	12.72	5.87	0.00	41.98	39.53
FRS	c	0.000	6.77	6.11	0.00	42.34	44.78

TABLE XI (Continued)

---

a. From the center of the pellet.
b. Not separated into sections.
c. Freshly sulfided catalysts.

APPENDIX H

DETAILS OF MODEL DERIVATIONS

Detail derivations of mass balance equations over a single catalyst pellet and over the reactor bed itself will be given in this appendix. The initial and boudary conditions, and the translations of all the equations into dimensionless form have been shown in Chapter VI, therefore, will not be presented here. Notation details are listed at the end of the derivations.

Mass Balance over a Single Catalyst Pellet

Main Reactant

For unsteady states reaction-diffusion problem, a mass balance for species A on a spherical shell of thickness Δr within a single catalyst particle can be written as:

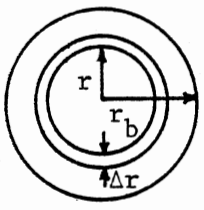

$$N_{Ar}|_r \cdot 4\pi r^2 - N_{Ar}|_{r+\Delta r} \cdot 4\pi(r+\Delta r)^2 + R_A \cdot 4\pi r^2 \Delta r \rho_p$$

$$= \varepsilon_p \frac{\partial C_{Ap}}{\partial t} \cdot 4\pi r^2 \Delta r \qquad \text{(H-1)}$$

Here $N_{Ar}|_r$ is the mass of A passing in the r-direction through an imaginary spherical surface at a distance r from the center of the sphere. The source term $R_A \cdot 4\pi r^2 \Delta r \rho_p$ gives the mass of A being produced by chemical reaction and the accumulation term $\varepsilon_p \, \partial C_{Ap}/\partial t \cdot 4\pi r^2 \Delta r$ gives the mass change in the shell of thickness Δr. Division by $4\pi\Delta r$ and letting $\Delta r \to 0$ gives:

$$\lim_{r \to 0} \frac{(r^2 N_{Ar})|_r - (r^2 N_{Ar})|_{r+\Delta r}}{\Delta r} + r^2 \rho_p R_A = r^2 \varepsilon_p \frac{\partial C_{Ap}}{\partial t} \qquad \text{(H-2)}$$

or

$$- \frac{\partial}{\partial r} (r^2 N_{Ar}) + r^2 \rho_p R_A = r^2 \varepsilon_p \frac{\partial C_{Ap}}{\partial t} \qquad \text{(H-3)}$$

The effective diffusivity, D_{Ae}, in the porous medium can be defined by the equation:

$$N_{Ar} = - D_{Ae} \frac{\partial C_{Ap}}{\partial r} \qquad \text{(H-4)}$$

From Equation (9) in Chapter VI, the reaction rate of A is given as

$$R_A = -k_A (1 - q_p)^M C_{Ap} \qquad \text{(H-5)}$$

Where k_A is the intrinsic reaction rate and q_p is the dimensionless coke content. When Eq. (H-4) and (H-5) are inserted into Eq. (H-3), one gets:

$$-\frac{\partial}{\partial r}(r^2 D_{Ae} \frac{\partial C_{Ap}}{\partial r}) - \rho_p r^2 k_A (1-q_p)^M C_{Ap} = \varepsilon_p r^2 \frac{\partial C_{Ap}}{\partial t} \qquad \text{(H-6)}$$

Coke Deposit

Since no diffusion is possible for deposited coke, the mass balance for coke, Q_p, can be written directly from Eq. (10):

$$R_q = -\frac{\partial Q_p}{\partial t} = k_q(1 - q_p)^N C_{Ap} \qquad \text{(H-7)}$$

Eq. (H-6) and (H-7) correspond to Eq. (14) and (15), respectively, in Chapter VI.

Mass Balance Over the Reactor Bed

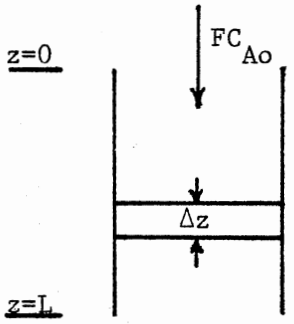

Main Reactant

The mass balance for the main reactant, A, over the fixed bed reactor can be written as:

$$FC_{Ab}\big|_z - FC_{Ab}\big|_{z+\Delta z} + S\,\Delta z\,\rho_b\,R_{A,obs} = S\,\Delta z\,\varepsilon_b\,\frac{\partial C_{Ab}}{\partial t} \qquad \text{(H-8)}$$

where FC_{Ab} is the rate of mass of A passing in the z-direction through a cross face at z position. The term $S\,\Delta z\,\rho_b\,R_{A,obs}$ and the term $S\,\Delta z\,\varepsilon_b\,\partial C_{Ab}/\partial t$ are the rates of reaction and accumulation, respectively, of A in a disk of thickness Δz. Division by $S\Delta z$ and letting $\Delta z \to 0$ gives:

$$-\frac{F}{S}\frac{\partial C_{Ab}}{\partial z} + \rho_b k_{A,obs} = \varepsilon_b \frac{\partial C_{Ab}}{\partial t} \qquad \text{(H-9)}$$

For pseudo first order reaction, the observed reaction rate can be written as:

$$R_{A,obs} = -k_A \eta_A C_{Ab} \qquad \text{(H-10)}$$

Substitute Eq (H-10) into (H-9), yields:

$$-\frac{F}{S}\frac{\partial C_{Ab}}{\partial z} - \rho_b k_A \eta_A C_{Ab} = \varepsilon_b \frac{\partial C_{Ab}}{\partial t} \qquad \text{(H-11)}$$

Coke Deposit

The mass balance for the first order, coking reaction in a fixed bed reactor can be written directly as:

$$\frac{\partial Q_b}{\partial t} = k_{q,obs} C_{Ab} = k_q \eta_q C_{Ab} \qquad \text{(H-12)}$$

Eq. (H-11) and (H-12) correspond to Eq. (29) and (30), respectively, in Chapter VI.

Notations

C_{Ab} = concentration of A in the bulk liquid, kg/m^3

C_{Ap} = concentration of A in the catalyst pellet, kg/m^3

D_{Ae} = effective diffusivity, m^2/s

F = oil feed rate, m^3/s

k_A = rate constant for the main reaction, $m^3/s/kg\text{-catalyst}$

k_q = rate constant for the coking reaction, $m^3/s/kg\text{-catalyst}$

$k_{A,obs}$ = observed rate constant for the main reaction, $m^3/s/kg\text{-catalyst}$

k_q,obs = observed rate constant for the coking reaction, $m^3/s/kq\text{-catalyst}$

L = total reactor length, m

M = order of catalyst site dependency for the main reaction

N = order of catalyst site dependency for the coking reaction

N_{Ar} = mass flux across a spherical surface of radius r, $kg/s/m^2$

Q_b = average coke content in the catalyst pellet, g-coke/g-catalyst

Q_M = maximum coke content allowable in the catalyst pellet, g-coke/g-catalyst

Q_p = local coke content in the catalyst pellet, g-coke/g-catalyst

q_p = dimensionless coke content, Q_p/Q_M

R_A = rate of the main reaction, kg/s/gk-catalyst

R_q = rate of the coking reaction, kg/s/kg-catalyst

$R_{A,obs}$ = observed rate of the main reaction, kg/s/kg-catalyst

$R_{q,obs}$ = observed rate of the coking reaction, kg/s/kg-catalyst

r = radial position of the catalyst pellet, m

Δr = radius increment, m

S = cross section area of the reactor, m^2

t = time on stream, s

z = longitudinal position of the reactor, m

Δz = length increment, m

Greek

ρ_b = packed catalyst density in the reactor, kg/m^3

ρ_p = catalyst bulk density, kg/m^3

ε_b = porosity of the catalyst bed

ε_p = porosity of the catalyst pellet

η_A = effectiveness of the main reaction

η_q = effectiveness of the coking reaction

APPENDIX I

FINITE DIFFERENCE EQUATIONS AND COMPUTER PROGRAMS

In this appendix, the dimensionless equations in Chapter VI will be translated into finite difference equations using an explicit finite difference method (Carnahan et al. 1974). The computer programs for solving these equations are listed in Tables XII and XIII.

Finite Difference Equations

Equations Over the Catalyst Pellet

The finite difference equations for first and second order derivatives of concentration and diffusivity are:

$$\frac{\partial Y_{m,n}}{\partial x} = \frac{Y_{m+1,n} - Y_{m-1,n}}{2(\Delta x)} \tag{I-1}$$

$$\frac{\partial^2 Y_{m,n}}{\partial x^2} = \frac{Y_{m+1,n} - 2Y_{m,n} + Y_{m-1,n}}{(\Delta x)^2} \tag{I-2}$$

$$\frac{\partial D_{m,n}}{\partial x} = \frac{D_{m+1,n} - D_{m-1,n}}{2(\Delta x)} \tag{I-3}$$

$$\frac{\partial Y_{m,n}}{\partial \theta_p} = \frac{Y_{m,n+1} - Y_{m,n}}{(\Delta \theta_p)} \tag{I-4}$$

$$\frac{\partial Q}{\partial \theta_p} = \frac{Q_{m,n+1} - Q_{m,n}}{(\Delta \theta_p)} \tag{I-5}$$

Where Y and Q are used instead of y_p and q_p in Chapter VI for convenience; m and n are node numbers of position and time respectively; and Δx and $\Delta\theta_p$ are position and time increments respectively.

The diffusion term in equation (19) in Chapter VI can be expanded as:

$$\frac{1}{x^2}\left(\frac{\partial}{\partial x} Dx^2 \frac{\partial Y}{\partial x}\right) = D \frac{\partial^2 Y}{\partial x^2} + \frac{\partial D}{\partial x}\frac{\partial Y}{\partial x} + \frac{2D}{x}\frac{\partial Y}{\partial x} \qquad \text{(I-6)}$$

for $x > 0$; at $x = 0$, $\partial Y/\partial x = 0$, equation (I-6) becomes:

$$\frac{1}{x^2}\left(\frac{\partial}{\partial x} Dx^2 \frac{\partial Y}{\partial x}\right) = D \frac{\partial^2 Y}{\partial x^2} \qquad \text{(I-7)}$$

with equations (I-1)-(I-6), equations (19)-(26) in Chapter VI can be written as:

$$\begin{aligned} Y_{m,n+1} = {} & Y_{m,n} - \frac{h_A^2(\Delta\theta p)}{h_q^2 \varepsilon_{m,n}} (1 - Q_{m,n})^M Y_{m,n} \\ & + \frac{(\Delta\theta_p)}{m(\Delta x)^2 h_q^2 \varepsilon_{m,n}} \Big\{ [4(1+m)D_{m,n} + mD_{m+1,n} \\ & - mD_{m-1,n}] Y_{m+1,n} - 8 m D_{m,n} Y_{m,n} \\ & + [-mD_{m+1,n} + 4(m-1)D_{m,n} + mD_{m-1,n}] Y_{m-1,n} \Big\} \end{aligned} \qquad \text{(I-8)}$$

$$Q_{m,n+1} = (1-Q_{m,n})^N Y_{m,n} (\Delta\theta_p) + Q_{m,n} \qquad \text{(I-9)}$$

$$\varepsilon_{m,n+1} = 1-\gamma Q_{m,n+1} \qquad \text{(I-10)}$$

$$D_{m,n+1} = \beta\varepsilon_{m,n+1} e^{-4.6\lambda_o/(\varepsilon_{m,n+1})^{1/2}} \qquad \text{(I-11)}$$

with initial conditions

at $n = 0$ and $0 < m < K$,

$$Y_{m,o} = 1 \quad \text{and} \quad Q_{m,o} = 0 \tag{I-12}$$

and boundary conditions

at $m = K$ and $n > 0$,

$$Y_{K,n} = 1 \tag{I-13}$$

at $m = 0$ and $n > 0$,

$$\frac{\partial Y_{o,n}}{\partial x} = 0 \text{ or } Y_{-1,n} = Y_{1,n} \tag{I-14}$$

Where K is the total number of the space divided. The second boundary condition yields a special case of equation (I-8): at $m = 0$ and $n > 0$,

$$Y_{o,n+1} = Y_{o,n} - \frac{h_A^2(\Delta\theta_p)}{h_q^2 \varepsilon_{o,n}} (1 - Q_{o,n})^M Y_{o,n} + \frac{2(\Delta\theta_p)}{h_q^2(\Delta x)^2 \varepsilon_{o,n}} (Y_{1,n} - Y_{o,n}) \tag{I-15}$$

The effectiveness factor of the main reaction at time interval n can now be integrated in finite difference from as:

$$\eta_{A_n} = 3(\Delta x)^3 \left[\frac{3}{8} (1-Q_{K,n})^M Y_{K,n} M^2 + \frac{1}{8}(1-Q_{K-1,n})^M Y_{K-1,n}(K-1)^2 + \sum_{m=1}^{K-1}(1-Q_{m,n})^M Y_{m,n} m^2\right] \tag{I-16}$$

The same equation can be used to calculate the effectiveness factor of the coking reaction, η_{qn}, when M is replaced by N.

Equations Over the Reactor Bed

The basic finite difference equations for first order derivatives are:

$$\frac{\partial U_{i,j}}{\partial z} = \frac{U_{i,j} - U_{i-1,j}}{(\Delta z)} \tag{I-17}$$

$$\frac{\partial U_{i,j}}{\partial \theta_b} = \frac{U_{i,j+1} - U_{i,j}}{(\Delta \theta_b)} \tag{I-18}$$

$$\frac{\partial V_{i,j}}{\partial \theta_b} = \frac{V_{i,j+1} - V_{i,j}}{(\Delta \theta_b)} \tag{I-19}$$

Where U and V are used instead of y_b and q_b in equations (38) and (39) to represent the reactant and coke concentrations in the reactor bed; i, j represent node numbers for the space and the time respectively. Equations (33)-(36) in Chapter VI can now be written in finite difference forms as:

$$U_{i,j+1} = [1 - (\Delta\theta_b)G\,\eta_{Aj}]U_{i,j} - \frac{(\Delta\theta_b)E}{(\Delta z)}(U_{i,j} - U_{i-1,j}) \tag{I-20}$$

$$V_{k,j+1} = V_{i,j} + (\Delta\theta_b)\eta_{qj}\,U_{i,j} \tag{I-21}$$

initial conditions

at $j = 0$ and $0 < i < I$,

$$U_{i,o} = 1 \text{ and } V_{i,o} = 0 \tag{I-22}$$

boundary conditions

at $i = 0$ and $j > 0$

$$U_{o,j} = 1 \tag{I-23}$$

Where I is the total number of space divided. Details of other notations are presented in Chapter VI.

TABLE XII

COMPUTER PROGRAM FOR SOLVING MASS BALANCE EQUATIONS OVER A SINGLE CATALYST PELLET

```
      $JOB            ,TIME=(00,05)
      C
      C
      C
      C   THIS PROGRAM IS DEVELOPED TO NUMERICALLY SOLVE REACTION-
      C   PARALLEL DEACTIVATION PROBLEM IN THE CATALYST PELLET.
      C
      C
      C  * THE FOLLOWING CONSTANTS AND PARAMETERS MUST BE SUPPLIED BY
      C    THE USER:
      C    NNUM   = TOTAL NUMBER OF TIME STEP
      C    MNUM   = TOTAL NUMBER OF RADIUS DIVIDED
      C    NFQPT  = FREQUENCY OF TIME STEP TO BE PRINTED
      C    MFQPT  = FREQUENCY OF RADIUS STEP TO BE PRINTED
      C    DTHETA = TIME INCREMENT
      C    RKA    = INTRINSIC RATE CONSTANT FOR THE MAIN REACTION,
      C             ML/S/G-CATALYST
      C    RKA    = INTRINSIC RATE CONSTANT FOR THE COKING REACTION,
      C             ML/S/G-CATALYST
      C    RADIUS = EQUIVALENT CATALYST PELLEL RADIUS, CM
      C    QM     = MAXIMUN COKE CONTENT, G-COKE/G-CATALYST
      C    CAB    = BULK CONCENTRATION OF THE REACTANT, G/ML
      C    PORO   = CATALYST POROSITY
      C    CATDEN = CATALYST PELLET DENSITY,G/ML
      C    COKDEN = COKE DENSITY, G/ML
      C    SD     = CRITICALL SOLUTE DEAMETER, ANGSTROM
      C    PDO    = PORE DIAMETER OF THE FRESHLY SULFIDED CATALYST, ANGSTROM
      C    DA     = BULK DIFFUSIVITY OF THE REACTANT, SQ. CM/S
      C    PARTI  = PARTITION COEFFICIENT
      C    TAU    = TORTUOSITY OF THE CATALYST
      C
      C
      C
 1          IMPLICIT REAL*8 (A-H,O-Z), INTEGER(I-N)
 2          DIMENSION FAI(100),SAI(100),SIGMA(100),D(100),FAIO(100)
     *            ,FAI2(100),SAI2(100),SIGMA2(100),D2(100)
      C
 3          READ (5,*) NNUM,MNUM,NFQPT,MFQPT
 4          READ (5,*) DTHETA,RKA,RKQ
 5          READ (5,*) RADIUS,QM,CAB,PORO,CATDEN,COKDEN
 6          READ (5,*) SD,PDO,DA,PARTI,TAU
 7          DZAI = 1.0/MNUM
 8          RATIO = DTHETA/DZAI/DZAI
 9          ALFA = SD/PDO
10          GAMA = QM*CATDEN/PORO/COKDEN
11          DAO = DEXP(-4.6*ALFA)*DA*PORO/PARTI/TAU
12          H = RADIUS*DSQRT(CATDEN*RKA/DAO)
13          HQ = RADIUS*DSQRT(RKQ*CAB*PORO/DAO/QM)
14          RAT = H*H*DTHETA/HQ/HQ
15          RATT = DTHETA/(DZAI*DZAI*HQ*HQ)
16          BETA = PORO*DA/(PARTI*TAU*DAO)
17          WRITE (6,700) NNUM,MNUM,DTHETA,DZAI,RATIO,
     *                  RADIUS,QM,CAB,PORO,CATDEN,COKDEN,
     *                  SD,PDO,PARTI,TAU,DA,DAO,
     *                  RKA,RKQ,H,HQ,ALFA,GAMA,RAT,RATT
18   700    FORMAT(1H1,///,I15,' = NUMBER OF TIME INCREMENT',
     *         /,I15,' = NUMBER OF RADIUS INCREMENT',
     *         /,D15.5,' = TIME INCREMENT',
     *         /,D15.5,' = RADIUS INCREMENT',
     *         /,D15.5,' = RATIO ',
```

TABLE XII (Continued)

```
     *          /,D15.5,' = RADIUS OF THE CATALYST PELLET,CM',
     *          /,D15.5,' = MAXIMUN COKE CONTENT, G/G-CATALYST',
     *          /,D15.5,' = BOUNDARY CONCENTRATION, G/ML',
     *          /,D15.5,' = PELLET POROSITY',
     *          /,D15.5,' = PELLET DENSITY, G/ML',
     *          /,D15.5,' = COKE DENSITY, G/ML',
     *          /,D15.5,' = SOLUTE DIAMETER, ANGSTROM',
     *          /,D15.5,' = PORE DIAMETER, ANGSTROM',
     *          /,D15.5,' = PARTITION COEFFICIENT',
     *          /,D15.5,' = TORTUOSITY',
     *          /,D15.5,' = BULK DIFFUSIVITY, SQ.CM/SEC',
     *          /,D15.5,' = EFFECTIVE DIFFUSIVITY, SQ.CM/SEC',
     *          /,D15.5,' = MAIN REACION RATE CONSTANT, ML/SEC/G',
     *          /,D15.5,' = COKING REACTION CONSTANT, ML/SEC/G',
     *          /,D15.5,' = THIELE MODULUS FOR THE MAIN REACTION',
     *          /,D15.5,' = THIELE MODULUS FOR THE COKING REACTION',
     *          /,D15.5,' = ALFA, SEE THE PROGRAM',
     *          /,D15.5,' = GAMA, SEE THE PROGRAM',
     *          /,D15.5,' = RAT,  SEE THE PROGRAM',
     *          /,D15.5,' = RATT, SEE THE PROGRAM')
19         WRITE (6,709)
20  709    FORMAT(1H1,///,1X,'DIMENSIONLESS PARAMETERS:',
     *              /,7X,'N = TIME',
     *              /,7X,'M = POSITION',
     *              /,5X,'FAI = REACTANT CONCENTRATION',
     *              /,5X,'SAI = LOCAL COKE CONCENTRATION',
     *              /,5X,'AVE.COKE = AVERAGE COKE CONTENT',
     *              /,5X,'EFQ = EFFECTIVENESS FACTOR FOR THE COKING',
     *              /,5X,'EFA = EFFECTIVENESS FACTOR FOR THE MAIN')
21         WRITE (6,710)
22  710    FORMAT(///,8X,'N',9X,'M',4X,'FAI(M,N)',5X,'SAI(M,N)',
     *       5X,'AVE. COKE',
     *       7X,'EFQ',10X,'EFA',/)
    C
    C  WHEN N=0
23         N=0
    C    WHEN M=0
24         FAIOO = 1.0
    C    WHEN M=1 TO MAXMIUM
25         DO 1100 M=1,MNUM
26           FAIO(M) = 1.0
27  1100   CONTINUE
28         MMI = MNUM-1
29         EFO = 3.0*(FAIO(MNUM)-FAIO(MMI))/H/H/DZAI
30         M = 0
31         WRITE(6,810) N,M,FAIOO,EFO
32         DO 3000 M=1,MNUM
33           IF ((M/MFQPT)*MFQPT.NE.M) GO TO 3000
34           WRITE(6,810) N,M,FAIO(M)
35  810      FORMAT(2(I10),D13.5,39X,D13.5)
36  3000   CONTINUE
    C  END OF N=0
37         FAIC = FAIOO
38         SAIC = 0.0
39         SIGMAC = 1.0
40         DO 3337 M = 1,MNUM
41           FAI(M) = FAIO(M)
42           SAI(M) = 0.0
43           SIGMA(M) = 1.0
44  3337   CONTINUE
```

TABLE XII (Continued)

```
      C
      C  WHEN N=1
45          N = 1
      C     WHEN M=0
46            FAIC2 = (1.0-RAT)*FAI00+2.0*RATT*(FAI0(1)-FAI00)
47            SAIC2 = FAIC*DTHETA
48            SIGMC2 = 1.0-GAMA*SAIC
49            SS = SIGMAC
50            DC2 = (DEXP(-4.6*ALFA/DSQRT(SS)))*BETA
      C     WHEN M=1
51            FAI2(1) = (1.0-RAT)*FAI0(1)+2.0*RATT*(FAI0(2)-FAI0(1))
52            SAI2(1) = FAI(1)*DTHETA
53            SIGMA2(1) = 1.0+GAMA*SAI(1)
54            SST = SIGMA(1)
55            D2(1) = (DEXP(-4.6*ALFA/DSQRT(SST)))*BETA
      C     WHEN M IS LARGER THAN 1
56            DO 1200 M=2,MMI
57              MH = M+1
58              ML = M-1
59              FAI2(M) = (1.0-RAT)*FAI0(M)+RATT/M*((1.0+M)*FAI0(MH)-
             *                2.0*M*FAI0(M)-(1.0-M)*FAI0(ML))
60              SAI2(M) = FAI(M)*DTHETA
61              SIGMA2(M) = 1.0-GAMA*SAI(M)
62              SSI = SIGMA(M)
63              D2(M) = (DEXP(-4.6*ALFA/DSQRT(SSI)))*BETA
64    1200    CONTINUE
65            M = MNUM
66            FAI2(M) = 1.0
67            SAI2(M) = DTHETA
68            SIGMA2(M) = 1.0-GAMA*SAI(M)
69            SSTI = SIGMA(M)
70            D2(M) = (DEXP(-4.6*ALFA/DSQRT(SSI)))*BETA
71            EF = 3.0*D2(MNUM)*(FAI2(MNUM)-FAI2(MMI))/H/H/DZAI
72             WRITE (6,802) N,FAIC2,SAIC2,SAIC2,EF,EF
73            DO 3500 M=1,MNUM
74              IF ((M/MFQPT)*MFQPT.NE.M) GO TO 3500
75              WRITE (6,800) M,FAI2(M),SAI2(M)
76    3500    CONTINUE
77            FAIC = FAIC2
78            SAIC = SAIC2
79            SIGMAC = SIGMC2
80            DC = DC2
81            DO 3336 M=1,MNUM
82              FAI(M) = FAI2(M)
83              SAI(M) = SAI2(M)
84              SIGMA(M) = SIGMA2(M)
85              D(M) = D2(M)
86    3336    CONTINUE
      C  END OF N=1
      C  WHEN N IS LARGER THAN 1
87            DO 1300 N=2,NNUM
88              NL = N-1
      C     WHEN M=0
89              FAIC2 = FAIC*(1.0-RAT/SIGMAC*(1.0-SAIC)**0.5)+
             *                2.0*RATT/SIGMAC*(FAI(1)-FAIC)
90              SAIC2 = (1.0-SAIC)**2*FAIC*DTHETA+SAIC
91              SIGMC2 = 1.0-GAMA*SAIC
92              SSNI = SIGMAC
93              DC2 = (DEXP(-4.6*ALFA/DSQRT(SSNI)))*BETA
      C       WHEN M=1
```

TABLE XII (Continued)

```
 94           FAI2(1) = FAI(1)*(1.0-RAT/SIGMA(1)*
     *            (1.0-SAI(1))**0.5)+RATT/4.0/SIGMA(1)*
     *            (FAI(2)*(8.0*D(1)+D(2)-DC)-
     *            8.0*D(1)*FAI(1)+FAIC*(DC-D(2)))
 95           SAI2(1) = (1.0-SAI(1))**2*FAI(1)*DTHETA+SAI(1)
 96           SIGMA2(1) = 1.0-GAMA*SAI(1)
 97           SSNN = SIGMA(1)
 98           D2(1) = (DEXP(-4.6*ALFA/DSQRT(SSNN)))*BETA
      C      WHEN M IS LARGER THAN 1
 99           DO 1400 M=2,MMI
100             MH = M+1
101             ML = M-1
102             FAI2(M) = FAI(M)*(1.0-RAT/SIGMA(M)*
     *               (1.0-SAI(M))**0.5)+RATT/(4.0*M*SIGMA(M))*
     *               (FAI(MH)*(4.0*(1.0+M)*D(M)+(D(MH)-D(ML))*M)-
     *               8.0*M*D(M)*FAI(M)+FAI(ML)*
     *               (D(ML)*M-4.0*(1.0-M)*D(M)-D(MH)*M))
103             SAI2(M) = (1.0-SAI(M))**2*FAI(M)*DTHETA+SAI(M)
104             SIGMA2(M) = 1.0-GAMA*SAI(M)
105             SSK = SIGMA(M)
106             D2(M) = (DEXP(-4.6*ALFA/DSQRT(SSK)))*BETA
107  1400     CONTINUE
108           M = MNUM
109           FAI2(M) = 1.0
110             SAI2(M) = (1.0-SAI(M))**2*FAI(M)*DTHETA+SAI(M)
111             SIGMA2(M) = 1.0-GAMA*SAI(M)
112             SSK = SIGMA(M)
113             D2(M) = (DEXP(-4.6*ALFA/DSQRT(SSK)))*BETA
114           IF ((N/NFQPT)*NFQPT.NE.N) GO TO 3335
115           CZAI = DZAI*DZAI*DZAI
116           ANUM = (0.25*(3.0*MNUM+MMI))**2
117           AVCOKE = 0.0
118           EFA = 0.0
119           EFQ = 0.0
120           DO 3290 M=2,MMI
121             AVCOKE = AVCOKE +SAI2(M)*M*M
122             EFA = EFA+(1.0-SAI2(M))**0.5*FAI2(M)*M*M
123             EFQ = EFQ+(1.0-SAI2(M))**2*FAI2(M)*M*M
124  3290     CONTINUE
125           AVCOKE = 3*(AVCOKE+0.125*(3.0*SAI2(MNUM)+SAI2(MMI))*ANUM)*CZAI
126           EFA = 3.0*(EFA+0.125*(3.0*(1.0-SAI2(MNUM))**0.5*FAI2(MNUM)+
     *           (1.0-SAI2(MMI))**0.5*FAI2(MMI))*ANUM)*CZAI
127           EFQ = 3.0*(EFQ+0.125*(3.0*(1.0-SAI2(MNUM))**2*FAI2(MNUM)+
     *           (1.0-SAI2(MMI))**2*FAI2(MMI))*ANUM)*CZAI
128           EF = 3.0*D2(MNUM)*(FAI2(MNUM)-FAI2(MMI))/H/H/DZAI
129           WRITE (6,802) N,FAIC2,SAIC2,AVCOKE,EFQ,EFA
130  802      FORMAT(I10,9X,'0',8(D13.5))
131           DO 3333 M=1,MNUM
132             IF ((M/MFQPT)*MFQPT.NE.M) GO TO 3333
133             WRITE (6,800) M,FAI2(M),SAI2(M)
134  3333     CONTINUE
135  3335    FAIC = FAIC2
136          SAIC = SAIC2
137          SIGMAC = SIGMC2
138          DC = DC2
139          DO 3338 M=1,MNUM
140            FAI(M) = FAI2(M)
141            SAI(M) = SAI2(M)
142            SIGMA(M) = SIGMA2(M)
143            D(M) = D2(M)
```

TABLE XII (Continued)

```
144    3338   CONTINUE
145    1300  CONTINUE
       C  END OF COMPUTING CYCLE
146    800    FORMAT(10X,I10,4(D13.5))
147           WRITE (6,789)
148    789    FORMAT(1H1)
149           STOP
150           END

       $ENTRY
```

TABLE XIII

COMPUTER PROGRAM FOR SOLVING MASS BALANCE EQUATIONS OVER A REACTOR BED

```
      $JOB           ,TIME=(00,05)
      C
      C
      C
      C    THIS PROGRAM IS DEVELOPED TO NUMERICALLY SOLVE REACTION-
      C    PARALLEL DEACTIVATION PROBLEM IN THE REACTOR BED.
      C
      C
      C
      C  * THE USER HAVE TO SUPPLY THE EFFECTIVENESS FACTORS OF THE MAIN AND
      C    THE COKING REACTIONS AS FUNCTIONS OF THIELE MODULUS AND TIME
      C    ON STREAM.  THESE FUNCTIONS OF EFFECTIVENESS FACTORS CAN BE
      C    CALCULATED NUMERICALLY FROM THE EQUATIONS OVER THE SINGLE CATALYST
      C    PELLET.  THE USER ALSO HAVE TO SUPPLY THE FOLLOWING CONSTANTS
      C    AND PARAMETERS:
      C
      C    NBMAX  = TOTAL NUMBER OF TIME INCREMENT
      C    MBMAX  = TOTAL NUMBER OF SPACE INCREMENT
      C    NBFQ   = FREQUENCY OF TIME STEP TO BE PRINTED
      C    MBFQ   = FREQUENCY OF SPACE STEP TO BE PRINTED
      C    DTIME  = TIME INCREMENT
      C    RKA    = INTRINSIC RATE CONSTANT FOR THE MAIN REACTION,
      C             ML/S/G-CATALYST
      C    RKA    = INTRINSIC RATE CONSTANT FOR THE COKING REACTION,
      C             ML/S/G-CATALYST
      C    RADIUS = EQUIVALENT CATALYST PELLEL RADIUS, CM
      C    QM     = MAXIMUN COKE CONTENT, G-COKE/G-CATALYST
      C    CAF    = INLET CONCENTRATION OF THE REACTANT, G/ML
      C    PORO   = CATALYST POROSITY
      C    CATDEN = CATALYST PELLET DENSITY,G/ML
      C    COKDEN = COKE DENSITY, G/ML
      C    SD     = CRITICALL SOLUTE DEAMETER, ANGSTROM
      C    PDO    = PORE DIAMETER OF THE FRESHLY SULFIDED CATALYST, ANGSTROM
      C    DA     = BULK DIFFUSIVITY OF THE REACTANT, SQ. CM/S
      C    PARTI  = PARTITION COEFFICIENT
      C    TAU    = TORTUOSITY OF THE CATALYST
      C    ST     = LIQUID VOLUME HOURLY SPACE TIME
      C    BEDEN  = CATALYST PACKED DENSITY, G/ML
      C
      C
      C
 1          IMPLICIT REAL*8 (A-H,O-Z), INTEGER(I-N)
 2          DIMENSION FAIB(100), SAIB(100), ETAB(100),ETQB(100)
           *          ,FAID(100), SAID(100), ETAD(100),ETQD(100)
      C
 3          READ (5,*) SLOPA1,SLOPA2,SLOPQ1,SLOPQ2
 4          READ (5,*) RKA,RKQ,ST,CAF,QM,BDEN
 5          READ (5,*) NBMAX,MBMAX,NBFQ,MBFQ,DTIME
 6          READ (5,*) SD,PDO,DA,PORO,TAU,RADIUS,CATDEN
 7          MAI = MBMAX-1
 8          DAO = DEXP(-4.6*SD/PDO)*DA*PORO/TAU
 9          HA = RADIUS*DSQRT(CATDEN*RKA/DAO)
10          HQ = RADIUS*DSQRT(RKQ*CAF*PORO/DAO/QM)
11          DLENS = 1.0/MBMAX
12          E = QM/(CAF*RKQ*ST)
13          G = RKA*BDEN*QM/CAF/RKQ
14          WX = DTIME*E/DLENS
15          WRITE (6,4010) NBMAX,MBMAX,DLENS,DTIME,RKA,RKQ,ST,CAF,QM,BDEN
           *                ,SD,PDO,DA,DAO,PORO,TAU,RADIUS,CATDEN,HA,HQ
16     4010  FORMAT(1H1,///,I5,' = NUMBER OF TIME INCREMENT',
```

TABLE XIII (Continued)

```
     *       /,I15, ' = NUMBER OF SPACE INCREMENT',
     *       /,D15.4,' = SPACE INCREMENT',
     *       /,D15.4,' = TIME INCREMENT',
     *       /,D15.4,' = RATE CONSTANT OF THE MAIN REACTION, ML/S/G',
     *       /,D15.4,' = RATE CONSTANT OF THE COKNG REACTION, ML/S/G',
     *       /,D15.4,' = LIQUID VOLUME HOURLY SPACE TIME',
     *       /,D15.4,' = CONCENTRATION OF THE REACTANT, G/ML',
     *       /,D15.4,' = MAXIMUM COKE DEPOSITION, G-COKE/G-CATALYST',
     *       /,D15.4,' = BED CATALYST DENSITY, G/ML',
     *       /,D15.4,' = SOLUTE DIAMETER, ANGSTROM',
     *       /,D15.4,' = PORE DIAMETER, ANGSTROM',
     *       /,D15.4,' = BULK DIFFUSIVITY SQ.CM/SEC.',
     *       /,D15.4,' = EFFECTIVE DIFFUSIVITY SQ.CM/SEC.',
     *       /,D15.4,' = CATALYST PELLET POROSITY',
     *       /,D15.4,' = TORTUOSITY',
     *       /,D15.4,' = CATALYST PELLET RADIUS, CM',
     *       /,D15.4,' = CATALYST PELLET DENSITY, G/ML',
     *       /,D15.4,' = THIELE MODULUS FOR MAIN REACTION',
     *       /,D15.4,' = THIELE MODULUS FOR COKING REACTION')
17        WRITE (6,4020)
18   4020 FORMAT(1H1,5X,'TIME',6X,'DEPTH',7X,'CONC',12X,'EF',12X,'EFQ ',
     *          12X,'COKE',9X,'AVE COKE',//)
     C
     C   WHEN N = 0
     C     AT REACTOR ENTRANCE
19          FAIBC = 1.0
20          SAIBC = 0.0
21          ETABC = 3.0*(1.0/DTANH(HA)-1.0/HA)/HA
22          ETQBC = 3.0*(1.0/DTANH(HA)-1.0/HA)/HA
23          ETAO = ETABC
24          ETQO = ETQBC
     C      AFTER REACTOR ENTRANCE
25          DO 5010 MB=1,MBMAX
26            FAIB(MB) = 1.0
27            SAIB(MB) = 0.0
28            ETAB(MB) = 3.0*(1.0/DTANH(HA)-1.0/HA)/HA
29            ETQB(MB) = 3.0*(1.0/DTANH(HA)-1.0/HA)/HA
30   5010     CONTINUE
31        NKO = 0
32        WRITE (6,4050) NKO,ETABC
33   4050 FORMAT(I10,25X,D15.4,/)
     C
     C   WHEN TIME GREATER THAN 0
34        DO 5020 NB=1,NBMAX
     C      AT REACTOR ENTRANCE
35          SAIDC = SAIBC + DTIME*ETQBC*FAIBC
36          ETADC = ETAO+SLOPA1*SAIBC+SLOPA2*SAIBC*SAIBC
37          ETQDC = ETQO+SLOPQ1*SAIBC+SLOPQ2*SAIBC*SAIBC
     C      AT MB=1
38          FAID(1) = (1.0-DTIME*G*ETAB(1))*FAIB(1)-WX*(FAIB(1)-FAIBC)
39          SAID(1) = SAIB(1) +DTIME*ETQB(1)*FAIB(1)
40          ETAD(1) = ETAO+SLOPA1*SAIB(1)+SLOPA2*SAIB(1)*SAIB(1)
41          ETQD(1) = ETQO+SLOPQ1*SAIB(1)+SLOPQ2*SAIB(1)*SAIB(1)
     C      AFTER REACTOR ENTRANCE
42          DO 5030 MB=2,MBMAX
43            MBH = MB+1
44            MBL = MB-1
45            FAID(MB) = (1.0-DTIME*G*ETAB(MB))*FAIB(MB)-
     *                   WX*(FAIB(MB)-FAIB(MBL))
46            SAID(MB) = SAIB(MB)+DTIME*ETQB(MB)*FAIB(MB)
```

TABLE XIII (Continued)

```
47              ETAD(MB) = ETAO+SLOPA1*SAIB(MB)+SLOPA2*SAIB(MB)*SAIB(MB)
48              ETQD(MB) = ETQO+SLOPQ1*SAIB(MB)+SLOPQ2*SAIB(MB)*SAIB(MB)
49    5030      CONTINUE
50              IF ((NB/NBFQ)*NBFQ.NE.NB) GO TO 5050
51              AVCOK = 0.5*SAIDC
52              DO 6020 MB=1,MAI
53                AVCOK = AVCOK+SAID(MB)
54    6020      CONTINUE
55              AVCOK = (AVCOK+0.5*SAID(MBMAX))*DLENS
56              MKO = 0
57              WRITE(6,4030) NB,MKO,FAIBC,ETADC,ETQDC, SAIDC,AVCOK
58    4030      FORMAT(2(I10),5(D15.4))
59              DO 6030 MB=1,MBMAX
60                IF ((MB/MBFQ)*MBFQ.NE.MB) GO TO 6030
61                WRITE(6,4040) MB,FAID(MB),ETAD(MB),ETQD(MB),SAID(MB)
62    4040        FORMAT(10X,I10,4(D15.4))
63    6030      CONTINUE
64    5050        SAIBC = SAIDC
65                ETABC = ETADC
66                ETQBC = ETQDC
67                DO 5040 MB = 1,MBMAX
68                  FAIB(MB) = FAID(MB)
69                  SAIB(MB) = SAID(MB)
70                  ETAB(MB) = ETAD(MB)
71                  ETQB(MB) = ETQD(MB)
72    5040        CONTINUE
73    5020    CONTINUE
74            WRITE (6,4033)
75    4033    FORMAT(1H1)
76            STOP
77            END

      $ENTRY
```

VITA

Hong-Ju Chang

Candidate for the Degree of

Doctor of Philosophy

Thesis: COKE DEACTIVATION DURING CATALYTIC COAL OILS HYDROTREATMENT

Major Field: Chemical Engineering

Biographical:

Personal Data: Born in Taiwan, Republic of China, December 21, 1951 to Mr. and Mrs. C. Y. Chang.

Education: Attended the Taichung First Senior High School, Taichung, Taiwan; received the degree of Bachelor of Science in Chemical Engineering from Tunghai University, Taichung, Taiwan in June, 1973; received the degree of Master of Science in Chemical Engineering from Oklahoma State University, Stillwater, Oklahoma in December, 1977; completed the requirements for the degree of Doctor of Philosophy at Oklahoma State University in December, 1982.

Professional Experience: Lieutenant, Chinese Army, October 1973 to August 1975; Process Engineering, United Polymer Corporation, Toufen, Taiwan, November 1975 to July 1976; Graduate Research Associate, Oklahoma State University, Stillwater, Oklahoma, September 1978 to July 1982.

Professional Affiliations: American Institute of Chemical Engineers; American Chemical Society.